Doctoral theses at NTNU, 2016:256

Anja B. Estensen Klausen

Early age crack assessment of concrete structures

Experimental investigation of decisive parameters

Doctoral thesis

Anja B. Estensen Klausen

ISBN 978-82-326-1850-7 (printed ver.)
ISBN 978-82-326-1851-4 (electronic ver.)
ISSN 1503-8181

NTNU
Norwegian University of
Science and Technology

Doctoral theses at NTNU, 2016:256

NTNU
Norwegian University of
Science and Technology
Thesis for the Degree of
Philosophiae Doctor
Faculty of Engineering Science and Technology
Department of Structural Engineering

NTNU
Norwegian University of
Science and Technology

Anja B. Estensen Klausen

Early age crack assessment of concrete structures

Experimental investigation of decisive parameters

Thesis for the Degree of Philosophiae Doctor

Trondheim, september 2016

Norwegian University of Science and Technology
Faculty of Engineering Science and Technology
Department of Structural Engineering

NTNU
Norwegian University of
Science and Technology

NTNU
Norwegian University of Science and Technology

Thesis for the Degree of Philosophiae Doctor

Faculty of Engineering Science and Technology
Department of Structural Engineering

ISBN 978-82-326-1850-7 (printed ver.)
ISBN 978-82-326-1851-4 (electronic ver.)
ISSN 1503-8181

Doctoral theses at NTNU, 2016:256

Printed by NTNU Grafisk senter

Preface

This doctoral thesis is submitted to the Norwegian University of Science and Technology (NTNU) for the degree Philosophiae Doctor (PhD). The research has been carried out at the Department of Structural Engineering at NTNU in Trondheim. The main supervisor has been Professor Terje Kanstad (NTNU) and the co-supervisor has been Øyvind Bjøntegaard (The Norwegian Public Roads Administration).

The current PhD project was initiated through COIN (Concrete Innovation Centre, 2007 – 2014, www.coinweb.no), which was a Centre for Research-based Innovation established by The Research Council of Norway. The described activities have been a part of COIN Focus Area 3.1 “Crack free concrete structures”.

The PhD work has been financed by NTNU and COIN, in addition to highly appreciated contributions from SINTEF. In 2015 and 2016, the PhD work also received financial support from the User-driven Research-based Innovation project DaCS (Durable advanced Concrete Solutions).

The PhD project started in October 2009 and the thesis was submitted in May 2016. The candidate had a maternity leave of 11 months during this period of time.

The writer, Anja B. Estensen Klausen, declares that this thesis with all its presented work is her own. The thesis contains no material that has previously been submitted for a degree at this university or any other institution.

Anja B. Estensen Klausen
Trondheim, May 2016

Acknowledgements

This thesis would not have been possible without all the people who have contributed and supported me over these last six years. For this I am tremendously grateful.

First of all, I would like to thank my main-supervisor Professor Terje Kanstad; thank you for never giving up on the equipment or me, but always encouraging and supporting me with your valuable knowledge, positivity and never-ending optimism. I would also like to thank my co-supervisor PhD Øyvind Bjøntegaard; thank you for sharing your profound knowledge on the topic, your valuable feedback and suggestions and for always answering my never-ending stream of questions. I am also very grateful to Professor Emeritus Erik Sellevold; thank you for taking the time to read my manuscript and providing me with your very useful comments and suggestions. Your feedback during the final stage was very motivating and inspiring.

I would also like to express my gratitude to the personnel in both the NTNU and SINTEF laboratories; thank you for all the support and help I have received with my experiments, for enduring my long-lasting (and justified…) suspicion towards the experimental equipment, for positive discussions and for exercise advices. I also owe my thanks to my colleagues at both SINTEF and NTNU; thank you for providing a pleasurable working environment, for sharing your knowledge and for your genuine and contagious love for concrete. I very much enjoy being a part of the SINTEF and NTNU concrete family.

I also highly appreciate the support from my family and friends; thank you for believing in me, encouraging me, listening to me and dragging me out of my concrete-bubble from time to time, providing highly appreciated quality time and laughter. I am also grateful to my floorball team-mates; thank you for pleasurable exercises, excellent victories as well as social highlights with competitions and loads of laughs.

Finally, a special thank you goes to my husband Jan Tore for encouraging me to take on this thesis and thereafter sticking by me and supporting me along the way. I am also very grateful to my children for being who they are and for constantly reminding me that early age concrete is not the only important thing in life. Thank you, Jan Tore, Jostein, Majken, Ina and Even.

Abstract

Concrete in the hardening phase is subjected to volume changes caused by thermal dilation and autogenous deformation. If these volume changes are restrained they may lead to cracking and further to functionality-, durability, and esthetical problems. The volume changes of concrete and the associated cracking risk can however be predicted by the use of calculation methods to assess the concrete's early age structural behaviour. On the basis of such calculations and corresponding laboratory experiments, proper choice of concrete type, mineral additives and execution methods on-site can be taken to minimize or avoid cracking. Hardening phase crack risk assessment of concrete structures is the main topic of the current PhD work.

The overall aim of the current study has been to contribute to an increased basic knowledge and understanding of early age concrete material properties (behavior) and also to investigate calculation methods to assess the concrete's structural behavior under realistic temperature curing conditions.

Five concretes with a varying amount of fly ash, 0 %, 17 %, 25 %, 33 % and 45 %, have been investigated (the fly ash content is given as percentage of the total amount of "cement + fly ash"). For each concrete, an extensive experimental test program has been performed; including heat development, compressive strength, tensile strength, E-modulus in tension and compression, creep in tension and in compression, autogenous deformation development and restrained stress development. During testing, considerable focus was given to the effect of curing temperature, i.e. 20 ^{o}C isothermal versus realistic temperature conditions. The obtained test results have been used as a basis for restrained stress calculations performed with the calculation approaches Excel, CrackTeSt COIN and DIANA. By using laboratory experiments and analytical approaches, the concretes' strain- and stress development and crack risk has been assessed. The concretes' crack risk was reduced with increasing fly ash content in spite of a corresponding reduction in strength; this was mainly because the maximum temperature also was strongly reduced.

The experimental test program has also included numerous tests in the Temperature-Stress Testing Machine (TSTM), which has been reconstructed and verified during the current work. The reconstruction has provided a more advanced management of the experiments and more extensive output from each test. By applying a representative degree of restraint and temperature history, the TSTM is now able to directly simulate the stress development of a given section of a concrete structure. In addition, the TSTM has been used as the answer for early age stress calculations, thus allowing for an evaluation and/or calibration of 1) the chosen calculation approaches and 2) the appurtenant material parameters determined from the previously described experimental test series.

The work conducted in this thesis forms the basis for future enhancement on the knowledge on materials modeling, structural behavior, concrete mix-design and execution methods.

Sammendrag

I herdefasen utsettes betongen for volumendringer forårsaket av termisk dilatasjon og autogen deformasjon. Dersom disse volumendringene er fastholdte, kan de føre til opprissing av betongen og videre til redusert funksjonalitet, bestandighet og estetikk. Betongens volumendringer og den tilhørende risikoen for opprissing kan imidlertid estimeres og evalueres ved hjelp av beregningsmetoder basert på betongens egenskaps-, tøynings- og spenningsutvikling i herdefasen. På grunnlag av slike beregninger og tilhørende laboratorieforsøk, kan rissrisikoen reduseres og om mulig også unngås ved hjelp av f.eks. betongens sammensetning og utførelsesmetoder.

Det overordnede målet i denne studien har vært å bidra til en økt grunnleggende kunnskap og forståelse av betongens materialegenskaper i tidlig alder, og også å undersøke beregningsmetoder for å vurdere betongens tøynings- og spenningsutvikling under realistiske temperaturbetingelser.

Fem betonger med en varierende mengde flyveaske, 0 %, 17 %, 25 %, 33 % og 45 %, har blitt undersøkt (flyveaskeinnholdet er gitt som prosent av den totale mengden av «sement + flyveaske»). For hver betong er det gjennomført et omfattende forsøksprogram, inkludert varmeutvikling, trykkfasthet, strekkfasthet, E-modul under strekk og trykk, kryp i strekk og i trykk, autogen deformasjon og spenningsutvikling. Betydelig fokus er viet effekten av herdetemperatur, dvs. 20 °C isoterme herdeforhold versus realistiske temperaturforhold. Forsøksresultatene har blitt brukt som basis for spenningsberegninger gjennomført i programmene Excel, CrackTeSt COIN og DIANA. Ved hjelp av laboratorieforsøk og beregningsmetoder har betongenes rissrisiko blitt estimert og redusert ved hjelp av tilsetning av flyveaske.

Forsøksprogrammet har også inkludert en rekke tester i en moderne spenningsrigg (Temperature-Stress Testing Machine - TSTM), som har blitt rekonstruert og verifisert under det nåværende arbeidet. Oppdateringen av spenningsriggen har medført en mer avansert styring av forsøkene samt mer omfattende resultater fra hver test. Ved å bruke en representativ fastholdningsgrad og temperaturhistorie er spenningsriggen nå i stand til direkte å simulere spenningsutviklingen i en konstruksjons kritiske snitt. Spenningsriggen har også blitt brukt som fasit for spenningsberegninger, og har slik dannet et grunnlag for vurdering og kalibrering av 1) de valgte beregningsmetodene og 2) de tilhørende materialparametere bestemt fra den tidligere beskrevne forsøksserien.

List of publications

In addition to the work presented in the current thesis, the author has contributed to the following work:

Conference papers

Klausen, Anja Estensen; Terje Kanstad and Øyvind Bjøntegaard (2015): *Updated Temperature-Stress Testing Machine (TSTM): Introductory tests, calculations, verification and investigation of variable fly ash content.* Proceedings of CONCREEP 10, Vienna, Switzerland

Klausen, Anja Estensen; Kanstad, Terje; Bjøntegaard, Øyvind (2014): *Updated Temperature-Stress-Testing-Machine (TSTM): Introductory Tests, Calculations and Verification*. Proceedings of the XXII Nordic Concrete Research Symposium, Reykjavik, Iceland

Schlicke, Dirk; Nguyen, Viet Tue; Klausen, Anja Estensen; Kanstad, Terje; Bjøntegaard, Øyvind (2014): *Structural Analysis and Crack Assessment of Restrained Concrete Walls - 3D FEM Simulation and Crack Assessment.* The 1st Concrete Innovation Conference, Oslo Norway

Bjøntegaard, Øyvind; Klausen, Anja Estensen; Kanstad, Terje (2013): *On materials testing and crack risk evaluation of hardening concrete structures.* Workshop Proceedings "Understanding the Fundamental Properties of Concrete" Celebrating Professor Erik J. Sellevold on his 75th birthday, 25th-26th April 2013, Trondheim, Norway

Kanstad, Terje; Kjellmark, Gunrid; Klausen, Anja Birgitta Estensen; Bjøntegaard, Øyvind (2011): *Updated Temperature-Stress-Testing Machine (TSTM): Introductory test results and determination of material properties development.* Proceedings of XXI Nordic Concrete Research Symposium, Finland

Reports

Kjellmark, Gunrid and Anja Estensen Klausen (2015): *Mechanical properties and calculation of model parameters for concrete with Norcem cement and variable fly ash content.* COIN Project Report (55), ISBN: 978-82-536-1454-0, SINTEF Building and infrastructure, Trondheim, Norway

Kjellmark, Gunrid and Anja Estensen Klausen (2015): *Mechanical properties and calculation of model parameters for concrete with Aalborg cement and variable fly ash content.* COIN Project Report (56), ISBN: 978-82-536-1455-7, SINTEF Building and infrastructure, Trondheim, Norway

Klausen, Anja Estensen (2014): *Temperature development in on-site curing boxes.* COIN Project Report (54), ISBN 978-82-536-1429-8, SINTEF Building and infrastructure, Trondheim, Norway

Klausen, Anja Estensen (2013): *Temperature-Stress Testing Machine - User Manual.* Norwegian University of Science and Technology (NTNU), Trondheim, Norway

Scientific lectures

Klausen, Anja Estensen (2015): "*Ung betong: oppvekst like viktig for betong som for oss (in English: Early age concrete: Childhood - as important for concrete as for us)*" Norsk Betongdag og SINTEF-NTNU Betonginformasjonsdag 2015, Trondheim, Norway

Table of contents

Abbreviations, notations and Greek letters

Abbreviations

AD	Autogenous Deformation
cem	Cement
COIN	Concrete Innovation Centre (2007-2014)
CTE	Coefficient of Thermal Expansion
CV	Coefficient of Variation
DPL	Double Power Law
FA	Fly Ash
LVDT	Linear Variable Displacement Transducer
NTNU	Norwegian University of Science and Technology
PhD	the degree Philosophiae Doctor
RH	Relative humidity
SD	Standard Deviation
TD	Thermal Dilation
TSTM	Temperature-Stress Testing Machine

Notations

a	Cooling factor
A	Activation energy parameter
b	Binder
B	Activation energy parameter
c	Specific heat capacity
C_i	Crack index
d	Creep model parameter
E	E-modulus
E_{28}	28-day E-modulus
E_T	Activation energy
E_{TSTM}	E-modulus obtained from the TSTM
f_c	Compressive strength
f_t	Tensile strength
f_{ts}	Tensile splitting strength

h	Convection coefficient
$H(T)$	Rate of hydration
$J(t,t')$	Compliance function
k_{FA}	Efficiency factor fly ash
k_{silica}	Efficiency factor silica
M	Maturity time
n_t	Model parameter tensile strength
n_E	Model parameter E-modulus
p	Creep model parameter
Q	Heat development
R	Degree of restraint
s	Material model time-development parameter
t	Time
t'	Time at loading
t_0	Start time for stress development
t_{eq}	Equivalent time
T	Temperature
T_{julabo}	Temperature in the Julabo
T_{TSTM}	Temperature measured in the TSTM
T_{Dil}	Temperature measured in the Dilation Rig
T_{max}	Maximum temperature
ΔT	Temperature change
w	Water

Greek letters

α	Degree of hydration
ε	Strain
ε_{as}	Autogenous deformation (AD)
ε_T	Thermal strain (TD)
ρ	Density
σ	Stress
φ_0	creep coefficient

1 Introduction

1.1 Background and motivation

Concrete is a strong, universal and favourable construction material which has been used since the building of Rome 2000 years ago. Modern use of concrete can be defined as the introduction of reinforced concrete in the late 1880s and the onset of industrial production of cement. From then on, a rapid development followed, and concrete is today the most used building material in the world. Although concrete as a building material has got many benefits, more challenging areas also exist. One of them is the concrete's volume changes, especially in the hardening phase, which may lead to cracking and further to reduced functionality, durability and aesthetics. The volume changes of concrete and the associated cracking risk can however be predicted by use of calculation methods to assess the concrete's early age structural behaviour. On the basis of such calculations, proper choice of concrete type and execution methods on-site can be taken to minimize or avoid cracking. Hardening phase crack risk assessment of concrete structures is the main topic of the current PhD work.

Problems with high temperatures and thermal cracking in hardening concrete were first treated in the literature during the 1920s. At this time, a period of construction of large-scale massive concrete dams began in the USA, and it was for the first time documented that early cracking in concrete members was associated with temperature rise due to hydration. During the construction of the Hoover dam in 1931 – 1935, new knowledge and techniques with regards to early age cracking were established; the significance of the chosen cement due to heat generation and strength growth, as well as the use of embedded cooling pipes to reduce the temperature increase.

Originally, concrete curing technology was based on calculations of temperature- and strength developments. However, already in 1946 Löfquist measured the strain development and characterized the strain capacity in restrained concrete specimens subjected to realistic temperature histories [Löfquist, 1946]. Several years later, in the late 1960s, increased focus was given to the importance of the degree of restraint, and consequently the first attempts to estimate the magnitude of stresses due to restrained thermal deformations and compare them with the increasing tensile strength of the concrete at early ages were made [RILEM, 1998]. In addition, with the increased use of high strength concretes, it became clear that also autogenous deformation contributes significantly to early age stress generation.

Despite the well documented importance of both restraint and autogenous deformation when it comes to cracking in the hardening phase, many specifications in handbooks [NPRA, 2009] and design codes are still based on temperature gradients. This is simple, but clearly insufficient since temperature is only one of several interplaying factors. Modern curing technology, which is dealt with in the current thesis, takes into account the

most relevant properties, as well as the strain- and stress development in the structure; thus is much more accurate.

Since the RILEM Munchen conference [RILEM, 1994], the concrete group at NTNU has been strongly involved in the early age cracking field both on the materials, the experimental and the computational aspects. The work has taken place both within EU- and national projects involving industrial, institutional and university participants. Numerous publications and participations at international conferences and workshops have resulted, as well as the following PhD theses: [Bjøntegaard, 1999], [Bosnjak, 2000], [Takacs, 2002], [Atrushi, 2003] and [Ji, 2008].

The topic early age crack assessment still faces a series of challenges: despite the research conducted during the recent years, severe cracking due to restrained volume changes can be found in today's structures. To increase the applicability of early age crack assessment, changes in regulations (i.e. standards and guidelines) are necessary. For instance, Eurocode 2 does not include anything on this topic. Furthermore, to maintain a solid basis for crack assessment calculations, it is important to continuously improve and update the existing material data bases, in particular due to new binders. In addition, when it comes to early age crack assessment, some of the research results found in the literature are few or rarely consistent and thus need further elaboration; e.g. autogenous shrinkage versus swelling, temperature effect on autogenous shrinkage, tensile versus compressive creep, as well as the general applicability of the linear viscoelasticity for aging materials.

1.2 Objectives and scope

The overall aim of the current PhD work was to contribute to an increased basic knowledge and understanding of early age concrete material properties (behavior) and also to investigate calculation methods to assess the concrete's structural behavior under realistic temperature curing conditions. This was pursued by defining the following objectives:

- Finalize and verify the reconstruction of the TSTM System[1] to provide a more advanced management of the experiments and more extensive outcome from each test (e.g. optional degree of restraint and incremental E-modulus development)
- Provide knowledge about the effect of concrete composition and mineral additives, exemplified by fly ash content, on strain and stress development and cracking sensitivity in concrete structures
- Check the validity and improve existing material models necessary to assess the structural behaviour of early age concrete

[1] The Temperature-Stress Testing Machine (TSTM) System at NTNU

The objectives were to a large extent approached experimentally, providing an extensive experimental test program which has been performed during the current work. The main focus has been on strain and stress development and the effect of curing temperature, i.e. 20 ^{o}C isothermal versus realistic temperature conditions. The additional analytical approach had two purposes: both to improve and verify the models themselves, and also as an evaluation of the experiments. The hypothesis has been to assess and reduce the concretes' sensitivity to cracking by using mineral additives (in the current work exemplified by fly ash) with the means of laboratory experiments and analytical approaches.

The current project deals with strain and stress development in the concrete hardening phase. This behavior is magnified in massive concrete structures, and thus the project is limited to deal with such structures as for example walls on slabs, large culverts and dams.

Plastic shrinkage cracking in fresh concrete is a different though related area, which is not covered by the current PhD study. Likewise, the effect of drying shrinkage is not considered since concrete is covered by formwork for several days after casting, as well as the fact that drying shrinkage in massive concrete structures (after formwork removal) will only be a surface effect with minor impact on the overall hardening phase restraint stresses.

As stated in the title, the thesis focuses on early age crack assessment of concrete structures. Mechanical properties at later ages (e.g. 28 and 91 days) are however also determined and included in the results. A reason for this is that the models used to describe the mechanical properties development at early ages often are based on the 28-day property value which often is used to characterize the quality of the concrete. Recently, it has also been considered to establish such models based on the 91-day property value, since it within the Eurocode committees is considered to replace the 28-days values with the 91-days values as quality reference. The relation between the property development at early ages and the corresponding 28- and 91 day property value is thus of considerable interest. In addition, it has been seen that some massive concrete structures (e.g. dams) require a considerable amount of time (years) to lose their hydration-generated heat, correspondingly prolonging the "risk of cracking" phase and thus underlining the importance of mechanical property values also at later ages.

1.3 Outline of the thesis

The thesis is organized in 10 chapters. The first chapter is an introduction to the topic, defining the background and the given objectives and scope of work. Chapter 2 presents a brief literature review on early age stress development, while Chapter 3 gives a description of the theoretical approach used for the currently performed early age stress calculations.

In Chapter 4, a description of the mix design of the investigated concretes as well as the experimental test programme is given.

Chapter 5 describes the experimental equipment used during the current study: The Temperature-Stress Testing Machine (TSTM) System at NTNU which consists of a Dilation Rig and a Temperature-Stress Testing Machine (TSTM). The TSTM System was subjected to a reconstruction during the current work, and Chapter 6 describes the succeeding verification and documentation program.

An extensive mechanical test programme has been carried out with the aim to establish a basis for early age stress calculations. Chapter 7 gives a presentation of the test results and the corresponding established material parameters further used in the calculations. Results from the test program performed in the TSTM and the Dilation Rig are given in Chapter 8.

A brief summary of the influence of fly ash content on the various investigated properties is given in Chapter 9, while Chapter 10 presents the main conclusions and the future perspectives of the current topic.

2 Early age stress development, literature review

2.1 Introduction

Hardening phase volume changes in concrete, caused by the hydration reactions, are proven to be of considerable importance. If these movements are restrained by the geometry of the concrete structure or from casting joints against adjoining structural parts, stresses will generate in the newly cast concrete and may further lead to cracking. Volume changes caused by autogenous deformation and thermal dilation are the predominant driving forces to stress generation and cracking in concrete structures. The amount of stress generated by autogenous deformation and thermal dilation in a given time interval depends on the degree of restraint by the surrounding structures and the stiffness properties (E-modulus and creep/relaxation) of the concrete. The stress development in a concrete structure during the hardening phase is illustrated in a schematic diagram in Figure 2.1. [RILEM, 1998, 2000, 2001, 2002, 2003, 2006]

Research in the "early cracking" field has expanded strongly internationally since the early 90`ies with the RILEM Munchen conference as a starting point [RILEM, 1994]. This has resulted in several major conferences devoted directly to the topic, or as special sessions at larger meetings, e.g. [JCI, 1998], [RILEM, 1998, 2000, 2001, 2002, 2003, 2006] and [Concreep 10, 2015]. In addition, large numbers of papers have been published in regular journals.

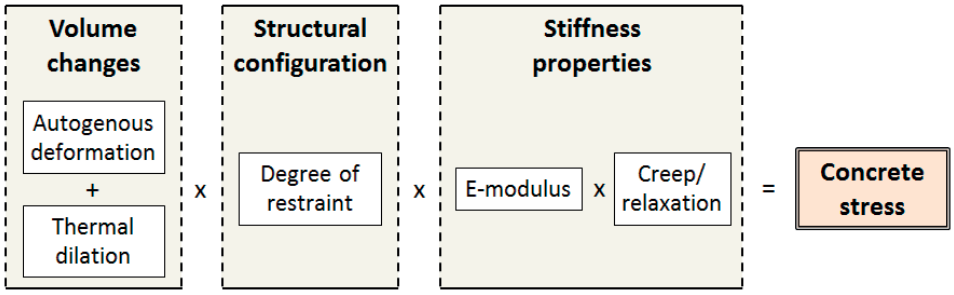

Figure 2.1; Stress development during the hardening phase, from [Bjøntegaard, 2011]

2.2 Volume changes in the hardening phase

2.2.1 Thermal dilation

The temperature induced volume change, Thermal Dilation (TD), is of major importance in stress analyses at early ages. Indeed, historically TD was considered in practice the only source before the use of higher strength concrete made autogenous deformation unavoidable as a significant contribution to stress generation (the 1994 Munchen conference had the title "Thermal Cracking in Concrete at Early Ages"). TD is caused by

temperature changes due to heat of hydration and environmental conditions. The relation between the temperature change ΔT and the thermal strain ε_T is given by the Coefficient of Thermal Expansion, CTE:

$$\varepsilon_T = CTE \cdot \Delta T \qquad \text{Equation 2.1}$$

Due to practical reasons, a constant value of CTE = $10.0 \cdot 10^{-6}$ /°C is normally used for calculation purposes. However, the CTE is actually found to be a complex parameter which varies with both concrete mix constituents and time (degree of self-desiccation), [Sellevold et al., 2006]. After casting, the CTE drops from an initial high value to a minimum value over the first 12-14 hours, and thereafter the CTE gradually increases with time, [Bjøntegaard, 1999], [Hedlund, 2000], [Bjøntegaard et al., 2001], [Bjøntegaard et al., 2004b], [Loser et al., 2010], [Maruyama et al., 2011] and [Wyrzykowski et al., 2013]. The initial rapid drop in CTE is also described by [Shoukry et al., 2011] and [Kim et al., 2011]. Additional CTE measurements over time are found in [Pane et al., 2008] and [Bjøntegaard et al., 2012]. [Emborg, 1989] differentiated between the coefficient of thermal expansion (heating phase, 8 - 24 hours) and contraction (cooling phase, 24 – 168 hours). The same method is described by [Hedlund, 1996] and [Westman, 1999], who both found that the coefficient of thermal expansion had a higher value than the corresponding contraction.

A model simulating the CTE development over the first 7 days is presented in [Wyrzykowski et al., 2013]. The model is based on the relative humidity (RH) dependence upon temperature ($\Delta RH/\Delta T$), acknowledging the previously described CTE dependence on moisture content (degree of self-desiccation) [Sellevold et al., 2006]. A CTE model based on the maturity principle was proposed by [Bjøntegaard et al., 2004a].

2.2.2 Autogenous deformation

Autogenous deformation (AD) is a consequence of chemical shrinkage: the absolute volume of hydration products is less than the total volume of the reactants (cement and water). A part of this inner volume loss also appears as an external shrinkage which is the AD [Lynam et al., 1934]. The main mechanism behind the AD is assumed to be self-desiccation due to reduction in the water saturation as water is consumed by the on-going cement hydration in the concrete, i.e. capillary forces (negative pore water pressure) [Radocea, 1992], [Justnes et al., 1996], [Jensen et al., 1996], [Bjøntegaard, 1999], [Lura, 2003] and [Bjøntegaard, 2011]. Volume changes caused by AD are found to be especially predominant in high performance concrete. This is related to the increased degree of self-desiccation caused by the low water/binder ratio and the addition of silica fume [Sellevold et al., 1982], [Sellevold et al., 1988], [Jensen et al., 1995], [Jensen et al., 1996], [Lura, 2003] and [Lee et al., 2003].

The AD development has been found to be strongly influenced by the concrete curing temperature [Houk et al., 1969], [Bjøntegaard, 1999], [Jensen et al., 1999], [Hedlund et al., 2001b], [Bjøntegaard et al., 2004b] and [Kim et al., 2011], and both [Bjøntegaard, 1999]

and [Jensen et al., 1999] concluded that the traditional maturity concept is not applicable to AD development. Various attempts to model the AD development have been found in the literature: e.g. [Hedlund, 2000] and [Hedlund et al., 2001b] (based on the maturity principle), and [Koenders, 1997], [Lura et al., 2003] and [Grondin et al., 2010] (based on capillary tension approach). [Kim et al., 2011] found a close correlation between the AD development and hydration temperature at an early age.

2.3 Degree of restraint

In a restrained concrete structure, the previously described volume changes will cause stress generation. Hardening concrete structures can be subjected to internal or external restraint. The restraint condition of a given section in a concrete structure depends on its location and the general configuration of the structure. For a wall cast on a stiff foundation/slab, the degree of restraint will vary over the structure and can be found by 2D or 3D linear elastic restraint analyses. With respect to risk of cracking, the critical section of a wall is the most unfortunate combination of high restraint and high curing temperature. For a wall cast on a stiff foundation/slab, the degree of restraint for the critical section (i.e. approximately one wall thickness away from the casting joint) will typically be $R = 0.37 – 0.70$ [Kanstad et al., 2001a].

Descriptions, calculations and discussions regarding the degree of restraint in early age concrete structures are found in e.g. [Emborg, 1989], [Larson, 2001], [Hedlund et al., 2001a], [Kanstad et al., 2001a], [Nilsson, 2003] and [Bjøntegaard, 2011].

2.4 Material models and relevant material properties

2.4.1 Degree of hydration and maturity

After casting, concrete gradually develops strength and stiffness as the reaction of cement and water takes place. It is well known that the concrete hydration rate increases with increasing temperature. Hence, the property development (i.e. the development of hydration products) of hardening concrete is dependent on time and temperature, and can be described and modelled based on the degree of hydration or by the maturity principle.

The degree of hydration, α, describes the development of hydration reactions of the cement and can be defined in several ways [Freiesleben Hansen, 1978], [Byfors, 1980] and [De Schutter et al., 1996]. Two common definitions are *"the ratio of amount of reacted cement to the original amount of cement"* and *"the ratio of chemically bound water to the quantity of chemically bound water at complete hydration"*. For engineering purposes, the quantity of heat developed has also been justified used as a measure of the degree of hydration. The degree of hydration is then defined as *"the ratio of quantity of heat developed to the quantity of heat developed at complete hydration"*. The choice of definition for the degree of hydration is usually related to the test methods available.

Also the maturity principle can be used for defining the property development of concrete (i.e. the state of hardening) at all times from mixing and through the hardening phase, see [Saul, 1951], [Rastrup, 1954], the pioneer for the model used today by [Freiesleben Hansen et al., 1977], [Chengju, 1989], [Pedersen, 1994] and [Bjøntegaard, 2011]. The maturity principle defines a relation between concrete curing temperature and strength development. [De Schutter, 2004] wrote that *"The maturity principle states that samples of a given concrete will acquire the same strength when equal maturities are reached, irrespective of their temperature histories"*. The equivalent age t_{eq} is highly related to and often also denoted maturity. The equivalent age is defined as the time that a concrete would have to be cured at a reference temperature (usually 20 ^{o}C) to achieve the same maturity as the concrete undergoing the actual curing history [Rastrup, 1954]. The Arrhenius function is the temperature function most commonly used with the maturity principle. The temperature function, also called the affinity ratio, describes the relation between the concrete hydration rate and the curing temperature.

[De Schutter, 2004] compared the degree of hydration concept with the maturity method and stated that both methods principally yield the same results and conclusion. He also found that both models can be recognized as valid tools for modelling the total thermo-viscoelastic behaviour of early age concrete. A brief discussion on the degree of hydration concept versus the maturity concept is also given in [Breugel, 2001].

2.4.2 Start time for stress development, t_0

The start time for stress development, t_0, is defined as the time at which the E-modulus reaches significant values so that the occurring volume changes can produce measurable stresses. Hence, at t_0, both strength and stiffness are defined to be zero, but beyond this they start to develop significant values. From this follows that the stress-inducing deformations are those occurring beyond t_0, and therefore the natural start of the thermal dilation and autogenous deformation is t_0, [Bjøntegaard et al., 1999], [Bjøntegaard et al., 2000] and [Kanstad et al., 2003b].

t_0 can be determined directly from E-modulus versus time data, from compressive strength tests, from semi-adiabatic calorimetry tests or from measured stress development in a Temperature-Stress Testing Machine, [Bjøntegaard et al., 1999] and [Kanstad et al., 2003a, b]. [Lura et al., 2009] showed how acoustic emission can be used to indicate the time when the fluid–solid transition occurs in a cement paste (i.e. time-zero), while [Carette, 2015] described a newly developed methodology for ultrasonic determination of setting time which was found to correlate well with the corresponding setting time deduced from standardized ASTM test methods.

2.4.3 Heat development

The hydration of concrete is an exothermic process, and a considerable amount of heat can be generated during the hardening phase. The rate of heat generation is dependent on both the degree of hydration and the actual temperature. The concrete heat development is often measured by adiabatic or semi-adiabatic calorimetry tests [Freiesleben Hansen, 1978], [Morabito, 1998].

Several models simulating the concrete heat development can be found in the literature. The generally used model in Norway is maturity-based and was proposed by [Freiesleben Hansen et al., 1977]. It should be noticed that the used Arrhenius equation is purely empirical, and that it should not be interpreted as a model of the hydration processes [Freiesleben Hansen et al., 1982]. Another model, developed and commonly used in Sweden, is described in e.g. [Byfors, 1980], [Emborg, 1989], [Jonasson, 1994], [JEJMS Concrete AB, 2009-2012] and [Jonasson et al., 2010]. A heat development model valid for Portland cement and blast furnace slag cement was developed by [De Schutter et al., 1995]. In this model, the heat production rate is calculated as a function of the actual temperature and the degree of hydration, where both influences are described separately by different functions.

2.4.4 Compressive strength, tensile strength and E-modulus

As previously described, concrete gradually develops strength and stiffness during the hardening phase as the hydration products form. The cement hydration, and hence the material properties development, is dependent on time and temperature.

Although the *compressive strength* of concrete is a fundamental and much studied concrete property, it is not decisive for early age cracking. Compressive strength is however relatively easy to determine, and is therefore often used in correlation with other properties which are decisive for early age stress development (tensile strength and E-modulus). At an engineering level (macroscale level), there are at least five different concepts which can be used to describe the development of compressive strength during the hydration process: the porosity concept, the gel-space ratio concept, the degree of hydration concept, the maturity principle and chemistry-oriented strength laws [Breugel, 2001].

The *tensile strength* of concrete is a vital parameter when it comes to early age cracking. Tensile strength can be determined directly by uniaxial tensile strength tests, or indirectly by splitting tensile strength tests or bending tests. The indirect tensile splitting test is considered favourable from a laboratory perspective due to the difficulties experienced with direct tensile methods, e.g. [Kanstad et al., 2001b]. However, the direct uniaxial tensile strength is the desired input parameter for stress calculations.

The concrete *E-modulus* is also an important parameter for early age stress calculations. The E-modulus can be determined both by compressive tests and tensile tests. Usually, the tensile and compressive E-modulus are assumed to be the same both for early age and

mature concrete [Kanstad et al., 2003a]. However, this relation seems to be somewhat unclear as some studies state that the tensile E-modulus tends to be higher than the compressive E-modulus, e.g. [Brooks et al., 1977], [Onken et al., 1995] and [Yoshitake et al., 2013].

An extensive number of test results on compressive strength, tensile strength and E-modulus are reported in the literature, e.g. [Brooks et al., 1977], [Byfors, 1980], [Shkoukani et al., 1991], [Westman, 1995], [De Schutter et al., 1996], [Khan et al., 1996], [Bjøntegaard et al., 2003], [Kanstad et al., 2003a], [Bjøntegaard, 2004], [Pane et al., 2008], [Ji, 2008], [Bjøntegaard et al., 2012] and [Kjellmark et al., 2015]. Similarly, also a wide number of models describing the materials property development can be found, a selection of which are summarized in e.g. [Byfors, 1980], [Emborg, 1998], [Hedlund, 2000], [Kanstad et al., 2003b] and [Bjøntegaard et al., 1999]. A "degree of hydration"-based description of the material properties was presented by [De Schutter et al., 1996]. Alternatively, the mechanical properties development has also been described by the maturity-based heat development model proposed by [Freiesleben Hansen et al., 1977].

The developments of compressive strength, tensile strength and E-modulus are not found to be linear correlated, see the relative development presented in Figure 2.2. Several studies have reported that the tensile strength tends to grow relatively faster than the compressive strength, e.g. [Byfors, 1980], [Yoshitake et al., 2013], [Khan et al., 1996], [Kanstad et al., 2001b] and [Kjellmark et al., 2015]. Similarly, also the E-modulus have been found to increase at a higher rate than the compressive and tensile strength [Byfors, 1980], [De Schutter et al., 1996], [Kanstad et al., 2001b] and [Kjellmark et al., 2015]. This is unfortunate with respect to early age cracking as the stress development in early age concrete is dependent on the E-modulus, while the risk of cracking is directly dependent on the tensile strength.

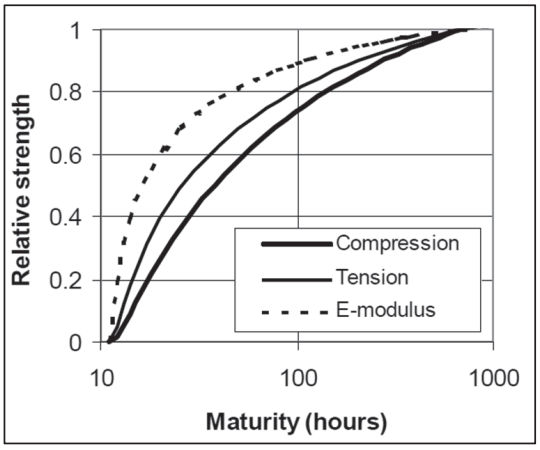

Figure 2.2; Relative development of compressive strength, tensile strength and E-modulus [Kanstad et al., 2001b]

2.5 Creep and relaxation

The time-dependent stress response of concrete is a complex and much studied phenomenon which is usually described by creep or relaxation. Creep is the time-dependent deformation of concrete subjected to a constant load, while relaxation is the reduction in stress over time for concrete subjected to a constant deformation, see Figure 2.3. Creep and relaxation are closely connected physically, and in concrete structures they often occur in combination with each other. In engineering practice, the term creep is often used to denote both creep and relaxation of stresses [Neville, 1970]. Creep is closely connected to the E-modulus, and creep should thus be considered in combination with the E-modulus development when evaluated.

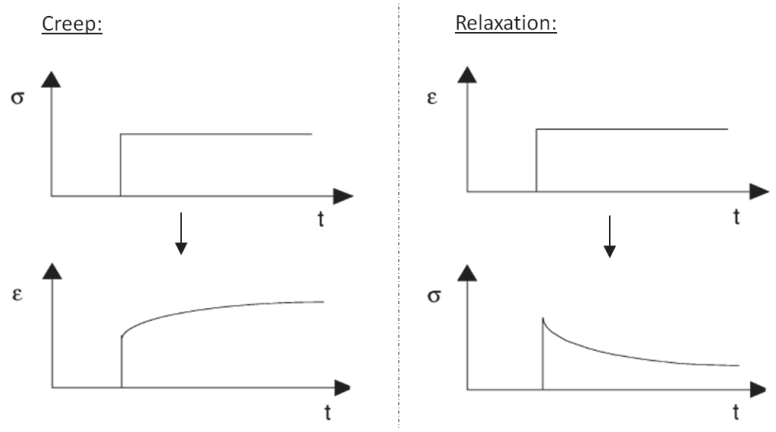

Figure 2.3; Creep (left) and relaxation (right), from [Bosnjak, 2000]

When a sustained stress is removed, the concrete undergoes an instantaneous recovery. The instantaneous recovery is followed by a time-dependent recovery, also denoted creep recovery, Figure 2.4. The creep recovery is found to be smaller than the proceeding creep regardless of the ages at loading and unloading [Neville, 1970]. In addition, the E-modulus at the initial stress application is lower than the E-modulus at the succeeding stress removal. Consequently, concrete subjected to a sustained stress which is subsequently unloaded exhibits both instantaneous and time-dependent strains, in addition to an irrecoverable strain also denoted residual strain, Figure 2.4.

Creep of concrete is a complex property which has been found to be dependent on a number of factors, e.g. load level, type of stress (compressive versus tensile), temperature, loading age, w/b ratio, size of specimen and concrete mix constituents [Neville, 1970]. Numerous studies on creep and its influences are found in the literature, the research results are however rarely consistent. For instance, while several studies conclude that (long time) tensile creep is larger than compressive creep, e.g. [Illston, 1965], [Brooks et

al., 1977], [Atrushi, 2003] and [Ji et al., 2012], other studies presents contradictorily results, e.g. [Hagihara et al., 2000] and [Gutsch, 2001].

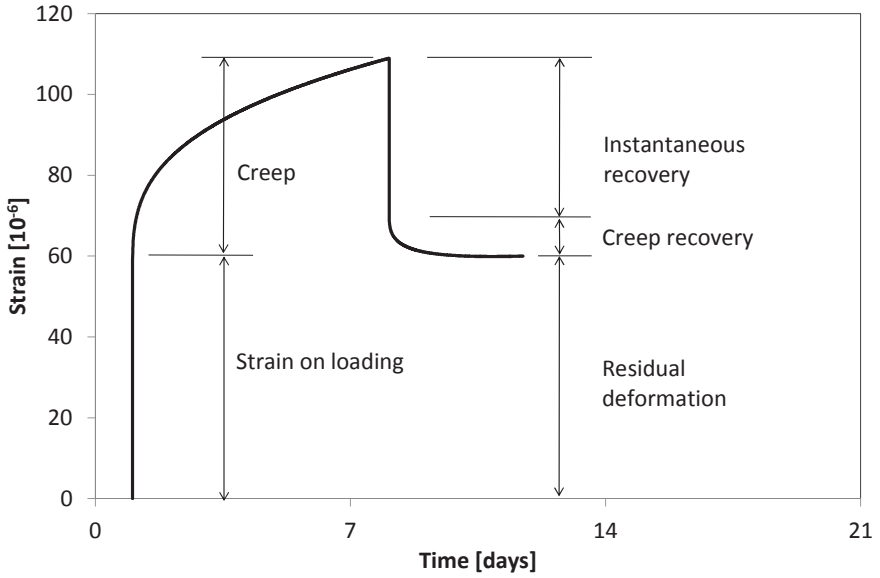

Figure 2.4; Instantaneous and creep recoveries, from [Neville, 1970]

Several mathematical models simulating creep and relaxation have been proposed over the years. Descriptions of the mechanisms of creep in concrete, in addition to creep test results and calculation methods, are given in e.g. [Illston, 1965], [Byfors, 1980], [Kanstad, 1990], [RILEM, 1994], [Bazant et al., 1995], [Westman, 1995], [RILEM, 1998], [Bosnjak, 2000], [Bazant, 2001], [Jonasson et al., 2001], [Takacs, 2002], [Atrushi, 2003], [Ji, 2008] and [Concreep 10, 2015].

2.6 Crack index

The risk of concrete cracking in a given case can be described by a crack index, C_i. The crack index is a time-dependent ratio between the concrete's self-induced tensile stress and its tensile strength. A calculated crack index of 1.0 or higher indicates that the actual tensile stress exceeds the tensile strength, and hence cracking will occur. In calculations, the allowed crack index is often limited to 0.7 as safety, which comprises an incorporation of statistical spread of the concrete properties, as well as uncertainties on-site (climate, etc.) and in the calculations.

In some countries, a safety factor (the inverse of the crack index) is used instead of a crack index, e.g. [Koenders, 1997] and [Nilsson, 2003].

3 Early age stress development, theoretical approach

3.1 Introduction

Early age stress calculations have been performed with the aim to back-calculate stress developments measured in the recently updated Temperature-Stress Testing Machine (TSTM). The following sections give a description of the theoretical approach used as basis for these calculations. As described in the previous chapter, early age concrete is subjected to volume changes, Section 3.2. If these volume changes are restrained, Section 3.3, stresses will start developing in the concrete structure. The amount of stress generated in a given time interval is also dependent on the E-modulus and the time-dependent stress response of the concrete, Section 3.4 and Section 3.5. Further is the concrete's probability of cracking evaluated by its crack index as described in Section 3.6, while Section 3.7 presents the three different calculation programs used for the TSTM stress calculations: TSTM-sim (Excel), CrackTeSt COIN and DIANA.

A comparison of stress developments calculated by the different calculation programs, together with the corresponding measured stress histories, is given in Chapter 8.3.

3.2 Volume changes in the hardening phase

In the currently performed TSTM stress calculations, free deformation measured in parallel Dilation Rig tests were used as input describing the early age volume changes, i.e. the thermal dilation (TD) and the autogenous deformation (AD), of the given concrete.

As described in Chapter 2, the Coefficient of Thermal Expansion (CTE) is a complex parameter which varies both with time and moisture content. However, in the current study the often used simplification of a constant CTE over time has been applied. For the majority of the performed test, the CTE was determined by temperature loops at the end of the tests, see Chapter 7.8. Based on these results, one constant CTE was determined for each concrete. The constant CTE approximation has had no impact on the stress calculations, as they were based on the total measured free deformation (TD + AD). A constant CTE will however introduce an inaccuracy to the deduced AD. Figure 3.1 illustrates the effect on obtained AD when using a constant CTE as opposed to a CTE which varies with time, CTE(t). The CTE development over time was estimated by the maturity-based model proposed by [Bjøntegaard et al., 2004a]. The model was applied an assumed minimum CTE value of $7.5 \cdot 10^{-6}$ /°C at the start time for stress development t_0 and a long-term value deduced from the given test. Figure 3.1 shows that the simplification of a constant CTE causes an early parallel displacement of the AD curve (increased contraction). The deviation occurs in a phase where the deduced AD curves have been found to show certain anomalies, and these should therefore not be emphasized. As already stated, the currently performed stress calculations are based on the total measured deformation and are thus not affected by the choice of CTE. In addition, if using the

deduced AD in combination with another temperature history, the simplification of a constant CTE would only have a limited influence on the stress development, as the early parallel displacement of AD occurs in a phase where the E-modulus is still rather low. The main point is therefore that the currently used constant CTE will cause a small overestimation (in form of an early parallel displacement) of the real AD development.

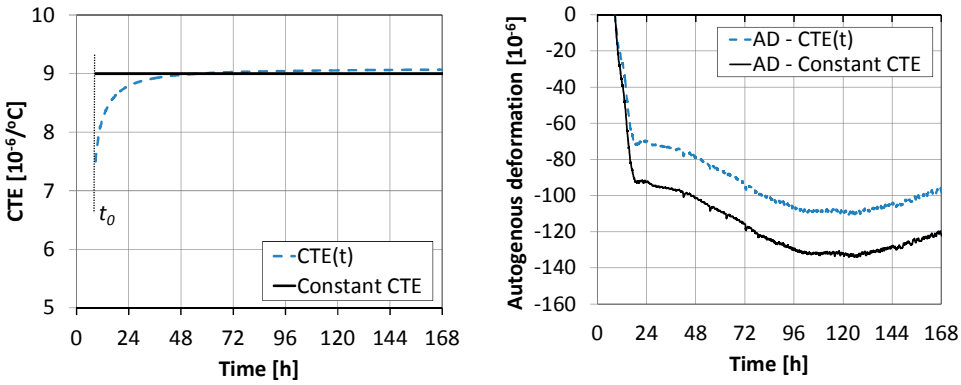

Figure 3.1; CTE as a function of time CTE(t) versus a constant CTE (left), and corresponding deduced autogenous deformation (right)

3.3 Degree of restraint

The early age stress calculations were established to perform "back-calculations" of the stress development measured in the updated TSTM. Consequently, the degree of restraint applied to the stress calculations were the same as applied to the TSTM during testing, i.e. 100 % for isothermal tests and 50 % for realistic temperature tests (i.e. defined as the ratio between restrained and total deformation in the TSTM tests times 100 %).

3.4 Material models and relevant materials properties

3.4.1 Maturity

In the current work, the maturity principle has been used to describe the effect of curing temperature on the concrete's heat and property development. The reference temperature is set to be 20 ^{o}C, and the Arrhenius equation has been used as temperature function [Freiesleben Hansen et al., 1977] and [Freiesleben Hansen et al., 1982]. According to the Arrhenius principle, the rate of hydration *H(T)* can be expressed as shown in Equation 3.1.

$$H(T_i) = exp\left(\frac{E_T(T_i)}{R} \cdot \left(\frac{1}{293} - \frac{1}{273 + T_i}\right)\right) \qquad \text{Equation 3.1}$$

where H is the hydration rate function, R is the gas constant, T is the temperature and E_T is the activation energy: $E_T = A + B(20\text{-}T_i)$, where $B = 0$ for $T > 20^oC$ and B has a given value for $T < 20\ ^oC$, and A has a fixed value for all temperatures.

The increase in maturity within a time increment is then $H(T_i) \cdot \Delta t_i$. The equivalent time (which in the current work has been denoted maturity time M) at a certain concrete age (after n intervals) is then the sum of all maturity growth increments as shown in Equation 3.2:

$$M = t_{eq} = \sum_{i=1}^{n} H(T_i) \cdot \Delta t_i \qquad \text{Equation 3.2}$$

where M is the maturity time, t_{eq} is equivalent time, H is the hydration rate function and T is the temperature

3.4.2 Start time for stress calculations t_0

For each concrete, the start time for stress calculations t_0 has been found by: 1) compressive strength tests over time, 2) semi-adiabatic calorimetry tests and 3) measured stress development in the TSTM. The results are compared and discussed in Chapter 7.5, and for the stress calculations it was concluded to use t_0 found directly from TSTM stress measurements, which is assumed to be the most reliable approach.

3.4.3 Heat development

The concretes' hydration heat evolvements were determined by semi-adiabatic calorimeter tests, see Chapter 4.3.2. For each test, the measured temperature development was converted to isothermal heat development and adiabatic temperature development by an Excel-run calculation routine [Smeplass, 1988, 2001] which is briefly described in the following: the applied log intervals Δt_i (e.g. 15 minutes) are converted into corresponding maturity time by the Freiesleben Hansen model given in Equation 3.2. Further, for each Δt_i, the following calculations are performed:

- The concretes' heat development ΔQ_{si} is calculated from Equation 3.3
- The heat loss to the surroundings ΔQ_{ti} is calculated by Equation 3.4.

The heat development is calculated from the temperature change in the concrete, while the heat loss calculation is based on the assumption that the heat flow out of the given curing box is proportional to the temperature difference between the concrete and the surroundings. This proportionality coefficient is called the "cooling factor", a, and it is specific for each tests and its corresponding test conditions. a is calculated by demanding a

small given heat development value over a defined time interval for high maturity ages, where the hydration (and the corresponding heat development) is close to zero. For instance, a common criteria for ANL cement has been dQ/dm = 0.1 kJ/kg·h for the time interval 150 – 200 maturity hours. The isothermal heat development is found by adding up the heat development ΔQ_{si} and the heat loss ΔQ_{ti} over each time interval, Equation 3.5, and plotting it as a function of maturity.

$$\Delta Q_{si} = \Delta T_{ci} \cdot c \cdot \rho \qquad \text{Equation 3.3}$$

where ΔQ_{si} is the heat growth in the time interval Δt_i, ΔT_{ci} is the corresponding concrete temperature change, c is the specific heat capacity and ρ is the density

$$\Delta Q_{ti} = (T_{ci} - T_{ai}) \cdot c \cdot \rho \cdot \Delta t_i \cdot a \qquad \text{Equation 3.4}$$

where ΔQ_{ti} is the heat loss in the time interval Δt_i, $(T_{ci} - T_{ai})$ is the temperature difference between the concrete and the surroundings in the time interval Δt_i, c is the specific heat capacity, ρ is the density and a is the cooling factor

$$Q_n = \sum_{i=1}^{n} (\Delta Q_{si} + \Delta Q_{ti}) \qquad \text{Equation 3.5}$$

where Q_n is the heat development obtained at time interval n, ΔQ_{si} is the heat growth in the time interval Δt_i and ΔQ_{ti} is the heat loss in the time interval Δt_i

The adiabatic temperature development at a given time of maturity is found by converting the total accumulated heat development into a temperature increase, Equation 3.6. The appurtenant adiabatic time (i.e. the time needed to achieve the corresponding maturity under adiabatic temperature conditions) is found by adjusting Δt_i by the ratio between the semi-adiabatic hydration rate and the corresponding adiabatic hydration rate, Equation 3.7.

$$T_{An} = \sum_{i=1}^{n} \frac{\Delta Q_i}{c \cdot \rho} \qquad \text{Equation 3.6}$$

where T_{An} is the adiabatic temperature at time interval n, ΔQ_i is the total accumulated heat development obtained at time interval Δt_i, c is the specific heat capacity and ρ is the density

$$t_{An} = \sum_{i=1}^{n} \Delta t_i \cdot \frac{H(T_{ci})}{H(T_{Ai})} \qquad \text{Equation 3.7}$$

where t_{An} is adiabatic time corresponding to T_{An} at the time interval n, $H(T_{ci})$ is the hydration rate for the actual measured temperature at the time interval Δt_i, and $H(T_{ci})$ is the hydration rate for the corresponding adiabatic temperature development

Finally, the calculation routine establishes a heat development model by fitting the Freiesleben Hansen model, Equation 3.8 [Freiesleben Hansen, 1978] and [Pedersen, 1994], to the obtained heat development results.

$$Q(t_e) = Q_\infty \cdot exp\left(-\left(\frac{\tau}{t_e}\right)^\alpha\right) \qquad \text{Equation 3.8}$$

where $Q(t_e)$ is the heat generation as a function of maturity time t_e, Q_∞ is the final heat after "infinite" time as well as a curve fitting parameter, together with τ and α

For the currently performed early age stress calculations, the heat- and temperature development in the concrete has been applied as an externally imposed temperature history. The applied temperature histories were the actual temperature history measured during the corresponding TSTM tests. These realistic TSTM temperature histories were calculated in CrackTeSt COIN prior to testing, and they were based on discrete heat development values as a function of maturity (i.e. the semi-adiabatic calorimetry test results prior to the previously described model-fitting), see Chapter 7.3.

In CrackTeSt COIN, the concrete heat development can either be described by discrete values or as given by Equation 3.9 [JEJMS Concrete AB, 2009-2012] and [Jonasson et al., 2010].

$$W = C \cdot W_c \cdot exp\left(-\lambda_1 \cdot \left[ln\left(1 + \frac{t_e}{t_1}\right)^{-\kappa_1}\right]\right) \qquad \text{Equation 3.9}$$

where W is the heat generation as a function of maturity time t_e, C is the cement content, W_c is the final heat after "infinite" time, and λ_1, κ_1 and t_1 are curve fitting parameters

3.4.4 Compressive strength, tensile strength and E-modulus

For the TSTM stress calculations in Excel, the compressive strength, tensile strength and E-modulus were modelled by Equation 3.10, which is a modified version of CEB-FIP MC 1990 [CEB-FIP, 1991], see [Kanstad et al., 2003b] and [Bjøntegaard, 2011]:

$$X(t_e) = X(28) \cdot \left\{exp\left[s \cdot \left(1 - \sqrt{\frac{672 - {t_0}^*}{t_e - t_0}}\right)\right]\right\}^n \qquad \text{Equation 3.10}$$

where $X(t_e)$ is the mechanical property as a function of maturity t_e, $X(28)$ is the property at 28 days, s and n are curve-fitting parameters, and $t_0 = {t_0}^*$ is the start time for stress development [maturity time], the parameter t_0 was introduced by [Kanstad et al., 2003b], while ${t_0}^*$ was later introduced in the program CrackTeSt COIN [Jonasson et al., 2010] and [JEJMS Concrete AB, 2009-2012].

Consequently, the equations describing the compressive strength, tensile strength and E-modulus in the Excel calculations are as presented in Equation 3.11, Equation 3.12 and Equation 3.13, respectively. The s-parameter is the same for all properties, while the n-parameter is varying. The 28-days properties as well as the curve-fitting parameters were determined by parallel mechanical testing, see Chapter 7.4.

$$f_c(t_e) = f_{c28} \cdot \left\{ exp\left[s \cdot \left(1 - \sqrt{\frac{672 - t_0}{t_e - t_0}} \right) \right] \right\}^{n_c}$$ where $n_c = 1$ Equation 3.11

$$f_t(t_e) = f_{t28} \cdot \left\{ exp\left[s \cdot \left(1 - \sqrt{\frac{672 - t_0}{t_e - t_0}} \right) \right] \right\}^{n_t}$$ Equation 3.12

$$E_c(t_e) = E_{c28} \cdot \left\{ exp\left[s \cdot \left(1 - \sqrt{\frac{672 - t_0}{t_e - t_0}} \right) \right] \right\}^{n_E}$$ Equation 3.13

In DIANA, the strength and stiffness properties were applied the analyses in form of discrete values as a function of maturity obtained from the models as presented above. In CrackTeSt COIN, however, a somewhat different model has been used to describe the compressive and tensile strength development, see [Jonasson et al., 2010] and [JEJMS Concrete AB, 2009-2012]. The CrackTeSt COIN curve-fitting parameters were determined by fitting the CrackTeSt COIN models to the property development described by Equation 3.11 and Equation 3.12.

3.5 Creep

The concrete's time-dependent stress response has been modelled based on the theory of linear viscoelasticity for ageing materials. This theory implies that the creep strains under a constant stress are linearly related to the stress level, Equation 3.14.

$$\varepsilon(t) = J(t, t') \cdot \sigma$$ Equation 3.14

where t is the concrete age, t' is the concrete age at which the actual stress σ was applied, $\varepsilon(t)$ is the creep strain, and $J(t,t')$ is the compliance function.

The principle of superposition applied ageing of concrete can be interpreted as *"…the strains produced at any time t by a stress increment applied at age t' < t are independent of the effects of any stress applied earlier or later"* [Neville, 1970]. Thus, by combining the theory of linear viscoelasticity with the principle of superposition, the total strain for a variable stress history can be expressed by Equation 3.15. This means that the stress at a certain position and point in time depends on the entire stress history. Correspondingly, the total stress for a variable strain history can be expressed by Equation 3.16.

$$\varepsilon(t) = \int_0^t J(t,t') \cdot d\sigma(t') + \varepsilon_{as}(t) + \varepsilon_T(t) \qquad \text{Equation 3.15}$$

where $J(t,t')$ is the compliance function of time t for a stress induced at time t', $\varepsilon_{as}(t)$ is autogenous deformation and $\varepsilon_T(t)$ is thermal dilation

$$\sigma(t) = \int_0^t R(t,t') \cdot [d\varepsilon(t') - d\varepsilon^0(t')] \qquad \text{Equation 3.16}$$

where $R(t,t')$ is the relaxation function of time t for a strain induced at time t', $d\varepsilon(t')$ is the strain increment and $d\varepsilon^0(t')$ is the stress-independent strain increment at time t'

The Excel calculations were based on superposition of creep curves (Equation 3.15), where the compliance function $J(t,t')$ was described by the Double Power Law, Equation 3.17 [Bazant et al., 1976]. The Excel calculation routine is presented in Section 3.7.2, and the applied creep parameters were determined from parallel creep tests, see Chapter 7.7.

$$J(t,t') = \frac{1}{E_c(t'_{eq})}\left[1 + \varphi_0 \cdot {t'_{eq}}^{-d} \cdot (t-t')^p\right] \qquad \text{Equation 3.17}$$

where t is the concrete age, t' is the concrete age at which the actual stress was applied, t_{eq}' is the maturity at t', $E_c(t_{eq}')$ is the E-modulus at t_{eq}', and φ_0, d and p are creep model parameters

In CrackTeSt COIN, the time-dependent stress response of concrete is described by a Maxwell Chain model, i.e. the calculations are based on relaxation curves (Equation 3.16). Because of this, the above described creep parameters were converted to relaxation data by the program RELAX [Jonasson et al., 2001] prior to the TSTM simulations in CrackTeSt COIN.

The creep/relaxation behaviour of concrete can be modelled by several different approaches in DIANA. For the currently performed TSTM stress calculations, two different approaches were used: 1) The Double Power Law model and 2) Direct input of the Maxwell Chain model. For the latter approach, the relevant creep parameters were converted to relaxation data by the program RELAX [Jonasson et al., 2001].

3.6 Crack index

The calculated stress development obtained for the various concretes have been compared and the various concretes evaluated by their crack index, C_i. For this purpose, the crack index is defined as the time-dependent ratio of the concrete's self-induced tensile stress to its average tensile strength as expressed by Equation 3.18.

$$C_i(t) = \frac{\sigma(t)}{f_t(t)} \qquad \text{Equation 3.18}$$

where C_i is the crack index, σ is the occurring tensile stress and f_t is the tensile strength

3.7 Restrained stress development in the TSTM – calculation approaches

3.7.1 General

Three different calculation approaches have been used to simulate the uniaxial stress development in the TSTM:

- TSTM-sim: a specially designed 1D calculation program run in Excel
- The special-purpose program CrackTeSt COIN
- The multi-purpose FE program DIANA

The current section gives a presentation of the above listed calculation approaches. A comparison of the calculated stress developments with corresponding measured stress histories is given in Chapter 8.3.

3.7.2 TSTM-sim (Excel)

3.7.2.1 Introduction

A calculation routine denoted TSTM-sim, simulating the uniaxial stress development in the TSTM at a given degree of restraint, was programmed in Excel and Visual Basic [Microsoft Office, 2010]. This section gives a description of the established calculation routine and algorithm.

3.7.2.2 Simulation steps

Figure 3.2 gives a schematic description of the different steps in the calculation routine. The simulation steps are described in the following:

STEP 1: The first step in the calculation routine is to collect, organize and insert the required input data into the designated cells in the Excel workbook. The necessary input data comprises: 1) Material parameters describing the given concrete, 2) Free deformation and temperature measured in the parallel Dilation Rig test and 3) Temperature measured in the TSTM.

STEP 2: After the required input data is inserted, the maturity, E-modulus and tensile strength development over time is calculated.

STEP 3: The third step in the calculation routine is to define the time intervals to be used in the stress and strain calculations. The Dilation Rig test results contain recorded data for a considerable amount of points in time. For the current stress and creep calculations, it is

necessary to reduce the amount of points in time, i.e. to define longer time intervals. Therefore, a Visual Basic macro which copies recorded data rows with a certain interval into a new worksheet was established. The interval size can be defined by the user; for instance each 30th minute up until 100 hours and each 60th minute beyond 100 hours.

STEP 4: The fourth step in the routine is to calculate the creep- and stress development for each time interval defined in step 3. The calculations are implemented in a Visual Basic macro as described in the next section.

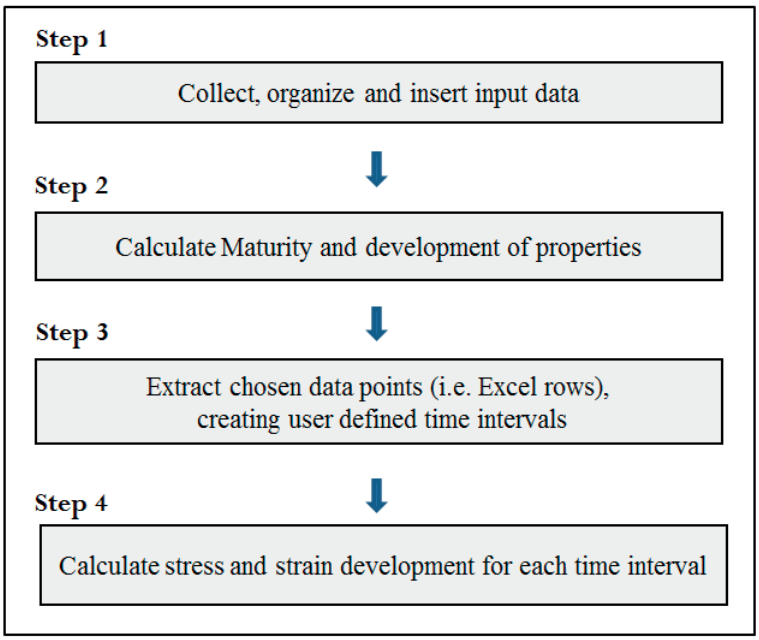

Figure 3.2; TSTM-sim: restrained stress calculations in Excel – simulation method, schematic diagram

3.7.2.3 Calculation algorithm

As described in Section 3.5, the total strain for a variable stress history can be determined with the principle of superposition as shown on discrete form in Equation 3.19. The sum of autogenous deformation $\varepsilon_{as}(t)$ and thermal dilation $\varepsilon_T(t)$ in the equation equals the free deformation measured in the Dilation Rig.

$$\varepsilon(t) = \sum_{0}^{t} J(t,t') \cdot \Delta\sigma(t') + \varepsilon_{as}(t) + \varepsilon_T(t) \qquad \text{Equation 3.19}$$

where $J(t,t')$ is the compliance function of time t for a stress increment $\Delta\sigma(t')$ induced at time t', $\varepsilon_{as}(t)$ is autogenous deformation and $\varepsilon_T(t)$ is thermal dilation

For the given calculations, the compliance function *J(t,t')* has been described by the Double Power Law, Equation 3.20.

$$J(t,t') = \frac{1}{E_c(t'_{eq})}\left[1 + \varphi_0 \cdot {t'_{eq}}^{-d} \cdot (t-t')^p\right] \qquad \text{Equation 3.20}$$

where t is the concrete age, t' is the concrete age at which the actual stress was applied, t_{eq}' is the maturity at t', $E_c(t_{eq}')$ is the E-modulus at t_{eq}', and φ_0, d and p are creep model parameters

A strain increment $\Delta\varepsilon_r$ generated in the time interval between t_{r-1} and t_r is derived in the following. Total strain at time t_{r-1} is given by Equation 3.21, while the total strain at the succeeding time t_r is given by Equation 3.22.

$$\varepsilon(t_{r-1}) = \sum_{q=1}^{r-1} J\left(t_{r-1}, t_{q-1/2}\right) \cdot \Delta\sigma_q + \varepsilon_{as}(t_{r-1}) + \varepsilon_T(t_{r-1}) \qquad \text{Equation 3.21}$$

$$\varepsilon(t_r) = \sum_{q=1}^{r} J\left(t_r, t_{q-1/2}\right) \cdot \Delta\sigma_q + \varepsilon_{as}(t_r) + \varepsilon_T(t_r) \qquad \text{Equation 3.22}$$

where $t_{q-1/2}$ is the time in the middle of the stress increment on a linear scale

Consequently, the strain increment $\Delta\varepsilon_r$ generated in the given time interval is given by Equation 3.23 - Equation 3.24.

$$\Delta\varepsilon_r = \varepsilon(t_r) - \varepsilon(t_{r-1}) \qquad \text{Equation 3.23}$$

$$\Delta\varepsilon_r = J\left(t_r, t_{r-1/2}\right) \cdot \Delta\sigma_r + \sum_{q=1}^{r-1} \Delta J\left(t_r, t_{q-1/2}\right) \cdot \Delta\sigma_q + \Delta\varepsilon_{rFREE} \qquad \text{Equation 3.24}$$

where $\Delta J\left(t_r, t_{q-1/2}\right) = J\left(t_r, t_{q-1/2}\right) - J\left(t_{r-1}, t_{q-1/2}\right)$ and $\Delta\varepsilon_{rFREE}$ is the free deformation (i.e. sum of ε_{as} and ε_T) in the given time interval

Equation 3.24 can also be written as shown in Equation 3.25 and Equation 3.26.

$$\Delta\varepsilon_r = \Delta\sigma_r / E'' + \Delta\varepsilon'' \qquad \text{Equation 3.25}$$

$$\text{i.e.} \quad \Delta\sigma_r = E''(\Delta\varepsilon_r - \Delta\varepsilon'') \qquad \text{Equation 3.26}$$

where

$$E'' = \frac{1}{J(t_r, t_{q-1/2})} \qquad \text{Equation 3.27}$$

$$\Delta\varepsilon'' = \sum_{q=1}^{r-1} \Delta J\left(t_r, t_{q-1/2}\right) \cdot \Delta\sigma_q + \Delta\varepsilon_{rFREE} \qquad \text{Equation 3.28}$$

During a test in the TSTM, the total strain increment generated over a time interval, i.e. $\Delta\varepsilon_r$ in Equation 3.26, is given by the actual degree of restraint. For example, if the degree of restraint is 100 % (fully restrained), the TSTM is not allowed to move, hence $\Delta\varepsilon_r = 0$. For a degree of restraint between 0 and 100 % (i.e. 0 – 1.0), the total strain increment $\Delta\varepsilon_r$ is as shown in Equation 3.29.

$$\Delta\varepsilon_r = -R \cdot \Delta\varepsilon'' + \Delta\varepsilon'' = (1 - R) \cdot \Delta\varepsilon'' \qquad \text{Equation 3.29}$$

From Equation 3.26 and Equation 3.29, it follows that the stress induced over a given time interval is as presented in Equation 3.30.

$$\Delta\sigma_r = -R \cdot E'' \cdot \Delta\varepsilon'' \qquad \text{Equation 3.30}$$

The procedure of the final calculation algorithm is first to find *E"* (Equation 3.27), then $\Delta\varepsilon''$ (Equation 3.28) and eventually $\Delta\sigma_r$ (Equation 3.30) for each defined time interval. Thereafter, $\sigma(t)$, $\varepsilon_{creep}(t)$ and $\varepsilon(t)$ are determined. Equation 3.28 is a comprehensive equation which requires numerous summations and calculation steps, and it is therefore found practical to perform the current calculation in Visual Basic. The Visual basic macro calculates the development of creep strain $\varepsilon_{creep}(t)$ and total strain $\varepsilon(t)$ by Equation 3.31 and Equation 3.32, respectively.

$$\varepsilon_{creep}(t) = \sum_{q=1}^{r} J(t, t') \cdot \Delta\sigma(t') \qquad \text{Equation 3.31}$$

$$\varepsilon(t_r) = \sum_{q=1}^{r} J\left(t_r, t_{q-1/2}\right) \cdot \Delta\sigma_q + \varepsilon_{as}(t_r) + \varepsilon_T(t_r) \qquad \text{Equation 3.32}$$

The calculated results are presented both as discrete values and as graphs.

During the current study, the specially designed program run in Excel was modified to open for a more comprehensive calculation algorithm with regard to the viscoelastic behaviour. The modified stress calculation, denoted "TSTM-sim-mod", differentiates between creep in compression, creep recovery and creep in tension, see Figure 3.3. The appurtenant sets of creep parameters (creep in compression, creep recovery and creep in tension) were determined from dedicated creep tests in the TSTM System as presented in Chapter 7.7.

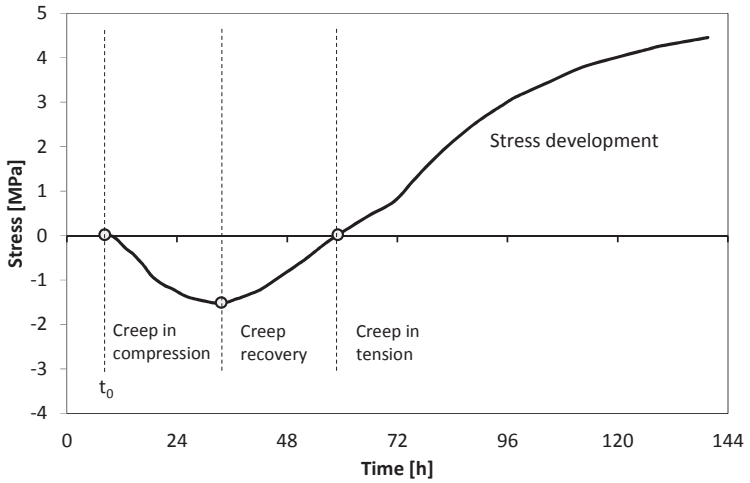

Figure 3.3; Enhanced stress calculation (TSTM-sim-mod): creep in compression, creep recovery and creep in tension

3.7.3 CrackTeSt COIN

3.7.3.1 General

A uniaxial stress analysis simulating the stress development in the TSTM was established in CrackTeSt COIN [JEJMS Concrete AB, 2009-2012], which is a 2D special-purpose program which calculates temperature, strength, stress and cracking risk development in hardening concrete structures.

3.7.3.2 CrackTeSt COIN model and input-data

The geometry of the modelled TSTM cross-section is given in Figure 3.4. CrackTeSt COIN creates a computation mesh consisting of a number of sub-blocks (elements). The program requires eight elements or more across the cross-section to obtain sufficient accuracy in the computation. The element mesh generated by the program for the current analysis is shown in Figure 3.4.

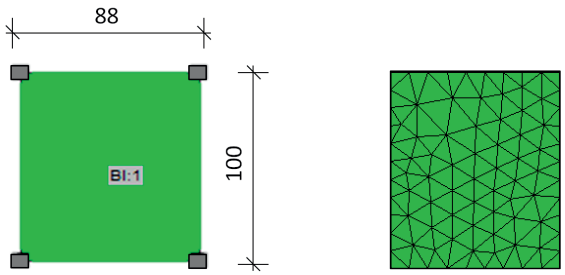

Figure 3.4; CrackTeSt COIN TSTM model: geometry (left) Finite element model (right) [mm]

The concrete temperature development is applied as an external temperature history over time. The concrete convection is set to be high, and thus, the external temperature directly controls the temperature development in the concrete model. As a control of the chosen temperature application, the temperature input was compared with the succeeding concrete temperature development obtained from the analysis. The measured free dilation in the dilation rig is applied the TSTM model as: 1) thermal dilation induced by the enforced temperature development, as well as 2) autogenous deformation applied as concrete shrinkage.

The TSTM model is applied full restraint during isothermal tests (i.e. no translation as well as no rotation around the x-axis nor the y-axis) and a restraint of 50 % for tests subjected to realistic temperatures.

In CrackTeSt COIN, the time-dependent stress response is described by a Maxwell chain model, i.e. the calculations are based on relaxation curves. The creep parameters were thus converted to relaxation data by the program RELAX [Jonasson et al., 2001] prior to the TSTM simulations in CrackTeSt COIN.

3.7.3.3 Analysis - Numerical solution technics

An early age stress calculation in CrackTeSt COIN consists of a heat flow analysis followed by a structural analysis.

All temperature calculations in CrackTeSt COIN are conducted in a two-dimensional plane. The results from the heat analysis are: temperature development, equivalent time (maturity time), compressive strength and boundary heat flow. CrackTeSt COIN automatically converts the heat flow results into input data for the structural analysis.

In the structural analysis, the same element mesh as for the heat analysis is used. However, the structural analyses only considers stresses in the orthogonal direction to the plane where the temperature development was calculated. Two different stress conditions are available in CrackTeSt COIN, which both are based on the Navier-Bernoulli hypothesis (i.e. plane sections remain plane): linear line analysis and plane surface analysis. In the

current calculations, the plane surface model was used, i.e. the stresses vary in the xy-plane according to the boundary conditions given by the user.

The result from the structural analysis includes compressive- and tensile strength development, stress development, stress/strength ratio (i.e. the crack index) and strain ratio.

3.7.4 DIANA

3.7.4.1 Introduction

A third uniaxial TSTM simulation method was established by the multi-purpose 3D FEM-program DIANA [TNO DIANA $_{BV}$, 2010], and this method is described in the following sections.

3.7.4.2 DIANA model

The modelled TSTM's geometry and dimensions are shown in Figure 3.5. Only the central section of the TSTM, i.e. the length between the measuring bolts (700 mm) was modelled. The two short ends were modelled as vertical symmetry surfaces. Each element size in the TSTM model was defined to be ¼ of the specimen's cross-section, i.e. 44 mm x 50 mm x 116.7 mm, see Figure 3.5.

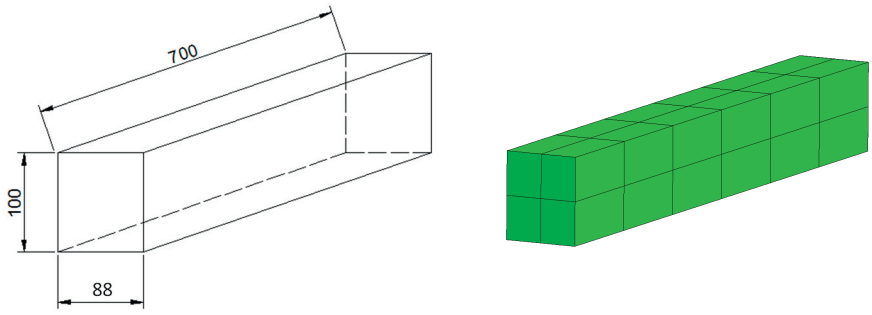

Figure 3.5; DIANA model of the TSTM: geometry (left) finite element model (right) [mm]

In DIANA, the TSTM simulation was performed as a staggered flow-stress analysis. This involves a transient heat flow analysis followed by a structural analysis. For this purpose, three different types of elements were used. For the structural analysis, the twenty-node isoparametric solid brick element CHX60 was applied, Figure 3.6 (left). DIANA recognizes the type of analysis from the module that is invoked, and prior to a heat flow analysis any structural element with material properties appropriate for the analysis type will be converted internally to a flow element. The structural element CHX60 is converted into the flow element HX8HT, an eight-node isoparametric brick element, Figure 3.6 (middle). To describe the heat convection along the outside surfaces of the concrete

structure, the flow element BQ4HT was used, Figure 3.6 (right). The BQ4HT element is linear interpolated, i.e., it has no mid-sides nodes. Therefore, the BQ4HT elements are incompatible with the CHX60 elements that are used for the structural model. In the Design environment of iDIANA, the meshing procedure will not allow the incompatibility of elements. A work-around solution for this problem was found by copying the surface along the boundary by translation over a zero distance. New points were created on the copied surface, the boundary element mesh was generated, and, finally, coincident nodes were merged.

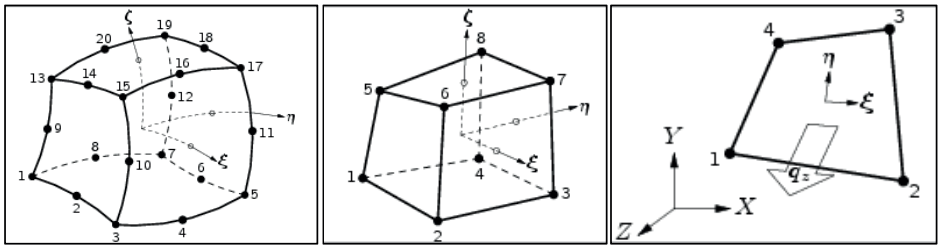

Figure 3.6; left: CHX60, solid brick element, 20 nodes, middle: HX8HT, flow brick element, 8 nodes, right: BQ4HT, flow element, quadrilateral boundary, 4 nodes [TNO DIANA BV, 2010]

Similarly as for the CrackTeSt COIN analyses, the temperature development in the modelled concrete specimen was applied as an external temperature history over time. The convection along the concrete boundaries was set to be high, the concrete hydration was set to be zero, and thus, the applied external temperature boundary condition directly controls the temperature development in the modelled TSTM specimen. To verify the chosen temperature application, the temperature input was compared with the temperature development actually obtained during the analysis.

The applied boundary constraints consist of symmetry conditions along the modelled symmetry lines, i.e. restraint from movement out of the symmetry plane. In addition, two horizontal supports, as well as one sideway support, were applied each of the two short ends, see Figure 3.7.

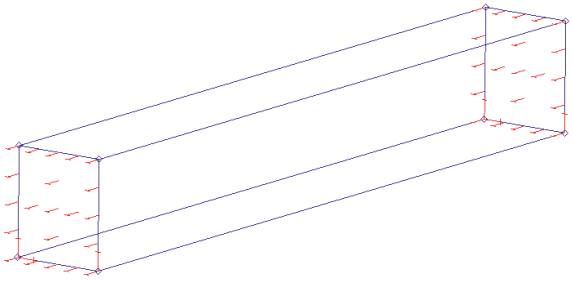

Figure 3.7; DIANA boundary constraints

The measured free dilation in the dilation rig was applied the TSTM model as a time dependent prescribed displacement, hence the thermal expansion and the shrinkage strains in the material model were set to zero since they were already taken into account by the Dilation Rig measurements.

In DIANA, both the Double Power Law and Maxwell chains are available when describing the creep/relaxation behaviour of the concrete. For the Double Power Law, the required creep parameters are: the creep coefficient φ_0, creep model parameters d, p, and the development point of the Taylor series approximation of the Power law, t_d. According to TNO DIANA BV (2010), best results are obtained if t_d is halfway the investigated time interval. As opposed to the current Excel calculations, the DIANA-calculation's creep ratio, $\varphi(t,t')$, is not maturity dependent. For the calculations based on relaxation and Maxwell chains, the given creep parameters were transformed to relaxation data by the program RELAX [Jonasson et al., 2001].

3.7.4.3 Analysis - Numerical solution technics

The TSTM simulation was run as a staggered flow-stress analysis: a transient heat flow analysis was first performed, and further used as input for the following transient nonlinear structural analysis.

A transient heat flow analysis basically involves two steps: initiation of a linear or nonlinear transient analysis, and solution of the equations for the specified time steps. The required output for the heat analysis was set to be: nodal temperatures and equivalent age. DIANA automatically converts the heat flow results to temperatures and maturity as input data for the transient nonlinear structural analysis. DIANA also applies a maturity model to convert the time dependent transient heat flow results into input for the structural analysis.

For the structural analysis, the DIANA default iteration method Regular Newton-Raphson with a maximum of five iterations was chosen. In the Regular Newton-Raphson iteration the stiffness relation is evaluated for each iteration. The Regular Newton-Raphson method yields a quadratic convergence characteristic, which means that the method converges to the final solution within only a few iterations. However, the quadratic convergence is only guaranteed if a correct stiffness matrix is used and if the prediction is already in the neighbourhood of the final solution. If the initial prediction is far from the final solution, the method easily fails because of divergence. In short: the Regular Newton-Raphson method usually needs only a few iterations, but each iteration is relatively time consuming. As convergence criteria, the norms of the force and displacement fields are applied. The tolerance on the reference norm is by default $\varepsilon = 10^{-3}$. DIANA terminates the iteration process if one of the specified criteria is satisfied.

The required output for the structural analysis was set to be the development of displacement, strain and stress.

4 Concrete mix design and test programme

4.1 Introduction

This chapter describes the mix design of the concretes investigated in the following laboratory experiments, as well as the experimental test programme.

A series of five concretes with variable fly ash (FA) content has been included in the current work. Four of the concretes, containing 0 %, 17 %, 25 % and 33 % FA, were originally defined within the COIN sub-project FA 3.1 "Crack Free Concrete Structures" [COIN, 2007-2014]. During the current work, one more concrete containing 45 % FA was added to the concrete series. The detailed mix compositions are given in Section 4.2.

For each concrete, the following test programme has been carried out:

- Heat development
- Mechanical properties under 20 ^{o}C isothermal curing conditions
- Mechanical properties, investigating the effect of curing temperature
- Creep tests in the TSTM System
- Restrained stress tests in the TSTM System (free deformation in the Dilation Rig and restrained stress development in the TSTM), under both isothermal and realistic temperature curing conditions

A survey of the test programme is given in Section 4.3.

4.2 Concrete mix design

The concretes' name and total FA content (in parenthesis as % by weight of cement + FA content) are listed below, and their composition (as well as total FA content and water-to-binder ratio) is given in Table 4.1.

- *ANL Ref.* *(0 % FA)*
- *ANL FA* *(17 % FA)*
- *ANL FA +8FA* *(25 % FA)*
- *ANL FA +16FA* *(33 % FA)*
- *ANL FA +28FA* *(45 % FA)*

ANL Ref. is the reference concrete. It contains no fly ash, and it is made with Portland cement CEM I "Norcem Anlegg" (ANL) [NS-EN 197-1:2011]. The fly ash concretes, on the other hand, are made with Portland-fly ash cement CEM II / A-V "Norcem Anlegg FA" (ANL FA). All concretes were made with a water-to-binder ratio of 0.4 and a cement paste volume of 292 l/m^3. The fly ash content was increased by replacing cement with fly ash 1:1 by weight, while keeping the water-to-binder ratio and the cement paste volume constant. The fly ash content is given as percentage of the total amount of cement + FA, see Equation 4.1. All concretes contain 5 % silica fume (by weight of cement + FA) with an efficiency factor k_{silica} = 2.0. For research purposes, the efficiency factor for extra added

fly ash (i.e. beyond what is part of the cement) was set to k_{FA} = 1.0. According to [NS-EN 206:2013+NA:2014], the efficiency factor for added fly ash is 0.7 for design purposes. The choice of efficiency factor (1.0 versus 0.7) for added fly ash will have an influence on the calculated (effective) water-to-binder (*w/b*) ratio, as indicated in Equation 4.2 and Table 4.1.

Table 4.1; Mix design, FA-content and water to binder ratio [kg/m^3]

	ANL Ref. [kg/m3]	***ANL FA*** [kg/m3]	***ANL FA +8FA*** [kg/m3]	***ANL FA +16FA*** [kg/m3]	***ANL FA +28FA*** [kg/m3]
Cement*	372.3	365.3	324.1	284.3	229.8
FA_{cem}	0.0	60.6	53.8	47.2	38.1
FA_{added}	0.0	0.0	36.0	71.1	118.5
Silica	18.6	18.3	18.0	17.6	17.4
Free water	163.8	160.7	158.5	156.2	153.3
Sand 0-2	201.1	201.1	201.1	201.1	201.1
Sand 0-8	740.2	740.2	740.2	740.2	740.2
Sand 4-8	275.0	275.0	275.0	275.0	275.0
Gravel 8-16	614.1	614.1	614.1	614.1	614.1
Admixture	2.05	2.01	1.78	1.56	1.56
Theoretical density	2400	2390	2380	2370	2360
Assumed air content	2.0	2.0	2.0	2.0	2.0
Total FA-content, FA/(cem+FA) **	**0 %**	**17 %**	**25 %**	**33 %**	**45 %**
Silica-content, Silica/(cem+FA)	5 %	5 %	5 %	5 %	5 %
w/b **k_{FA_added} = 1.0**	**0.40**	**0.40**	**0.40**	**0.40**	**0.40**
w/b k_{FA_added} = 0.7	0.40	0.40	0.41	0.42	0.44

*) *ANL Ref.: cement batch EG1-14, fly ash concretes: cement batch TF5-14*

**) *The FA-content for each concrete is calculated by Equation 4.1*

During the current PhD study, the ANL and ANL FA cements (EG1-10 and TF3-11) had to be replaced with new cement batches (EG1-14 and TF5-14) due to lack of material. The majority of the experimental program in the current study was performed with the cement batches EG1-14 and TF5-14, however, the test series on mechanical properties under 20 ^{o}C isothermal conditions were tested with EG1-10 and TF3-11. In addition, separate cement batches were used at NORCEM when performing compressive strength tests for determination of activation energy. The cement analyses for the various cement batches are given in Appendix A. The ANL FA cement batches show a slight variation in FA content, however, this has been considered negligible and the FA contents of the defined concrete series have been calculated based on cement batch TF3-11 as presented in Table 4.1.

$$FA\ content = \frac{FA_{cem} + FA_{added}}{(Cement + FA_{cem} + FA_{added})} \cdot 100\% \qquad \textit{Equation 4.1}$$

$$w/b = \frac{water}{(Cement + k_{silica} \cdot Silica + k_{FA} \cdot FA_{added})} \qquad \textit{Equation 4.2}$$

Each concrete contains four fractions of aggregate: 0-2 mm, 0-8 mm, 4-8 mm and 8-16 mm from NorStone AS, Årdal, Norway. Årdal aggregate is dominated by granite and gneiss, and it is used as standard laboratory aggregate in Norway.

The fly ash was supplied by NORCEM, and the composition and physical properties are given in Appendix A.

The polycarboxylate based superplasticizer Sika ViscoCrete RMC-420 was used for all concrete mixes.

4.3 Test programme

4.3.1 Introduction

The original plan was to study various effects of fly ash content on hardening concrete. A mechanical test programme including heat development, compressive strength, tensile strength, E-modulus, free deformation and restrained stress development was planned and started. However, during the first tests in the newly modified TSTM System, it became clear that the experimental equipment needed comprehensive adjustments and verification testing. This adjustment- and verification period became quite time-consuming, and therefore the experimental programme had to be postponed. Because of this, the verification and documentation of the equipment itself have been given thorough discussions, Chapter 6. Despite the reduced time for actual parameter studies, there are

reasons to claim that the totality of the experimental programme has become quite comprehensive. An overview of the experimental programme is given in the following:

- *Heat development*, used as basis for realistic temperature calculations.
- *Mechanical properties under 20 °C isothermal curing conditions* including: compressive strength over time (activation energy), compressive strength, splitting tensile strength, direct uniaxial tensile strength, E-modulus in compression and E-modulus in tension. The results were used for material parameter determination as basis for early age stress calculations.
- *Mechanical properties - effect of curing temperature*. These tests included compressive strength, direct tensile strength and E-modulus in tension under both 20 °C isothermal- and realistic temperature curing conditions. The results were used for an evaluation of whether or not the curing temperature should be taken into consideration when deciding material parameters for early age stress calculations.
- *Creep tests in the TSTM System*. These results were used for evaluation and determination of creep parameters as basis for early age stress calculations.
- *Restrained stress tests in the TSTM System.* A test programme of restrained stress tests (measuring thermal dilation and autogenous deformation in the Dilation Rig and restrained stress development in the TSTM) was carried out for the concretes previously described. Some of the tests were performed under 20 °C isothermal conditions, but the emphasis was given to the realistic temperature tests (realistic temperature history, see Section 7.3) with temperature histories representing both summer- and winter conditions.

4.3.2 Heat development

Semi-adiabatic calorimeter tests (NTNU-box, 15 litres samples) were performed to determine the hydration heat evolvement of the concretes for each of the two cement batches of both ANL and ANL FA (as described in Section 4.2). Since extra FA was added in three concretes in combination with ANL FA, this multiple testing involved all concretes (except the later added *ANL FA +28FA*). An overview of the performed semi-adiabatic calorimeter tests is given in Table 4.2.

During the given heat development tests, the temperature development in the concretes were measured and converted to isothermal heat development as a function of maturity, see Chapter 3.4.3. The heat loss to the environment was compensated for by assuming that the heat flow out of the box was proportional to the temperature difference between the concrete and the environment. The proportionality coefficient is called “cooling factor” and can be measured or calculated. This method is standardized and described in [NS 3657:1993].

Table 4.2; Heat development test series for the two batches of ANL and ANL FA cement

Concrete	*Cement batch*	
	EG1-10/TF3-11	*EG1-14/TF5-14*
ANL Ref	1	1
ANL FA	1	1
ANL FA +8FA	1	1
ANL FA +16FA	1	1
ANL FA +28FA	-	1

4.3.3 Mechanical properties under 20 °C isothermal conditions

Compressive strength, splitting tensile strength, direct uniaxial tensile strength, E-modulus in compression and E-modulus in tension were tested under 20 °C isothermal conditions. An overview of the mechanical tests is given in Table 4.3.

The mechanical test series was performed within the COIN sub-activity FA 3.1 “Crack Free Concrete Structures” [COIN, 2007-2014], and the experimental set-up as well as test results for four of the concretes are reported in [Kjellmark et al., 2015]. However, the later added concrete *ANL FA +28FA* is only reported in the current work. While the concretes in the COIN test series were tested at 2 and 28 days, the later added concrete *ANL FA +28FA* was also tested at 91 days to include the long term property development often seen for fly ash concretes.

In addition to the presented tests, NORCEM performed compressive strength tests over time with cubes stored under isothermal conditions at 5 °C, 20 °C and 35 °C for all concretes. The four concretes *ANL Ref.*, *ANL FA*, *ANL FA +8FA* and *ANL FA +16FA* were tested in 2013, while the later added concrete *ANL FA +28FA* was tested in 2015 with a different batch of ANL FA cement. The NORCEM test results are evaluated in the present study, and as planned they were used to determine the activation energy for the concretes.

Table 4.3; Mechanical test programme, 20 °C isothermal conditions

Concrete	**Test**	**No of spec.**	**Test age** [Md]
ANL Ref.	Compressive strength	3	28
	Tensile splitting strength	3 + 3	2, 28
	Direct uniaxial tensile strength	2 + 2	2, 28
	E-modulus (tension)	2 + 2	2, 28
	E-modulus (compression)	3 + 3	2, 28
ANL FA	Compressive strength	3	28
	Tensile splitting strength	3 + 3	2, 28
	Direct uniaxial tensile strength	2 + 2	2, 28
	E-modulus (tension)	2 + 2	2, 28
	E-modulus (compression)	3 + 3	2, 28
ANL FA +8FA	Compressive strength	3	28
	Tensile splitting strength	3 + 3	2, 28
	Direct uniaxial tensile strength	2 + 2	2, 28
	E-modulus (tension)	2 + 2	2, 28
	E-modulus (compression)	3 + 3	2, 28
ANL FA +16FA	Compressive strength	3	28
	Tensile splitting strength	3 + 3	2, 28
	Direct uniaxial tensile strength	2 + 2	2, 28
	E-modulus (tension)	2 + 2	2, 28
	E-modulus (compression)	3 + 3	2, 28
ANL FA +28FA	Compressive strength	3 + 3 +3	3, 28, 91
	Tensile strength	2 + 2 + 2	3, 28, 91
	E-modulus (tension)	2 + 2 + 2	3, 28, 91

4.3.4 Additional mechanical testing – effect of curing temperature

Due to observations in connection with the TSTM tests, additional mechanical tests were initiated in order to study the effect of temperature history on the compressive strength, tensile strength and E-modulus in tension. These additional tests involved the concretes *ANL Ref.* and *ANL FA +16FA*. Half of the test specimens were cast in temperature-controlled moulds and subjected to a realistic temperature history as described in Section 7.3. The other half were cast into regular moulds and cured under 20 ^{o}C isothermal conditions. All specimens were unmoulded and wrapped with aluminium foil at 14 days, and further cured under 20 ^{o}C isothermal conditions. An overview of these tests is given in Table 4.4.

Table 4.4; Additional mechanical test programme, effect of curing temperature

Concrete	**Test**	**Curing conditions**	**No of spec.**	**Test age** [Md]
ANL Ref.	Direct tensile strength, incl. E-modulus in tension	Isothermal	2 + 2	28, 91
		Realistic temp.	2 + 2	28, 91
	Compressive strength	Isothermal	3 + 3	28, 91
		Realistic temp.	3 + 3	28, 91
ANL FA +16FA	Direct tensile strength, incl. E-modulus in tension	Isothermal	2 + 2	28, 91
		Realistic temp.	2 + 2	28, 91
	Compressive strength	Isothermal	3 + 3	28, 91
		Realistic temp.	3 + 3	28, 91

4.3.5 Creep in tension and compression

Due to observations in connection with the "back-calculations" of stresses measured in the TSTM System, own creep tests were performed for the two concretes *ANL FA* and *ANL FA +16FA*. An overview of these creep tests is presented in Table 4.5.

The creep tests were conducted in the TSTM System at a constant temperature of 20 ^{o}C: one test measuring creep in compression and one test measuring creep in tension. The execution of the creep tests is further described in Section 7.7.

As described in Chapter 5, the TSTM System consists of a TSTM (restrained stress development) and a "dummy" Dilation Rig (free deformation). Hence, the creep tests given in Table 4.5 were accompanied by 20 ^{o}C Dilation Rig tests measuring autogenous deformation, which is a prerequisite for separating load-dependent and -independent strains in early age creep tests.

Table 4.5; Creep tests performed in the TSTM System, 20 °C isothermal conditions

Concrete	Test	No of tests	Load age [h (days)]	Stress level [MPa]	Duration [days]
ANL FA	Creep in tension	1	218 (9)	1.0	19
	Creep in compression	1	24 (1)	1.0	8
ANL FA +16FA	Creep in tension	2*	218 (9)	1.0	33
	Creep in compression	1	24 (1)	1.0	8

*) *The test was repeated due to a LVDT support failure two days after loading*

4.3.6 TSTM System

As previously discussed, there was a need to go deep into the mode of action of the TSTM in verification tests. This included several reproducibility tests (nominally identical tests) during the process of trial and error. Some of these tests are naturally not reported since they were done in a phase with continuously adjustments of hardware and software.

For each concrete, one restrained stress test under 20 °C isothermal conditions and one under realistic temperature summer conditions were planned in the TSTM System. However, due to the previously described delay, it was decided to give emphasis to the realistic temperature tests. Some tests were also repeated with adjusted temperature histories due to the change of cement batch and the corresponding change in heat development (described in Section 7.3). As realistic temperature TSTM tests were prioritized, *ANL FA*, *ANL FA +8FA* and *ANL FA +28FA* were not tested under 20 °C isothermal conditions

Increased FA content systematically reduces hydration heat; this is the traditional finding and beneficial effect. However, the tensile strength, which is equally important, is found to be reduced and also time-development slows down. It has been seen that the tensile strength for high volume fly ash concretes can be very slow at low/moderate temperatures, and it is suspected that this effect may override the beneficial effect of reduced heat development. It was therefore decided to include two restrained stress tests under semi-adiabatic temperatures representing Norwegian winter conditions in the given TSTM test programme.

An overview of the tests performed in the TSTM System is given in Table 4.6, where the Dilation Rig and TSTM have been run in parallel for all tests. In addition to these main tests, the TSTM System test programme has also involved tests with variable degree of restraint, creep tests (see Section 4.3.5) as well as faulty measurements (power failure, etc.). A complete list of all TSTM System tests is given in Table 4.7, where the tests have

been listed chronologically. It should be noticed that although the realistic temperature histories for the fly ash concretes were based on either cement batch TF3-11 or cement batch TF5-14, all corresponding TSTM tests were actually performed with cement batch TF5-14, see Table 4.7 for details.

Table 4.6; Restrained stress tests in the TSTM System, overview

	Isothermal 20 °C	**Realistic temperature history**		
		Summer*		**Winter***
		*Cement batch EG1-10/TF3-11**	*Cement batch EG1-14/TF5-14**	*Cement batch TF5-14**
ANL Ref	3	4	-	-
ANL FA	-	1	2	1
ANL FA +8FA	-	1	-	-
ANL FA +16FA	1	2	1	-
ANL FA +28FA	-	-	1	1

*) *The applied temperature history in the test is based on heat evaluation data for each individual cement batch, the tests were however mainly performed with EG1-10 and TF5-14, as described in Table 4.7*

Table 4.7; Restrained stress tests in the TSTM System

Test no.	Concrete	Cement	Temperature	Dilation Rig	TSTM	Comment
V01 26.08.2013	*ANL Ref.*	EG1-10	20 °C isothermal	Duration = 18 days	R = 100 % Duration = 18 days	
V02 17.09.2013	*ANL Ref.*	EG1-10	20 °C isothermal	Duration = 13 days	R = 70 % Duration = 13 days	
V04 08.10.2013	*ANL Ref.*	EG1-10	Realistic temp. (EG1-10)	Duration = 5 days	R = 70 % Duration = 5 days	Failure in tension
V03 03.12.2013	*ANL Ref.*	EG1-10	Realistic temp. (EG1-10)	Duration = 6 days	R = 50 % Duration = 6 days	Failure in tension
V03-2 13.12.2013	*ANL Ref.*	EG1-10	Realistic temp. (EG1-10)	Duration = 6 days	R = 50 % Duration = 5 days	Failure in tension
V05 20.12.2013	*ANL FA*	TF3-11	20 °C isothermal	Duration = 3 days	R = 100 % Duration = 3 days	Power failure after 3 days
V06 21.02.2014	*ANL Ref.*	EG1-10	20 °C isothermal	Duration = 10 days	R = 100 % Duration = 10 days	
V07 01.04.2014	*ANL Ref.*	EG1-10	Realistic temp. (EG1-10)	Duration = 4 days	R = 70 % Duration = 4 days	Air-conditioner failed
V08 10.04.2014	*ANL Ref.*	EG1-10	Realistic temp. (EG1-10)	Duration = 3 days	R = 50 % Duration = 3 days	Software problems
P3.1-1 15.05.2014	*ANL Ref.*	EG1-10	Realistic temp. (EG1-10)	Duration = 7 days	R = 50 % Duration = 7 days	Failure in tension
P3.1-2 27.05.2014	*ANL FA*	TF5-14	Realistic temp. (TF3-11)	Duration = 10 days	R = 50 % Duration = 6 days	Failure in tension
P3.1-3 11.06.2014	*ANL FA +8FA*	TF5-14	Realistic temp. (TF3-11)	Duration = 8 days	R = 50 % Duration = 8 days	Failure in tension
P3.1-4 26.06.2014	*ANL FA +16FA*	TF5-14	20 °C isothermal	Duration = 32 days	R = 100 % Duration = 32 days	Air-conditioner failed after 21 days

Test no.	Concrete	Cement	Temperature	Dilation Rig	TSTM	Comment
P3.1-5 03.09.2014	*ANL FA +16FA*	TF5-14	Realistic temp. (TF3-11)	Duration = 26 days	R = 50 % Duration = 13 days	
P3.1-6 01.10.2014	*ANL Ref.*	EG1-14	Realistic temp. (EG1-10)	Duration = 18 days	R = 50 % Duration = 20 days	
C01 23.10.2014	*ANL FA +16FA*	TF5-14	20 °C isothermal	Duration = 18 days	Creep in compression Duration = 18 days	Creep test
C02 11.11.2014	*ANL FA +16FA*	TF5-14	20 °C isothermal	Duration = 29 days	Creep in tension Duration = 29 days	LVDT support failed
C03 17.12.2014	*ANL FA +16FA*	TF5-14	20 °C isothermal	Duration = 35 days	Creep in tension Duration = 35 days	Creep test
P3.1-7 29.01.2015	*ANL FA +16FA*	TF5-14	Realistic temp. (TF3-11)	Duration = 48 days	R = 50 % Duration = 48 days	Repetition
C04 24.03.2015	*ANL FA*	TF5-14	20 °C isothermal	Duration = 14 days	Creep in compression Duration = 14 days	Creep test
C05 10.04.2015	*ANL FA*	TF5-14	20 °C isothermal	Duration = 18 days	Creep in tension Duration = 18 days	Creep test
P3.1-8 08.05.2015	*ANL FA*	TF5-14	Realistic temp. (TF5-14)	Duration = 10 days	R = 50 % Duration = 10 days	Dil.Rig temperature-control failure
P3.1-9 22.05.2015	*ANL FA*	TF5-14	Realistic temp. (TF5-14)	Duration = 17 days	R = 50 % Duration = 17 days	
P3.1-10 11.06.2015	*ANL FA*	TF5-14	Realistic temp. winter co	Duration = 24 days	R = 50 % Duration = 8 days	Winter conditions
P3.1-11 08.07.2015	*ANL FA +28FA*	TF5-14	Realistic temp. (TF5-14)	Duration = 49 days	R = 50 % Duration = 49 days	
P3.1-12 27.08.2015	*ANL FA +16FA*	TF5-14	Realistic temp. (TF5-14)	Duration = 18 days	R = 50 % Duration = 6 days	Failure in tension
P3.1-13 16.09.2015	*ANL FA +28FA*	TF5-14	Realistic temp. winter co	Duration = 84 days	R = 50 % Duration = 84 days	Winter conditions

5 The TSTM System

5.1 General

In 1969, the Cracking Frame was developed in München, Germany [Springenschmid, 1998]. The Cracking Frame measures the stress response of concrete at early ages to changing temperatures in a concrete specimen with high, but unknown, restraint. In 1984, Springenschmid et al. developed the improved Temperature-Stress Testing Machine (TSTM) which was temperature- and deformation-controlled giving 100 % restraint. Today, several different TSTM variants and other similar devices measuring stress development in hardening concrete are found around the world, for instance [Springenschmid et al., 1994], [Hedlund, 2000], [Czerny et al., 2005], [Amin et al., 2009] and [Darquennes et al., 2011].

The TSTM System at NTNU, Figure 5.1, consists of a Dilation Rig and a Temperature-Stress Testing Machine (TSTM), both connected to a Temperature-control System (Julabo FP45). The TSTM System is located in a conditioned room which holds a constant temperature of 21 °C ± 0.5 °C. The Dilation Rig, the TSTM and the temperature-control system Julabo FP45 are described in the following sections.

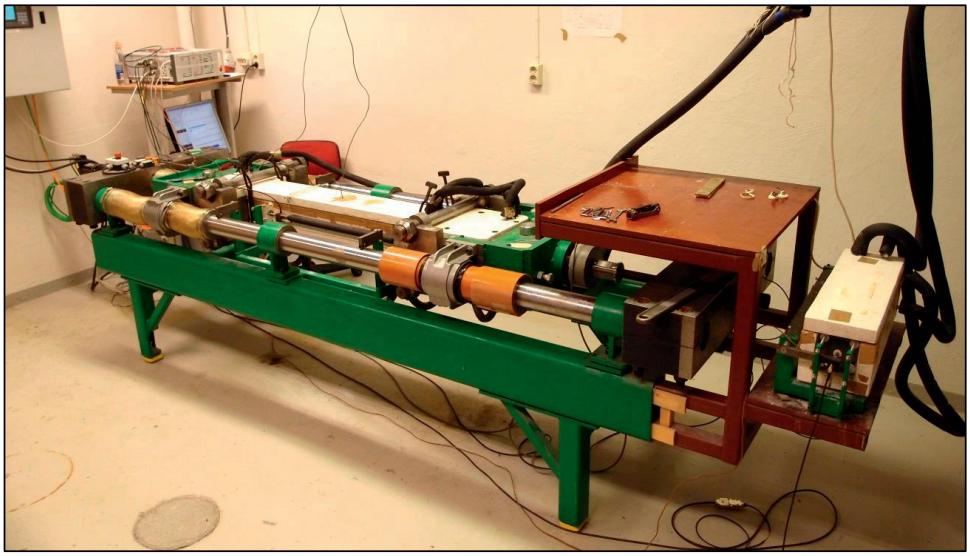

Figure 5.1; The TSTM system at NTNU: the TSTM (left) and the Dilation Rig (right)

The Dilation Rig measures free deformation, i.e. thermal dilation and autogenous deformation, of a sealed concrete specimen. The TSTM is constructed to measure the stress generation of a sealed concrete specimen through the hardening phase at a chosen degree of restraint. The degree of restraint can be varied in the range between 0 and 100 %. The temperature-control system makes it possible to prescribe and apply isothermal or realistic temperature histories to the two concrete specimens in the TSTM System.

Basically, the free deformation measured in the Dilation Rig is the source of the restraint stresses measured in the TSTM. The free deformation data can be used both as input for curing technology programs and to back-calculate the stress measured in the parallel TSTM test.

The TSTM System at NTNU is well established and documented. The TSTM System was built in 1995 and has since been a part of several PhD studies and research projects at NTNU: [Bjøntegaard, 1999], [Bosnjak, 2000], [Atrushi, 2003], [Ji, 2008], the European Brite-EuRam project IPACS (1997-2001, project leader Scancem AB) and Concrete Innovation Centre COIN (2007-2014, project leader SINTEF) among others. During the years 2008 - 2013, the software for logging and management of the TSTM has been updated. In addition, the instrumentation system has been improved to achieve the necessary accuracy and robustness of the system.

For active users, a more detailed description of the experimental equipment is provided in the TSTM System user manual [Klausen, 2013]. A presentation of the originally constructed TSTM System is given in [Bjøntegaard, 1999].

5.2 The Dilation Rig

The Dilation Rig measures free deformation, i.e. thermal dilation and autogenous deformation, of a concrete specimen. Illustrations of the Dilation Rig are given in Figure 5.2, providing explanations of some of the words and expression used in the current section. Pictures of the Dilation Rig and some of its components are shown in Figure 5.3 - Figure 5.4.

The Dilation Rig constitutes a formwork into which a 100x100x460 mm horizontal oriented concrete specimen is cast. The formwork is made of 5 mm thick cobber plates surrounded by 5 mm copper pipes with circulating water connected to a temperature-control unit. The formwork and the copper pipes are covered with insulation, Figure 5.2. Movable end plates made of polystyrene and steel, respectively, are placed at each short end of the formwork. The end plates are supported by end steel supports. Prior to start of length measurements, the end steel support is loosened and moved, allowing the end plates and hence the concrete specimen to move freely during the experiment.

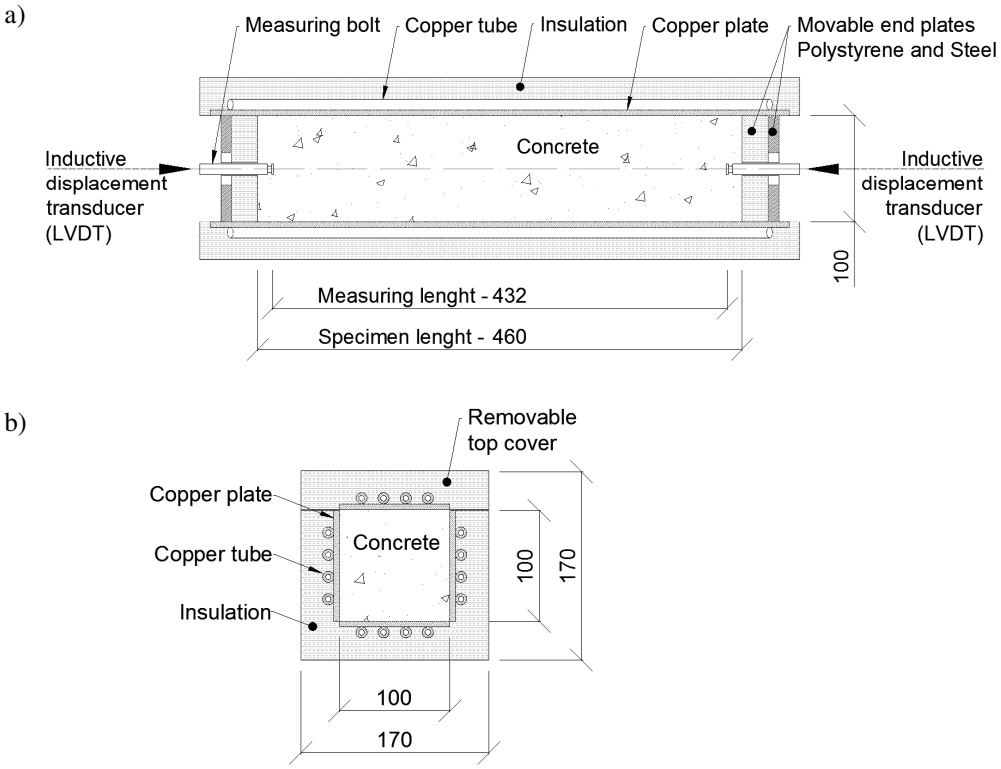

Figure 5.2; Sketch of the Dilation Rig (a) Dilation Rig cross-section (b) [mm]

Before casting, the Dilation Rig formwork is lined with two layers of plastic with talcum powder in between, Figure 5.3. After casting, the concrete specimen is well covered with the excess plastic. In addition, the concrete is covered with aluminium foil. The aluminium foil is bent and fixed with tape to the outer walls of the mould. Finally, the top cover is placed onto the mould, Figure 5.3.

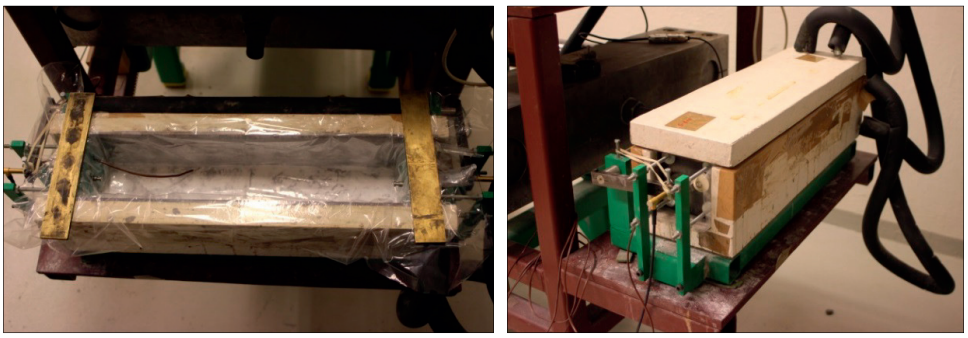

Figure 5.3; The Dilation Rig: before casting (left) after casting (right)

During the recent reconstruction, the Dilation Rig was provided with a new length measurement setup. Now, measuring bolts are cast into each short end of the concrete specimen, Figure 5.2. The measuring bolts have diameter = 8 mm and length = 70 mm, whereof 15 mm is embedded in the concrete. Each measuring bolt is provided with a 5 mm notch to secure anchorage in the concrete specimen, Figure 5.4. The measuring bolts are made of invar steel with a low coefficient of thermal expansion to reduce temperature induced movements of the measuring bolts. The temperature in the measuring bolts is found to follow the temperature measured in the concrete specimen. The temperature induced length change of the measuring bolts is calculated and compensated for in every experiment, see Chapter 6.2.3.

Before conducting an experiment, an inductive displacement transducer (LVDT) is mounted at each short end, Figure 5.4. The LVDTs measure the length change of the concrete specimen by measuring the movement of the embedded measuring bolts previously described.

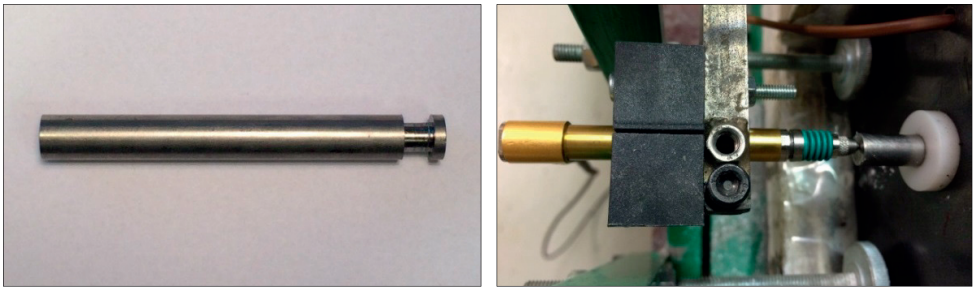

Figure 5.4; The Dilation Rig: measuring bolt (left) mounted LVDT in action (right)

When conducting an experiment in the Dilation Rig, the following data are recorded:

- Concrete length displacement, measured by two LVDTs
- Concrete temperature, measured with a Type K thermocouple
- Surrounding air temperature, measured in water with a Type K thermocouple

Temperature measurements are started immediately after casting. Length change measurements are initiated after approximately 2 hours, depending on the concrete and its early stiffening characteristics.

A more detailed description of the Dilation Rig and the procedures required when performing an experiment are provided in the TSTM System user manual [Klausen, 2013].

5.3 The Temperature-Stress Testing Machine (TSTM)

The Temperature-Stress Testing Machine (TSTM) measures the stress generation of a concrete specimen through the hardening phase at a chosen degree of restraint. An illustration of the TSTM is given in Figure 5.5, providing an explanation of some of the words and expressions used in the following. Pictures of the TSTM and some of its components are given in Figure 5.6 and Figure 5.7.

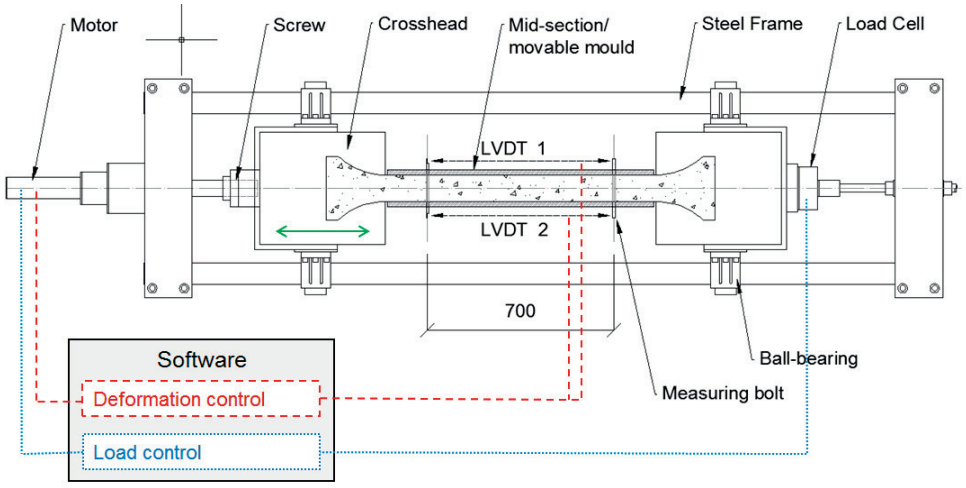

Figure 5.5; Sketch of the TSTM

The TSTM consists of an outer steel frame which, nearly frictionless, supports two movable crossheads and a movable mid-section. Together, the two crossheads and the mid-section constitute a formwork into which the horizontally oriented concrete specimen is cast. The TSTM formwork is composed in the same way as the Dilation Rig formwork: with 5 mm copper plates surrounded by 5 mm copper tubes (containing circulating temperature-controlled water) covered by insulation. The crossheads and the top covers are also temperature controlled, providing a uniform temperature history in the whole concrete specimen during testing.

The TSTM concrete specimen is shaped as a «dog bone». The central 700 mm of the mid-section, the measuring length, has a rectangular cross-section with dimensions: 88 mm (width) x 100 mm (height). Outside the measuring length, the width of the concrete cross-section increases linearly on both sides until it reaches 100 mm at the crossheads. The cross-section width continues to increase gradually up to 225 mm within the crosshead, thus providing restraint for the concrete specimen.

Prior to casting, two measuring bolts are installed in the TSTM mid-section with a distance of 700 mm, defining the measuring length, Figure 5.5 and Figure 5.6. The measuring bolts go through the temperature-controlled mould, and are embedded in the concrete during casting. The concrete specimen deformation is measured as the length change between the

two measuring bolts by two inductive displacement transducers (LVDTs), one on each side of the concrete specimen. The LVDTs are mounted in the following way: 1) by fixed support to measuring bolt II and 2) by spring support over the top cover close to measuring bolt I, Figure 5.6b.

A load cell is mounted to the right crosshead, Figure 5.5, measuring the restraining force transferred through the concrete cross-section during testing.

a)

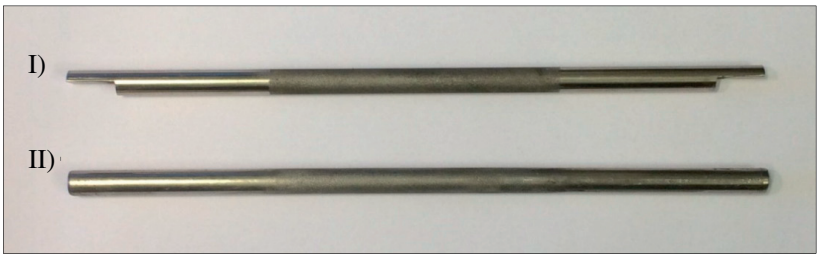

b)

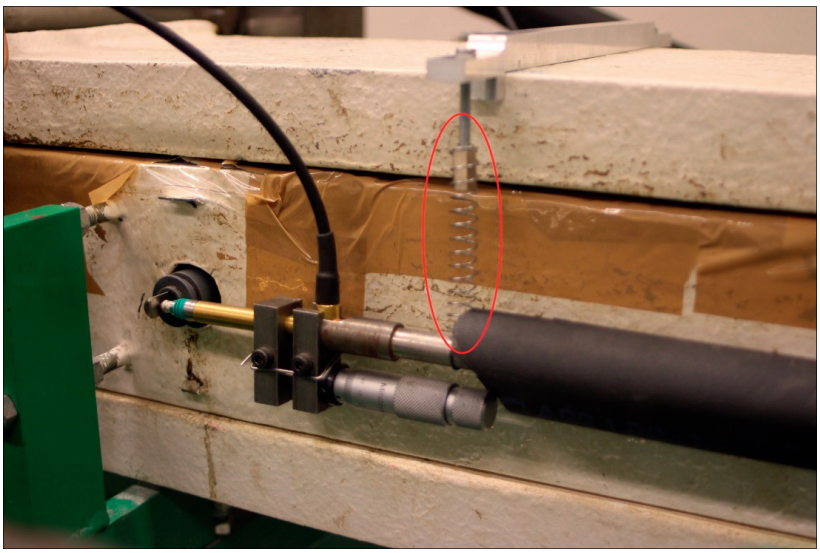

Figure 5.6; The TSTM: measuring bolts (a) mounted LVDT in action (b)

Prior to casting, the TSTM mid-section is lined with two layers of plastic with talcum powder in between, Figure 5.7. After casting, the concrete specimen is well covered with aluminium foil. The aluminium foil is bent and fixed with tape to the top and outer walls of the mould. Finally, the top cover is placed onto the mould Figure 5.7.

When conducting an experiment in the TSTM, the following data are recorded:

- Concrete length displacement, the average measured by two LVDTs
- Force, measured by the load cell
- Concrete temperature, measured by a Type K thermocouple
- Surrounding air temperature, measured in water by a Type K thermocouple

The temperature measurements start immediately after casting. The TSTM feedback system is usually started 5-8 hours after mixing, depending on the concrete and its early stiffening characteristics.

Figure 5.7; The TSTM: before casting (left) after casting (right)

During the years 2008 - 2013, the TSTM System was upgraded with new software and a new length measurement setup as described above. The new software is connected to the LVDTs and the load cell, as well as to a high precision screw moving the left crosshead, Figure 5.5. The magnitude of the crosshead movement induced by the software is decided by: 1) the length change in the concrete measured by the LVDTs, 2) the load measured by the Load Cell and 3) the user defined parameters in the software. The TSTM is by this both deformation-controlled and load-controlled. In addition, the new software allows the user to choose a desired degree of restraint in the range between 0 and 100 %, where the degree of restraint is defined as the ratio between restrained and total deformation in the TSTM tests times 100 %. As a result, the TSTM is now able to directly simulate the stress development in a given section of a concrete structure.

When the measured deformation reaches its threshold value during an experiment, the software is activated and a crosshead movement is induced. When such an activation event, i.e. screw regulation, is started, data are stored 10 times a second until the regulation is completed. This feature provides a substantial stress-strain relation for each regulation during an experiment. The concrete E-modulus can be calculated based on the recorded data, providing an E-modulus development over time in the hardening phase for the concrete in question.

The deformation increment is decided by considering the following requirements 1) to obtain enough data to determine the incremental E-modulus, see Chapter 6.3.7 and 2) to achieve a stress versus time development curve which is not too coarse. For stress development tests applied a degree of restraint of 50 %, a suitable deformation increment was found to be 0.006 mm.

The TSTM System can be used for several types of experiments. In addition to the previously described restrained stress measurements, also creep and relaxation tests as well as determination of restraint stresses due to drying shrinkage can be performed, [Ji, 2008] and [Bjøntegaard et al., 2004c]. In the current work, the TSTM System has been used for both restrained stress measurements as well as a series of creep tests. Both creep in compression, creep recovery and creep in tension have been investigated. When performing a creep test in the TSTM System, a load is applied the concrete specimen and then kept at a constant load-level while simultaneously measuring the length change. The resulting creep data can then be found by subtracting the parallel free deformation measurements (Dilation Rig) from the length change measured in the TSTM.

A more detailed description of the TSTM and the procedures required when performing a test in the TSTM System is provided in the TSTM user manual [Klausen, 2013].

5.4 The Temperature-control System

In both Rigs in the TSTM System, 5 mm copper pipes with circulating water are placed on the outer side of each of the formwork copper plates. The copper tubes are connected in series to a cooling/heating regulator Julabo FP45 by insulated plastic tubes. The temperature-control system makes it possible to prescribe and apply isothermal or realistic temperature histories to the two concrete specimens.

The temperature-control unit Julabo FP45 consists of a circulator head and a heating/cooling unit, and can provide heating, cooling and isothermal conditions for the concrete specimens. The Julabo working temperature range is -42 – 200 ^{o}C. The Julabo heating/cooling unit is normally filled with soft/decalcified water, but alternative liquid can be used for temperatures below 5 ^{o}C. A picture of the Julabo FP45 is given in Figure 5.8, while operating instructions for the Julabo FP45 are found in the Julabo Operating Manual [GmbH, 2013].

Figure 5.8; The temperature-control unit Julabo FP45

Due to heat loss to the surroundings, $\Delta T_{heat\ loss}$, the temperature programmed in the Julabo is not exactly equal to the temperature obtained in the centre of the concrete specimens in the TSTM System. To achieve the desired temperature in the concrete specimens, a relation between the temperature entered in the Julabo, T_{julabo}, and the achieved TSTM concrete temperature, $T_{concrete}$, is found. This is done by programming temperature increments in the Julabo, and measuring the corresponding achieved temperatures in the concrete specimens.

$$T_{julabo} = T_{concrete} + \Delta T_{heat\ loss} \qquad \textit{Equation 5.1}$$

6 Verification and documentation of the TSTM System

6.1 Introduction

In 2008, a reconstruction of the TSTM System was initiated within the COIN project's sub-activity FA 3.1 "Crack free concrete structures". The construction work has mainly been related to the TSTM, while for the Dilation Rig the work has been limited to some modifications. The main objectives of the reconstruction of the TSTM were to obtain: 1) a more advanced management and control of the experimental equipment, and 2) a more extensive output from each test. These objectives were achieved by providing the TSTM System with a new and more advanced software for management and logging. However, after the new software was installed, a series of verification tests indicated that the TSTM System was no longer providing reliable results. The new software was found to require a higher accuracy of the instrumentation system; hence, a new measurement setup had to be established and installed for the software to achieve satisfactory control of the TSTM. In addition, the verification test series also revealed other irregularities, and several different adjustments and actions were initiated to correct, improve and complete the TSTM System. For a time it seemed as if for every error found and solved, a new source of error was uncovered. Hence, the reconstruction and verification of the TSTM System has required far more time and effort than originally planned. In 2014, after numerous adjustments and corrections, the TSTM System was finally found to produce reliable and reproducible results, and the TSTM test programme could be initiated.

The given section describes the verification and documentation of the TSTM System. Brief descriptions of the troubleshooting conducted during the verification period are given, and some potential sources of errors during testing are discussed.

6.2 The Dilation Rig

6.2.1 General

The Dilation Rig was provided with a new length measurement setup during the above described verification period. The Dilation Rig remains otherwise as it was originally built, and is therefore still covered by verification tests and discussions carried out during the original construction and verification performed by [Bjøntegaard, 1999]. At that time it was concluded that the sealing of the Dilation Rig was satisfactory, as verified by weight loss measurements of the Dilation Rig during testing. It was also concluded that friction between the mould and concrete specimen was not a basic problem and that the sum of the two LVDTs represented the true movement of the concrete sample. These previous findings are supported in the current work, at least in the way that the reproducibility is very good today, see Section 6.2.5.

Reabsorption of bleed water may influence these types of tests. The risk and effect of bleeding during Dilation Rig tests are evaluated in Section 6.2.2. The new length

measurement setup in the Dilation Rig is presented and discussed in Section 6.2.3. To what extent the Dilation Rig is influenced by its surroundings is discussed in Section 6.2.4, while the reproducibility of the updated Dilation Rig is presented in Section 6.2.5.

6.2.2 Bleeding

The risk and effect of bleeding during testing in the TSTM System has been evaluated. [Bjøntegaard, 1999] found that the presence of bleed water had a disturbing effect in linear Dilation Rig tests: if bleeding has taken place before setting, the bleed water will be reabsorbed by the concrete as self-desiccation occurs after setting, resulting in reduced autogenous shrinkage or even expansion after setting, at least for a period of time. During the current work, visual inspections of the concrete specimens during testing have given no indications of bleeding. In addition, the literature shows that the phenomena «reabsorption of bleed water» occurs in the early ages (5-10 hours after water addition), while the current scope of work is the stress-generating part of the deformations which occurs after final setting. Bleed water reabsorption would only have a minor effect on the stress-generating part of the deformations, at least when the bleeding tendency is moderate as appears to be the case for the tested w/b = 0.4 concrete. Hence, in the current study, no regular routine of removing bleed water was initiated. This conclusion is supported by the good reproducibility found in Section 6.2.5.

6.2.3 Measurement setup

During the reconstruction of the TSTM System, the Dilation Rig was provided with new LVDTs, new measuring bolts and a new LVDT/measuring bolt setup, Figure 6.1.

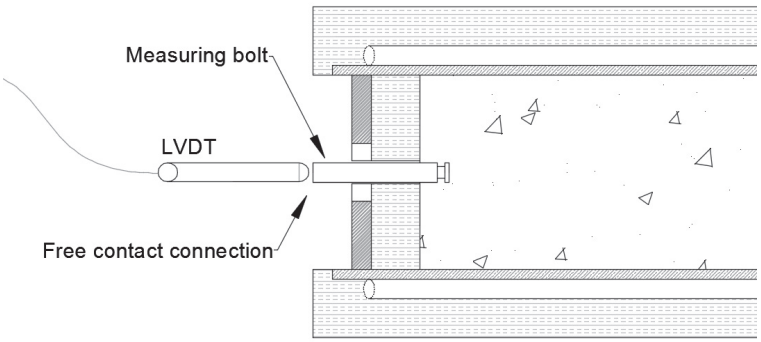

Figure 6.1; Dilation Rig – free length change measurement setup

Previously, the measuring rods were fixed to the LVDTs. In the new length measurement setup, the LVDTs rest freely against the measuring bolts, providing a spring-loaded free

contact connection between the measuring bolts and the LVDTs, Figure 6.1. In this way, potential transversal constraining forces (bending forces) caused by differential vertical movement of the measuring bolts and the LVDTs are avoided. Previously, such constraining forces have been seen to produce significant friction in the LVDT. In addition, the new set up reduces mechanical wear, which is believed to make the LVDTs more durable.

The new measuring bolts have a diameter of 8 mm and a length of 70 mm, whereof 15 mm are embedded in the concrete. The measuring bolts are made of invar steel with a low coefficient of thermal expansion (CTE = $1.18 \cdot 10^{-6}$ /^{o}C) to reduce thermal deformation of the measuring bolts and thereby reduce the thermal disturbance in the length change measurement of the concrete specimen. Still, the temperature development and the corresponding thermal deformation of the measuring bolts should be determined and compensated for in each experiment.

The measuring bolts are not expected to have a uniform temperature distribution during an experiment. The part of the measuring bolt which is embedded in the concrete is assumed to follow the concrete temperature when imposing temperature changes to the concrete specimen. The free part of the measuring bolt will develop a temperature gradient due to heat exchange with the surroundings. A relation between specimen temperature and average bolt temperature has therefore been established for routine and simple compensation of bolt movements during every test.

The temperature development in the free end of the measuring bolts was measured during an experiment where a realistic temperature history was applied the specimen, Figure 6.2. It should be noted that the used thermocouples have an accuracy of ± 1.0 ^{o}C for the current temperature range. The measured temperature change in the free end of the bolts was found to be 55 % of the temperature change measured in the given concrete specimen. This relation was quite constant during the entire experiment.

A uniform average bolt temperature was estimated based on the assumed (and simplified) temperature distribution over the bolt length as illustrated in Figure 6.3. Combined with the previously found relation between measured concrete temperature and the temperature in the free end of the bolt, the average temperature change of the measuring bolt was approximated to be 75 % of the temperature change measured in the concrete specimen during an experiment.

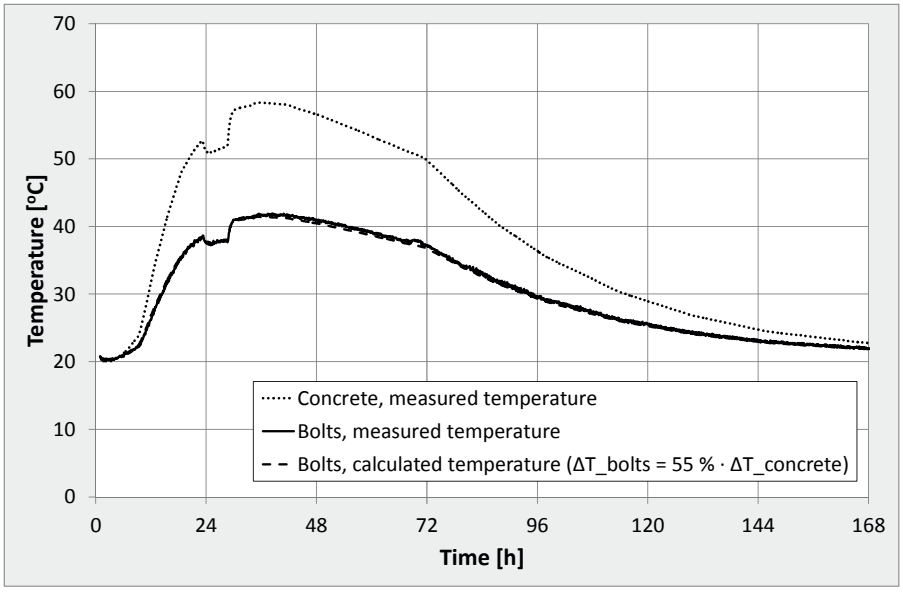

Figure 6.2; Dilation Rig – temperature development measuring bolts

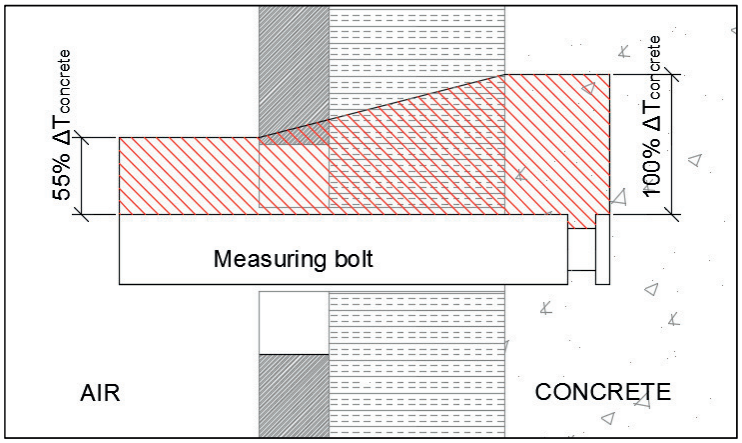

Figure 6.3; Dilation Rig – assumed temperature distribution over the measuring bolt length

The temperature induced length change of the measuring bolts has been calculated and compensated for in every experiment. The calculations were based on a measuring bolt temperature as described above and on a measuring length setup as given in Figure 6.4.

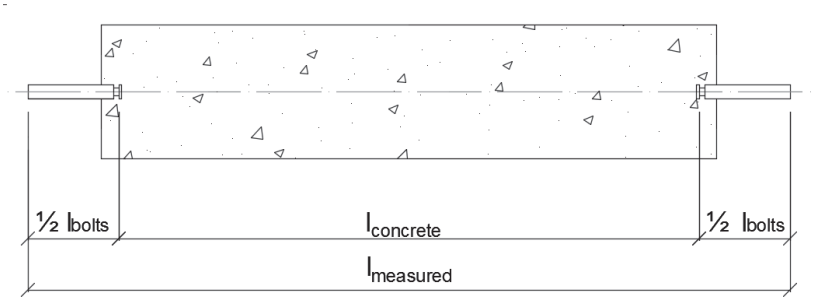

Figure 6.4; Dilation Rig – estimation of thermal deformation disturbance by the measuring bolts

The relation between the total measured length change, the length change of the concrete and the length change of the measuring bolts is as follows:

$$\Delta l_{measured} = \Delta l_{concrete} + \Delta l_{bolts}$$

$$\Delta l_{concrete} = \Delta l_{measured} - \Delta l_{bolts}$$

$$\Delta l_{concrete} = \Delta l_{measured} - CTE_{bolts} \cdot \Delta T_{bolts} \cdot l_{bolts}$$

where $\Delta l_{concrete}$ = concrete length change, $\Delta l_{measured}$ = total measured length change in the LVDTs, CTE_{bolts} = $1.18 \cdot 10^{-6}$ /°C and ΔT_{bolts} = $(0.75 \cdot \Delta T_{concrete})$ = the temperature change in the measuring bolts, l_{bolts} = 140 mm

The effect of compensating for the thermal dilation of the measuring bolts was evaluated by looking at the *ANL Ref.* test subjected to a realistic temperature history, which was the test with the highest maximum temperature (62 °C). The total measured concrete deformation (expansion) at the maximum temperature was found to be 0.124 mm. When using the relation established above, the actual concrete deformation is really 0.119 mm. It then follows that the compensation constitutes 4 %, i.e. that the measured strain is 4 % higher than the true specimen behaviour. If assuming that the bolts obtained the same temperature change as the concrete specimen (100 %), the total concrete deformation becomes 0.117 mm (compensation is 5%). These numbers indicate that thermal deformations of the bolts should be compensated for, but that the simplifications regarding the temperature distribution and the following accuracy of the concrete/bolt temperature relation is not crucial. It is therefore put trust in the established calculation procedure, where the temperature change in the bolts is set to be 75 % of the temperature change measured in the concrete specimen. This conclusion complies with [Bjøntegaard, 1999] who found that Dilation Rig measuring bolts with a diameter of 7 mm had a temperature equal to 66 % of the temperature measured in the concrete, and that this percentage would increase with increasing diameter of the measuring bolt.

6.2.4 External influence

During the reconstruction of the TSTM System, verification tests showed that the measured length change in the Dilation Rig was affected by both the surrounding temperature and air humidity. It was discovered that the newly installed plastic brackets holding the LVDTs were hygroscopic and highly influenced by both room temperature and air humidity. The plastic brackets were therefore replaced by brackets made of invar steel. In addition, in order to enhance climate room control, the room was in 2014 equipped with a new temperature-control unit (Daikin FTXS-K) as well as with a new air humidity-control unit (Condair FAN3S). The climate room control is now much better; the temperature is kept stable at 21 ^{o}C ± 0.5 °C and the air humidity is kept stable at 50 % ± 1.5 %.

By increasing the room temperature while keeping the concrete temperature constant in trial tests, the Dilation Rig length change disturbance is now found to be in the order of 4.0 μstrains / ^{o}C change in air temperature. As the Dilation Rig is located in a conditioned room which normally holds a constant temperature of 21 °C ± 0.5 °C, this external temperature disturbance must be regarded to be satisfactory small.

Infrequently, the Dilation Rig can be subjected to jolts caused by experiments in the surrounding locations. Such jolts will most likely be discovered as they produce definite leaps in the measured data for both the Dilation Rig and the TSTM, which later can be compensated for.

6.2.5 Reproducibility

Several verification- and introductory tests have been performed in the Dilation Rig. Repeated nominally identical tests (based on separate concrete batches) indicate good reproducibility for both isothermal and realistic temperature conditions. A survey of repeated Dilation Rig tests are given in Table 6.1 and the test results are presented in Figure 6.5 - Figure 6.8. Positive deformation values are expansion, while negative values are contraction.

Table 6.1; Dilation Rig reproducibility: repeated nominally identical tests

Concrete	Temperature conditions	No. of tests	Figure
ANL Ref.	20 ^{o}C isothermal	3	Figure 6.5
	Realistic temp. history	4	Figure 6.6
ANL FA +16FA	20 ^{o}C isothermal	4	Figure 6.7
	Realistic temp. history	2	Figure 6.8

Figure 6.5 shows measured autogenous deformation for three nominally identical 20 ^{o}C isothermal tests performed with the reference concrete, *ANL Ref.*. Two of the tests do not

have any data measurements before 10 hours (after water addition), and therefore, all three curves have been zeroed at 10 hours. This point in time is later than the start time for stress development which was found to be t_0 = 8.8 maturity hours, see Section 7.5, but for reproducibility comparisons it was decided acceptable to zero the measurements at 10 h. The reproducibility in Figure 6.5 must be regarded as very satisfactory.

Four nominally identical realistic temperature tests performed with the reference concrete, *ANL Ref.,* are presented in Figure 6.6. The tests were performed under the same temperature development, representing the average temperature in a selected section of an 800 mm thick wall structure (see Section 7.3). The applied temperature history is also shown in Figure 6.6. The measurements have been zeroed at t_0 = 8.8 maturity hours, which is the starting point for stress development in the TSTM test for the given concrete, Section 7.5. One of the tests in Figure 6.6 was based on cement from a different batch than the other three tests. Results from the three tests performed with the same cement batch show very good agreement. The concrete with the newer cement batch differs somewhat from the other tests, but all in all, the reproducibility must be regarded as very good.

Figure 6.7 - Figure 6.8 present results from a series of tests performed with the concrete *ANL FA +16FA*. Figure 6.7 shows autogenous deformation for four tests run in the Dilation Rig under 20 ^{o}C isothermal temperature conditions, while Figure 6.8 gives the total deformation for two realistic temperature tests run with identical temperature histories. All curves have been zeroed at t_0 = 12 hours of maturity, as found in Section 7.5. Both isothermal and semi-adiabatic tests show very good reproducibility.

The tests presented in the current section were conducted during the years 2013-2014. Parallel to the testing, several adjustments and actions were initiated and performed to correct and complete the TSTM System (i.e. adjustments of the measuring bolts and length measurement setup, stabilisation of the surrounding temperature and air humidity conditions, change of cement batch, etc.). Hence, there are some variations in the experimental details among the performed tests. The tests performed with *ANL FA +16FA* (Figure 6.7 - Figure 6.8) are all conducted after the final completion of the TSTM System, and they are thus performed under nominally identical climate room and test set-up, as well as with the same batch of cement. As can be seen from Figure 6.7, the Dilation Rig gives a difference of only 7 μstrains both after 2 days and after 12 days. A numerical evaluation of the reproducibility of the *ANL Ref.* and *ANL FA +16FA* test results at two chosen points in time is presented in Table 6.2 and Table 6.3, respectively.

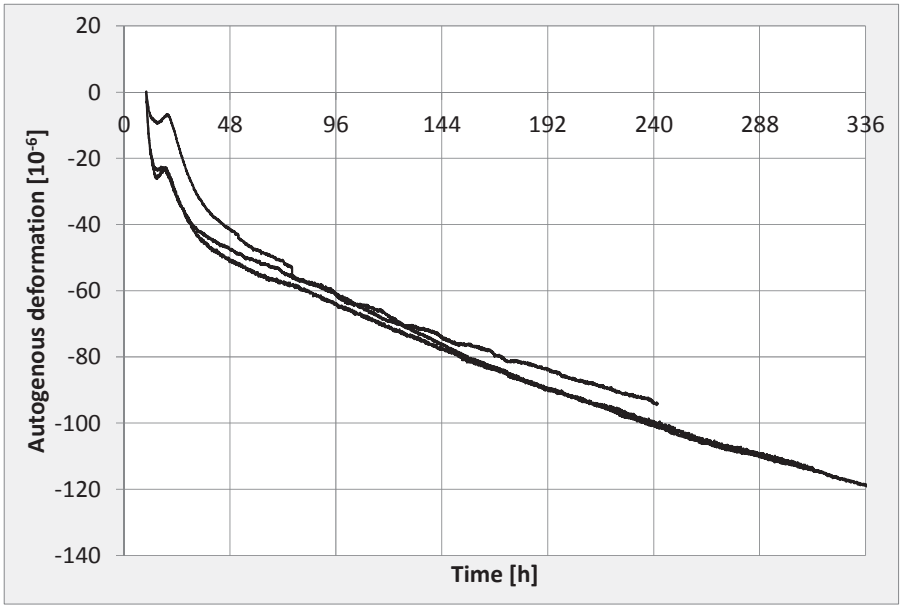

Figure 6.5; Dilation Rig reproducibility: autogenous deformation ANL Ref., 20 °C isothermal, zeroed at 10 hours

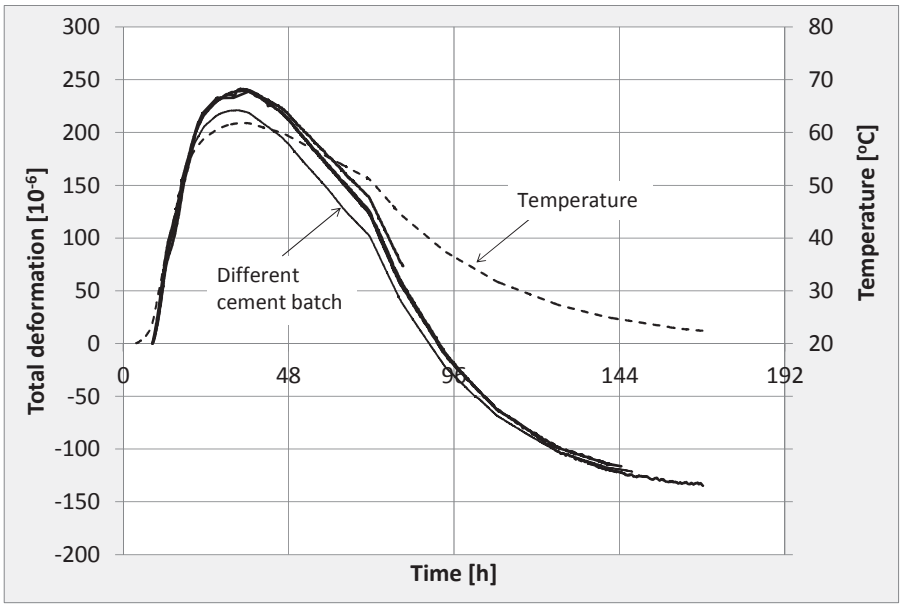

Figure 6.6; Dilation Rig reproducibility: total deformation ANL Ref., realistic temperature conditions, zeroed at t_0 = 8.8 h

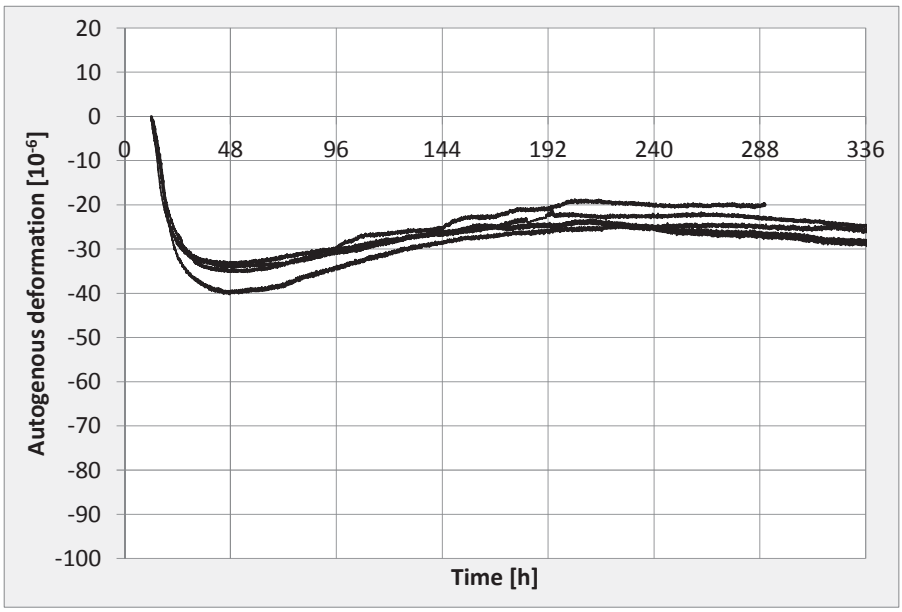

Figure 6.7; Dilation Rig reproducibility: autogenous deformation ANL FA +16FA, 20 °C isothermal temperature conditions, zeroed at t_0 = 12 h

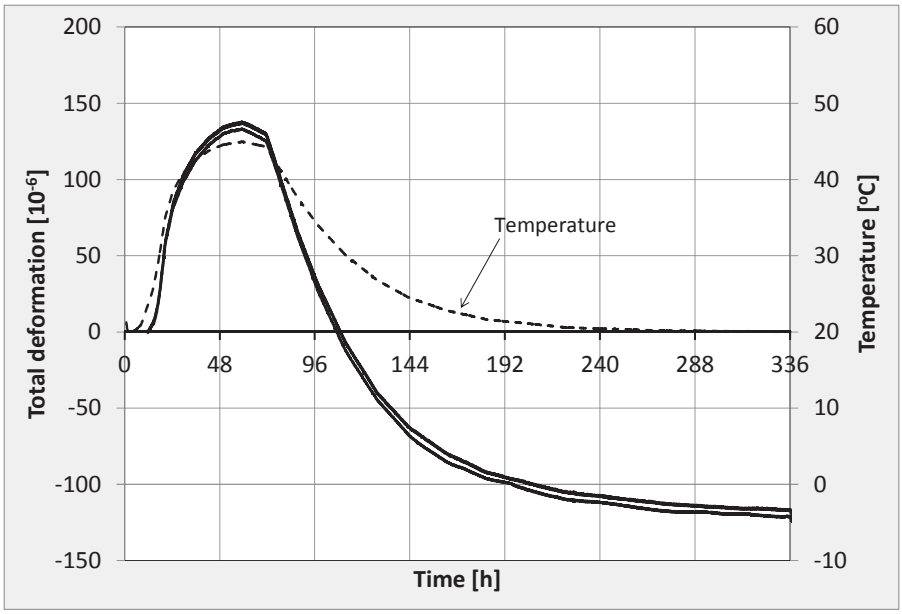

Figure 6.8; Dilation Rig reproducibility: total deformation ANL FA +16FA, realistic temperature conditions, zeroed at t_0 = 12 h

Table 6.2 shows that the reproducibility among the *ANL Ref.* tests is good. The standard deviations for three nominally identical 20 °C isothermal tests are only 4.0 and 3.0 µstrain after 48 and 240 hours, respectively. The four *ANL Ref.* tests with realistic temperature conditions show a slightly higher scatter in the test results at 48 hours. However, when removing the semi-adiabatic *ANL Ref.* test made with a different cement batch, the standard deviation after 48 hours for the remaining three nominally identical semi-adiabatic tests is reduced from 10.9 to 2.2 µstrain. Thus, the reproducibility for the *ANL Ref.* tests made from the same cement batch must be regarded as very good.

Table 6.2; Dilation Rig reproducibility: numerical evaluation of ANL Ref. tests

Test	**Age** [h]	**No of tests**	**Min** [µstrain]	**Max** [µstrain]	**Mean** [µstrain]	**SD** [µstrain]
20 °C isothermal	48	3	-51	-41	-47	4.0
	240	3	-101	-94	-98	3.0
Realistic temp.	48	4	189	217	208	10.9*
	144	3	-121	-116	-119	2.1

*) *Reduced to 2.2 when removing the test that applied a different cement batch*

Table 6.3; Dilation Rig reproducibility: numerical evaluation of ANL FA +16FA tests

Test	**Age** [h]	**No of tests**	**Min** [µstrain]	**Max** [µstrain]	**Mean** [µstrain]	**SD** [µstrain]
20 °C isothermal	48	4	-40	-33	-35	2.5
	288	4	-26	-19	-23	2.6
Realistic temp.	48	2	128	133	131	2.4
	288	2	-118	-115	-116	1.8

The numbers in Table 6.3 clearly proves that the reproducibly among the *ANL FA +16FA* tests are very good. The standard deviations for four nominally identical 20 °C isothermal tests are only 2.5 and 2.6 µstrain after 48 and 288 hours, respectively. The two semi-adiabatic tests give even better agreement, with a standard deviation of 2.4 µstrain after 48 hours, and 1.8 µstrain after 288 hours, but it must be taken into consideration that only two tests are included in this latter evaluation.

6.3 The TSTM

6.3.1 General

As previously described, the reconstruction of the TSTM has been challenging. Numerous obstacles and errors have been uncovered and located during the reconstruction period, requiring several modifications of the experimental equipment. The reconstruction has required far more effort and time than originally planned, and consequently, a considerable part of the current work has been dedicated to a continuous evaluation and modification of the TSTM System. Section 6.3.2 gives a brief summary of some of the main challenges encountered during the verification period. Section 6.3.3 – 6.3.7 discusses sources of errors and accuracy with regards to tests results, while Section 6.3.8 presents the reproducibility of the TSTM after the reconstruction.

6.3.2 Challenges during the TSTM reconstruction- and verification period

During the initial verification tests in 2010, the concrete specimens developed very early tensile failure (typically after 24 hours for 20 ^{o}C isothermal conditions). Comprehensive troubleshooting revealed that an interference voltage in the TSTM motor control induced a drift in the TSTM motor. The TSTM motor drift caused a very slow but regular movement of one of the anchoring crossheads, resulting in an unintended movement of the concrete specimen of about 0.2 mm/hour during the initial phase. This initial deformation was the reason for the early failure which was located in the transition zone between the crosshead and the specimen mould. The interference source was eliminated by: 1) adjusting the motor control noise limit settings and 2) isolating the motor control in a separate insulated box. With these actions, the initial drift of the TSTM motor was successfully eliminated.

Parallel to the previously described motor drift problem, a lot of time was spent on challenges regarding the interface between the new software and the experimental equipment. The software was developed and successively improved as an iterative process in combination with verification tests, and the process required a considerable amount of iterations. As one TSTM test was run for typically two weeks, the process became quite time consuming. Eventually, when the software was found to work as intended, a number of TSTM tests were run to find the appropriate parameter settings for routine/standard testing in the TSTM.

After passing all challenges described above, poor reproducibility of the TSTM length deformation was observed during manual motor control. This revealed that both new LVTDs as well as a new LVDT setup were required to achieve a higher degree of accuracy. Due to the low threshold values for TSTM deformation regulations (around five thousandth of a mm), high accuracy of length measurements and avoidance of sources of errors as for instance slippage are essential. As shown in Section 6.3.3, the new LVDT setup has been found to provide satisfying accuracy.

A further discovery was that the LVDTs were not equipped with protection sockets. This allowed talcum and dust to enter into the LVDT, which was found to cause friction and occasionally irregular measurements. Consequently, these LVDTs were removed and replaced by new LVDTs equipped with protection sockets.

Furthermore, the new software allowed separate measurements for the two LVDTs, one on each side of the concrete specimen. These measurements indicated eccentrically loading of the TSTM specimen. Several mechanical adjustments were then made to reduce the eccentricity. In addition, the outer steel frame in the TSTM System was lubricated to reduce friction in the ball bearings of the cross-heads during testing and the regulation speed was reduced, allowing the motor to respond more accurately to the software control.

Finally, a handful of unexpected external challenges have been encountered. There have been a number of power failures, one of which caused considerable damage to the experimental equipment. The forces of nature have also claimed their part in the reconstruction. During the verification period, there has been both flood and lightning, causing short circuits as well as air-condition failure, all with time consuming effort to solving them as they occurred.

6.3.3 Displacement measurements

As previously described, a new TSTM measurement setup had to be established and installed due to the strict accuracy requirements from the software. To study the accuracy of the LVDT measurement, the test specimen was uncovered and two strain gauges were glued to the specimen, one on each vertical side of the mid-section of the specimen. Load was applied manually by the motor control, and the length deformation was measured with the two LVDTs and with the strain gauges. The average deformation of the concrete specimen measured by the LVDTs and the strain gauges are given in Figure 6.9. When applying a load increment of 0.8 MPa, the deformation response measured by the LVDTs was approximately 4 % higher than measured by the strain gauges. However, when comparing these measurements, it should be remembered that while the strain gauges measure the length change over a rather small distance, the LVDTs measure the concrete length change over as much as 700 mm.

Figure 6.10 shows the length change measured by each specific LVDT and strain gauge on both sides of the TSTM concrete specimen. While the strain gauges measure a very similar length change on both sides, the LVDTs showed a difference of approximately 12 % between the right and the left side. Repeated load applications and appurtenant measurements gave the same results. The difference between the right and left LVDT measurement is most likely caused by an eccentricity in the experimental equipment as illustrated in Figure 6.11. While the strain gauges measure the length change over a rather small distance, the LVTDs measure the length change over 700 mm. The LVDTs would thus capture a potential eccentricity in the concrete specimen to a much larger extent than the strain gauges would. Taking into account the difference in measuring length, a 4 %

deviation in measured average length change between the LVDTs and the strain gauges must be considered as a very good agreement between the two measuring methods.

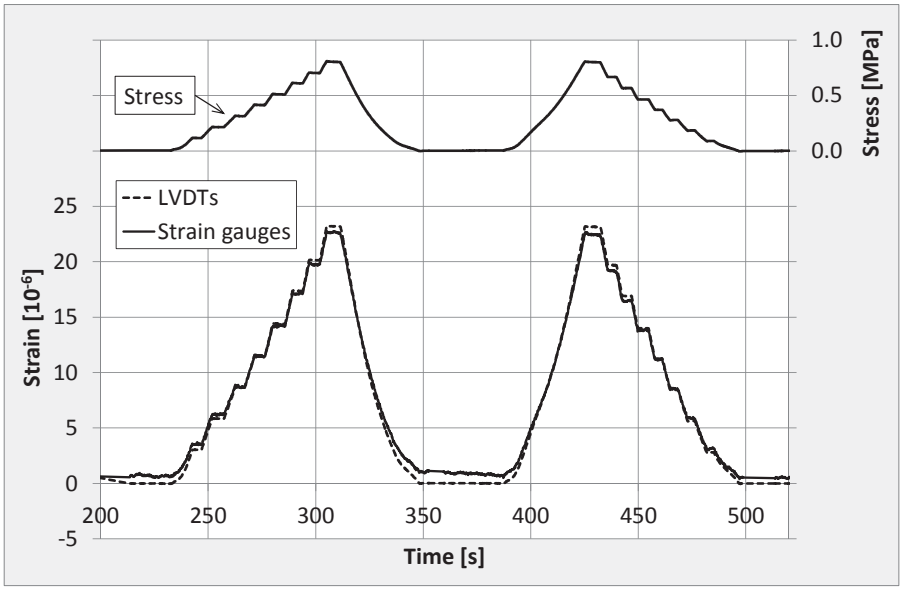

Figure 6.9; TSTM, strain gauges versus LVDTs

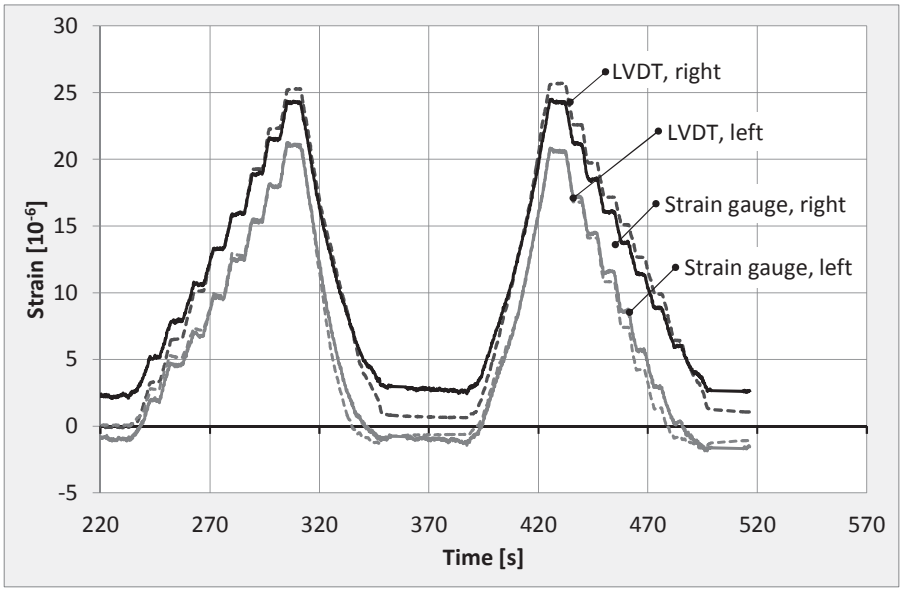

Figure 6.10; TSTM, strain gauges versus LVDTs with respect to eccentricity

A small uncertainty is connected to the strain gauge measurements as a small but increasing drift was discovered in the measurements over time. The drift was caused by a gradual failure in the glue with which the strain gauges were attached to the concrete specimen.

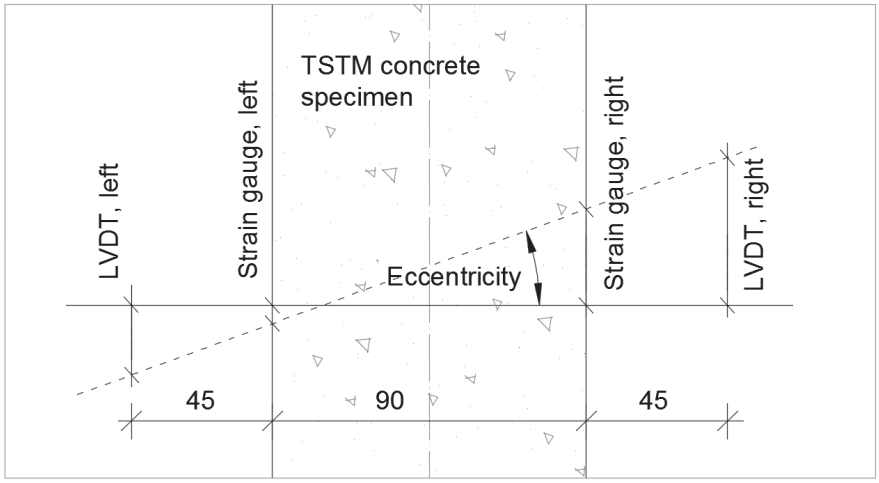

Figure 6.11; TSTM, length measurements and eccentricity

6.3.4 Load measurements

The original TSTM Load Cell (HBM 100kN) was providing stable results, but during a regular routine calibration in 2014, blind spots in the Load Cell measuring range were found. Due to the following risk of error during measurements, as well as the age of the original Load Cell, a new Load Cell (HBM Z4A) was calibrated and installed in May 2014.

6.3.5 External influence

Similar to the Dilation Rig as discussed earlier, also the TSTM was found to be influenced by the surrounding temperature. The temperature control in the room failed during one of the tests, and the room temperature increased with 7 ^{o}C. The measured stress showed a clear response as shown in Figure 6.12. The increase in room temperature of 7 ^{o}C resulted in a change in stress level of about 0.7 MPa, i.e. 0.1 MPa/^{o}C. As the TSTM now is located in a conditioned room normally keeping a constant temperature of 21 °C ± 0.5 °C, this external temperature influence will be very limited, and the potential influence will be only small fluctuations of the stress curve as the external room temperature oscillates.

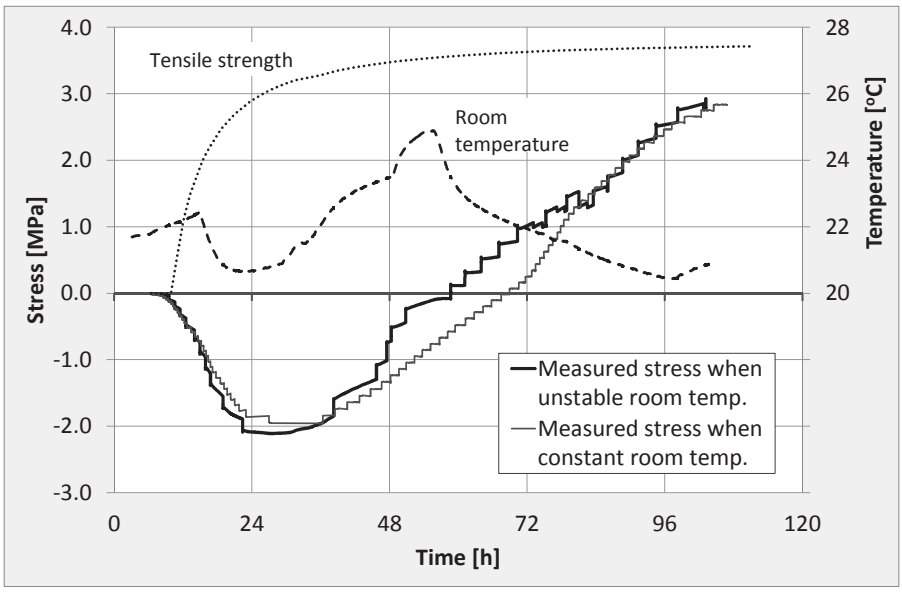

Figure 6.12; TSTM, stress development influenced by surrounding temperature

As for the Dilation Rig, the TSTM can infrequently be subjected to jolts caused by experiments in the surrounding locations. Such jolts will most likely be discovered and compensated for due to simultaneous leaps in the measured data for both the Dilation Rig and the TSTM.

6.3.6 Degree of restraint

One of the main advantages with the updated TSTM System is the possibility to select a degree of restraint (R) between 0 and 100 %. In the current section, an assessment of the chosen degree of restraint versus the actual obtained degree of restraint in the TSTM is conducted.

The degree of restraint R is entered as a parameter in the software, and it controls how much the concrete specimen is allowed to move. A degree of restraint of 0.0 (0 %) means that the specimen is free to move, while R = 1.0 (100 %) provides a fully restrained specimen. The application of the degree of restraint in the TSTM is illustrated in Figure 6.13. A threshold value for the measured length change in the TSTM, here denoted A, is entered as a parameter in the software. When this threshold value is reached, the software induces a feed-back regulation which moves the concrete specimen a distance $B = - R \cdot A$. Hence, the size of the software induced movement B for each regulation is decided by the degree of restraint R and the threshold value A chosen in the software.

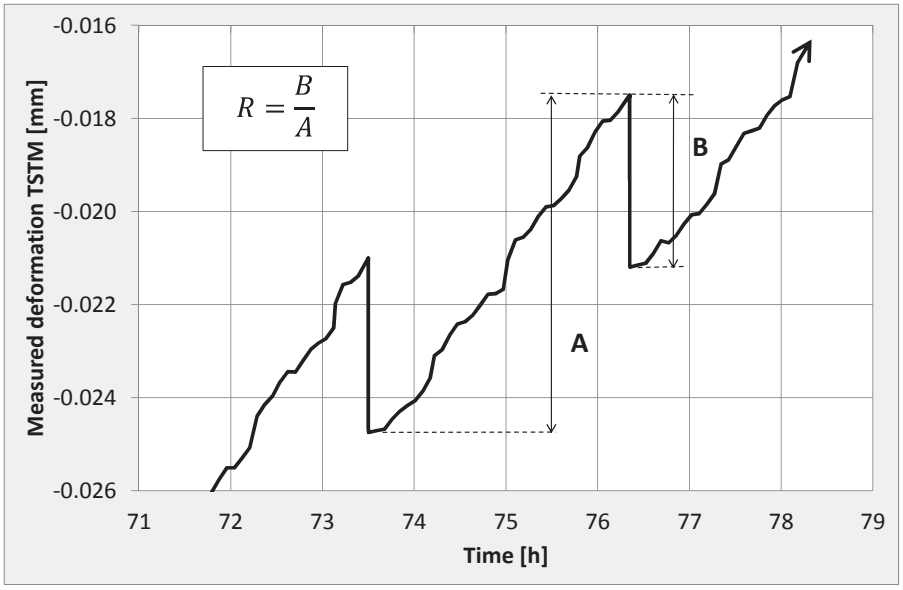

Figure 6.13; TSTM: degree of restraint

Initially, the measured feedback regulation B was found to be somewhat higher than $R \cdot A$. This was found to be caused by a small time delay in the system: as the software registered that the movement B was achieved and signalled for the motor to stop, the movement had already surpassed the value B, resulting in a larger feed-back regulation B than intended, and thus a higher achieved R than entered in the software. This was solved by adjusting and lowering the motor speed, allowing the software to react and respond quickly enough.

A close look at the strain-stress relation of a regulation showed that the force response was a little ahead of the length change, see Figure 6.14. This is assumed to occur due to 1) a small friction force in the crosshead support and/or 2) a small slippage in the LVDT contact points with the TSTM cast-in measuring bolts. The outer steel frame in the TSTM System was lubricated to reduce any friction. A small slippage Δ in the measurement each time the TSTM movement changes direction would influence the achieved R as given by Equation 6.1.

$$R = \frac{B + \Delta}{A + \Delta} \qquad \textit{Equation 6.1}$$

If the degree of restraint R is 100 % and thus $B = A$, the slippage Δ will have no influence on the achieved R. However, when decreasing the degree of restraint R and thus $B < A$, the slippage Δ will cause R to increase with decreasing B. By comparing the measured A and B with the entered R for several tests in the TSTM System, it was found that with a defined degree of restraint of R = 50 %, the actual degree of restraint in the System was approximately 54 %, i.e. 10 % higher than the degree of restraint applied in the software.

This relation is also dependent on the chosen deformation tolerance *A*, where the actually obtained *R* will decrease with an increasing *A*.

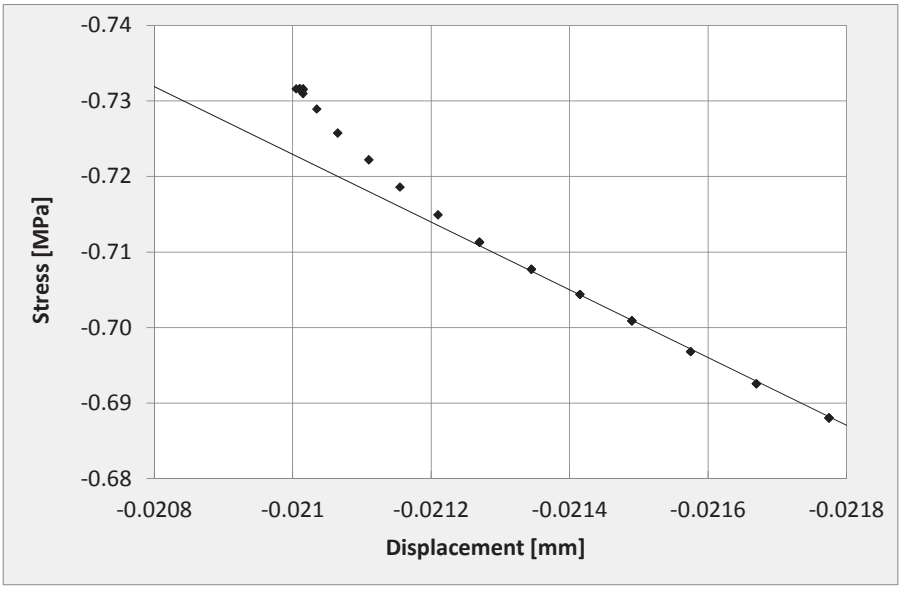

Figure 6.14; The initial stress-strain relation during a TSTM regulation

6.3.7 Incremental E-modulus development

When the TSTM deformation reaches its threshold value, the software is activated and a crosshead movement (regulation) is induced (see previous section and Section 5.3). When such an activation event is started, data are stored 10 times a second until the regulation is completed. This feature provides a comprehensive stress-strain relation for each TSTM regulation during an experiment, see Figure 6.15. From this stress-strain relation, an incremental E-modulus development (i.e. obtained from incremental loading) over time is provided for the concrete in question. The procedure used to determine the incremental E-modulus for each regulation in a TSTM test is described in the following: for each point in the measured stress-strain relation (illustrated in Figure 6.15), the E-modulus E_i was calculated as the secant E-modulus over a distance of 15 measuring points (i.e. between the points *i – 15* and *i*, representing a stress increment of approximately 0.06 MPa):

$$E_i = \frac{\sigma_i + \sigma_{(i-15)}}{\varepsilon_i + \varepsilon_{(i-15)}} \qquad \textit{Equation 6.2}$$

The E_i development over the stress-strain relation was plotted versus stress, and the incremental E-modulus was determined as the value the E_i development was approaching during the given regulation, see Figure 6.16.

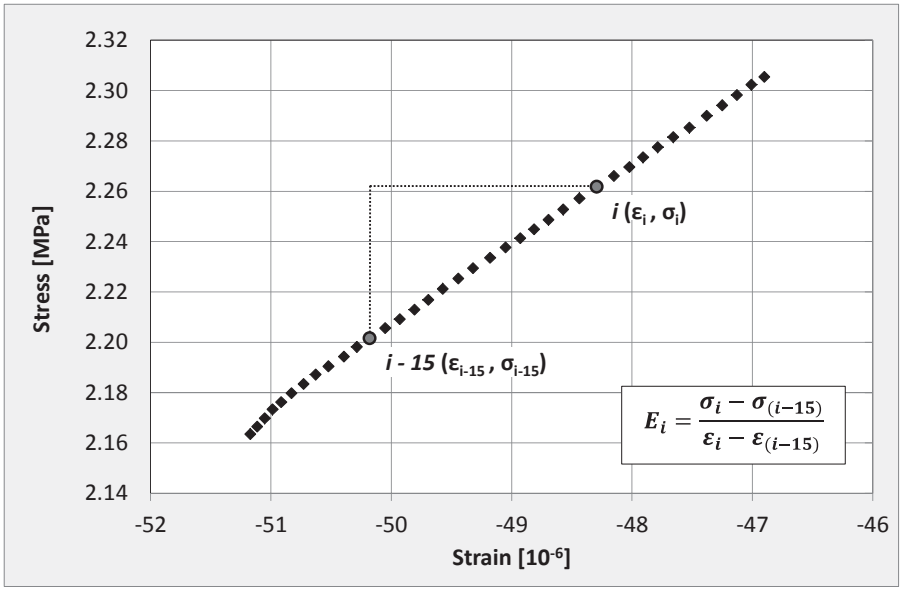

Figure 6.15; A typical stress-strain relation for a deformation-induced regulation during an experiment in the TSTM, ANL FA +16FA

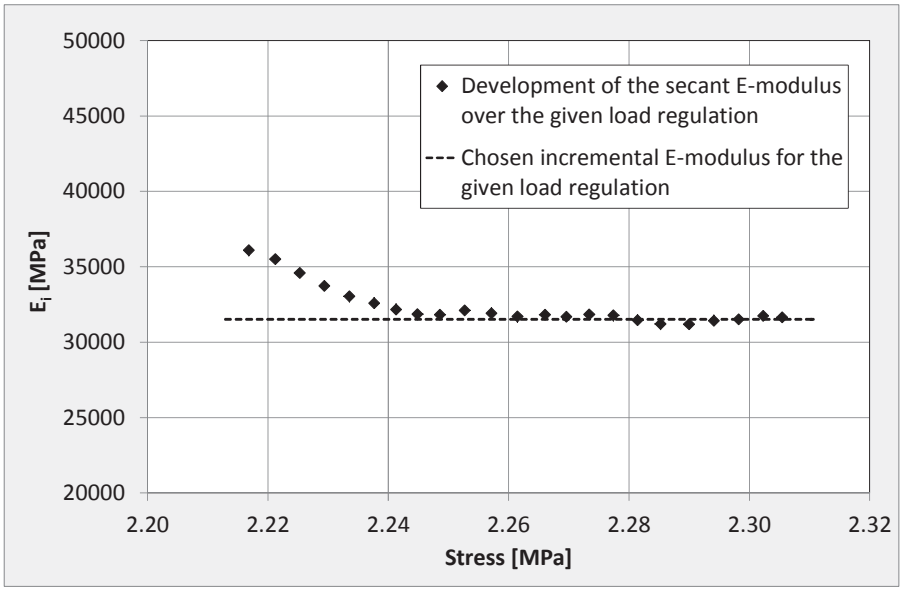

Figure 6.16; A typical secant E-modulus development E_i during a deformation-induced regulation in the TSTM, ANL FA +16FA

The incremental E-modulus development for *ANL FA +16FA* during a realistic temperature test in the TSTM is given in Figure 6.17. The figure also presents the E-modulus model based on mechanical testing, see Chapter 7.4. An elevated value (in this case 33400 MPa at 153 maturity hours, Figure 6.17) is seen for all tests as the TSTM movement changes direction from expansion to contraction, and it is most likely related to a small slowness/slippage in the TSTM System. The incremental E-modulus shows a somewhat faster development than the model, this is probably related to temperature effects caused by the realistic curing temperature as investigated and discussed in Chapter 7.6. The incremental E-modulus development provides a direct description of the actual E-modulus occurring in the given concrete specimen during testing in the TSTM System.

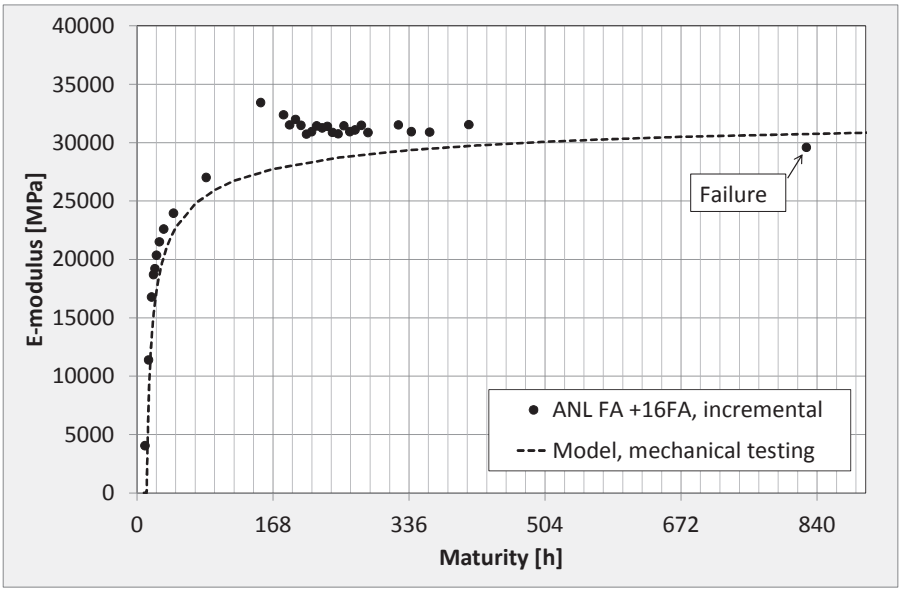

Figure 6.17; Incremental E-modulus development during a TSTM test, realistic temperature conditions, ANL FA +16FA

At the end of each performed TSTM tests, the specimen was unloaded and thereafter reloaded at a constant tensile strain rate until failure. This procedure provided an E-modulus at the end of the test determined from a continuous loading (quite similar to the uniaxial tensile strength test). The E-modulus at the end of the test has been calculated as the secant E-modulus between 10 % and 40 % of the ultimate tensile stress, i.e. over a stress increment in the order of magnitude of approximately 1.0 MPa.

The incremental E-modulus and the E-modulus at the end of the test are determined by two quite different approaches, but still they have been found to give rather similar results, see Chapter 8.5.2. To compare the two E-modulus approaches, the TSTM specimen was applied a compressive load of 0.8 MPa: first incrementally and then continuously, see Figure 6.18. The two consecutive loadings gave identical stress-strain relations regardless of the load application used, Figure 6.19. Further, the E_i development versus stress (E_i over

15 data steps as described above) were found for both loading conditions, Figure 6.20. E_i from the incremental load application starts at a somewhat higher value for each load increment, probably caused by an initial slowness in the system and/or a small slippage in the measuring devices. However, during each incremental loading, the E_i development gradually coincides with the E_i development determined from the continuous load application. Hence, using the final E_i value for each incremental loading will give an overall incremental E-modulus development equal to the E_i development obtained under a corresponding continuous loading.

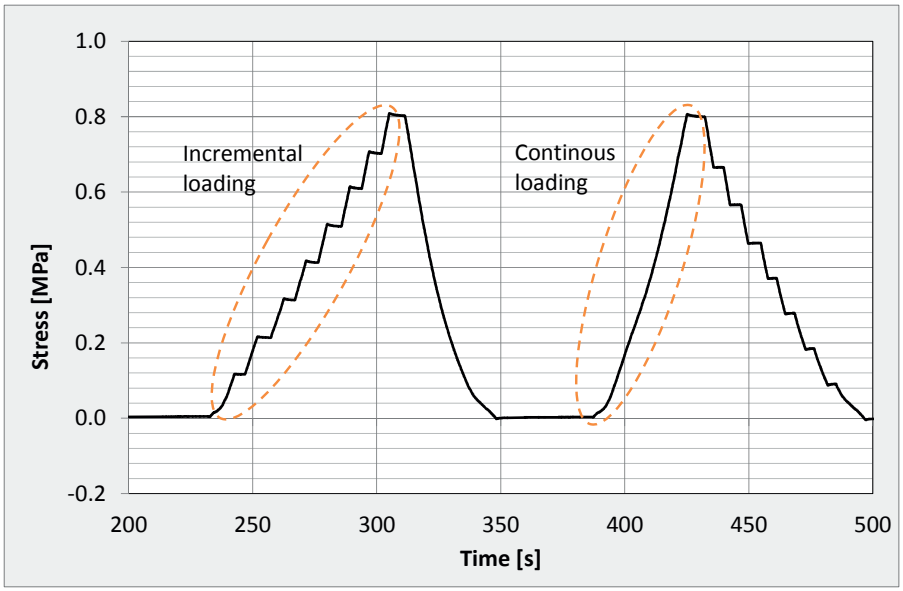

Figure 6.18; Incremental versus continuous compressive loading in the TSTM. ANL Ref.

While Figure 6.20 compares the E-modulus-stress relations for incremental and continuous compressive loading, a corresponding comparison under tensile loading conditions is given in Figure 6.21. One concrete specimen in the TSTM (*ANL FA +16FA*) was loaded in four different manners: 1) incrementally up to 0.6 MPa, 2) continuously up to 1.0 MPa, 3) continuously up to 1.4 MPa and 4) continuously until it developed failure in tension. All load applications resulted in the same E_i-stress relation. Although the incremental loading gave a relatively high E_i at the beginning of each load increment, the final value coincided with the E_i developments determined from the continuously applied loads. The incremental E-modulus development (i.e. the final E_i value for each load increment) does not directly reflect the ultimate E-modulus, as the latter is calculated over a larger interval. However, E_i will still represent the actual E-modulus development in the given concrete specimen with respect to stress calculations of the TSTM.

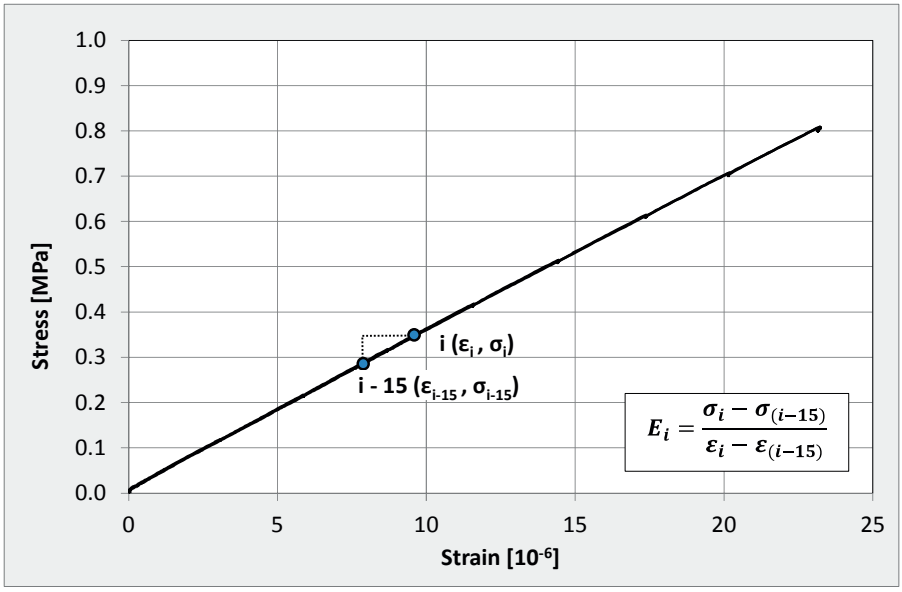

Figure 6.19; Stress-strain relation for both incremental and continuous compressive loading in the TSTM, ANL Ref.

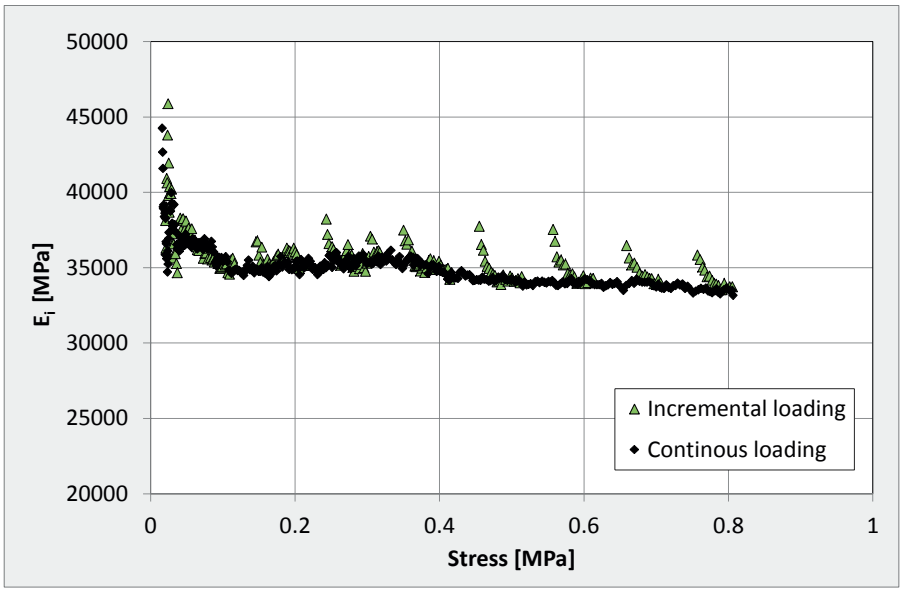

Figure 6.20; E_i development for incremental versus continuous compressive loading in the TSTM, ANL Ref.

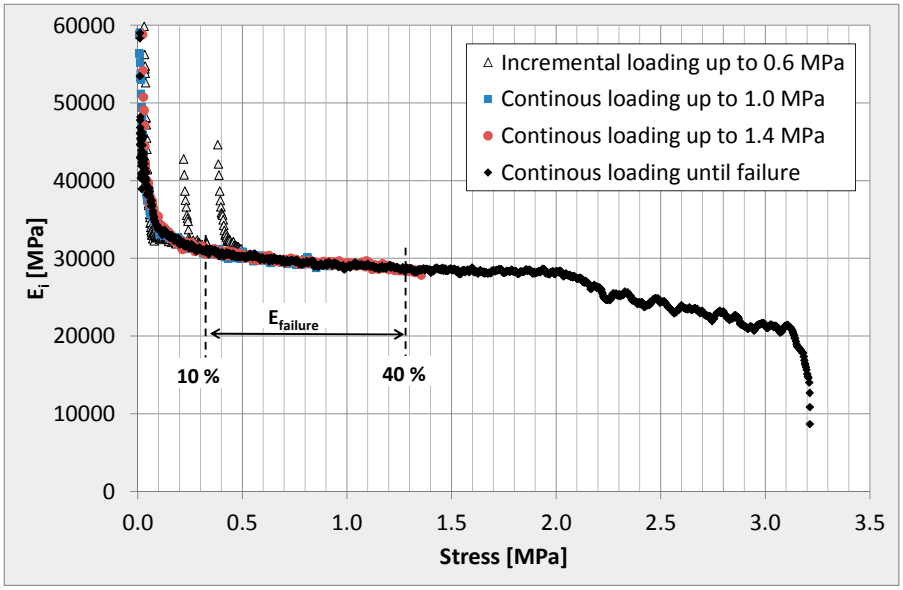

Figure 6.21; E_i development for incremental versus continuous tensile loading TSTM, ANL FA +16FA

In the literature, the tensile E-modulus is often described to be calculated from the "linear part of the stress-strain relation", e.g. [Yoshitake et al., 2012]. The shape of the currently found E_i-stress relations suggests however that there is no such "linear part". Instead, E_i is found to be gradually decreasing with increasing stress, Figure 6.21. This observation has been described by both [Neville, 1972] and [Brooks et al., 1977]. [Neville, 1972] stated that the magnitude of the curvature of the stress-strain relation depended on the rate of application of stress, and he concluded that "*Because the secant modulus decreases with an increase in stress, the stress at which the tensile E-modulus had been determined should always be stated.*" In the current work the following rates of stress applications have been used: 1) incremental loading: 0.04 MPa/s, 2) continuous loading: 0.03 MPa/s and 3) uniaxial tensile strength tests: 0.17 MPa/s.

To investigate if the presently found curvature of the stress-strain curve was related to the TSTM or if it was general, E_i-stress curves from TSTM tests were compared with corresponding curves deduced from uniaxial tensile strength tests, Figure 6.22. It should be noted that E_i for the mechanical tests are calculated over a larger stress interval than for the TSTM (0.40 MPa and 0.06 MPa, respectively). If a corresponding larger interval is chosen also for the TSTM data, a more even, however less detailed, E_i-stress curve would be obtained. Figure 6.22 shows that E_i obtained from uniaxial tensile strength tests show the same E_i-stress ratio as the TSTM (i.e. decreasing secant E-modulus with increasing stress). This conformity supports the validity of the results obtained from the TSTM, and it also suggests that the magnitude of the curvature of the stress-strain relation does not seem to

be dependent on the rate of application of stress, i.e. 0.04 MPa/s and 0.17 MPa/s for the TSTM and uniaxial tensile tests, respectively.

From the found shape of the E-modulus-stress relation, Figure 6.22, it follows that the E-moduli deduced from uniaxial tensile strength tests are very dependent on the stress interval from which they were determined. As previously described, in the current work, the tensile E-modulus has been calculated as the secant E-modulus between 10 % and 40 % of the ultimate tensile stress (from the SINTEF internal procedure KS 14-05-04-511). In the literature, several other such criteria have been found. [Onken et al., 1995] defined the tensile E-modulus as the average secant E-modulus between 5 % and 50 % of the tensile strength, while [Bjøntegaard, 1999] calculated the tensile E-modulus based on the data between the stress values 0.5 and 2.0 MPa. In a study by [Yoshitake et al., 2014], the tensile stress-strain curves in the tests were stated to be linear almost up to the maximum force, and thus the tensile E-modulus was defined from a gradient of the linear best fit. However, during the current literature study several articles were found which did not state the stress interval from which the tensile E-moduli were determined. This is unfortunate because neither the tensile E-modulus nor the relation between tensile and compressive E-moduli can automatically be compared or adopted between different studies unless the criteria from which the moduli were determined are the same. For instance, for the currently performed TSTM tests, using the data between 10 and 40 % of the tensile strength provided a tensile E-modulus at the end of the test which was approximately 1.0 GPa lower than if the data between 0.5 and 2.0 MPa had been used.

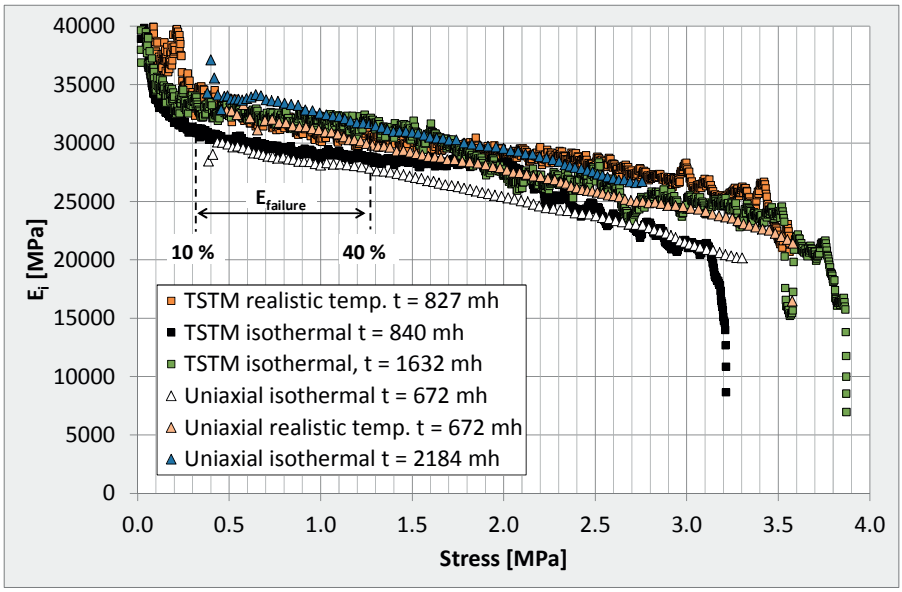

Figure 6.22; Tensile E-modulus from the TSTM and from uniaxial tensile strength tests, 20 ^{o}C isothermal conditions and realistic temperature conditions, ANL FA +16FA

6.3.8 Reproducibility

Several verification- and introductory tests have been performed in the TSTM. Repeated nominally identical tests indicate good reproducibility for both isothermal and realistic temperature conditions. The tests representing the TSTM reproducibility are summarized in Table 6.4 and the test results are presented in Figure 6.23 - Figure 6.27.

Table 6.4; TSTM reproducibility: repeated nominally identical tests

Concrete	Temperature conditions	No. of tests	Figure
ANL Ref.	20 ^{o}C isothermal	2	Figure 6.23
	Realistic temp. history	3	Figure 6.24
ANL FA	Realistic temp. history	2	Figure 6.25
ANL FA +16FA	20 ^{o}C isothermal	2	Figure 6.26
	Realistic temp. history	2	Figure 6.27

The tests presented in the current section were conducted during the years 2013-2015. Parallel to the testing, several adjustments and actions were initiated and performed to correct and complete the TSTM System (i.e. adjustments of the measuring length setup, adjustments of the software parameters, stabilisation of the surrounding temperature and air humidity conditions, change of cement batch, etc.). Hence, there are some variations in the experimental details among the performed tests. Numerical evaluations of the reproducibility of the tests presented in the current chapter are given in Table 6.5 - Table 6.7.

Figure 6.23 shows measured stress development for two TSTM tests performed with the reference concrete, *ANL Ref.*. The concrete specimens were applied a degree of restraint of 100 % and exposed to 20 ^{o}C isothermal temperature conditions. The two tests in Figure 6.23 were performed six months apart, and show very good reproducibility. Table 6.5 shows a standard deviation of only 0.02 MPa at both 48 and 192 hours for the two tests.

Stress developments measured for three realistic temperature TSTM tests performed with the reference concrete, *ANL Ref.,* are given in Figure 6.24. The degree of restraint was set to 50 %. The tests were performed with identical realistic temperature histories, which represents the average temperature in a selected section of an 800 mm thick wall structure exposed to Norwegian summer conditions, see Section 7.3. The applied realistic temperature history is given in Figure 6.24. The time duration of the tests varies. The numerical evaluation presented in Table 6.5 clearly proves that the reproducibly among the *ANL Ref.* tests are very good. The standard deviation for three nominally identical realistic temperature tests is only 0.03 MPa after 48 hours, while the standard deviation for the two tests still remaining at 96 hours is 0.06 MPa.

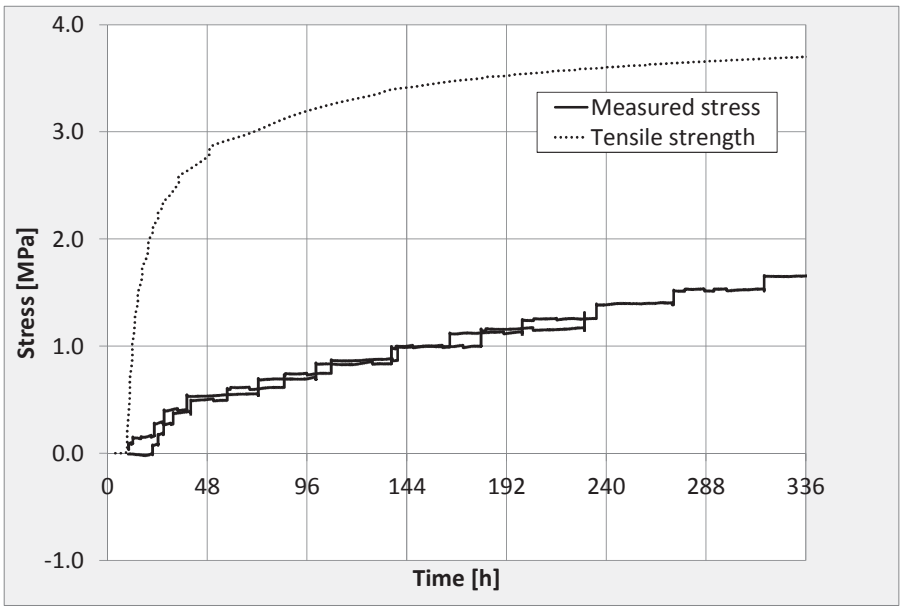

Figure 6.23; Two nominally identical tests in the TSTM. Concrete ANL Ref., 20 °C isothermal conditions, R = 100 %)

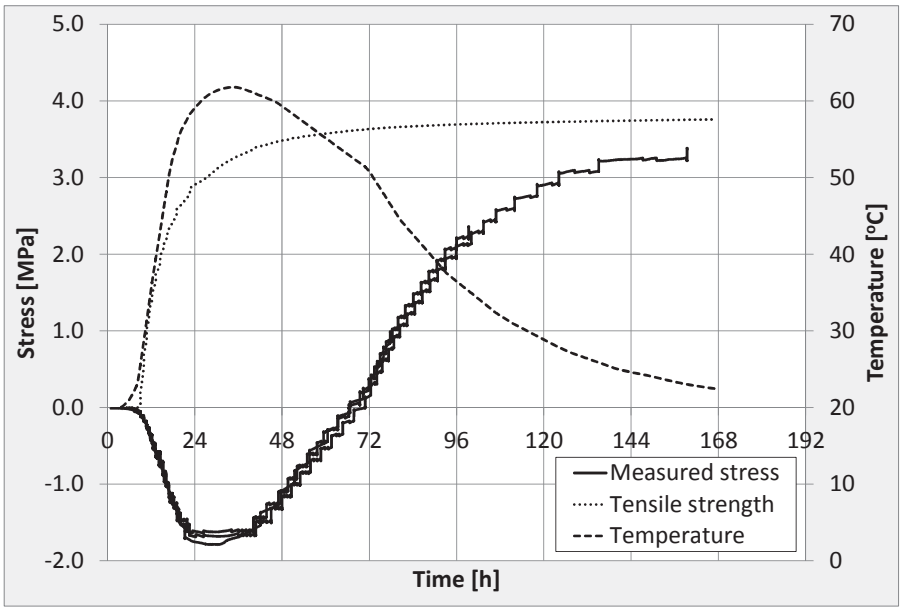

Figure 6.24; Three nominally identical tests in the TSTM. Concrete ANL Ref., realistic temperature conditions, R = 50 %

Table 6.5; TSTM reproducibility: numerical evaluation of ANL Ref.

Test	Age [h]	No of tests	Min	Max	Mean	SD
20 °C isothermal	48	2	0.50	0.53	0.52	0.02
	192	2	1.12	1.16	1.14	0.02
Realistic temperature	48	3	-1.16	-1.09	-1.12	0.03
	96	2	2.09	2.20	2.14	0.06

Figure 6.25 shows the measured restrained stress developments for two nominally identical realistic temperature *ANL FA* tests applied a degree of restraint of 50 %. The stress developments measured for the two tests are almost identical during the compression phase, but a small deviation seems to occur during the tensile stress development phase, i.e. after approximately 60 hours. Table 6.6 gives a standard deviation of 0.04 MPa at 48 hours, while the standard deviation after 80 hours is 0.15 MPa.

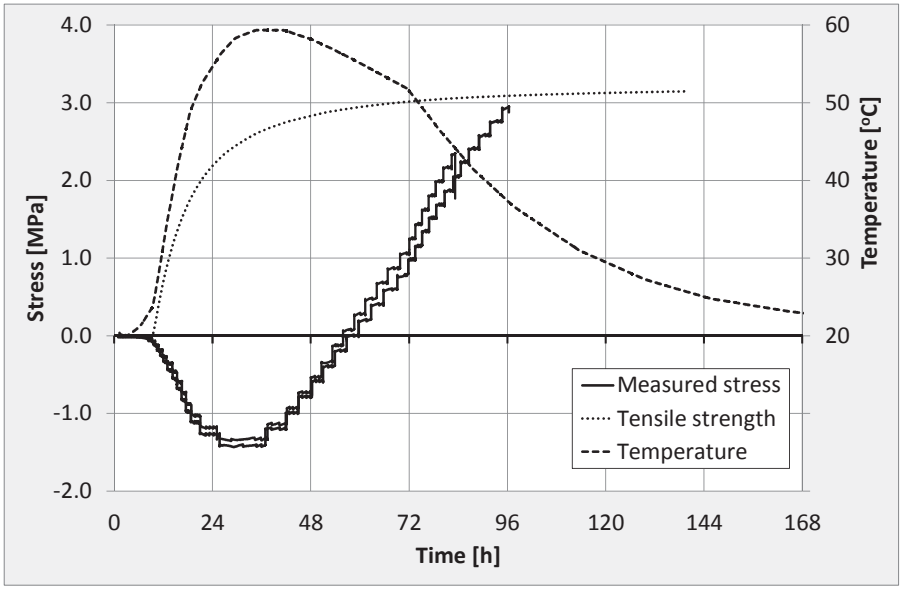

Figure 6.25; Two nominally identical tests in the TSTM. Concrete ANL FA, realistic temperature conditions, R = 50 %

Table 6.6; TSTM reproducibility: numerical evaluation of ANL FA

Test	Age [h]	No of tests	Min	Max	Mean	SD
Realistic temperature	48	2	-0.80	-0.71	-0.76	0.04
	80	2	1.70	2.00	1.85	0.15

Figure 6.26 - Figure 6.27 present results from tests performed with the concrete *ANL FA +16FA*. Figure 6.26 shows total deformation measured in the TSTM for two nominally identical creep tests run under 20 ^{o}C isothermal conditions. One of the tests failed approximately 24 hours after loading due to a failure in the LVDT spring support, but up until failure the length measurements are almost identical for the two nominally identical tests. The numerical evaluation presented in Table 6.7 shows that the standard deviation at 240 hours is only 0.2 µstrain for the two given tests, which must be considered very good.

Figure 6.27 shows measured stress development for two TSTM tests performed with *ANL FA +16FA* under realistic temperature conditions. The degree of restraint was set to 50 %. The compressive stress measured for the two tests are almost identical. Table 6.7 shows that the standard deviation after 48 hours is 0.03 MPa, which must be considered rather small. However, during the tensile stress development phase, i.e. after approximately 84 hours, an increasing deviation in measured stress development can be seen. After 240 hours, the difference in tensile stress between the two tests is 0.47 MPa, which gives a standard deviation of 0.24 MPa. The obtained difference in stress development may be partly explained by: 1) a small difference in the deformation tolerance chosen in the software for the two tests and 2) an observed scatter in E-modulus development between the two tests. The test with the highest tensile stress was applied a slightly lower deformation tolerance threshold value, causing a small increase in the actually obtained degree of restraint *R* when compared with the other test (in this case estimated to an increase in *R* of approximately 0.5 %), see Section 6.3.6. In addition, the test with the highest tensile stress development showed a higher incremental E-modulus (approximately 6.0 %) during the entire TSTM test, which could further partly explain the increase in tensile stress.

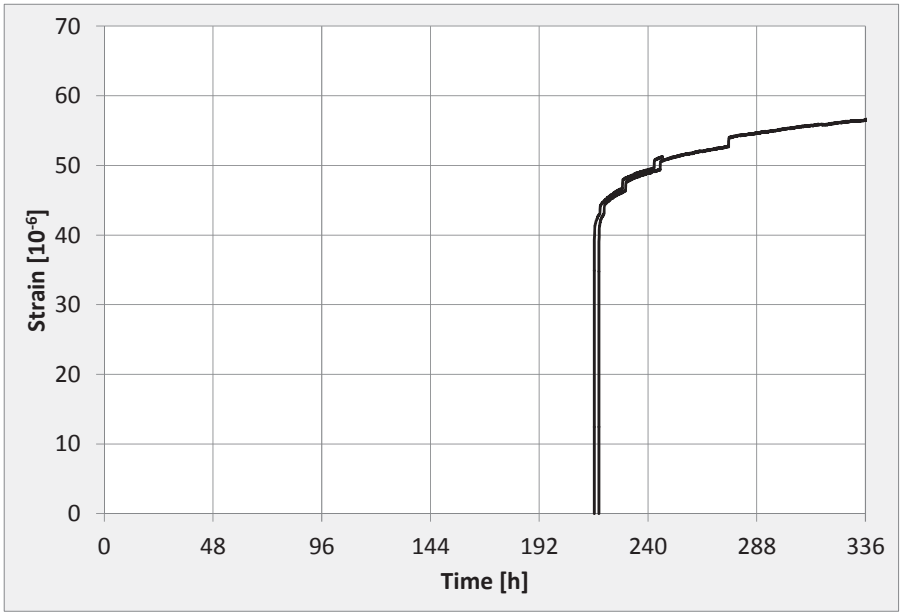

Figure 6.26; Two nominally identical creep tests in the TSTM. Concrete ANL FA +16FA, isothermal 20 °C

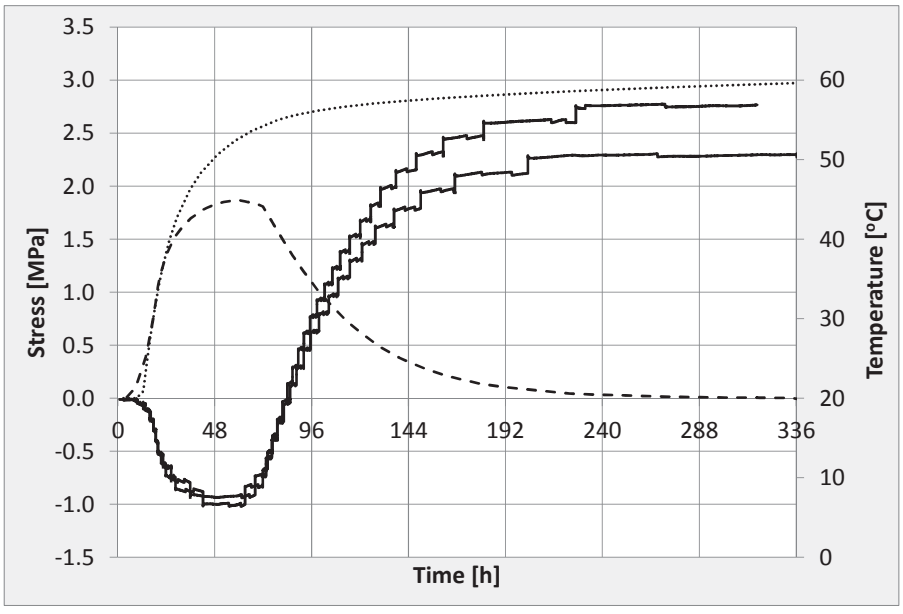

Figure 6.27; Two nominally identical tests in the TSTM. Concrete ANL FA +16FA, realistic temperature conditions, R = 50 %

Table 6.7; TSTM reproducibility: numerical evaluation of ANL FA +16FA

Test	Age [h]	No of tests	Min	Max	Mean	SD
20 °C isothermal (deformation [μstrain])	240	2	48.9	49.3	49.1	0.20
Realistic temperature (stress [MPa])	48	2	-1.00	-0.94	-0.97	0.03
	96	2	0.62	0.77	0.70	0.08
	240	2	2.29	2.76	2.53	0.24

6.4 Temperature Control

The Dilation Rig and the TSTM are both connected to the same temperature control unit: a Julabo FP45 (described in Section 5.4). Both rigs in the TSTM System are connected to the same temperature control unit, but in parallel, separate circuits. The length of the two separate circuits of tubes with circulating water is quite different for the two rigs. The current section discusses this issue and how to handle the temperature control system in order to achieve the same temperature history in both rigs.

It should be noticed that the accuracy of the Type T thermocouple used for temperature measurements in the current work is ± 1.0 °C. This should be taken into consideration during the evaluation.

Prior to a realistic temperature test in the TSTM System, a specific temperature history to be applied the concrete specimens is calculated based on the heat properties for the given concrete. However, due to heat loss to the surroundings, the temperature programmed in the Julabo (the Julabo water temperature) is not exactly equal to the temperature occurring in the centre of the two concrete specimens. Consequently, a calculation procedure to compensate for the difference between the following three temperature histories has been established:

1) Original calculated temperature history, $T_{calculated}(t)$
2) Temperature history programmed in the Julabo, $T_{julabo}(t)$
3) Temperature measured in the TSTM, $T_{TSTM}(t)$ (≈ the Dilation Rig $T_{Dil}(t)$)

A relation between $T_{julabo}(t)$ and $T_{TSTM}(t)$ was found by programming a series of temperature steps in the Julabo and comparing the programmed Julabo temperature with the corresponding temperature measured in the TSTM. The deviation between programmed and measured temperatures was found to be linearly increasing with increasing temperature level for both rigs. Figure 6.28 shows the original calculated

temperature $T_{calculated}(t)$ versus actually measured temperature in the specimen centre $T_{TSTM}(t)$ for four of the temperature histories used in the verification tests. The calculated temperature history programmed in the Julabo $T_{julabo}(t)$ (which is higher than $T_{calculated}(t)$ to compensate for the heat loss) is not given in the figure. The figure shows that the established relation between desired and programmed temperature gives rather good control.

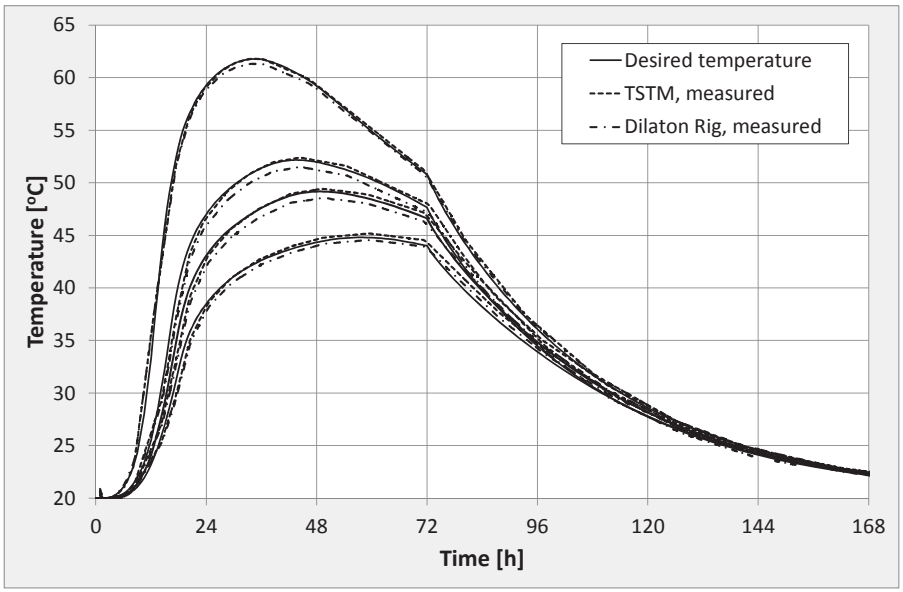

Figure 6.28; Temperature control: desired (calculated) temperature history versus temperature measured in the centre of the specimens of the TSTM and the Dilation Rig

In addition to the described difference between programmed temperature and temperature measured in the TSTM, there is also, as previously described, a deviation between the temperatures measured in the Dilation Rig, $T_{Dil}(t)$, and the TSTM, $T_{TSTM}(t)$. This temperature difference is corrected for in the evaluation phase, but it is still aspired to keep the difference as small as possible. Figure 6.29 shows the difference between the temperatures measured in the Dilation Rig and the TSTM during both isothermal and realistic temperature tests. For the isothermal tests, the temperature difference between the Dilation Rig and the TSTM is maximum 0.2 °C. For the realistic temperature tests, the temperature difference between the two rigs is, not surprisingly, found to be increasing with increasing temperature level. For the highest test temperature, T_{max} = 62 °C, the temperature measured in the TSTM is 0.9 °C higher than the temperature measured in the Dilation Rig, implying that the temperature control of the TSTM is more effective than for the Dilation Rig.

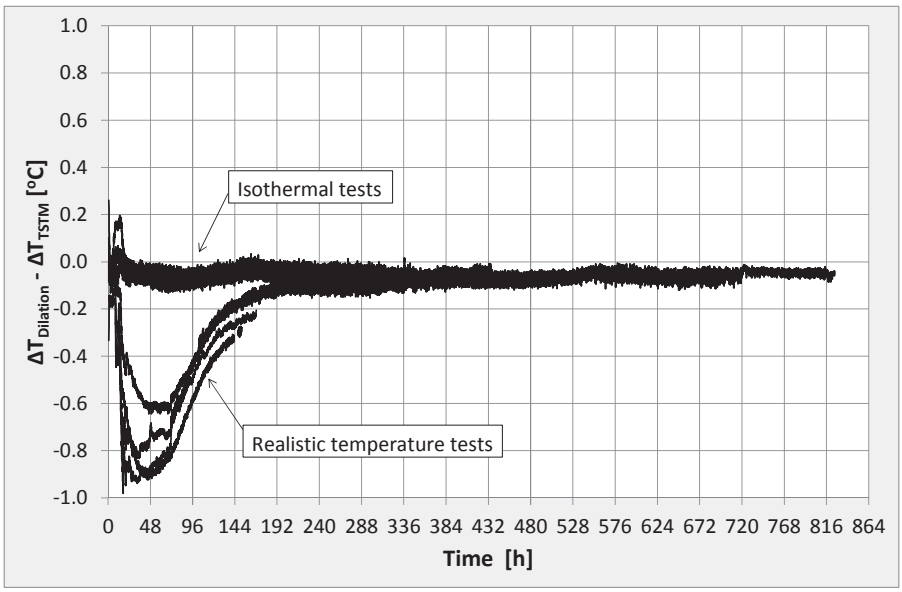

Figure 6.29; Temperature difference between measured temperature in the Dilation Rig and the TSTM for three isothermal tests and four realistic temperature tests

During spring 2015, corrosion in the quick release coupling between the temperature-control unit and the Dilation Rig was discovered. The corrosion had gradually damaged the coupling and reduced the inner water flow cross-section area and hence the temperature control efficiency. The damaged coupling was removed, and the temperature control in the Dilation Rig obtained increased efficiency, making the temperature control of the Dilation Rig more efficient than for the TSTM. This is as expected and explained by the path of the circulating water, which is about six times longer in the TSTM than in the Dilation Rig. As a measure to achieve the same temperature control efficiency for the two rigs, a butterfly valve was installed to narrow the cross-section of the Dilation Rig water supply. In this way, more or less identical temperature histories may now be obtained for the two rigs. Figure 6.30 shows the relation between the following four temperatures: 1) Calculated desired temperature, 2) Temperature programmed in the Julabo, 3) Temperature measured in the TSTM and 4) Temperature measured in the Dilation Rig, for a test performed after the butterfly valve was installed. The results reveal good temperature agreement between the two rigs in the TSTM System, as well as between the original calculated temperature and the temperature actually obtained in the two concrete specimens.

The majority of the tests performed in the current work were already carried out when the corrosion problem was discovered and the coupling was replaced. Hence, the above discussions and results are valid for most of the reported tests. Although the efficiency of the Dilation Rig has changed, the general conclusion is that when using data from Julabo temperature loops run in the TSTM System, a reliable and stable relation between imposed (programmed) temperature and measured temperature can be determined. By integrating

this relation into the calculation of the Julabo temperature input, a good control of the desired, imposed and obtained temperature history the concrete specimens during testing can be achieved.

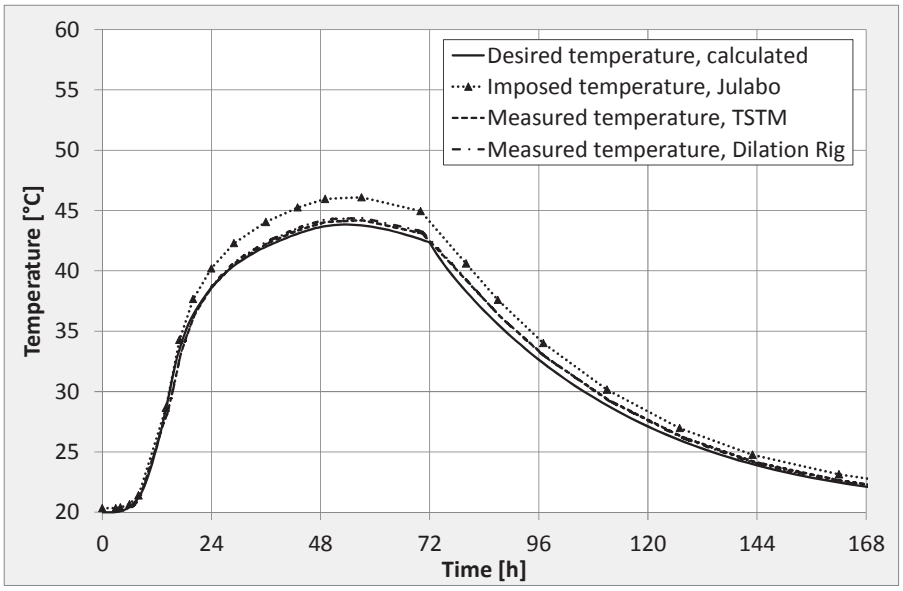

Figure 6.30; Temperature control: imposed temperature vs measured temperature, after removing the corroded quick release couplings

A uniform temperature distribution over the concrete specimens during testing is also important. This issue was investigated by [Bjøntegaard, 1999], who performed restrained stress tests with several thermocouples placed over the cross-section of the specimens. The conclusion was that the temperature in both specimens in the TSTM System was uniform during both isothermal tests and realistic temperature tests.

7 Experimental basis for stress calculations and determination of model parameters

7.1 Introduction

A mechanical test programme has been carried out with the aim to establish a basis of model parameters for early age stress calculations. The current section gives a presentation of the test results and the corresponding established material parameters. The following test series have been performed:

- Heat development from semi-adiabatic calorimeter tests
- Mechanical properties under 20 ^{o}C isothermal conditions
- Mechanical properties, effect of curing temperature history
- Creep tests in the TSTM System

The heat development results, Section 7.2, were used for calculations of realistic test temperatures, Section 7.3. Results from the mechanical test series under 20 ^{o}C isothermal conditions, Section 7.4, were used as a basis for model parameters determination for compressive strength, tensile strength and E-modulus. The test series that investigated the effect of curing temperature on the mechanical properties was used to evaluate whether or not the curing temperature had to be taken into consideration in terms of the end-value for each property, Section 7.6.

As described in Chapter 4, the concrete series consists of five concretes: *ANL Ref.*, *ANL FA*, *ANL FA +8FA*, *ANL FA +16FA* and *ANL FA +28FA*. The concretes have a fly ash content of 0 %, 17 %, 25 %, 33 % and 45 %, respectively, achieved by increasingly replacing cement with fly ash (the fly ash content is given as percentage of the total amount of cement + FA).

Based on the test results and corresponding evaluations presented in the following sections, a final set of material parameters has been established. The final material parameters, used as input during the later restrained stress analysis, are summarized in Section 7.9.

7.2 Heat development

The results from the semi-adiabatic calorimeter tests are presented as adiabatic temperature developments in Figure 7.1 - Figure 7.2, and as isothermal heat development in Figure 7.3 and Figure 7.4. A tabulated version of the isothermal heat development is given in Appendix B. As described in Section 4.2: during the current work, two batches of cement, EG1-10 (ANL cement) and TF3-11 (ANL FA cement), went short and had to be replaced with new ones, EG1-14 and TF5-14, respectively. Semi-adiabatic calorimeter tests were performed for the given concrete series for all cement batches. However, *ANL FA +28FA* was added to the concrete series after the cement batches were replaced, and its heat development is thus only measured with the new cement batch TF5-14. Figure 7.3 shows

the isothermal heat development results for the concrete series with the originally used cement batches (EG1-10 and TF3-11), and Figure 7.4 the repeated series with the new cement batches (EG1-14 and TF5-14) including also *ANL FA +28FA*. It can be seen directly from the two figures that the heat development for comparable concretes are quite different. However, the effect of increasing FA content is in both cases reduced heat increase, as expected. While the new ANL cement had a small decrease in heat development compared to the first batch, the new ANL FA cement had a considerable increase. Consequently, with the new cement batches there was less difference in heat development between *ANL Ref.* and the fly ash concretes based on ANL FA cement.

Table 7.1 presents the total adiabatic temperature increase after 20 and 60 hours. The table shows that the new batch of ANL FA cement, TF5-14 (which is the basis for all concretes containing FA), has a considerable impact on the concrete heat development, especially early in the hardening phase (i.e. before approximately 50 hours). For *ANL FA +16FA*, the use of cement batch TF5-14 compared to batch TF3-11 caused a 53% increase in adiabatic temperature rise after 20 hours. The corresponding increase in adiabatic temperature rise at 60 hours is 16 %. It is evident that the change of cement batch has had a major impact on the heat development for all the fly ash concretes.

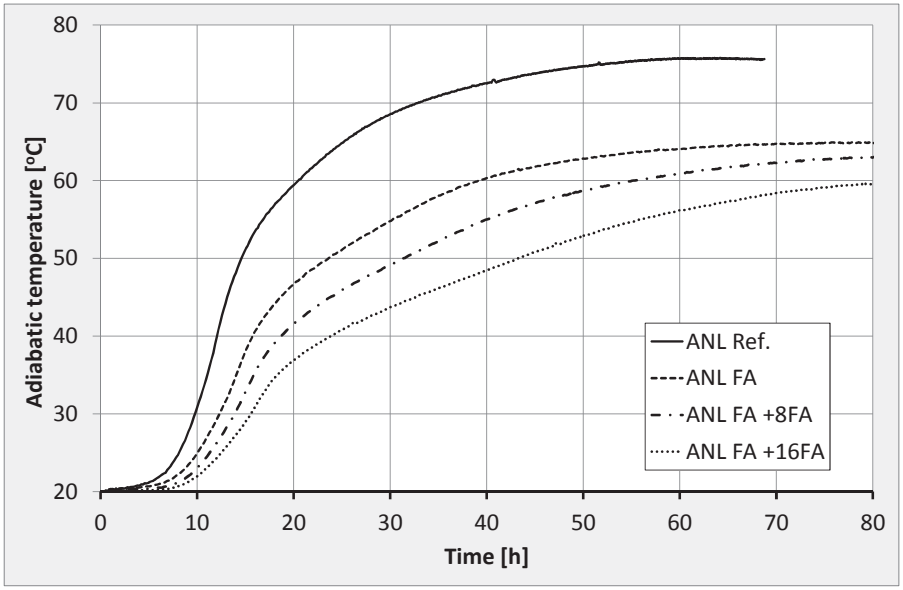

Figure 7.1; Adiabatic temperature development, cement batch EG1-10 and TF3-11

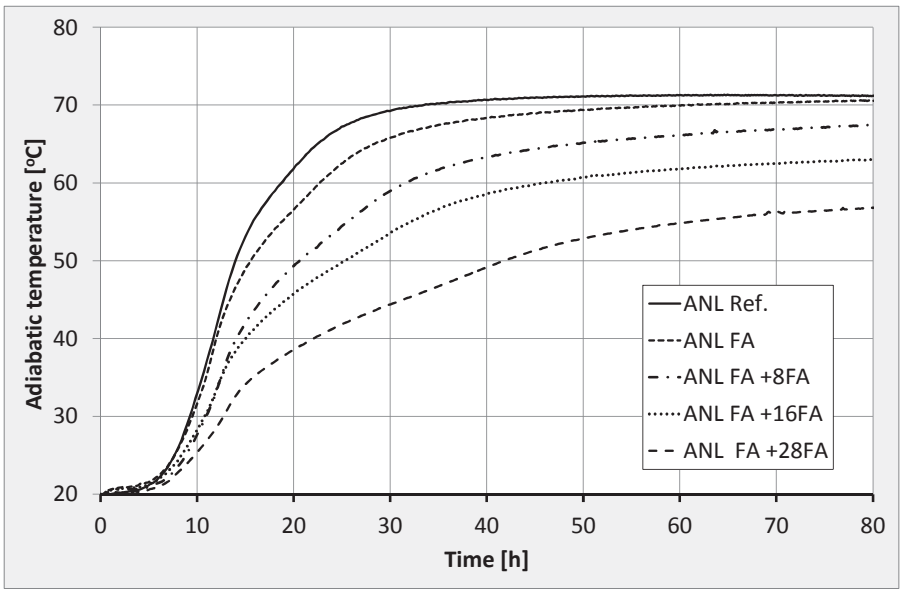

Figure 7.2; Adiabatic temperature development, cement batch EG1-14 and TF5-14

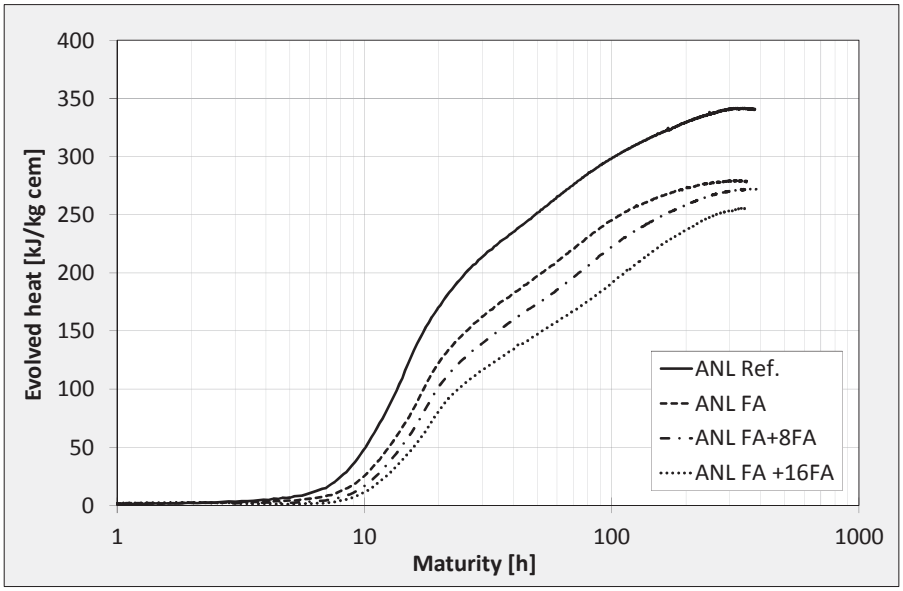

Figure 7.3; Isothermal heat development, cement batch EG1-10 and TF3-11

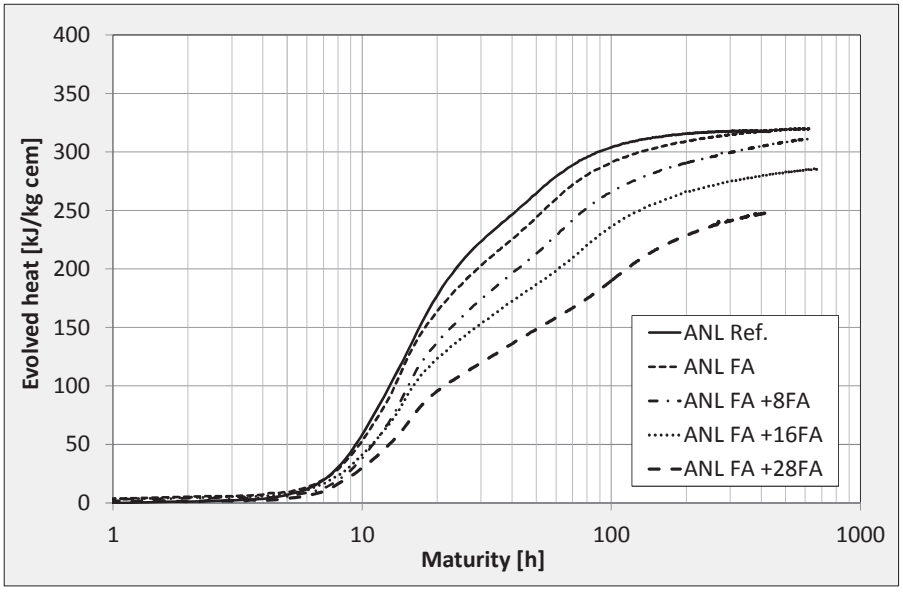

Figure 7.4; Isothermal heat development, cement batch EG1-14 and TF5-14

Table 7.1; Adiabatic temperature rise after 20 hours and 60 hours

Concrete	**Cement**	ΔT_{ad} **(20 h)** [°C]	$\frac{Cem_{new}}{Cem_{orig}}$ *	ΔT_{ad} **(60 h)** [°C]	$\frac{Cem_{new}}{Cem_{orig}}$ *
ANL Ref.	EG1-10	39.4	-	55.7	-
	EG1-14	41.8	1.06	51.3	0.92
ANL FA	TF3-11	26.7	-	44.1	-
	TF5-14	36.5	1.37	49.9	1.13
ANL FA +8FA	TF3-11	21.7	-	40.9	-
	TF5-14	29.2	1.35	46.1	1.13
ANL FA +16FA	TF3-11	16.8	-	36.2	-
	TF5-14	25.7	1.53	41.9	1.16
ANL FA +28FA	TF5-14	18.5	-	34.8	-

**) Adiabatic temperature rise for the new cement batches (EG1-14 and TF5-14) relative to the originally used cement batches (EG1-10 and TF3-11)*

7.3 Realistic temperature histories

The majority of the performed TSTM tests have been carried out under semi-adiabatic conditions, i.e. the concrete specimens have been subjected to a realistic temperature history during testing. These temperature histories were calculated with the program CrackTeSt COIN [JEJMS Concrete AB, 2009-2012]. The calculations were based on the heat development results reported in the previous section and on a wall structure as described in the following.

The wall is 800 mm thick and 4200 mm high, and it is cast onto a 1000 mm thick foundation, see Figure 7.5. The following calculation results (which are used later during the experiments to control the test temperatures) are the average temperature of a 200 x 800 mm cross section area marked in grey in Figure 7.5. Calculation presumptions, e.g. initial and ambient temperatures and heat convection coefficients, are summarized in Table 7.2 and Table 7.3. For each concrete, two temperature histories were calculated representing: 1) Norwegian summer conditions and 2) Norwegian winter conditions. The temperature histories representing summer conditions were calculated for both the original and new cement batches (discussed in the previous section). The winter temperature histories, however, were calculated only for the new cement batch. The calculation results are given in Figure 7.6, Figure 7.7 and Figure 7.8 (where the presented temperature curves are the average of the grey area in Figure 7.5). As expected, the calculated temperature rise in the given cross-section becomes both lower and slower with increasing fly ash content for both ambient temperature conditions regardless of cement batch.

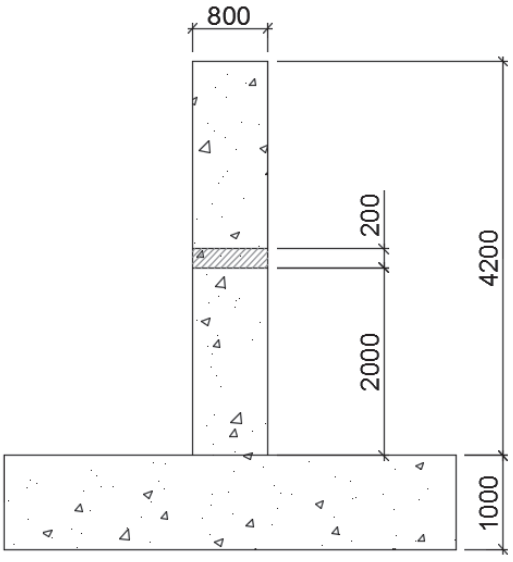

Figure 7.5; Wall structure used for temperature calculations [mm]

Table 7.2; Calculation presumptions: temperatures and formwork removal

	Summer	**Winter**
Initial concrete temperature	20 °C	10 °C
Initial foundation temperature	20 °C	10 °C
Ambient temperature	20 °C	5 °C
Removal of formwork	3 days	No removal

Table 7.3; Convection coefficients for the concrete boundaries

	$\mathbf{h_{surf}}$ [W/m^{2}K]	**Boundary**
Formwork	3.33	18 mm plywood, no wind
Free surface	12.6	Free surface, wind v = 1.5 m/s

Table 7.4 presents the maximum temperature T_{max} and the maximum temperature increase ΔT_{max} for all calculated temperature histories. The table clearly illustrates the fact that the new ANL FA cement batch, TF5-14, has considerable more heat than the original batch. Figure 7.9 compares calculated temperature results directly for original and new cement batches for *ANL Ref.* and *ANL FA*. For *ANL FA*, the change of cement batch causes a 9 °C (24 %) increase in ΔT_{max}. The main difference in temperature increase arises in the heat development phase, while the difference after the chosen demoulding time of 72 hours is not that pronounced. *ANL Ref.* is however not much influenced by the cement batch exchange, with a change in maximum temperature of only 2 %.

Due to the major difference in heat development (and thus concrete temperature development) for the two ANL FA cement batches TF3-11 and TF5-14, the initially calculated temperature histories based on TF3-11 no longer represent the same concrete structure when the new cement batch TF5-14 is used. This has been taken into consideration in the further evaluations.

The temperature histories representing winter conditions (Figure 7.8) were calculated based on the new cement batches (EG1-14 and TF5-14). As expected, winter conditions have a considerable influence on the calculated temperature history in the way that the temperature increase is lower than for summer conditions. When exposed to winter conditions, *ANL FA +28FA* has a maximum temperature of only 26.1 °C, while the maximum temperature during summer conditions was found to be 43.8 °C.

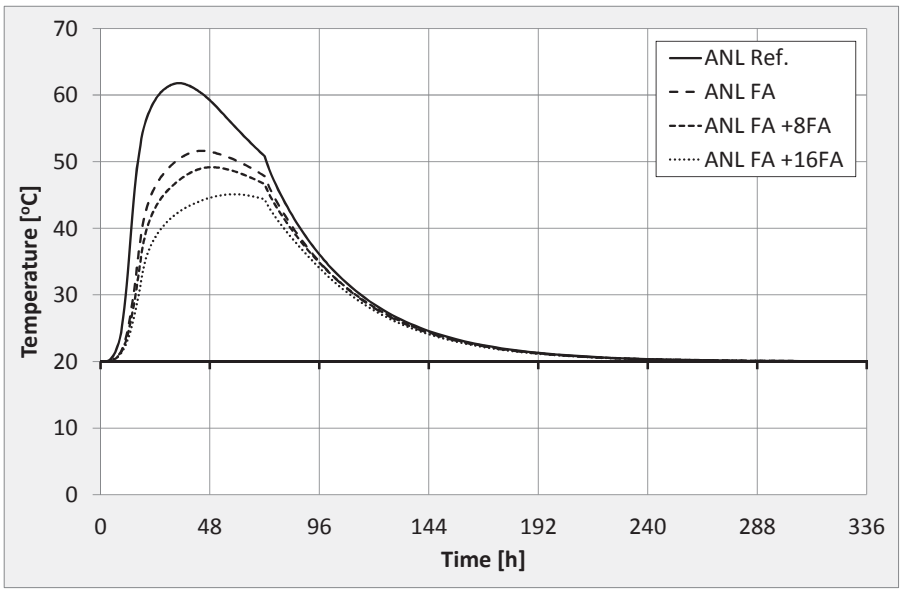

Figure 7.6; Average calculated wall temperature in selected area under summer conditions, original cement batch EG1-10 and TF3-11

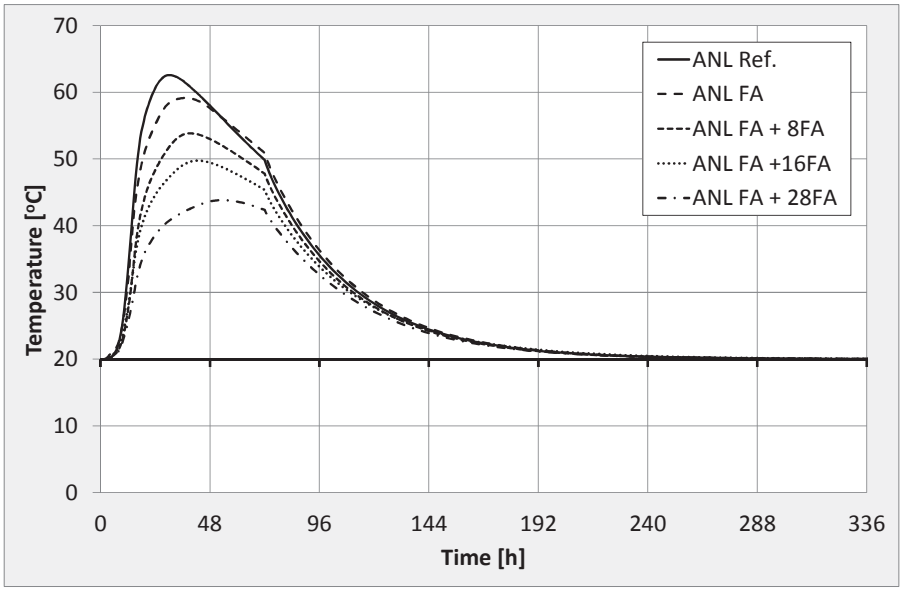

Figure 7.7; Average calculated wall temperature in selected area under summer conditions, new cement batches EG1-14 and TF5-14

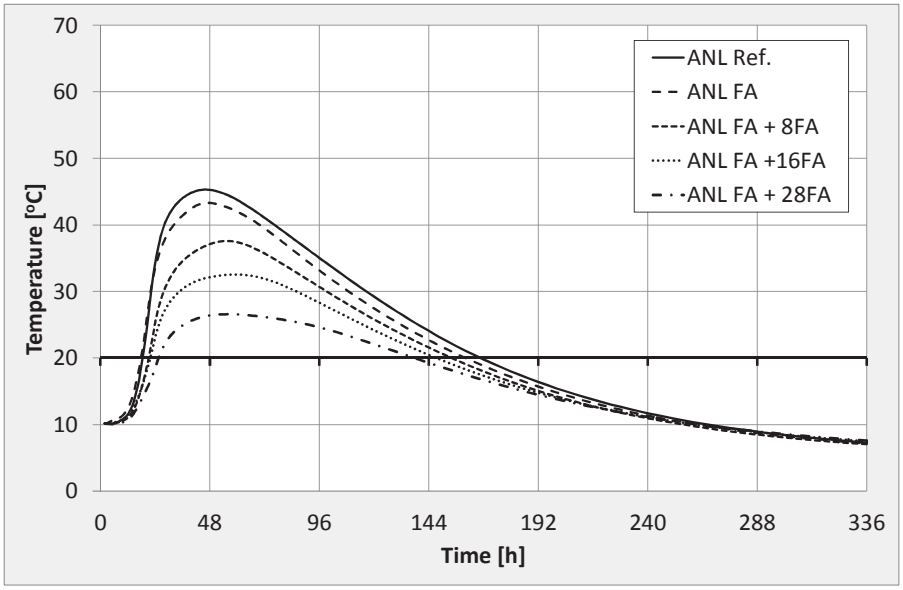

Figure 7.8; Average calculated wall temperature in selected area under winter conditions, new cement batches EG1-14 and TF5-14

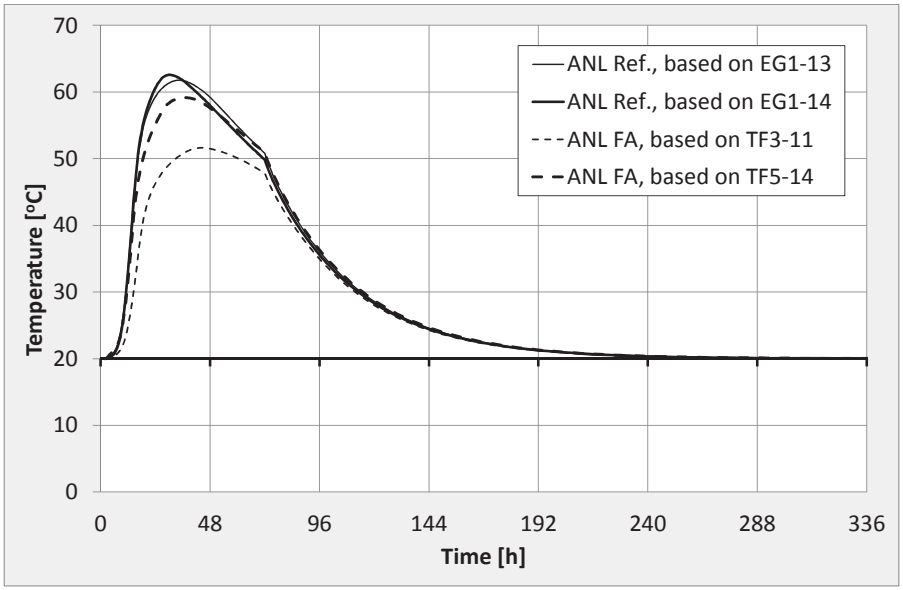

Figure 7.9; Average calculated wall temperature in selected area under summer conditions, ANL Ref. and ANL FA, all cement batches (EG1-13, EG1-14, TF3-11 and TF5-14)

Table 7.4; Maximum temperature T_{max} and maximum temperature increase ΔT_{max} for the investigated concretes

Concrete	**Season**	**Cement**[*]	T_{max} **wall**[**] [°C]	ΔT_{max} **wall**[**] [°C]	$\frac{\Delta T_{max\_new}}{\Delta T_{max\_orig}}$
ANL Ref.	Summer	EG1-10	61.8	41.8	-
		EG1-14	62.6	42.6	1.02
	Winter	EG1-10	45.3	35.3	-
ANL FA	Summer	TF3-11	51.6	31.6	-
		TF5-14	59.2	39.2	1.24
	Winter	TF5-14	43.3	33.3	-
ANL FA +8FA	Summer	TF3-11	49.2	29.2	-
		TF5-14	53.8	33.8	1.16
	Winter	TF5-14	37.6	27.6	-
ANL FA +16FA	Summer	TF3-11	45.1	25.1	-
		TF5-14	49.8	29.8	1.19
	Winter	TF5-14	32.6	22.6	-
ANL FA +28FA	Summer	TF5-14	43.8	23.8	-
	Winter	TF5-14	26.1	16.1	-

[*)] *The temperature calculations are based on heat development results from the listed cement, see previous section*

[**)] *The average value over a 200x800 cross-section*

7.4 Mechanical properties under 20 °C isothermal conditions

7.4.1 General

A test series on mechanical property development under 20 °C isothermal conditions has been carried out for the concretes *ANL Ref.*, *ANL FA*, *ANL FA +8FA* and *ANL FA +16FA*. The following tests were included in the test series:

- Compressive strength over time at 5 °C, 20 °C and 35 °C isothermal temperature, respectively (for determination of activation energy)
- Compressive strength
- Tensile strength (splitting and uniaxial)
- E-modulus (in compression and in tension)

While the compressive strength tests for activation energy determination were performed at NORCEM, all the other tests were performed at NTNU/SINTEF. The test series was conducted within the COIN project's sub-activity FA 3.1 "Crack Free Concrete Structures" [COIN, 2007-2014]. The results are reported in [Kjellmark et al., 2015], but a summary as well as an independent evaluation are given in the following. A corresponding test series was also performed for the later added concrete *ANL FA +28FA*. The latter results are only reported in the current work, and are thus more thoroughly described.

As described in Section 4.2, the originally used batches of cement were replaced with new cement batches during the given PhD work. As a result, the concretes *ANL Ref.*, *ANL FA*, *ANL FA +8FA* and *ANL FA +16FA* were tested for mechanical properties with the originally used batches of cement, while *ANL FA +28FA* was tested with the new cement batch. In order to investigate the effect of cement batch on mechanical properties, an additional limited mechanical test program was performed with *ANL Ref.* and *ANL FA* with the new cement batches. In contrast to the considerable effect on heat development (Section 7.2), the new cement batches only had a minor influence on the mechanical properties: a small increase in compressive strength for all concretes, as well as a small increase in tensile strength for *ANL Ref.* These results are reported in [Kjellmark, 2015] and they were not taken into consideration in the current work.

Material parameters for each concrete has been determined by fitting the material models described in Section 3.4 to the results from the mechanical test series. The current section gives an overview of the determined material parameters as well as the test results which they were based on. The results are reported in Section 7.4.2 - 7.4.5, while a discussion on results and influence of FA content is given in Section 7.4.6.

7.4.2 Activation Energy

The compressive strength tests (performed at NORCEM) at 5 °C, 20 °C and 35 °C for *ANL FA +28FA* are presented in Table 7.5. The corresponding results for the other concretes are given in Appendix C.

Table 7.5; NORCEM compressive strength test results at 5, 20 and 35 °C, ANL FA +28FA

5 °C		**20 °C**		**35 °C**	
Age [d]	[MPa]	Age [d]	[MPa]	Age [d]	[MPa]
1	0.9	0.5	3.0	0.25	1.4
1.5	3.2	0.67	5.3	0.33	4.6
2	6.0	1	8.4	0.5	8.3
3	9.0	2	15.5	0.67	10.7
4	12.7	3	19.3	1	14.8
5	15.0	7	27.2	2	22.4
7	19.1	28	48.6	4	33.3
28	29.9	-	-	28	66.2

The activation energy parameters *A* and *B* were found by the following procedure: the compressive strength model, Equation 3.11, was fitted to the compressive strength test results at 20 °C by using the method of least squares. Further, the maturity time-scale was adjusted by changing the A-parameter as to fit the 35 °C test results to the 20 °C model line, and by changing the B-parameter as to fit the 5 °C test results to the 20 °C model line. The obtained activation energy parameters are presented in Table 7.6. Compressive strengths (both measured and modelled) for *ANL FA +28FA* are plotted versus maturity in Figure 7.10, while corresponding figures for the other concretes are given in [Kjellmark et al., 2015].

Table 7.6; Activation energy parameters A and B

Concrete	***A*** $[J \cdot mol^{-1}]$	***B*** $[J \cdot mol^{-1} \cdot K^{-1}]$
ANL Ref.	31482	296
ANL FA	31487	197
ANL FA +8FA	32958	273
ANL FA +16FA	37023	0
ANL FA +28FA	42124*	53*

*) *Assumed values: A = 42000 and B = 0*

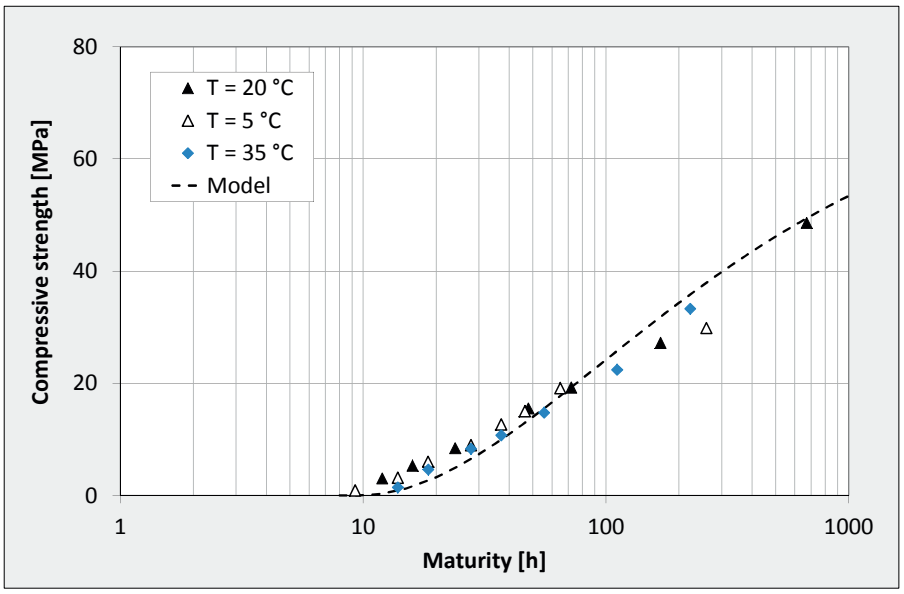

Figure 7.10; Measured and modelled compressive strength versus maturity, ANL FA +28FA

The activation energy parameters for *ANL FA +28FA* were needed for calculation purposes before the results from the activation energy tests were available. Therefore, the parameters were assumed to be: A = 42000 and B = 0 based on the results from the other concretes. The assumed values were very similar to the parameters later found from testing (Table 7.6). In addition, the choice of one of the two "*A* and *B"*- sets would not have any effect on the calculation results due to the fact that all material parameter determinations have been based on the chosen set of A and B. It was therefore decided to proceed with the assumed A and B values for *ANL FA +28FA* as they were already included in several calculations.

The effect of fly ash content on the activation energy parameters is discussed in Section 7.4.6.

7.4.3 Compressive strength

Standard 28-days 20 ^{o}C compressive strength tests were performed at both NORCEM and NTNU. A comparison of these results are presented in Table 7.7 and illustrated in Figure 7.11. The compressive strengths found by NORCEM were in average 9 MPa (13 %) higher than the corresponding strengths found by NTNU. The reason for the deviation between the two laboratories is unclear, however, it could be explained by different test equipment as well as differences in cement batches, gravel bathes and mixing procedures. *ANL FA +28FA* was also tested at 91 days at NTNU: f_{c91} = 60.9 MPa, implying a considerable property increase (34 %) between 28 and 91 days.

Table 7.7; Compressive strengths under 20 °C isothermal conditions at 28 days, NTNU and NORCEM

Concrete	f_{c28} NTNU [MPa]	f_{c28} NORCEM [MPa]
ANL Ref.	80.3	84.8
ANL FA	71.2	79.3
ANL FA +8FA	65.7	78.9
ANL FA +16FA	53.6	66.9
ANL FA +28FA	45.3	48.6

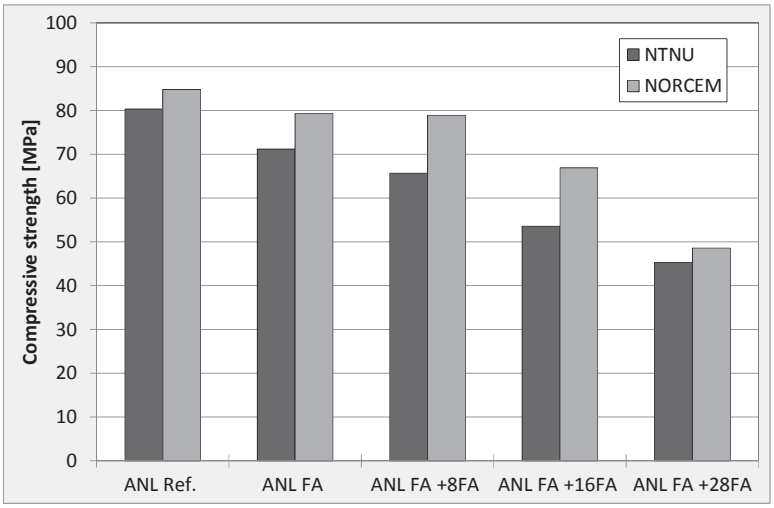

Figure 7.11; 28-days compressive strengths under 20 °C isothermal conditions, NTNU and NORCEM

The compressive strength model parameters were determined from the NORCEM test results (Section 7.4.2) by the procedure described in the following: first, t_0 was found by fitting the compressive strength model, Equation 3.11, to the 20 °C strengths by using the method of least squares. Further, f_{c28} and s were found by fitting Equation 3.11 to the compressive strength test results for all temperatures (5 °C, 20 °C and 35 °C) while using the activation energy parameters found in the previous section. The obtained model parameters t_0, f_{c28} and s are presented in Table 7.8.

As previously described, the compressive strengths found by NORCEM were higher than the corresponding values found by NTNU. As all tests, except compressive strength at different temperatures, were carried out at NTNU, it was decided to use only the activation

energy *A* and *B* and the time-development model parameter *s* obtained from the NORCEM results, while f_{c28} and t_0 were set according to the NTNU results. Hence, the model parameter f_{c28} was set to be the 28-day compressive strength found at NTNU and t_0 was determined by the procedures discussed in Section 7.5. The final derived compressive strength model parameters are presented in Table 7.8 and illustrated in Figure 7.12. The effect of fly ash content on the compressive strength is discussed in Section 7.4.6.

Table 7.8; Compressive strength model parameters, NORCEM and NTNU

	Based on NORCEM			**Based on NTNU/TSTM**	
Concrete	f_{c28} (NORCEM)	*s*	t_0 [Maturity hours]	f_{c28} (NTNU)	t_0 [Maturity hours]
ANL Ref.	78.8	**0.200**	8.9	**80.3**	**8.8**
ANL FA	77.8	**0.257**	7.5	**71.2**	**9.5**
ANL FA +8FA	77.1	**0.295**	7.5	**65.7**	**11.0**
ANL FA +16FA	67.9	**0.356**	7.0	**53.6**	**12.0**
ANL FA +28FA	49.4	**0.424**	8.0	**45.3**	**13.0**

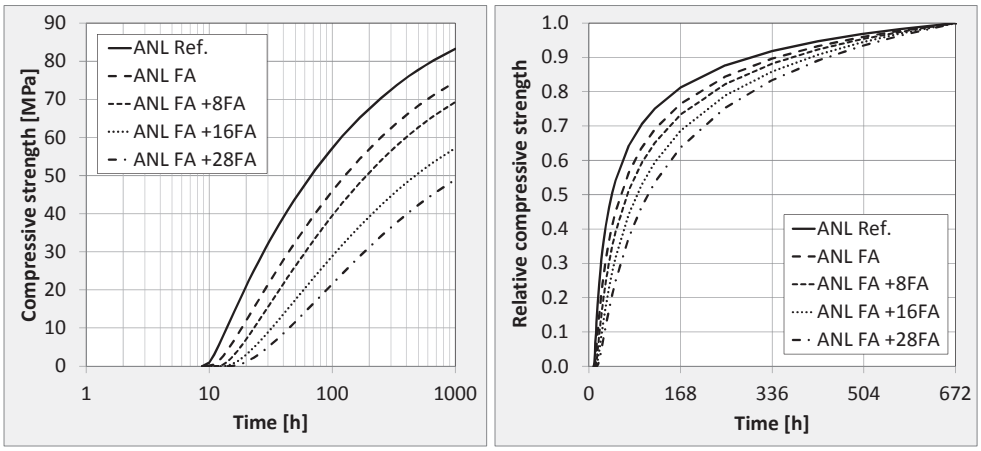

Figure 7.12; Compressive strength development (left) and relative compressive strength development (right), as expressed by the model

7.4.4 Tensile strength

The indirect tensile splitting test is considered the favourable test method from a laboratory perspective due to the difficulties experienced with direct tensile methods. However, the direct uniaxial tensile strength is the desired input parameter for stress calculations. Thus, a test series including both splitting strength and direct uniaxial strength under 20 °C isothermal curing conditions was performed in order to establish a relation between the two methods. The tensile strength test results are presented in Table 7.9 and illustrated in Figure 7.13. For the later added *ANL FA +28FA* however, only direct tensile strength tests were performed. It can be seen that the tensile strength both at 2 and 28 days decreases systematically with increasing fly ash content, except for the direct tensile strength result for *ANL FA* at 28 days (3.09 MPa). Based on 7 restrained *ANL FA* tests in the TSTM System, the 28-day direct uniaxial tensile strength was seen to be higher, on average 3.60 MPa. This result gives coherence with the other tensile strength test results, and it was therefore decided to use 3.60 MPa as the 28-day direct tensile strength for *ANL FA* (marked "TSTM" in Figure 7.13).

Table 7.9; Tensile strength test results (20 °C)

Concrete	**Tensile splitting strength** [MPa]		**Direct uniaxial tensile strength** [MPa]		
	2 days	*28 days*	*2 days*	*28 days*	*91 days*
ANL Ref.	3.69	5.07	2.80	3.92	-
ANL FA	2.72	4.59	2.42	3.09**	-
ANL FA +8FA	2.32	4.10	2.01	3.38	-
ANL FA +16FA	1.97	3.72	1.66	3.16	-
ANL FA +28FA	-	-	1.56*	3.02	3.99

*) *Tested at 3 days*

**) *Deviating result, it is argued and decided to proceed with the value f_{t28} = 3.60 MPa*

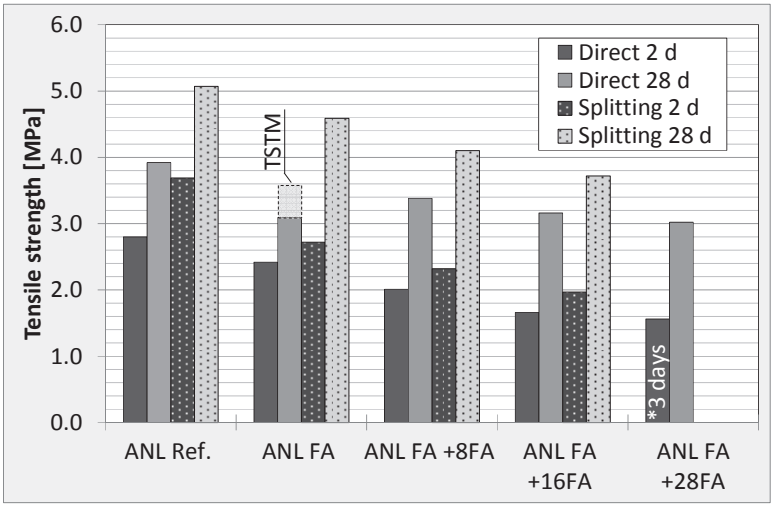

Figure 7.13; Tensile strength at 2 days and 28 days, 20 °C isothermal curing

The tensile strength model parameters were found by the procedure described in the following: a correlation between splitting and direct tensile strength was established, Equation 7.1, and the splitting test results were adjusted to direct tensile strength values, see [Kjellmark et al., 2015]. The tensile strength model parameters were found by fitting the tensile strength model described in Section 3.4, Equation 3.12, to the test results by using the method of least squares. Further, due to the limited number of test ages, the model parameter f_{t28} was fixed to the 28-day tensile strength (i.e. the average of direct strength and adjusted splitting strength).

$$f_t = 0.65 \cdot f_{ts} + 0.52 \qquad \textit{Equation 7.1}$$

where f_t is the uniaxial tensile strength and f_{ts} is the tensile splitting strength

The model parameters found for *ANL FA +28FA* were based on direct uniaxial tensile tests only. As opposed to the other concretes, *ANL FA +28FA* was also tested at 91 days, but for comparison and similarity reasons, only the test results at 2 and 28 days were used for the given tensile strength material model determination. Model parameters for the tensile strength development are presented in Table 7.10 and illustrated in Figure 7.14.

Table 7.10; Direct tensile strength, model parameters

Concrete	f_{t28} [MPa]	n_t
ANL Ref.	3.86	0.484
ANL FA	3.55	0.589
ANL FA +8FA	3.28	0.509
ANL FA +16FA	3.05	0.486
ANL FA +28FA	3.02	0.665

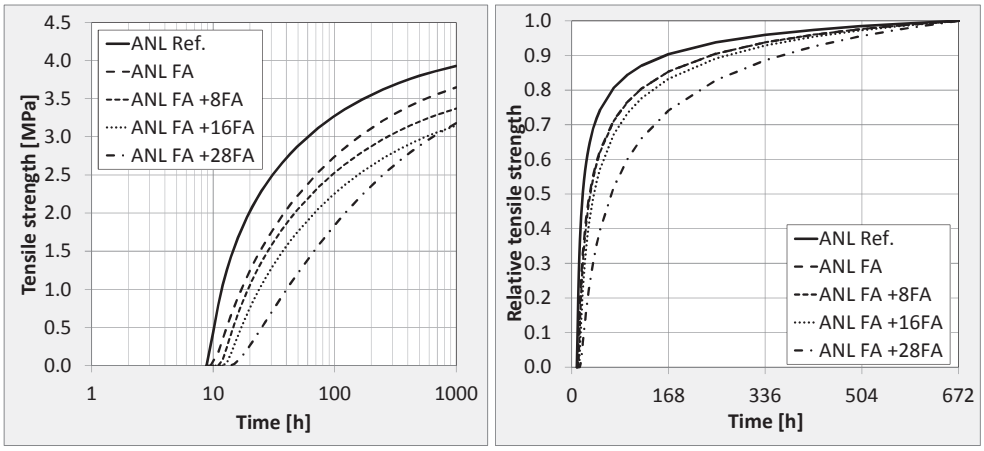

Figure 7.14; Direct tensile strength development (left) and relative tensile strength development (right), as expressed by the model

7.4.5 E-modulus

The compressive and tensile E-modulus test results under 20 °C isothermal curing conditions are presented in Table 7.11 and illustrated in Figure 7.15. The compressive E-modulus was determined according to [NS 3676:1987], while the tensile E-modulus was calculated as the secant E-modulus between 10 % and 40 % of the ultimate tensile stress. For *ANL Ref.,* the 28-day uniaxial tensile tests failed and therefore the 28-day tensile E-modulus had to be assumed. This was done by extrapolating the linear trend line from the 28-days results for the other concretes with higher FA content, as shown in Figure 7.22. From this procedure, the *ANL Ref.* 28-days tensile E-modulus was assumed to be 34.1 GPa.

The tensile E-modulus was found to be slightly higher than the compressive E-modulus for all concretes and test ages. This relation is however not compared with other studies as the

tensile-compressive E-modulus relation is found to be strongly dependent on the stress range from which the moduli were determined, see discussion in Chapter 6.3.7.

Table 7.11; E-modulus test results at 2 days and 28 days, 20 °C isothermal conditions

Concrete	**E-modulus in compression** [GPa]		**E-modulus in tension** [GPa]		
	2 days	*28 days*	*2 days*	*28 days*	*91 days*
ANL Ref.	25.3	30.8	27.0	-*	-
ANL FA	22.5	30.2	25.5	30.9	-
ANL FA +8FA	21.4	26.9	23.0	28.5	-
ANL FA +16FA	19.6	27.8	21.9	27.8	-
ANL FA +28FA	-	-	20.6**	24.9	28.4

*) *Test failed, value 34.1 GPa assumed based on trend lines*

**) *Tested at 3 days*

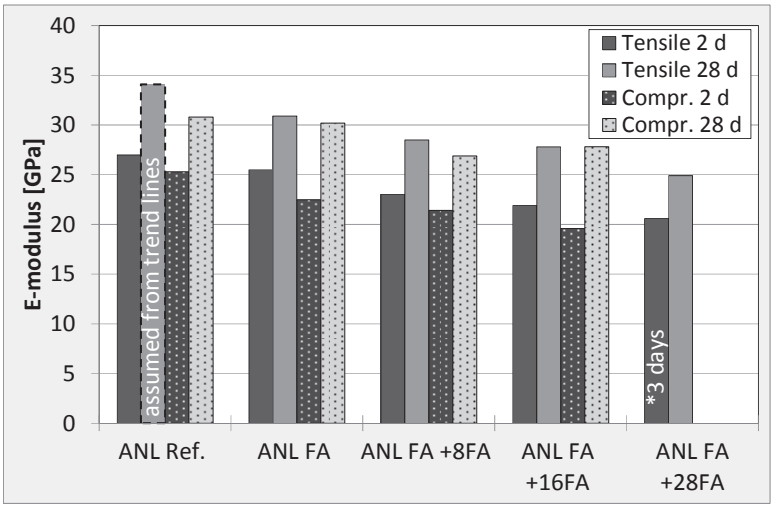

Figure 7.15; E-modulus test results at 2 days and 28 days

The model parameters describing the development of the E-modulus were determined in the following way: the model parameter E_{28} was set to the average of the 28-day E-modulus in compression and in tension, while the model time-development parameter n_E was found by best fit (least square) to the E-modulus test results (compression and tension) at 2 days, see Section 3.4, Equation 3.13. The model parameters found for *ANL FA +28FA* were based on E-modulus in tension only, since the compressive E-modulus was not

measured. The model parameters describing the E-modulus development are given in Table 7.12 and illustrated in Figure 7.16.

Table 7.12; Model parameters E-modulus

Concrete	E_{28} [GPa]	n_E
ANL Ref.	32.45	0.348
ANL FA	30.55	0.299
ANL FA +8FA	27.70	0.233
ANL FA +16FA	27.80	0.252
ANL FA +28FA	24.88	0.189

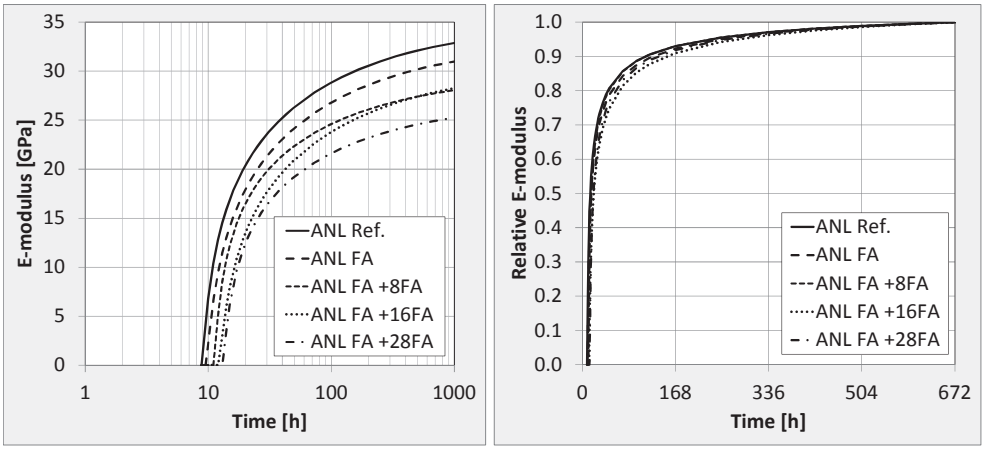

Figure 7.16; E-modulus development (left) and relative E-modulus development (right), as expressed by the model

7.4.6 Discussion of all mechanical properties test results

The influence of fly ash content on the activation energy parameters *A* and *B* are illustrated in Figure 7.17. The activation energy for temperatures above 20 °C (represented by the parameter *A*) was systematically increasing with increasing amount of fly ash. The same trend was seen for the parameter *A* in [Bjøntegaard, 2004], [Han et al., 2003] and [Bjøntegaard et al., 2012]. The influence of fly ash on the parameter *B* was not found to be as systematic, neither here nor in the literature. There was however a tendency of a decreasing *B* value with increasing amount of fly ash. The resulting activation energies for all concretes over the temperature interval -10 to 50 °C are shown in Figure 7.18. The overall effect of this, in terms of relative hydration rate (Equation 3.1 in Section 3.4.1), can

be seen in Figure 7.19. While the hydration rate for temperatures below 20 °C is quite similar for all concretes, the hydration rate is increasing with increasing amount of fly ash for temperatures above 20 °C.

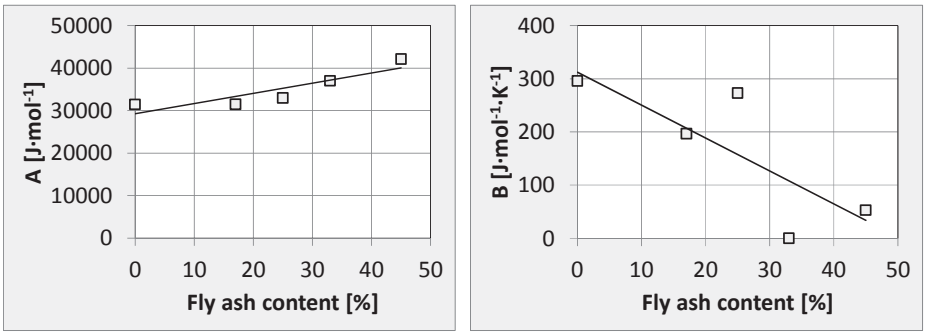

Figure 7.17; Activation energy parameters A (left) and B (right) versus fly ash content

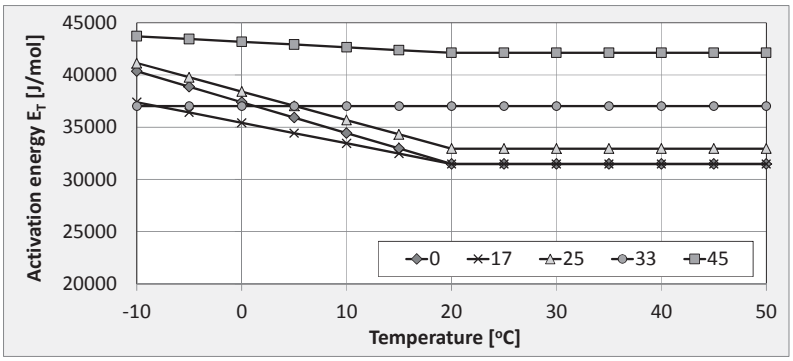

Figure 7.18; Activation energy E_T versus temperature for various fly ash contents [%], see Equation 3.1

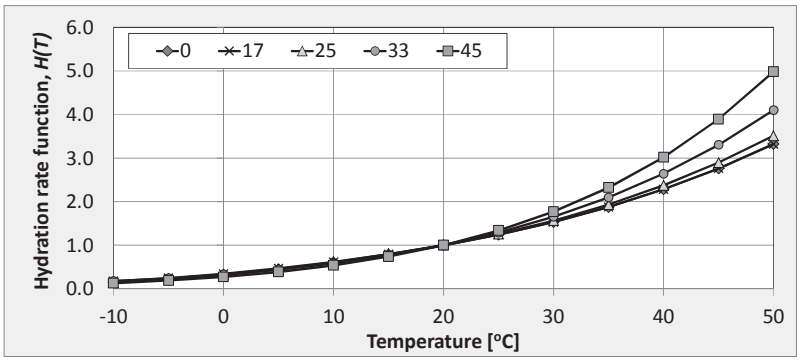

Figure 7.19; Hydration rate function H(T) versus temperature for various fly ash contents [%]

For all concretes, both the 2-day and 28-day values for compressive strength, tensile strength and E-modulus were found to decrease with increasing fly ash content, Figure 7.20 - Figure 7.22. This is as excepted, as the addition of pozzolanes is known to cause slower strength and temperature development than for ordinary Portland cement alone, [Neville, 1972], [Herholdt et al., 1979] and [Möller et al., 1982]. The same references also state that the ultimate strength developed over longer times may reach and/or even exceed the ones for ordinary Portland cement. This was however not seen in the given test series as the concretes were normally tested at 2 and 28 days only, which is not enough time for studying these effects, but still relevant for the intended use which is stress calculation in the early age. The long-term property development of fly ash concretes is addressed in Section 7.6. As previously described, the compressive- and tensile strengths as well as the E-modulus were all found to decrease systematically with increasing amount of fly ash. Similar trends have been found several places in the literature, but not always as clear and systematic as in the current work. A test series on mechanical property development reported by [Bjøntegaard et al., 2003] showed a consistent decrease in the 28-day compressive strength, tensile strength (direct and splitting strength), as well as E-modulus with increasing fly ash dosage under 20 ^{o}C isothermal conditions. [Ji, 2008], however, found that while both the 28-day compressive- and tensile strength decreased with increasing amount of fly ash, this was not the case for the 28-day E-modulus which actually increased with fly ash content for two of the concretes when compared to the reference. In [Bjøntegaard et al., 2012], both the 28-day compressive strength and E-modulus was reported to have a slight decrease with fly ash dosage, while the splitting tensile strength on the other hand showed a clear increase with fly ash content. Test results reported by [Pathak et al., 2012] showed a clear and systematically decrease in both compressive strength and tensile splitting strength with increasing amount of fly ash in self-compacting-concrete. [Case et al., 2013] measured compressive strengths at 7 and 28 days on concrete with 0, 15, 30 and 45 % fly ash. While the 7-day strength was found to be decreasing with increasing fly ash content, surprisingly no corresponding relation was seen for the 28-day strength.

In the present study, the only property that did not decrease with increasing fly ash dosage was the 28-day compressive E-modulus for *ANL FA +16FA,* which was slightly higher (3.5 %) than *ANL FA +8FA,* Figure 7.15. It is notable that the incremental E-moduli found directly from the TSTM tests were also decreasing with increasing fly ash content, see Section 7.8. Due to the rather high compressive 28-day E-modulus measured for *ANL FA +16FA,* the concretes *ANL FA +8FA* and *ANL FA +16FA* obtained a quite similar 28-day E-modulus model parameter, Table 7.12, Figure 7.16 and Figure 7.22.

It should be noted that when establishing the material models for tensile strength and E-modulus, only the 2-day result (average of two or three specimens) was used to determine the time development parameter n. This limited test program could provide some sensitivity to the outcome, especially for the tensile strength which usually has a larger scatter in test results than the other properties, see Section 7.6. However, the relative

tensile strength developments, illustrated in Figure 7.14, show that the shape of the curve changes systematically with increasing fly ash dosage, as one would expect.

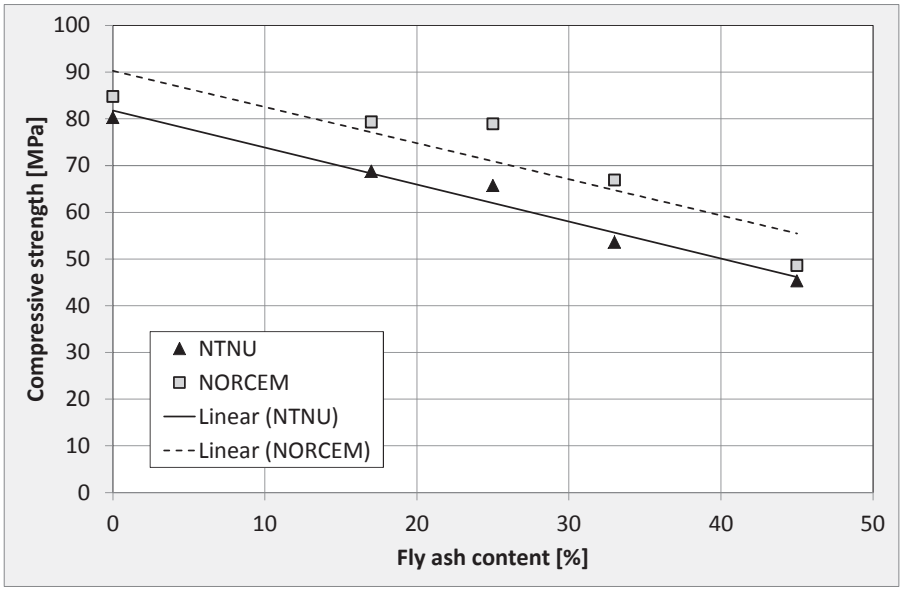

Figure 7.20; Compressive strength at 28 days, tested at NTNU and NORCEM (20 °C)

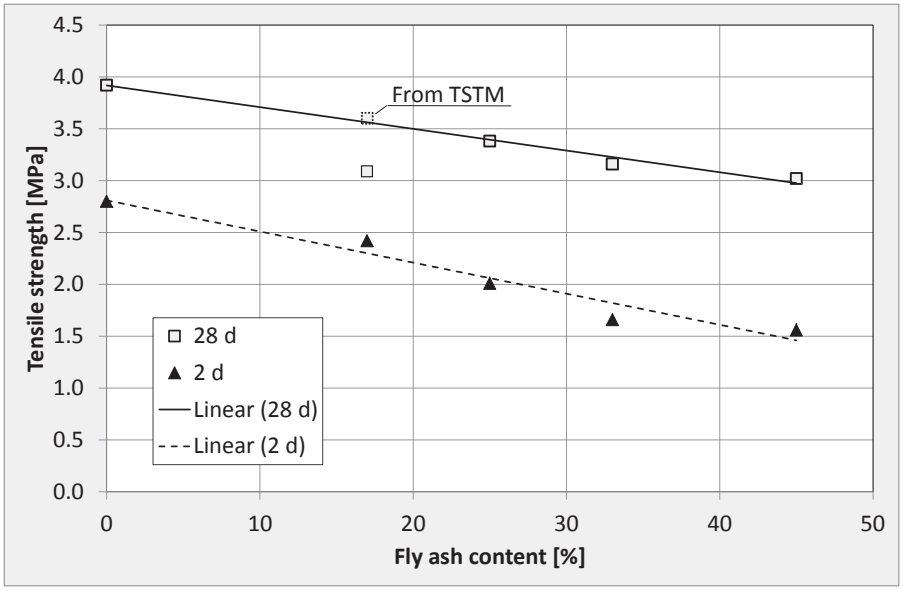

Figure 7.21; Direct tensile strength at 2 days and 28 days versus fly ash content, 20 °C isothermal curing conditions

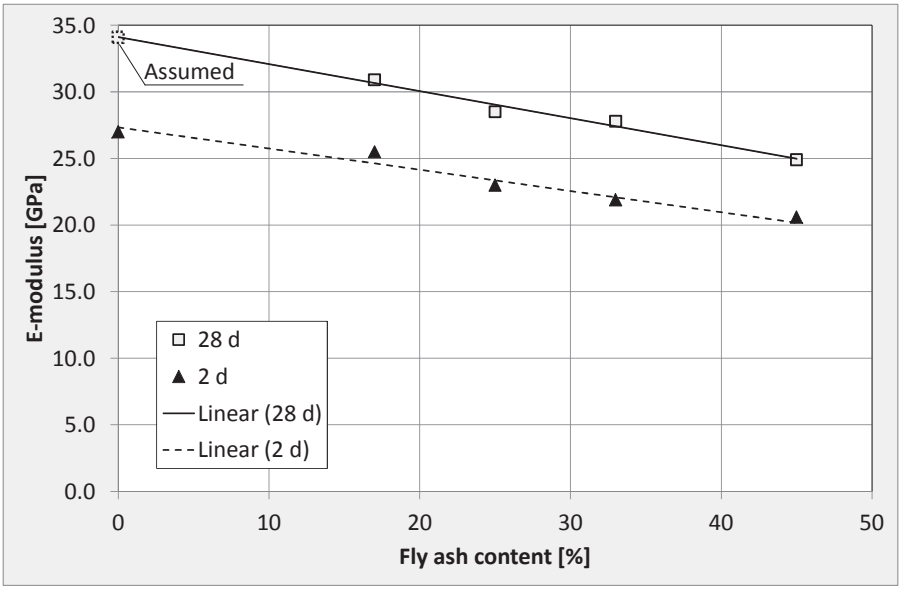

Figure 7.22; E-modulus in tension at 2 days and 28 days versus fly ash content, 20 °C isothermal curing conditions

7.5 t_0 – start time for stress development

The start time for stress development, t_0, is defined as the time at which the E-modulus reaches significant values so that the occurring volume changes can produce measurable stresses. The material models describing compressive strength, tensile strength and E-modulus (see Section 3.4) contain the same time parameter t_0. In addition, also the thermal dilation and autogenous deformation curves start at t_0, as there are no stress-inducing volume changes before t_0.

In the current work, t_0 has been determined by three different approaches:

- *From compressive strength tests over time performed at NORCEM*: Based on the presumption that all mechanical properties start to develop simultaneously, t_0 was found from compressive strength tests as described in Section 7.4.3.
- *From semi-adiabatic calorimetry tests performed at NTNU*: The start time determined from semi-adiabatic calorimetry tests is defined as the maturity time where the heat release is 12 kJ above the "baseline" heat release during the dormant period. This time is denoted t_{12kJ}. The t_0 –parameter was deduced by the following assumption found by [Bjøntegaard et al., 2000]: $t_0 = t_{12kJ} + 1.8$ hours.
- *From realistic temperature tests in the TSTM System (at NTNU)*: From TSTM tests, t_0 was defined as the maturity time when the measured restrained stress reached 0.1 MPa for tests performed under realistic (summer) temperature conditions [Bjøntegaard, 1999]. The tests performed under winter conditions provided a

somewhat later t_0 than tests under summer conditions. This is probably related to the fact that the activation energy is slightly different to that of the hardening phase [Smeplass, 2001], which has not been within the scope of the present study.

The obtained values for t_0 are presented in Table 7.13. While the t_0 values from the compressive strength tests were slightly decreasing with increasing fly ash content, t_0 from both the semi-adiabatic calorimetry tests and TSTM tests showed the opposite trend. The latter is expected due to previous experience. The realistic temperature tests in the TSTM System are considered to give the most trustworthy t_0 development. Hence, t_0 determined from the TSTM tests were decided used for early age stress calculations in the current work.

Table 7.13; Start time for stress development, t_0 [maturity hours]

Concrete	**Compr. Strength (NORCEM)**	**Semi-adiabatic calorimeter tests (NTNU)**				**TSTM* (NTNU)**
		Cement batches EG1-10 and TF3-11		*Cement batches EG1-14 and TF4-15*		
	t_0	t_{12kJ}	$t_0 = t_{12kJ} + 1.8$	t_{12kJ}	$t_0 = t_{12kJ} + 1.8$	t_0
ANL Ref.	8.9	7.0	8.8	7.0	8.8	**8.8**
ANL FA	7.5	8.8	10.6	7.5	9.3	**9.5**
ANL FA +8FA	7.5	9.3	11.1	7.8	9.6	**11.0**
ANL FA +16FA	7.0	10.2	12.0	7.5	9.3	**12.0**
ANL FA +28FA	8.0	-	-	8.4	10.2	**13.0**

*) *t_0 was deduced from TSTM tests performed with cement batches EG1-10 and TF4-15*

7.6 Additional mechanical testing – effect of curing temperature history

7.6.1 Introduction

Along with the mechanical test results discussed previously and parallel TSTM tests it was suspected that realistic temperature curing conditions could have an effect on the mechanical properties. Therefore, a series of mechanical testing was carried out with the aim to investigate the effect of curing temperature on compressive strength, tensile strength and E-modulus. The test series was performed with the concretes *ANL Ref.* and *ANL FA +16FA*. For both concretes, half of the specimens were cured under 20 ^{o}C isothermal conditions, while the other half were subjected to a realistic temperature history over the first 14 days. All specimens were unmoulded and wrapped with aluminium foil at 14 days, and further cured under 20 ^{o}C isothermal conditions. The specimens were tested at 28 and 91 days of maturity. A survey of the test series is presented in Chapter 4.3. The test results are presented in Section 7.6.2 – Section 7.6.4, followed by a discussion of the results in Section 7.6.5.

It should be noticed that the two given concretes were not subjected to the same realistic temperature history. Each concrete was subjected to its own semi-adiabatic temperature history representing a selected section of an 800 mm thick wall as described in Section 7.3. However, due to the new and more reactive fly ash cement used in *ANL FA +16FA*, the temperature histories currently used for *ANL Ref.* and *ANL FA +16FA* (which were based on the previous cement batch) no longer represent the same structural part. Consequently, the test results for the two given concretes have mainly been evaluated individually, rather than compared.

During the given test series, the temperature control system was slightly more efficient than originally assumed. This caused a 3 % increase in maximum temperature for *ANL Ref* as compared to the temperature history described in Section 7.3. During the given test series, the maximum temperature for *ANL Ref.* was 63.5 ^{o}C, while the maximum temperature for *ANL FA +16FA* was 45.0 ^{o}C.

7.6.2 Compressive strength

The results from the compressive strength tests are presented in Table 7.14 and illustrated in Figure 7.23 - Figure 7.24. Each result in the table is the average of 3 parallel cubes, while the figures show the value for each cube to give an illustration of the concentration of the results. A statistical evaluation of each set of parallel cubes shows that the internal variation is small. The coefficient of variation (CV) among the various sets lies between 0.3 % and 1.2 % for the compressive strength.

When exposed to a realistic temperature history, *ANL Ref.* showed a 12 % and 9 % reduction in compressive strength at 28 and 91 maturity days, respectively. A corresponding compressive strength reduction was not seen for the fly ash concrete *ANL FA +16FA*. However, as previously described, the two concretes were subjected to

different realistic temperature histories. *ANL Ref.* produces more hydration heat, and has therefore a higher maximum temperature (63.5 °C) during the test than *ANL FA +16FA* (45.0 °C). It is likely that this has influenced the temperature effect on the compressive strength for *ANL Ref.*.

ANL FA +16FA obtained a higher percentage increase in compressive strength between 28 and 91 maturity days than *ANL Ref.* However, for both concretes, the development from 28 maturity days to 91 maturity days (20 °C isothermal conditions) appears not to be affected by the preceding 0-14 days curing temperature, but the early strength reduction effect for *ANL Ref.* remains also after 91 days, as previously discussed.

Table 7.14; Compressive strength, effects of curing temperature

Concrete	**Test age** [Md]*	**Curing conditions**	**No of spec.**	**Mean** [MPa]	**SD** [MPa]	**CV** [%]
ANL Ref.	28	Isothermal	3	**84.0**	0.4	0.6
		Realistic temp.	3	**74.4**	0.9	1.2
	91	Isothermal	3	**86.8**	0.6	0.7
		Realistic temp.	3	**79.0**	0.8	1.0
ANL FA +16FA	28	Isothermal	3	**56.9**	0.4	0.7
		Realistic temp.	3	**59.9**	0.2	0.3
	91	Isothermal	3	**65.3**	0.6	0.9
		Realistic temp.	3	**63.9**	0.4	0.7

*) *Maturity days*

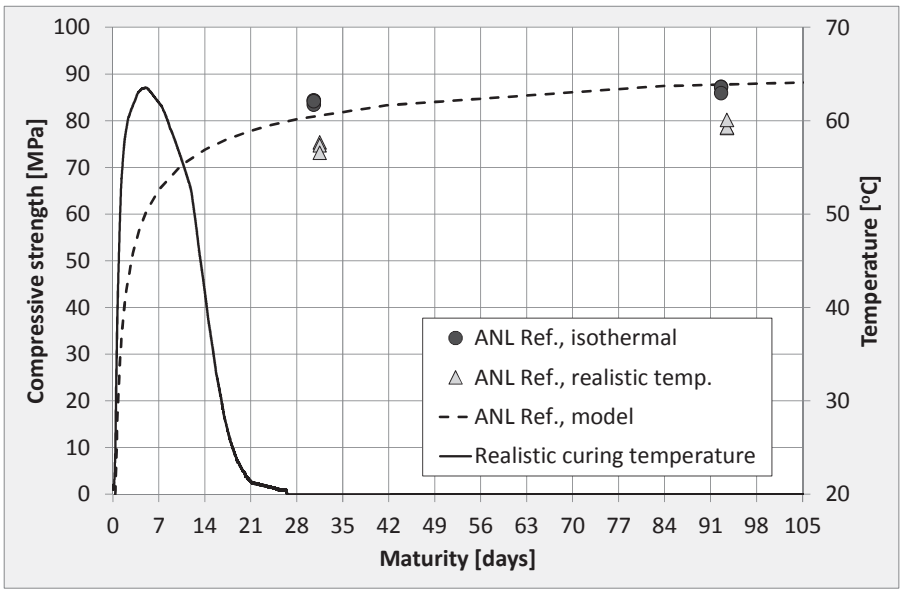

Figure 7.23; Curing temperature effects on compressive strength, ANL Ref.

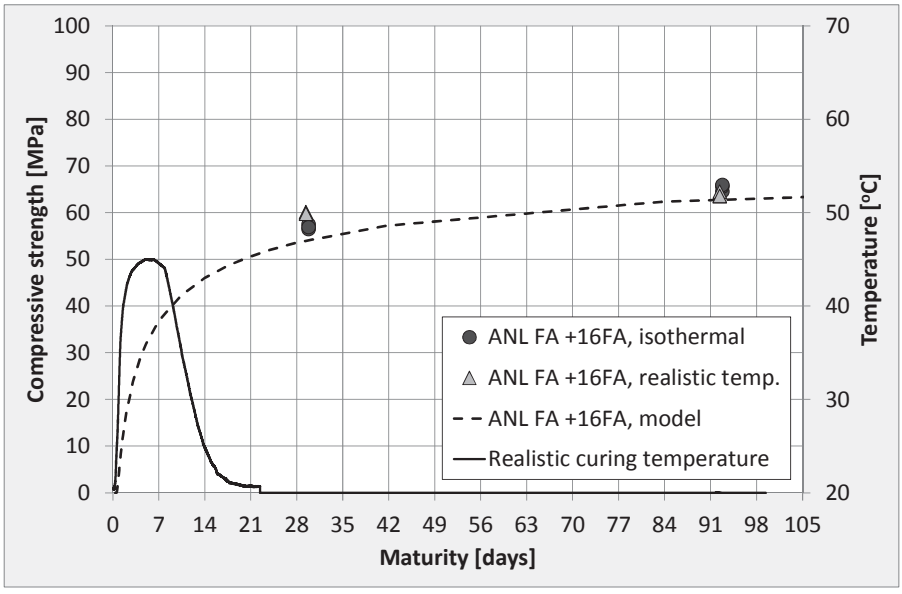

Figure 7.24; Curing temperature effects on compressive strength, ANL FA +16FA.

7.6.3 Tensile strength

The results from the direct tensile strength tests are presented in Table 7.15 and illustrated in Figure 7.25 - Figure 7.26. As given by the figures and the Coefficient of Variation (CV) in Table 7.15, there is a rather pronounced variation within the sets of 2 parallel prisms, especially for *ANL Ref.* at 28 maturity days of isothermal curing. By means of comparison, similar tests reported by [Kanstad et al., 2003b] had a CV of 3.9 – 9.2 % in sets consisting of 4 parallel prisms. The use of only 2 parallel prisms in the present study represents a rather limited selection, and the CV must thus be expected to have some variation.

The tensile strength results for the reference concrete *ANL Ref.* are presented in Figure 7.25. *ANL Ref.* shows a reduction in tensile strength for both test ages when exposed to a realistic temperature history during curing. In addition, the tensile strength for *ANL Ref.* decreases from 28 to 91 days of maturity when subjected to a realistic curing temperature. Considering the internal variation (SD), it can be discussed if this temperature effect is significant or if it is caused by variations in the test results. However, the reduction in tensile strength (0.4 MPa) is higher than the standard deviation (0.2 MPa), indicating that a tensile strength reduction between 28 and 91 maturity days may actually be the case.

Table 7.15; Tensile strength, effects of curing temperature

Concrete	**Test age** [Md]*	**Curing conditions**	**No of spec.**	**Mean** [MPa]	**SD** [MPa]	**CV** [%]
ANL Ref.	28	Isothermal	2	**4.7**	0.4	9.0
		Realistic temp.	2	**4.2**	0.2	4.4
	91	Isothermal	2	**4.6**	0.2	4.3
		Realistic temp.	2	**3.8**	0.1	1.9
ANL FA +16FA	28	Isothermal	2	**3.2**	0.1	3.7
		Realistic temp.	2	**3.3**	0.3	8.4
	91	Isothermal	2	**4.1**	0.2	4.9
		Realistic temp.	2	**4.0**	0.0	1.0

*) *Maturity days*

The tensile strength results for *ANL FA +16FA* are presented in Figure 7.26. For this concrete a negative effect of temperature on the tensile strength cannot be seen. The results show that tensile strength for both curing conditions continues to increase after 28 days maturity: the tensile strength increase is as high as around 1.0 MPa (approx. 25 %) between 28 and 91 maturity days for both temperature conditions. I.e., the fly ash concrete keeps developing tensile strength after 28 days of maturity in a much higher degree than

ANL Ref.. It is notable that the applied exponential material model (see Section 7.4) is not able to express the tensile strength increase beyond 28 days due to its formulation.

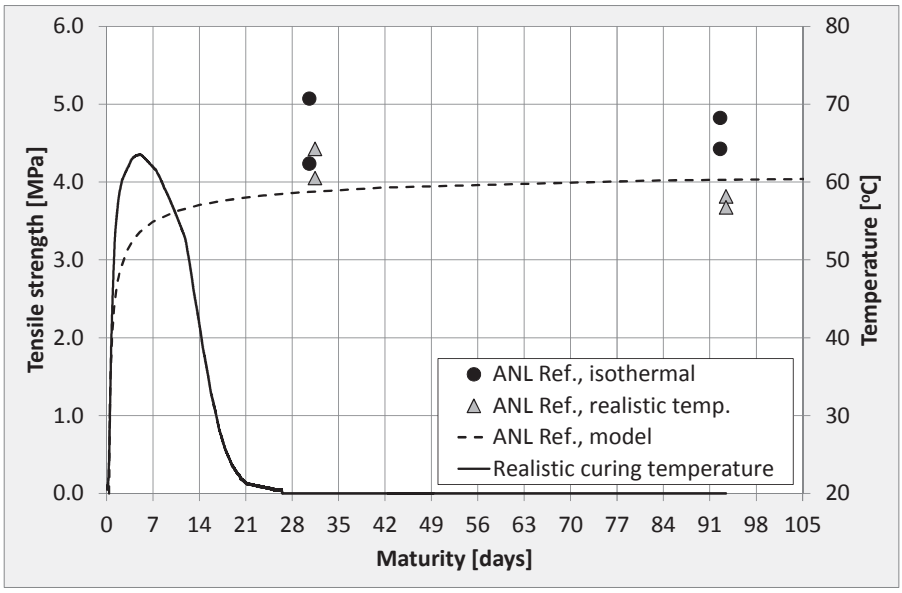

Figure 7.25; Curing temperature effects on tensile strength, ANL Ref.

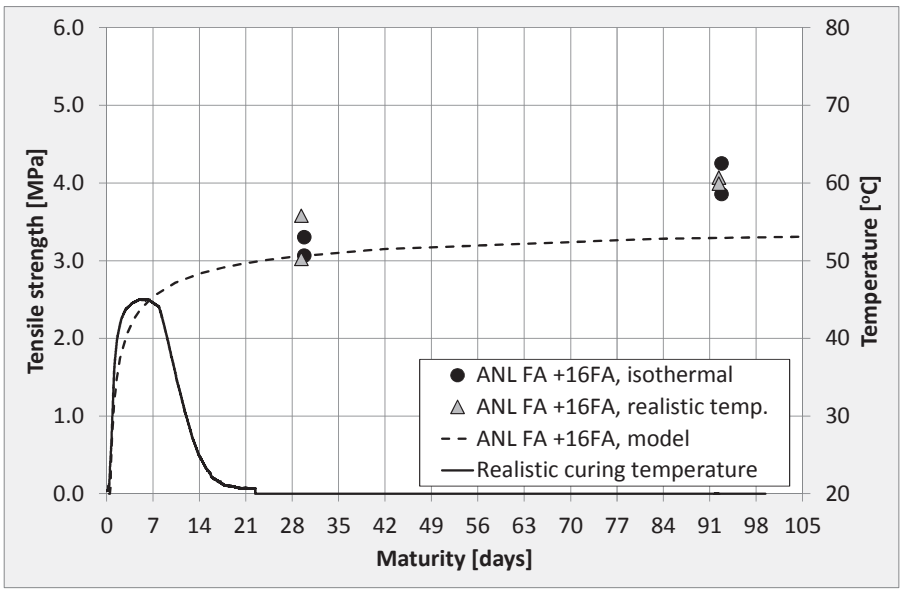

Figure 7.26; Curing temperature effects on tensile strength, ANL FA +16FA

7.6.4 E-modulus in tension

The tensile E-modulus test results are presented in Table 7.16 and illustrated in Figure 7.27 - Figure 7.28. The Coefficient of Variation (CV) is within 2.6 % for all tests, which must be regarded as quite satisfactory. Each test set consisted of only two specimens, which is rather limited. The E-modulus however generally shows rather low variability.

The reference concrete *ANL Ref.* shows a small reduction in E-modulus for both test ages when exposed to realistic curing temperatures. For *ANL FA +16FA* on the other hand, realistic curing conditions gives an 11 % increase in the E-modulus at 28 days of maturity.

Table 7.16; E-modulus - effects of curing temperature

Concrete	**Test age** [Md]*	**Curing conditions**	**No of spec.**	**Mean** [MPa]	**SD** [MPa]	**CV** [%]
ANL Ref.	28	Isothermal	2	**32200**	640	2.0
		Realistic temp.	2	**30500**	780	2.6
	91	Isothermal	2	**32800**	160	0.5
		Realistic temp.	2	**31000**	490	1.6
ANL FA +16FA	28	Isothermal	2	**27600**	600	2.2
		Realistic temp.	2	**30600**	180	0.6
	91	Isothermal	2	**31000**	510	1.7
		Realistic temp.	2	**30300**	50	0.2

*) *Maturity days*

While *ANL Ref.* shows the same E-modulus development between 28 and 91 maturity days for both curing conditions, *ANL FA +16FA* displays a pronounced difference in E-modulus development during the same time-span for isothermal versus realistic curing conditions. *ANL FA +16FA* shows a faster initial E-modulus development for the concrete specimens cured under realistic temperature conditions than for the specimens cured under isothermal conditions. The specimens cured under realistic temperature conditions seem to have reached their final level at 28 hours of maturity. While the specimens cured under 20 ^{o}C isothermal conditions continues to develop stiffness (E-modulus) after 28 days of maturity, this is not the case for the specimens subjected to realistic curing temperatures. At 91 maturity days, both curing conditions gave the same E-modulus level. Hence, both curing conditions obtain similar values for the E-modulus at 91 days, but they seem to follow a different path of getting there. The E-modulus model used in Section 7.4 (based on isothermal curing temperatures) will neither capture the more rapid E-modulus development before 91 maturity days for the concrete when exposed to a realistic

temperature history, nor the continuously development of the E-modulus between 28 and 91 days of maturity for fly ash concrete under 20 °C isothermal curing conditions.

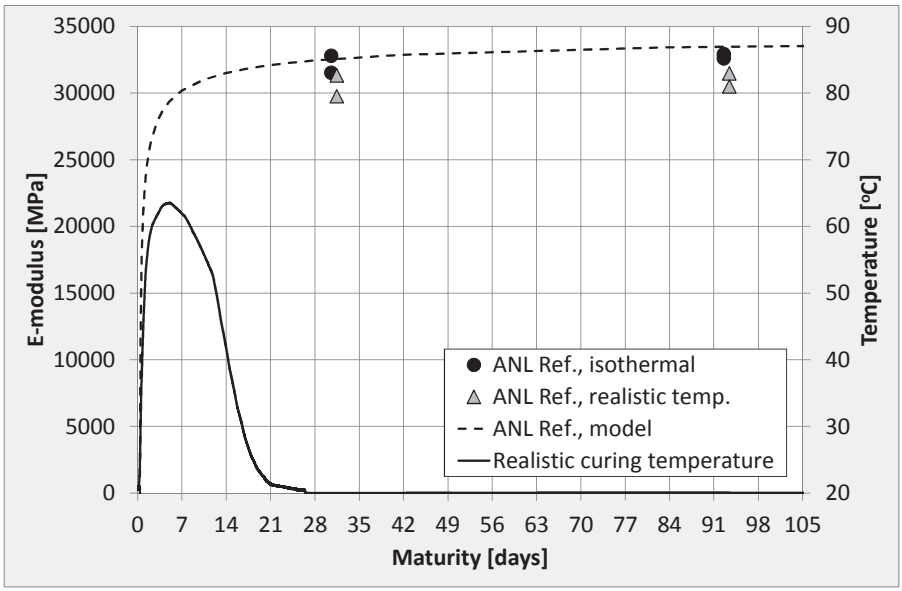

Figure 7.27; Curing-temperature effects on E-modulus in tension, ANL Ref.

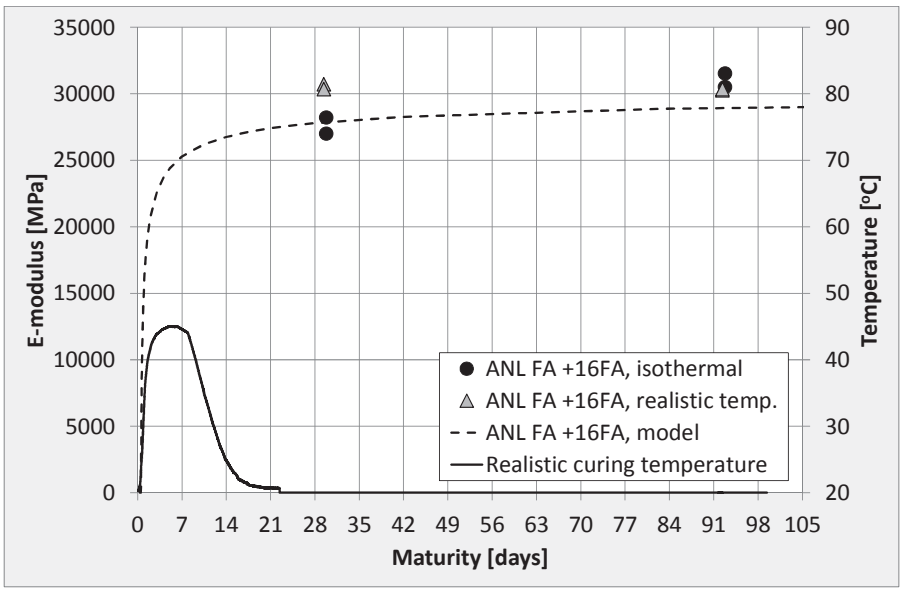

Figure 7.28; Curing-temperature effects on E-modulus in tension, ANL FA +16 FA

7.6.5 Discussion of test results

As previously described, the two different temperature histories used as realistic temperature curing conditions for *ANL Ref.* and *ANL FA +16FA,* respectively, no longer represent the same structural part. The test results for the two given concretes have therefore mainly been evaluated individually, rather than compared.

The scatter is smaller for the compressive strength- and the E-modulus test results than for the direct tensile strength results. The Coefficients of Variation (CVs) are within the range 0.3 – 1.2 % for the compressive strength results, 0.2 – 2.6 % for the E-modulus results and 1.0 – 9.0 % for the tensile strength results. However, as previously stated, the number of parallel specimens (only 2 at each test age) was limited. In a similar (but more extensive) mechanical test series, [Kanstad et al., 2003a], it was also found that the scatter was higher for tensile strength test results than for compressive strength. The reported CVs were in the range of 3.2 – 9.2 % for the 28-day tensile strength, which is in the same range as for the current work.

For *ANL Ref.*, all tested material parameters (compressive strength, tensile strength and E-modulus) were found to decrease (in a variable degree) when exposed to realistic temperature curing conditions. This trend was however not seen for the fly ash concrete *ANL FA +16FA,* where the compressive strength and tensile strength were found to be unaffected and the 28-day E-modulus was found to be increasing under realistic curing conditions. However, the absolute property values were always higher for *ANL Ref.* than for *ANL FA +16FA*, with exception of the 91 day tensile strength value for realistic curing conditions as described in Section 7.6.3.

As described, *ANL Ref.* showed a decrease in 28- and 91 day compressive strength when subjected to the given realistic temperature curing condition. This reduced compressive strength in mature age is believed to be caused by a coarser and more continuous pore structure induced by a high maximum temperature exposure [Sellevold et al., 1997]. Similar results have been found by other researchers, e.g. [Jonasson et al., 2014] (realistic temperature histories) and [Munch-Petersen et al., 2014] (isothermal temperature histories at different levels). The latter study found that including fly ash in the concrete reduced the compressive strength loss effect. In the current work, the compressive strength for *ANL FA +16FA* did not decrease when cured under realistic temperature conditions. This result is common and supported by for instance [De Weerdt et al., 2012], who studied the effect of curing temperature on the hydration (and compressive strength development) of cement paste with: 1) an ordinary Portland cement and 2) composite cements containing limestone powder and fly ash. It was found that when raising the (isothermal) curing temperature to 40 ^{o}C, the ordinary Portland cement showed an increased coarse porosity, resulting in a reduction of the long-term compressive strength. In the case of the composite cement, this increase in coarse porosity with increasing curing temperature was not observed. Instead the increased curing temperature enhanced the pozzolanic reaction of the fly ash and an increase in long-term compressive strength was observed. It was concluded that higher

curing temperatures are detrimental for the long-term compressive strength of ordinary Portland cement, but beneficial for the composite cement containing fly ash. However, when comparing the test results in the current test series, it should be remembered that *ANL FA +16FA* was exposed to a lower temperature increase during curing than *ANL Ref.*.

As already stated, the *ANL Ref.* E-modulus was found to decrease when subjected to the given realistic temperature history, while the 28-day E-modulus for *ANL FA + 16FA* was found to increase with as much as 11 %. By way of comparison, a mechanical test series of specimens cured under 20 ^{o}C isothermal conditions reported by [Bjøntegaard et al., 2003] showed that the 28-day E-modulus was decreasing with increasing amount of fly ash, while a mechanical test series of specimens cured under realistic temperature conditions performed one year later showed that the 28-day E-modulus did not decrease with an increasing amount of fly ash [Bjøntegaard, 2004]. This is in line with the current results, and as is a mechanical test series reported by [Kim et al., 2002], where it was found that while the 28-day E-modulus would increase at higher curing temperatures for fly ash concretes, the 28-day E-modulus for concrete without fly ash would decrease.

The given additional mechanical test series was originally initiated by restrained stress experiments in the TSTM System (Chapter 8). The tests in the TSTM System, involving incremental E-modulus determination, showed an increase of the E-modulus for fly ash concretes when subjected to realistic temperature curing conditions. The main objective of the current test series was to investigate this observation. The results from the given mechanical test series support the observed 28-day E-moduli increase for fly ash concretes cured under realistic temperature conditions in the TSTM.

While the tensile strength of *ANL Ref.* is constant, or even decreasing, between 28 and 91 days of maturity, the fly ash concrete keeps developing tensile strength after 28 days. The same trend is found for both compressive strength and E-modulus. Table 7.17 and Table 7.18 give an overview of the development of mechanical properties between 28 and 91 days of maturity. Table 7.17, which shows the mechanical property development under 20 ^{o}C isothermal conditions, also includes the mechanical test results for *ANL FA +28FA* (reported in Section 7.4). The mechanical property increase is given both as absolute values and as a percentage increase from 28 to 91 days of maturity. Under isothermal curing conditions, the compressive strength-, tensile strength- and E-modulus development between 28 and 91 days of maturity are clearly found to increase with increasing fly ash content.

Consequently, when exposed to 20 ^{o}C isothermal curing conditions, the fly ash concretes have a much more pronounced mechanical property development beyond 28 days than the reference concrete without fly ash. The model used to describe the material properties (Section 7.4) in the current work gives a good fit to the *ANL Ref.* results. However, for the fly ash concretes, the model fails to express the continuing development of properties beyond 28 days. For the fly ash concretes, the model combined with the 28-day E-modulus would considerably underestimate the 91-day E-modulus. On the other hand, by including

the 91-day E-modulus test results in the curve fitting, the model would overestimate the 28-day E-modulus and underestimate the 91-day E-modulus. Consequently, a new model describing the material property development of fly ash concretes should be considered established. This has however not been prioritized in the current study due to the previously defined scope of work, Chapter 1.

Table 7.17; Mechanical property increase (Δ) between 28 and 91 days, 20 °C isothermal curing conditions

	Δf_c [MPa]	Δf_t [MPa]	ΔE_t [MPa]
ANL Ref.	2.8 (3 %)	0	600 (2 %)
ANL FA +16FA	8.4 (15 %)	0.9 (27 %)	3400 (12 %)
ANL FA +28FA	15.6 (34 %)	1.0 (32 %)	3500 (14 %)

Table 7.18 presents the mechanical property increase between 28 and 91 days of maturity for specimens cured under realistic temperature conditions. There is no longer a clear relation between fly ash content and long-term property development. Hence, a material model based on 28-day testing of specimens cured under 20 °C isothermal conditions will not give an accurate description of the property development for a fly ash concrete exposed to realistic curing temperatures, as would be the case for in-situ concrete structures.

Table 7.18; Mechanical property increase (Δ) between 28 and 91 days, realistic curing conditions

	Δf_c [MPa]	Δf_t [MPa]	ΔE_t [MPa]
ANL Ref.	4.6 (6 %)	-0.4 (-9 %)	500 (2 %)
ANL FA +16FA	4.0 (7 %)	0.7 (21 %)	-300 (-1 %)

Considering the given mechanical test series in retrospect, one set of tests beyond 91 days could have been included. This would have given an indication of whether or not the *ANL FA +16FA* tensile strength and the E-modulus had reached an upper level, or if they would have continued to develop over time. This is especially relevant with respect to the *ANL FA +16FA* E-modulus under realistic curing conditions, which shows no increase in value between 28 and 91 days, and thus seems to already have reached an upper level due to the elevated curing temperature. However, the number of test specimens in the current test series was limited by the number of available temperature-controlled moulds.

7.7 Compressive and tensile creep tests in the TSTM System

7.7.1 General

In the current work, the concrete's time-dependent stress response has been modelled by the "Double Power Law" and the principle of linear superposition as described in Section 3.5. The creep parameters originally used in the current TSTM stress calculations, Table 7.19, were assumed on the grounds of previous experience with corresponding concretes described by [Atrushi, 2003] and [Bjøntegaard et al., 2012]. Due to obtained deviations between measured and calculated restrained stress development in the TSTM System, it was decided to investigate the validity of the applied creep parameters. Hence, a limited series of creep tests were performed for the concretes *ANL FA* and *ANL FA +16FA* (containing 17 % and 33 % fly ash, respectively, as % by weight of cement + FA-content). For each concrete, one compressive and one tensile creep test were carried out. The creep test methods and procedures are described in Section 7.7.2 and Section 7.7.3, while the results are presented in Section 7.7.4 - Section 7.7.6 and discussed in Section 7.7.7.

Table 7.19; Originally assumed creep parameters, based on results and discussions reported by [Bjøntegaard et al., 2012]

	φ_0	d	p
ANL Ref.	0.75	0.20	0.21
ANL FA	0.75	0.20	0.21
ANL FA +8FA	1.37	0.20	0.21
ANL FA +16FA	1.37	0.20	0.21

7.7.2 Creep tests in the TSTM System

The creep tests were performed in the TSTM System at a constant temperature of 20 ^{o}C. All tests were carried out in the following way:

1. Mixing and casting in the TSTM System; i.e. in the TSTM and the Dilation Rig (dummy) as described in Chapter 5.
2. After casting, the software was programmed to let the TSTM specimen move freely, while the load was kept at 0.0 ± 0.02 MPa
3. At the chosen loading time, a load corresponding to 1.0 MPa compressive or tensile stress was applied to the TSTM specimen. Immediately after applying the load, the software was programmed to let the TSTM specimen move freely and to keep the stresses at 1.0 ± 0.02 MPa

During all creep tests, the following data were measured: free deformation in the Dilation Rig, deformation in the TSTM, stress in the TSTM, and finally the temperature in the Dilation Rig, the TSTM and the room. The creep strain was found by subtracting (for creep

in compression) or adding (for creep in tension) the free deformation measured in the Dilation Rig from the deformation measured in the TSTM. As the applied stress was 1.0 MPa, the obtained creep strain curves also represent the compliance function *J(t,t')*.

In order to maximize the practical relevance of the creep tests, experimentally achieved restrained stress curves were used to choose time and magnitude of loading. Hence, a load of 1.0 MPa compressive or tensile stress was applied and removed from the concrete specimen according to the stress development curve previously obtained from the TSTM as illustrated in Figure 7.29.

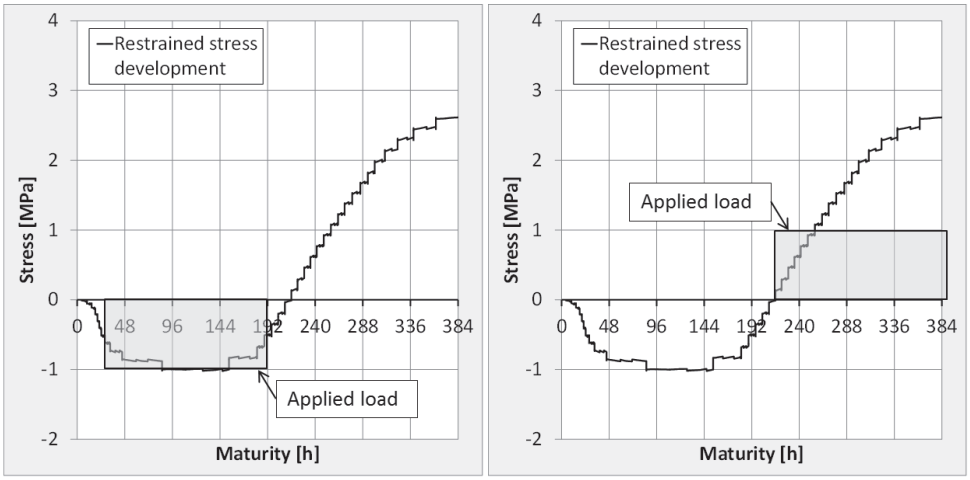

Figure 7.29; Applied load during TSTM creep tests designed according to the actual restrained stress for the given concrete: Creep in compression (left) Creep in tension (right), [Klausen et al., 2015]

It should be noticed that both compressive and tensile loads as well as compressive and tensile creep curves are presented with positive values in the following figures.

7.7.3 Creep model

In the current work, the time-dependent stress response of concrete has been modelled by the Double Power Law as described in Section 3.5. For each concrete, the creep test results were fitted to the compliance function:

$$J(t,t') = \frac{1}{E_c(t'_{eq})}\left[1 + \varphi_0 \cdot {t'_{eq}}^{-d} \cdot (t-t')^p\right] \qquad \textit{Equation 7.2}$$

where t [days] is the concrete age, t' is the concrete age at which the actual stress was applied, $E_c(t_{eq}')$ is the E-modulus at t_{eq}', t_{eq}' is the maturity at t', and φ_0, d and p are creep model parameters

First, the parameter d was determined by using the method of least squares when combining both test results (creep in compression and creep in tension). Secondly, the parameters φ_0 and p were found by two different approaches as described in the following:

- Using the method of least squares for only the given creep test result; i.e. creep in compression or creep in tension
- Using the method of least squares when combining both creep test results; i.e. creep in compression and creep in tension

Consequently, for each concrete three sets of creep parameters were determined: 1) creep in compression, 2) creep in tension and 3) creep in tension and compression combined.

As can be seen from Equation 7.2, the E-modulus is very important when determining the creep model parameters. For all performed creep tests, two E-moduli are presented: E_0, which is the E-modulus found based on mechanical testing (see Section 7.4) and E_{TSTM}, which is the E-modulus found directly from the stress/strain relation during loading in the TSTM in the given test (see Section 8.5). For all tests, E_{TSTM} was decided used when determining the creep model parameters as described above.

7.7.4 Creep test results for *ANL FA*

The current section presents the results from the two *ANL FA* creep tests. Figure 7.30 shows load and deformations measured in the Dilation Rig and the TSTM during the compressive creep test. In this test, a compressive stress of 1.0 MPa (which equals 5 % of the compressive strength at the time of loading) was applied at 25 hours. Figure 7.31 presents load and deformation measured in the Dilation Rig and the TSTM during the tensile creep tests, where 1.0 MPa tensile stress was applied at 218 hours. This stress level corresponds to 34 % of the tensile strength at the time of loading. For both tests, all strains are zeroed at the loading time. The creep curves obtained from the measurements are given in Figure 7.32

The E-modulus used when determining the creep model parameters for *ANL FA* are presented in Table 7.20. Both E-moduli approaches (E and E_{TSTM}) show good agreement with respect to the E-modulus development over time. The E-modulus determined directly from the TSTM for the given test, E_{TSTM}, was used when estimating the *ANL FA* creep model parameters.

Table 7.20; Creep tests, E-modulus at loading, ANL FA

ANL FA	**Time** [h]	E [MPa]	E_{TSTM} [MPa]
Creep in compression	25	20250	20400
Creep in tension	218	28800	28500

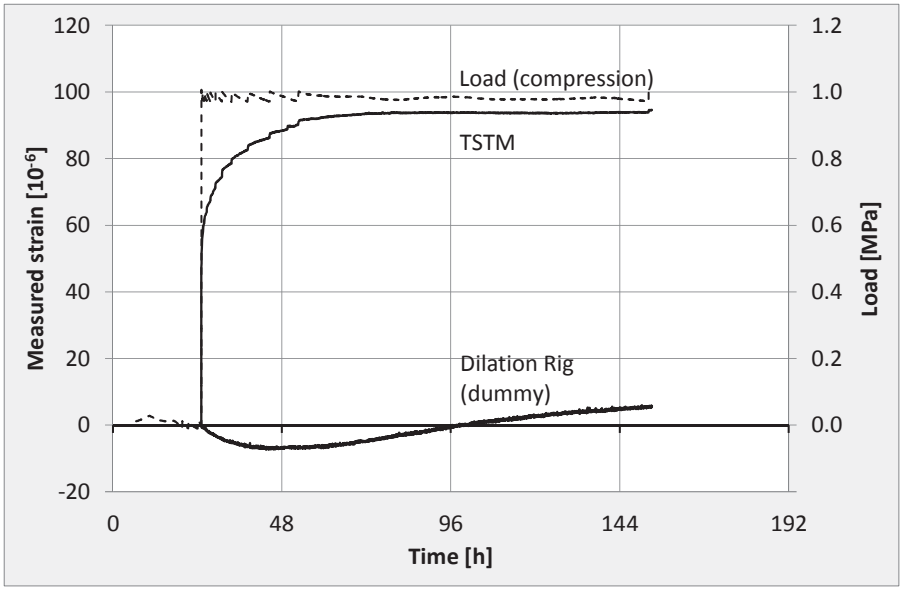

Figure 7.30; Compressive creep test: measured load and strains, ANL FA

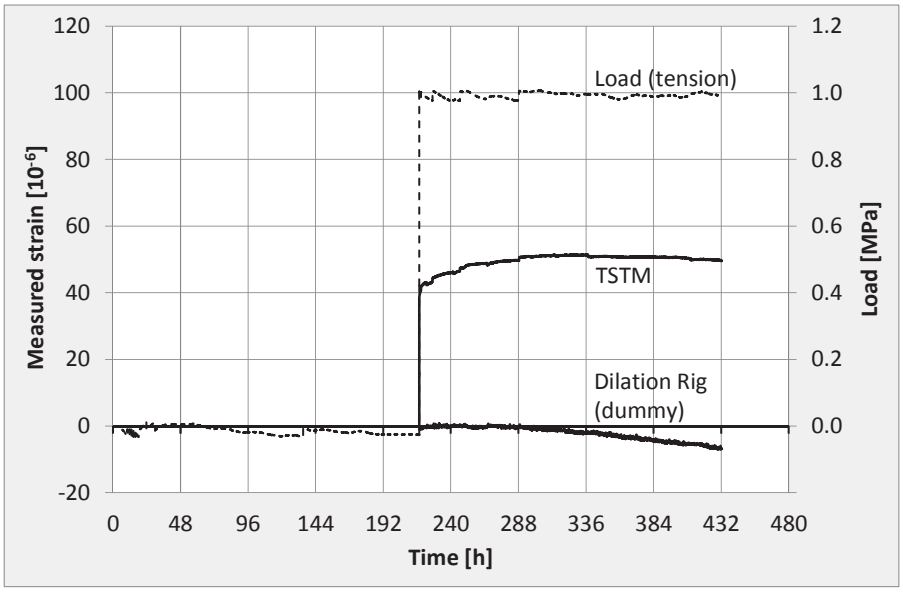

Figure 7.31; Tensile creep test: measured load and strains, ANL FA

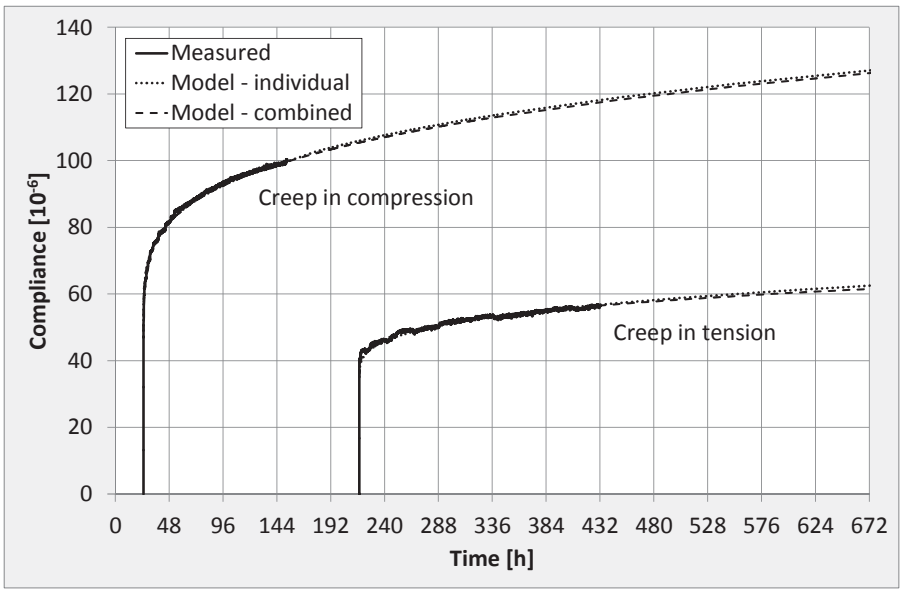

Figure 7.32; Measured and modelled creep strains, ANL FA

Table 7.21 presents the *ANL FA* creep model parameters determined by the method presented in the previous section. The table shows three sets of creep parameters: 1) creep in compression 2) creep in tension and 3) creep in compression and tension combined. From the results it seems as if creep in compression (φ_0 = 0.68) has a somewhat higher initial creep than creep in tension (φ_0 = 0.63), while creep in tension (p = 0.31) seems to have a slightly higher creep development over time than creep in compression (p = 0.26). Overall, the three different sets of creep parameters show a considerable resemblance.

The similarity between the obtained sets of creep parameters is also illustrated in Figure 7.32, which compares the measured creep results with the Double Power Law creep models when using the different sets of obtained creep model parameters. As can be seen from the figure, both sets of creep parameters determined individually from each test, as well as the creep parameters based on both tests combined, give a very good description of the measured creep both in compression and tension.

Table 7.21; Creep model parameters, ANL FA

ANL FA	φ_0	***d***	***p***
Creep in compression	0.68	0.32	0.26
Creep in tension	0.63	0.32	0.31
Combined creep	**0.67**	**0.32**	**0.28**

7.7.5 Creep test results for *ANL FA +16FA*

The current section presents the results from the *ANL FA +16FA* creep tests. During the first tensile creep test, one of the LVDTs spring supports failed 24 hours after loading. The test was therefore repeated and only the test results from the latter test are presented in the current section. However, up to the spring support failure the two nominally identical tests are very much alike, see Figure 6.26 in Section 6.3.8, strengthening the confidence in the results obtained from the given creep tests. Loads and deformations measured in the TSTM System during the compressive and tensile *ANL FA +16FA* creep tests are given in Figure 7.33 and Figure 7.34, respectively. For the compressive creep test, 1.0 MPa (representing 9 % of the compressive strength at the time of loading) was applied at 25 hours, while for the tensile creep test the load was applied at 218 hours. This stress level corresponds to 38 % of the tensile strength at the time of loading. For both tests, all strains are zeroed at the loading time.

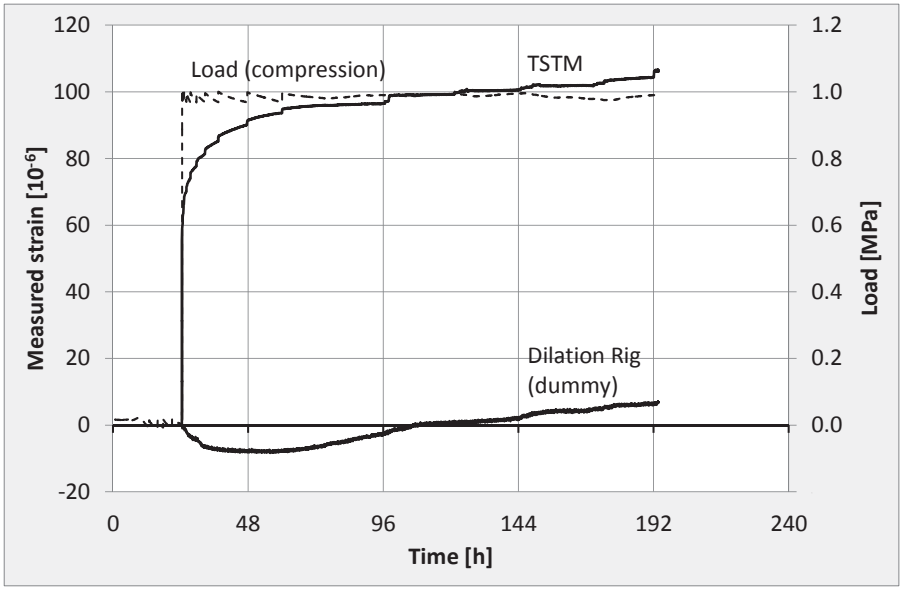

Figure 7.33; Compressive creep test: measured load and strains, ANL FA +16FA

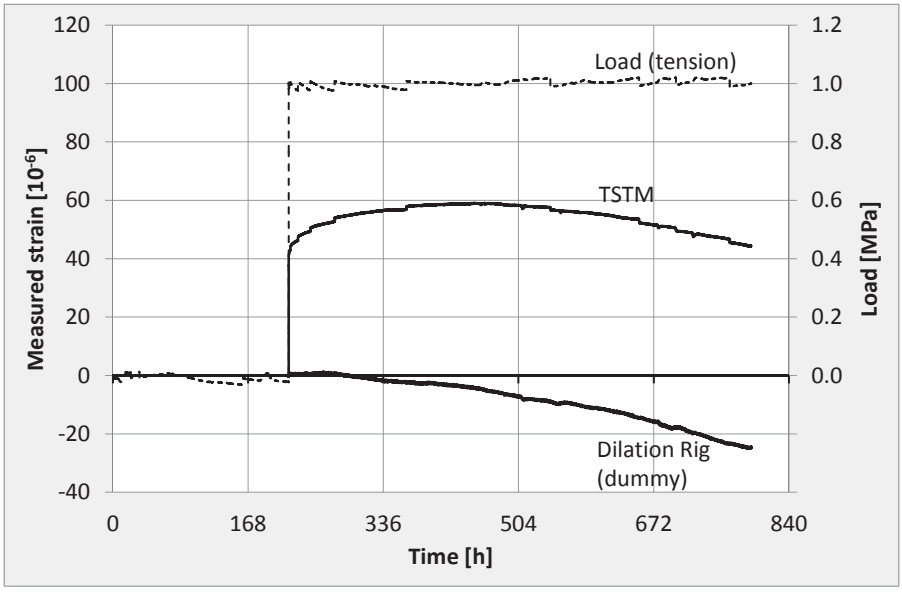

Figure 7.34; Tensile creep test: measured load and strains, ANL FA +16 FA

The E-moduli used when determining the *ANL FA +16FA* creep model parameters are presented in Table 7.22. The E-modulus found directly from the TSTM in the given creep test gives a higher value than the E-modulus estimated from mechanical testing, especially for creep in compression at 25 hours. This is probably caused by variation in test results, and as for *ANL FA*, E_{TSTM} was decided used in the current creep parameter estimation.

Table 7.22; Creep tests, E-modulus at loading, ANL FA +16FA

ANL FA +16FA	**Time** [h]	***E*** [MPa]	E_{TSTM} [MPa]
Creep in compression	25	15850	17700
Creep in tension	218	25900	26500

Table 7.23 presents the creep model parameters determined from the *ANL FA +16FA* creep test results. The parameters were found by the method presented in Section 7.7.3. The table shows three sets of creep parameters: 1) creep in compression, 2) creep in tension and 3) a combined set of parameters describing both creep in compression and creep in tension. For *ANL FA +16FA* it seems as if creep in tension ($\varphi_0 = 0.53$) has a slightly higher initial creep than creep in compression ($\varphi_0 = 0.48$), while creep in compression ($p = 0.35$) seems to have a somewhat higher creep development over time than creep in tension ($p = 0.31$). This is the opposite trend as seen for *ANL FA*. However, as for *ANL FA*, the three different sets of creep parameters are quite similar.

The resemblance between the obtained sets of creep model parameters is illustrated in Figure 7.35, which compares the measured creep results with the creep calculated from the obtained sets of creep model parameters. As for *ANL FA*, both sets of creep parameters determined individually from each of the creep tests, as well as the set of parameters determined based on both creep tests combined, give a very good description of the measured creep, both for creep in compression and creep in tension.

Table 7.23; Creep model parameters, ANL FA +16FA

ANL FA +16FA	φ_0	***d***	***p***
Creep in compression	0.48	0.22	0.35
Creep in tension	0.53	0.22	0.31
Combined creep	**0.49**	**0.22**	**0.33**

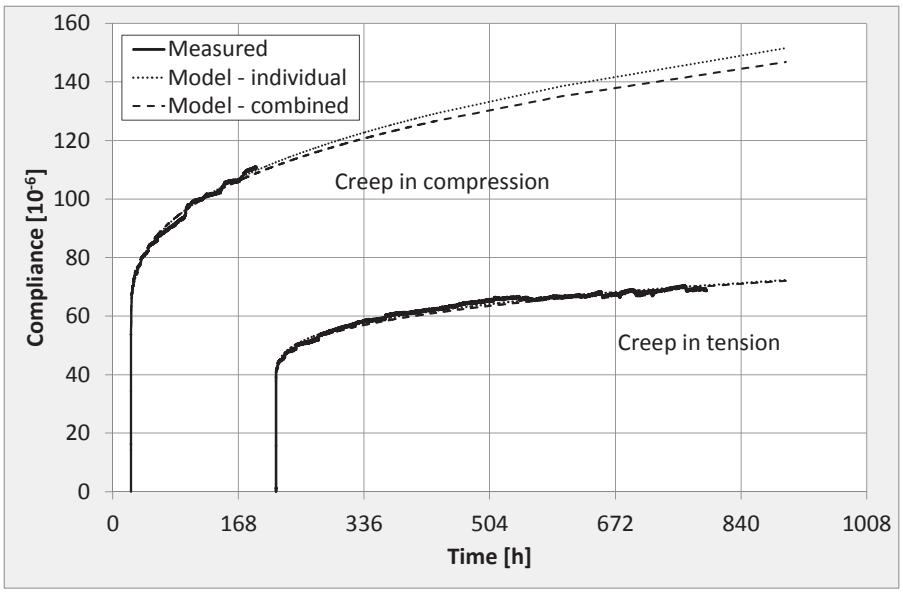

Figure 7.35; Measured and modelled creep strains, ANL FA +16FA

7.7.6 Creep recovery

The *ANL FA +16FA* compressive creep test was actually run for a longer time than given in Figure 7.33. The test was unloaded at 194 hours, and then the load (1.0 MPa) was reapplied at 291 hours. The measured load and strain for the entire test, including unloading and reloading, is given in Figure 7.36. The E-moduli determined at loading, unloading and reloading are given in Table 7.24. As in the previous sections, the E-

modulus obtained directly from the TSTM for the given creep test, E_{TSTM}, has been used in the creep modelling. When using the previously found creep parameters, Table 7.23, a significant deviation between measured and calculated creep is obtained from the time of unloading at 194 hours, Figure 7.37. Somewhat surprisingly, the best fit between measured and modelled creep is achieved when the creep recovery is set to zero. This result indicates that for the given concrete and time of loading/unloading, no creep strain is recovered when unloading the compressive load. These findings are supported by calculations performed in Chapter 8, which shows that the best agreement between restrained stress calculations and measured TSTM test results are provided when the creep recovery is set to zero. This result is further discussed in Section 7.7.7.

Table 7.24; Compressive creep test, E-modulus at loading, unloading and reloading, ANL FA +16FA

ANL FA +16FA	**Time** [h]	***E*** [MPa]	E_{TSTM} [MPa]
Creep in compression (loading)	25	15850	17700
Creep recovery (unloading)	194	25650	26000
Creep in compression (reloading)	289	26500	27300

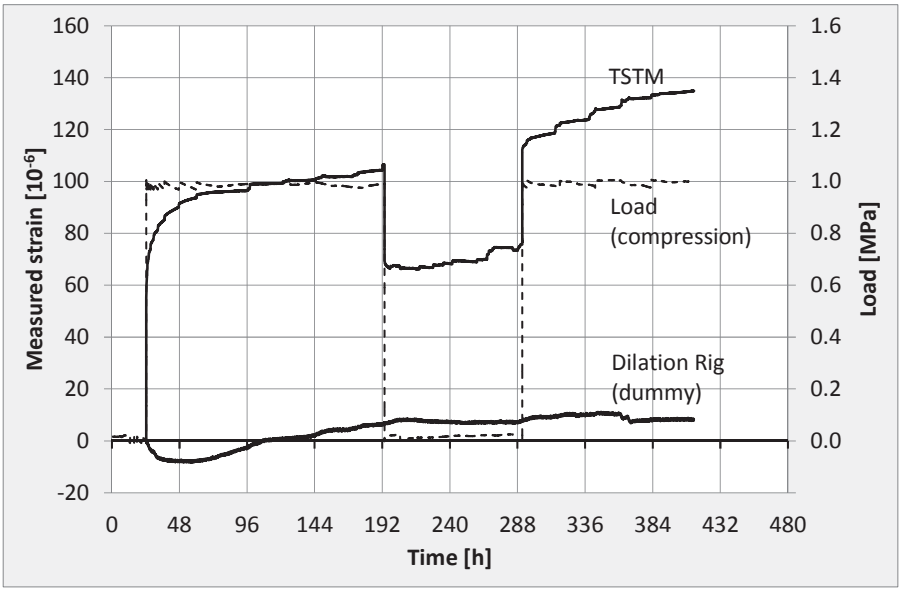

Figure 7.36; Compressive creep test including unloading and reloading, measured load and strains, ANL FA +16FA

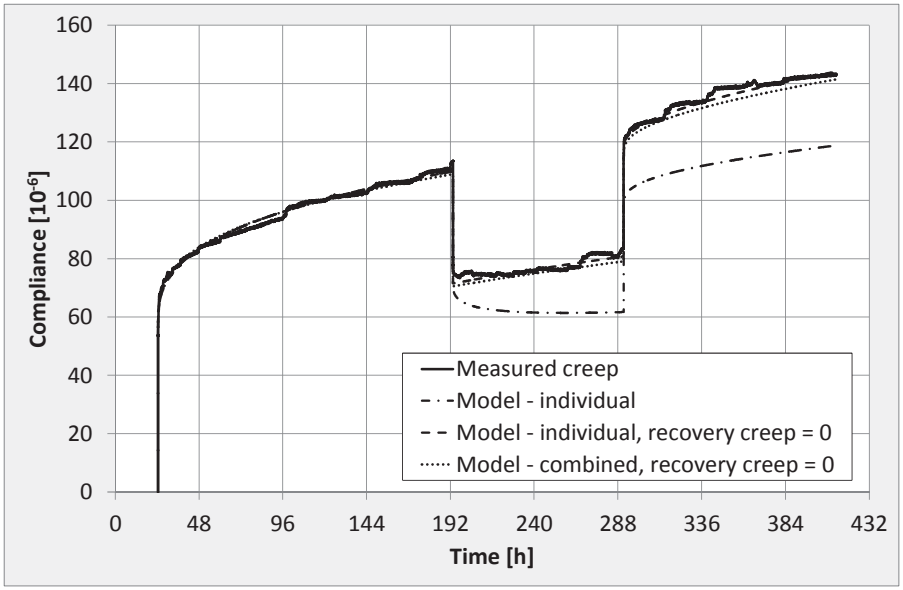

Figure 7.37; Measured and modelled creep strains, including creep recovery and reloading, ANL FA +16FA

7.7.7 Discussion of TSTM creep test results

The creep parameters deduced from the current creep tests (*ANL FA* and *ANL FA +16FA*) are summarized in Table 7.25. All sets of creep parameters must be considered in combination with the E-modulus of the given concrete when evaluating the actual creep development. Table 7.25 also shows the creep parameters for the reference concrete *ANL Ref.*, which were kept as originally assumed due to the good agreement between TSTM test results and corresponding restrained stress calculations. The creep parameters for the two remaining concretes, *ANL FA +8FA* and *ANL FA +28FA,* were further estimated based on the three sets of creep parameters already established and fly ash content.

The performed creep tests confirm that the fly ash concretes have a quite different viscoelastic behaviour than initially assumed. Originally, the creep was assumed to increase with an increasing amount of fly ash in the concrete as found by [Ji, 2008] and [Bjøntegaard et al., 2012]. The current creep test series shows that the creep is in fact increasing with increasing amount of fly ash (Figure 7.38), but not as much as originally assumed. For both tensile and compressive creep tests, the increase in creep at 336 hours is 7.1 % for *ANL FA +16FA* when compared to *ANL FA*. With the originally assumed sets of creep parameters, the corresponding increase in creep would have been as much as 43 % and 67 % for tensile and compressive creep, respectively. The opposite tendency, i.e. a decrease in creep with increasing fly ash content, has been found by other researchers, e.g. [Kuder et al., 2012] and [Wang et al., 2011]. A comprehensive series of creep tests

performed by [Sennour et al., 1989] showed, however, that while one type of fly ash would reduce creep, another type of fly ash would slightly increase the creep properties of the concrete.

Table 7.25; Creep parameters used in restrained stress calculations

	φ_0	d	p
ANL Ref.[*]	**0.75**	**0.20**	**0.21**
ANL FA	**0.67**	**0.32**	**0.28**
ANL FA +8FA[**]	0.60	0.24	0.31
ANL FA +16FA	**0.49**	**0.22**	**0.33**
ANL FA +28FA[**]	0.30	0.24	0.35

[*)] *assumed based on previous experience*
[**)] *estimated based on ANL Ref., ANL FA and ANL FA +16FA*

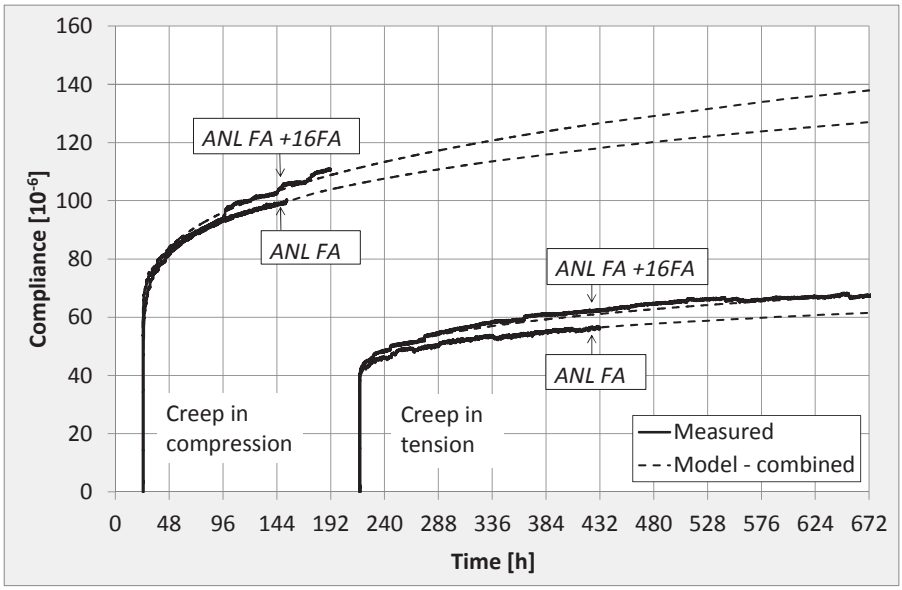

Figure 7.38; Measured and modelled creep strains, compliance function

Both [Atrushi, 2003] and [Ji et al., 2012] found that the creep behaviour in compression and tension was quite different for early age concretes containing mineral additives: while the initial creep and creep rate was higher for creep in compression than for creep in tension, the creep rate decreased continuously in time in a higher degree for the compressive creep than for the tensile creep. After a while, the compressive and tensile

creep curves would cross, leading to a higher tensile creep than compressive creep over time. Contradictorily, the results from the current creep test series show very similar creep behaviour in both compression and tension. The current compressive and tensile creep tests differ from [Atrushi, 2003] and [Ji et al., 2012] (as well as from many of the compressive versus tensile creep comparisons found in the literature) by the following conditions:

- Both compressive and tensile creep tests were performed with the same experimental equipment, the TSTM. Hence, all creep tests were performed on specimens with exactly the same dimensions and the same curing conditions.
- For both compressive and tensile creep tests, the test specimens were subjected to the same load level, i.e. 1.0 MPa. The time and magnitude of the loading in the current creep tests were decided from experimentally achieved restrained stress curves from the TSTM. This was done in order to maximize the relevance of the obtained creep parameters with respect to the restrained stress calculations of the TSTM. Contradictorily, for most of the compressive versus tensile creep comparisons found in the literature, a load corresponding to a percentage of the compressive cube strength or the uniaxial tensile strength, respectively, have been used during testing.

Due to the similar compressive and tensile creep behaviour found in the current test series, it was concluded to use the creep parameters found when combining compressive- and tensile creep test results during the final TSTM restrained stress calculations in Chapter 8. Comparisons between TSTM test results and corresponding restrained stress calculations showed that the creep parameters found from the performed creep tests gave a much better description of the creep behaviour of the fly ash concretes than the originally assumed parameters, which very much validates the obtained creep test results. The creep parameters used in the TSTM restrained stress calculations were found to have a considerable effect on the obtained stress curves, underlining the substantial importance of correct creep parameters when conducting restrained stress calculations.

During the *ANL FA +16FA* compressive creep test, the TSTM specimen was loaded at 25 hours, unloaded at 194 hours and then reloaded at 289 hours. Quite surprisingly, the result indicates no creep recovery when unloading the compressive load. These findings are supported by restrained stress calculations performed in Chapter 8, where the calculations give better agreement with the TSTM test results when creep recovery is set to zero. Although experimental results regarding creep recovery only was obtained for *ANL FA +16FA*, calculations in Chapter 8 indicate that this could be the case for all the fly ash concretes used in the current work. Correspondingly, [Staquet et al., 2005] found that numerical predictions of creep recovery by the principle of superposition deviated strongly from experimental data and that another creep recovery model was called for.

7.8 The coefficient of thermal expansion (CTE)

The coefficient of thermal expansion (CTE) was unfortunately not investigated and systematically determined during the current work. Initially, due to the challenging verification of the TSTM System, the main attention was given to the stress and displacement results. Although the CTE was determined for each test, it was found under different test conditions, e.g. concrete age, temperature steps and/or the time-span over which they were applied. Finally, far into the TSTM test series, one systematic temperature loop for CTE determination was introduced: temperature steps of ±3 ^{o}C around an initial temperature of 20 ^{o}C. However, also when using an identical temperature loop for each test, the CTE kept varying from test to test, also for nominally identical concretes. It was for instance seen that the tests subjected to winter temperature conditions provided a quite different CTE than the corresponding summer tests.

The main objective of the current work has been the stress calculations. As the total free deformation measured in the Dilation Rig was used as input, an accurate value for CTE was not considered to be decisive. A correct CTE value was however more important for the autogenous deformation (AD) results presented in Chapter 8.2, and a certain inaccuracy has been introduced to the deduced AD by the currently applied simplification of a constant CTE. This inaccuracy occurs as an early parallel displacement of the AD curve (increased contraction), see Chapter 3.2. For each concrete, the CTE was determined as an average value based on different tests with varying test conditions. The obtained CTE values are presented in Table 7.26, and they have (as previously described) been used for deduction of AD-curves as well as for early age stress calculations in Chapter 8.

Table 7.26; The Coefficient of Thermal Dilation

Concrete	CTE
ANL Ref.	9.0
ANL FA	9.1
ANL FA +8FA	9.0
ANL FA +16FA	9.2
ANL FA +28FA	9.4

7.9 Model parameters for restrained stress calculations - summary

The established basis of material parameters used for early age stress analysis is summarized in the following. The material parameters are based on the previously described models, tests and discussions. The model parameters *A* and *B*, describing the activation energy, are presented in Table 7.27, while the parameters describing the

compressive strength and the start time for stress calculations t_0 are given in Table 7.28. The determined tensile model parameters are shown in Table 7.29.

In Section 7.6, the 28-days E-modulus for the fly ash concrete was found to increase when subjected to realistic temperature curing conditions. The same trend has been seen for realistic temperature tests in the TSTM System. Based on these results, it was decided to use the 28-day E-modulus deduced from the TSTM tests for early age stress calculations. This was done by increasing the model parameter E_{28} according to TSTM test results, while keeping the other model parameter n_E as found in Section 7.4.5. The final E-modulus model parameters are given in Table 7.30.

The creep model parameters and the coefficients of thermal expansion are presented in Table 7.31 and Table 7.32, respectively.

Table 7.27; Activation energy model parameters

Concrete	***A*** [J·mol^{-1}]	***B*** [J·mol^{-1}·K^{-1}]
ANL Ref.	31482	296
ANL FA	31487	197
ANL FA +8FA	32958	273
ANL FA +16FA	37023	0
ANL FA +28FA	42000	0

Table 7.28; Compressive strength model parameters

Concrete	f_{c28} [MPa]	***s***	t_0 [Maturity hours]
ANL Ref.	80.3	0.200	8.8
ANL FA	71.2	0.257	9.5
ANL FA +8FA	65.7	0.295	11.0
ANL FA +16FA	53.6	0.356	12.0
ANL FA +28FA	45.3	0.424	13.0

Table 7.29; Tensile strength model parameters

Concrete	f_{t28} [MPa]	n_t
ANL Ref.	3.86	0.484
ANL FA	3.55	0.589
ANL FA +8FA	3.28	0.509
ANL FA +16FA	3.05	0.486
ANL FA +28FA	3.02	0.665

Table 7.30; E-modulus model parameters

Concrete	E_{28} [GPa]	n_E	$E_{28\ TSTM}$ [GPa]
ANL Ref.	32.45	0.348	32.80
ANL FA	30.55	0.299	31.50
ANL FA +8FA	27.70	0.233	31.00
ANL FA +16FA	27.80	0.252	30.50
ANL FA +28FA	24.88	0.189	29.50

Table 7.31; Creep parameters used in restrained stress calculations

Concrete	φ_0	d	p
ANL Ref.[*]	0.75	0.20	0.21
ANL FA	0.67	0.32	0.28
ANL FA +8FA[**]	0.60	0.24	0.31
ANL FA +16FA	0.49	0.22	0.33
ANL FA +28FA[**]	0.43	0.24	0.35

[*] *assumed based on previous experience*

[**] *estimated based on ANL Ref., ANL FA and ANL FA +16FA*

Table 7.32; The coefficient of thermal dilation, CTE

Concrete	**CTE**
ANL Ref.	9.0
ANL FA	9.1
ANL FA +8FA	9.0
ANL FA +16FA	9.2
ANL FA +28FA	9.4

8 The TSTM System - test results and restrained stress calculations

8.1 Introduction

A series of restrained stress tests has been run in the TSTM System. For each test, the following results have been obtained:

- Free deformation in the Dilation Rig,
  i.e. Thermal Dilation (TD) and Autogenous Deformation (AD)
- Stress development in the TSTM
- Incremental E-modulus development in the TSTM
- Final tensile strength and E-modulus at the end of the test in the TSTM

The tests performed in the TSTM System include various concretes and temperature histories, and the following notation has been used to identify the concrete and the temperature history in question:

"Concrete name (T_{init}/T_{max})"

where T_{init} is the initial temperature of the fresh concrete and T_{max} is the maximum concrete temperature during testing.

As described in Chapter 4, the given concrete series consists of five concretes with *w/b* = 0.40: *ANL Ref.*, *ANL FA*, *ANL FA +8FA*, *ANL FA +16FA* and *ANL FA +28FA*. The concretes have a fly ash content of 0 %, 17 %, 25 %, 33 % and 45 %, respectively, achieved by an increasing replacement of cement with fly ash (the fly ash (FA) content is given as percentage of the total amount of cement + FA). In addition, all concretes contain 5 % silica fume (by weight of cement + FA).

Section 8.2 presents autogenous deformation results deduced from free deformation measurements in the Dilation Rig. The autogenous deformation results have been (together with material parameters determined in Chapter 7) used as input for the TSTM stress calculations described in Section 8.3. Measured and calculated stress developments for all performed TSTM tests are presented in Section 8.4. Section 8.5 shows incremental E-moduli deduced from TSTM tests, as well as the final tensile strength and E-modulus obtained at the end of the tests (i.e. when loading until failure).

8.2 Autogenous deformation, Dilation Rig

8.2.1 General

For all tests in the TSTM System (both restrained stress tests and pure creep tests), free deformation has been measured in the Dilation Rig. The measured free deformation is the sum of thermal dilation (TD) and autogenous deformation (AD). AD has been deduced by removing TD from the measured total deformation, using coefficients of thermal expansion

(CTEs) as found in Chapter 7.8. As previously discussed, the current use of a constant CTE may introduce an inaccuracy to the deduced AD, see Chapter 3.2. However, under isothermal conditions, i.e. for the 20 °C isothermal tests as well as realistic temperature tests beyond two weeks, the AD is found directly from the measurements and is thus not dependent on the CTE. All AD curves presented in the following start at t_0 (i.e. $t_0 = t_{0,\ TSTM}$ as described in Section 7.5).

An overview of all tests performed in the Dilation Rig is given in Table 8.1. As previously described, all the realistic temperature tests in the TSTM were performed with individual temperature histories representing the given concrete cast in an 800 mm thick wall, see Chapter 7.3. It should however be noticed that while the calculated temperature histories were based on two different sets of cement batches as described in Table 8.1 and Chapter 7.3, most TSTM tests were actually performed with the cement batches EG1-10 (reference concrete) and TF5-14 (fly ash concretes), see Table 4.7. Section 8.2.2 – Section 8.2.6 present the deduced AD curves for each concrete, respectively. Comparisons and discussions of the obtained AD results are given in Section 8.2.7.

Table 8.1; Free deformation tests performed in the Dilation Rig, overview

	Isothermal 20 °C	**Realistic temperature conditions**		
		Summer*		**Winter***
		*Temperature from cement batch EG1-10/TF3-11**	*Temperature from cement batch EG1-14/TF5-14**	*Temperature from cement batch TF5-14**
ANL Ref	3	3	-	-
ANL FA	2	1	2	1
ANL FA +8FA	-	1	-	-
ANL FA +16FA	4	2	1	-
ANL FA +28FA	-	-	1	1

*) *The curing temperatures applied during testing are based on heat development from each individual concrete mixed with the listed cement batch, the tests were however actually performed with cement batch EG1-10 and TF5-14 (see Table 4.7). Summer and winter curing conditions are explained in Chapter 7.3.*

8.2.2 ANL Ref.

AD curves for three 20 °C isothermal *ANL Ref.* tests are given in Figure 8.1. The results show very similar behaviour in AD: a rapid contraction between t_0 and 12 hours, followed by a small period of stagnation between 12 and 20 hours which gradually transits into a small contraction over time until the test is ended.

AD deduced from three nominally identical tests with realistic temperature conditions (*ANL Ref. (20/62))* are presented in Figure 8.2. The CTE was set to $9.0 \cdot 10^{-6}$ /°C as found in Chapter 7.8. All AD curves show the same rapid contraction up to 24 hours. However, while one of the tests continues with a gradual contraction beyond 24 hours, the AD development in the two other tests seems to experience a small stagnation. One of the tests was ended after 90 hours. For the two tests run longer than 96 hours, it is noticeable that AD occurs as an expansion between 96 and 168 hours. A decreased CTE value (smaller than $7.0 \cdot 10^{-6}$ /°C) would remove this expansion, however, all CTE test results indicate that the CTE for *ANL Ref.* is $9.0 \cdot 10^{-6}$ /°C (see Chapter 7.8). After 168 hours (beyond which the temperature is 20 °C and AD is measured directly), the development of AD stops and the AD stays at a constant level for the rest of the test, i.e. for 13 days.

Figure 8.3 compares AD obtained under 20 °C isothermal conditions with AD obtained under realistic temperature conditions. The results show a very different behaviour of AD for isothermal tests when compared to the realistic temperature tests. The isothermal tests show a slower initial contraction, however, while AD under realistic temperature conditions flattens out after a week, the isothermal tests continue to contract gradually and eventually surpass the realistic temperature tests. AD versus maturity is given in Figure 8.4, which clearly shows that the temperature influence on AD could not be compensated for by the maturity principle.

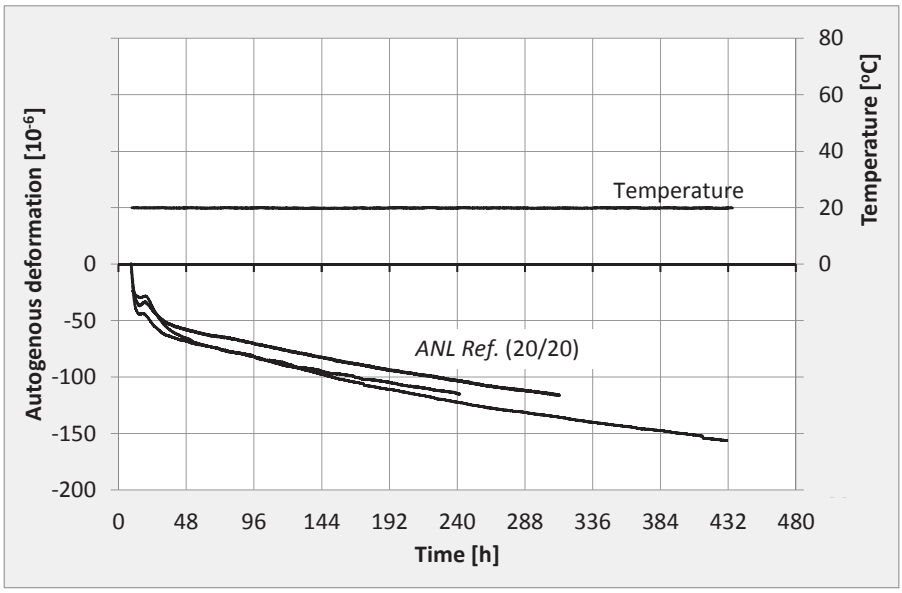

Figure 8.1; Measured autogenous deformation, ANL Ref., three nominal identical tests, 20 °C isothermal conditions

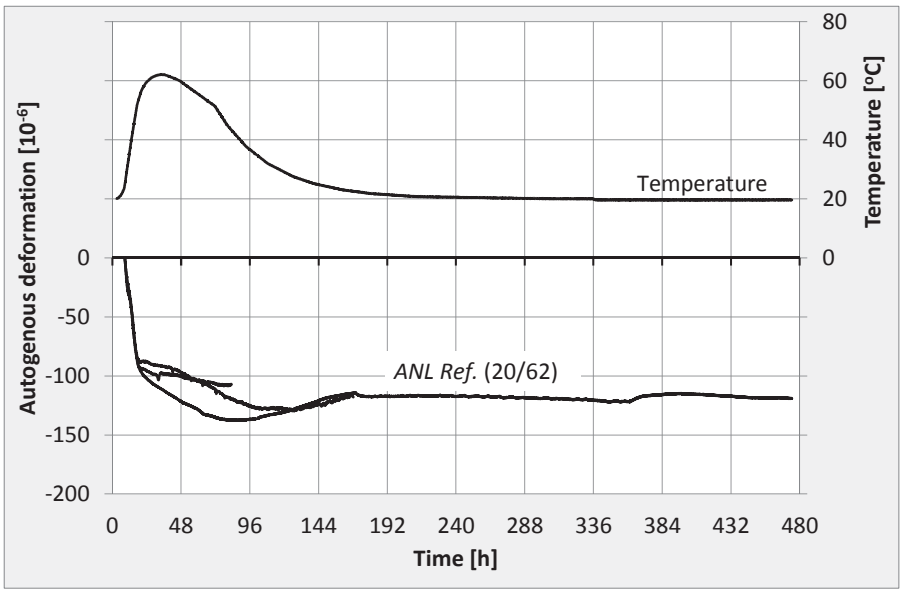

Figure 8.2; Measured autogenous deformation, ANL Ref., three nominal identical tests, realistic temperature conditions

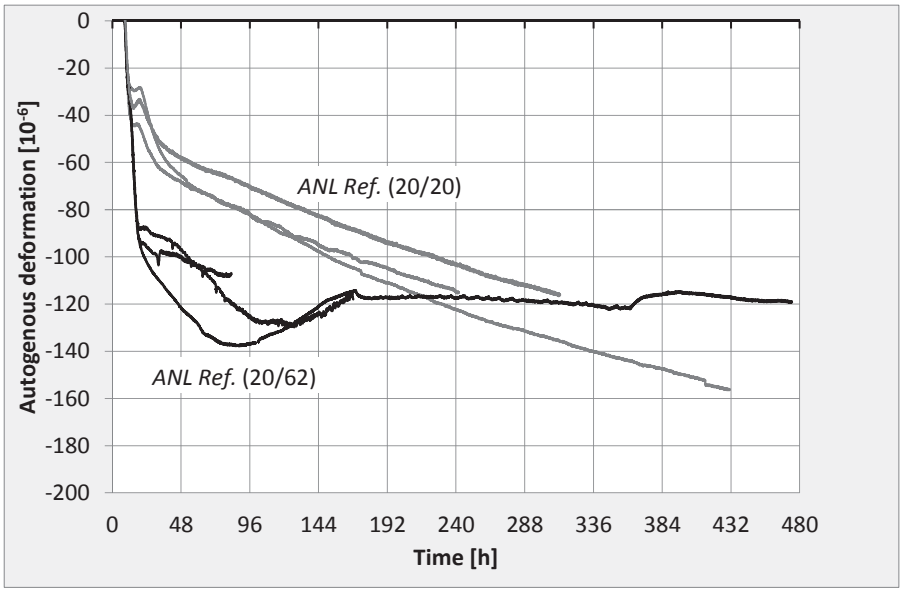

Figure 8.3; Measured autogenous deformation versus time, ANL Ref., all tests

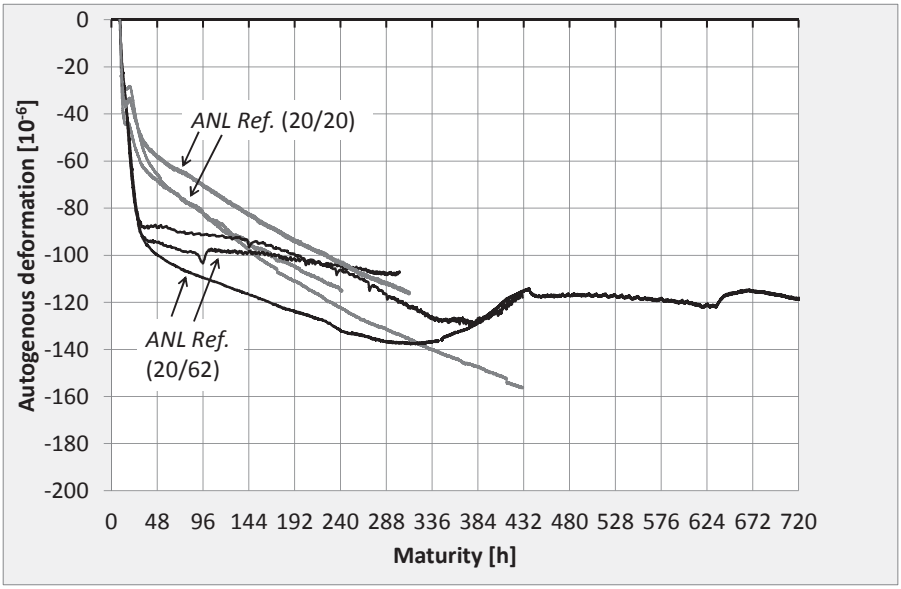

Figure 8.4; Measured autogenous deformation versus maturity, ANL Ref., all tests

8.2.3 ANL FA

AD curves from two nominally identical 20 °C isothermal *ANL FA* tests are given in Figure 8.5. The two AD curves are virtually identical; the lines in the graph appear on top of each other and cannot be visually separated. The AD curves show a contraction of 40 μstrains up to 24 hours, followed by a slow expansion over 10 days which gradually changes back into a very slow contraction. At 18 days, the total AD is still only -35 μstrains.

Figure 8.6 and Figure 8.7 show AD deduced from the following four *ANL FA* tests subjected to realistic temperature histories:

- *ANL FA (10/43)* winter conditions (the temperature history was based on heat evolution data from the TF5-14 cement batch)
- *ANL FA (20/59)* summer conditions (temp. based on the TF5-14 cement batch)
- *ANL FA (20/52)* summer conditions (temp. based on the TF3-11 cement batch)
- *ANL FA (20/34)* summer conditions (but with reduced temperature development caused by the temperature control system, see Section 6.4)

For all tests, the CTE was set to $9.1 \cdot 10^{-6}$ /°C as found in Chapter 7.8. The tests show a rapid AD development (contraction) up to 24 hours, which coincides with the heat development phase in the concrete. During the next three days, the AD behaviour seems to differ between the tests: while AD for *ANL FA (20/34)* turns into an expansion, the AD curves

for the other tests continue to contract. Approximately 5 days after mixing, the AD behaviour for all tests flattens out.

The AD curves for all *ANL FA* tests are compared in Figure 8.8 (versus time) and in Figure 8.9 (versus maturity). The figures show that there is a systematic increase in AD (contraction) with increasing maximum temperature, with exception of *ANL FA (10/43)*, which was the test with the lower fresh concrete temperature (winter conditions). However, when looking at the maximum temperature increase, $\Delta T_{max} = T_{max} - T_{init}$, AD (contraction) was found to be systematically increasing with increasing ΔT_{max} for all tests. After two weeks of maturity (336 hours), the AD was: -28, -51, -135, -146 and -181 μstrain, for a ΔT_{max} of 0, 14, 32, 33 and 39 °C, respectively. This observation is further discussed in Section 8.2.7.

All tests show a fast AD development (contraction) between t_0 and 24 hours. Between 24 hours and 144 hours, the rate of AD development seems to change systematically with ΔT_{max}. While *ANL FA (20/20)* and *ANL FA (20/34)* (the two tests with the lowest ΔT_{max}) experiences AD as an expansion between 24 and 144 hours, the other tests shows AD as a contraction which seems to be increasing with increasing ΔT_{max}. Beyond 144 hours, the AD development for the three tests with the highest ΔT_{max} more or less stops and stay at a constant level throughout the tests, while *ANL FA (20/20)* and *ANL FA (20/34)* keeps developing AD as a contraction, but at a rather limited rate.

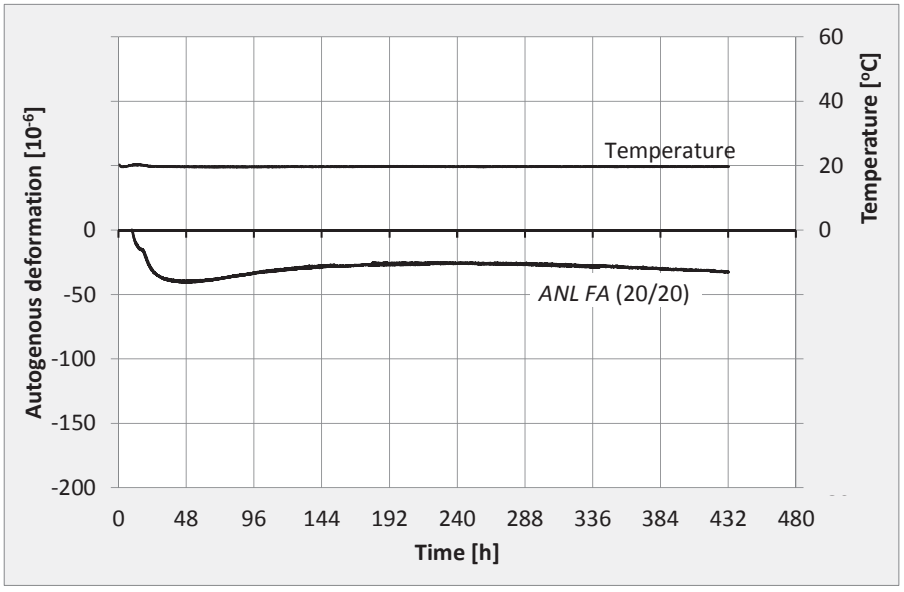

Figure 8.5; Measured autogenous deformation, ANL FA, two nominal identical tests, 20 °C isothermal conditions

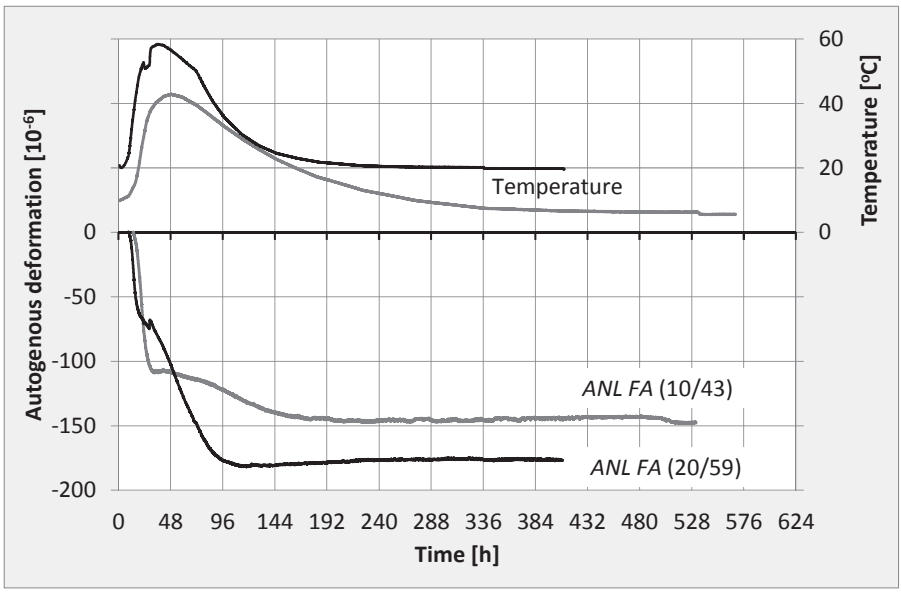

Figure 8.6; Measured autogenous deformation, ANL FA, realistic temperature tests: winter- and summer conditions based on cement TF5-14 heat development

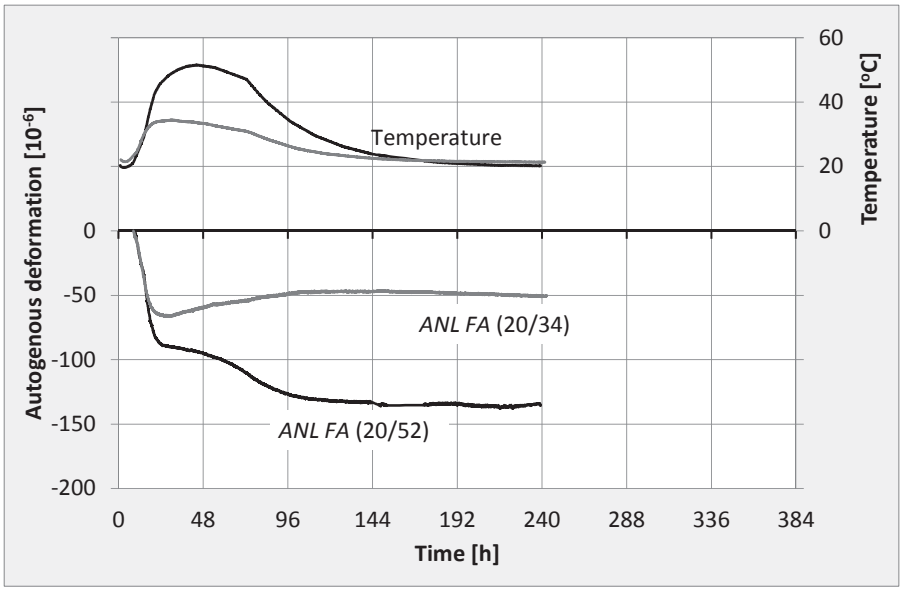

Figure 8.7; Measured autogenous deformation, ANL FA (20/34) and ANL FA (20/52), realistic temperature tests: summer conditions based on cement batch TF3-11

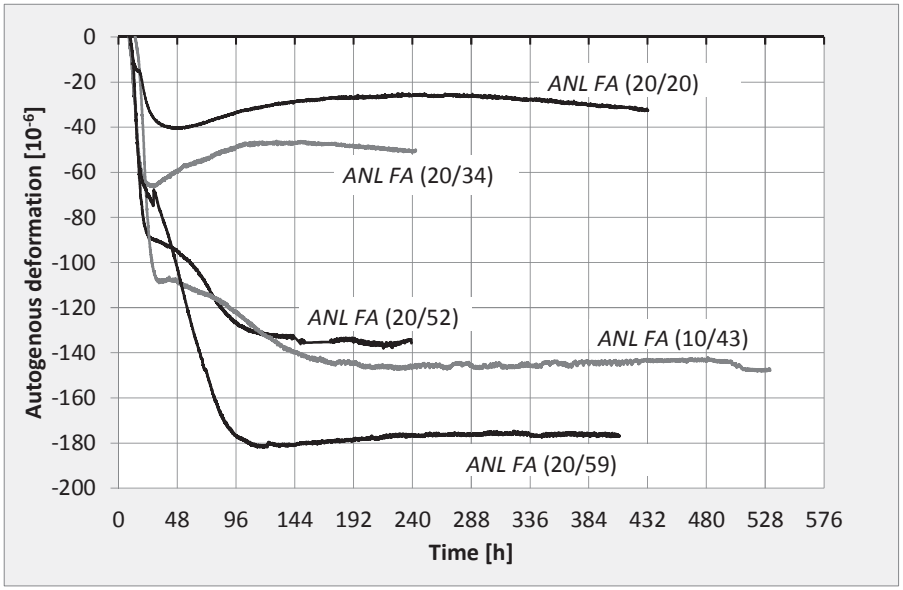

Figure 8.8; Measured autogenous deformation versus time, ANL FA, all tests

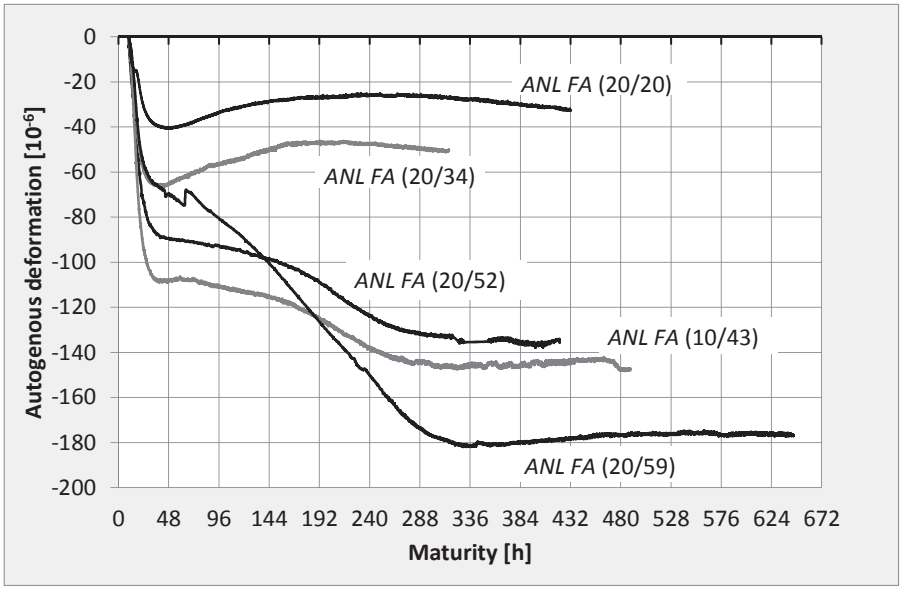

Figure 8.9; Measured autogenous deformation versus maturity, ANL FA, all tests

8.2.4 ANL FA +8FA

The deduced AD curve representing *ANL FA +8FA* under realistic temperature conditions is given in Figure 8.10. The concrete was subjected to a temperature history based on heat development data from the TF3-11 cement batch. A CTE of $9.0 \cdot 10^{-6}$ /°C was used as determined in Chapter 7.8. The AD results showed a rapid contraction between t_0 and 24 hours, followed by a slow but continuous contraction until the test was ended after 7 days.

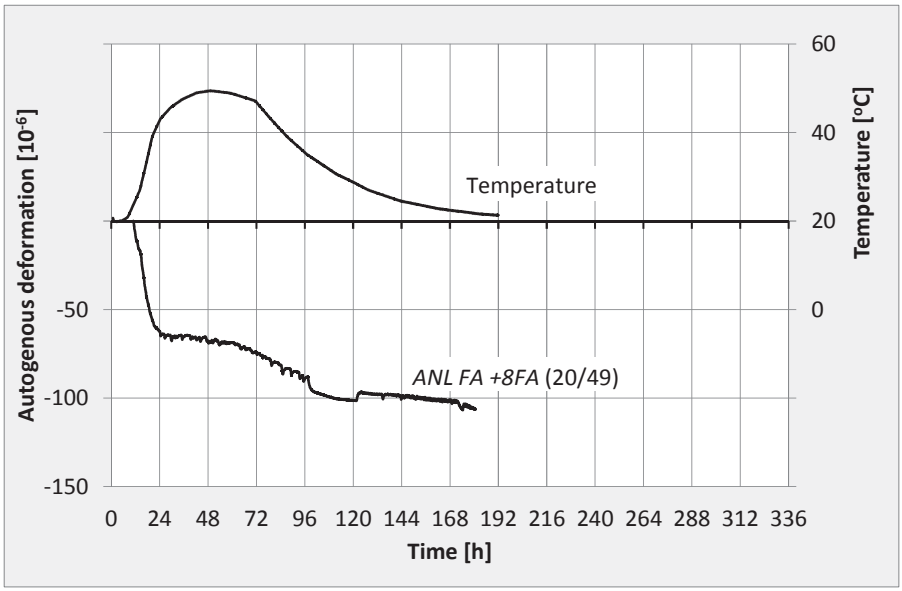

Figure 8.10; Autogenous deformation, ANL FA +8FA, realistic temperature conditions

8.2.5 ANL FA +16FA

Figure 8.11 shows AD curves deduced from four 20 °C isothermal *ANL FA +16FA* tests, three of which are creep tests. The tests were evaluated numerically in Chapter 6.2.5, and showed very good reproducibility with a standard deviation at 48 and 288 hours of only 2.5 and 2.6 µstrain, respectively. The AD curves show a fast initial contraction, followed by a small expansion which gradually changes back into a contraction after approximately 10 days. A slow but continuous contraction followed until the tests were ended (3-5 weeks).

AD curves deduced from the following 3 tests subjected to realistic temperature histories are presented in Figure 8.12:

- *ANL FA +16FA (20/45)* 2 nominally identical tests subjected to summer conditions. The temperature history was based on heat evolution data from the TF3-11 cement batch
- *ANL FA +16FA (20/50)* summer conditions (temperature based on the TF4-15 cement batch)

The CTE was set to $9.2 \cdot 10^{-6}$ /°C as found in Chapter 7.8. Figure 8.12 shows that the two *ANL FA +16FA (20/45)* tests provide very similar behaviour in AD. All the realistic temperature tests show a rapid contraction up to 24 hours, i.e. during the concrete heat development phase. However, while *ANL FA +16FA (20/45)* shows a gradual and constant AD contraction development from 24 hours and up to as much as 7 weeks when the test is ended, *ANL FA +16FA (20/50)* continuous with a rather fast increase in AD contraction also beyond the heat development phase until the curve flattens out after approx. three days.

AD curves for both isothermal and realistic temperature tests are presented in Figure 8.13 (versus time) and Figure 8.14 (versus maturity). An increasing maximum temperature seems to affect the rate of AD development between 24 and 168 hours. The isothermal tests experience an expansion, while the AD for the realistic temperature tests occurs as a contraction which is increasing with increasing maximum temperature.

The AD measured beyond 336 hours (2 weeks) is measured under 20 °C isothermal conditions for all tests, and is thus not influenced by the applied CTE. It is noticeable that both *ANL FA +16FA (20/20)* and *ANL FA +16FA (20/45)* keeps developing AD (contraction) at the same constant rate up until the tests are ended at 5 and 7 weeks, respectively.

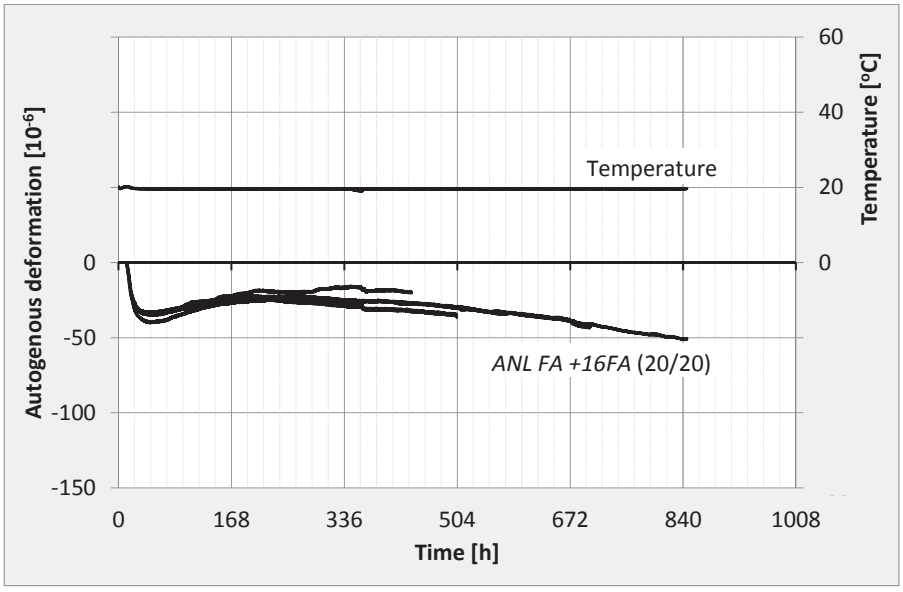

Figure 8.11; Measured autogenous deformation, ANL FA +16FA, four nominally identical tests, 20 °C isothermal conditions

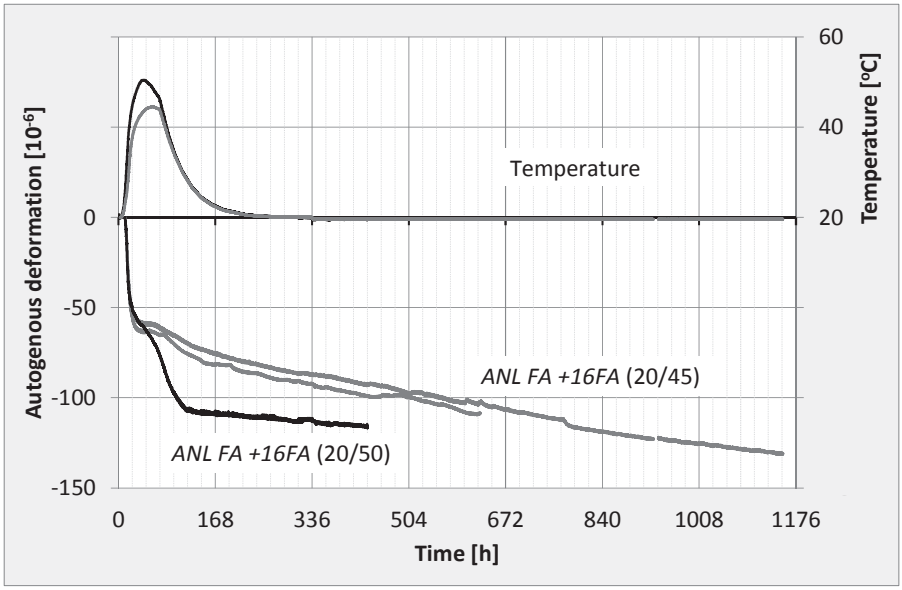

Figure 8.12; Measured autogenous deformation, ANL FA +16FA, three tests under realistic temperature conditions

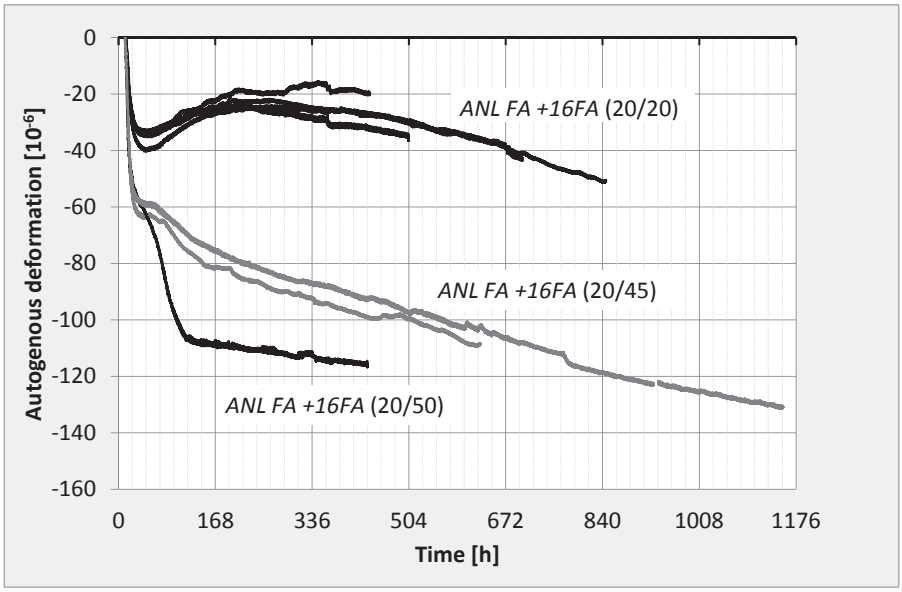

Figure 8.13; Measured autogenous deformation versus time, ANL FA +16FA, all tests

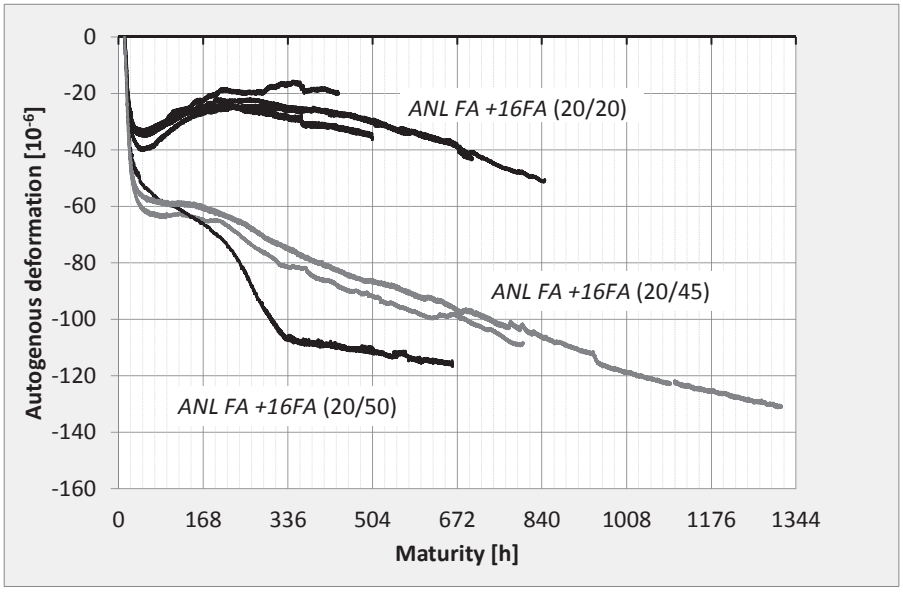

Figure 8.14; Measured autogenous deformation versus maturity, ANL FA +16FA, all tests

8.2.6 ANL FA +28FA

Two TSTM tests subjected to realistic temperature histories were performed with *ANL FA +28FA*:

- *ANL FA +28FA (10/26)* winter conditions (temperature history based on the TF4-15 cement batch)
- *ANL FA +28FA (20/44)* summer conditions (temperature based on the TF4-15 cement batch)

For *ANL FA +28FA (20/44),* a CTE of $9.4 \cdot 10^{-6}$ /^{o}C was used, see Chapter 7.8. However, for *ANL FA +28FA (10/26)*, the unplanned temperature increase and decrease at 336 hours gave a CTE of only $7.2 \cdot 10^{-6}$ /^{o}C. It was decided to use the CTE found directly from the TSTM test, i.e. CTE = $7.2 \cdot 10^{-6}$ /^{o}C, for *ANL FA +28FA (10/26).*

The AD curves are presented in Figure 8.15 (versus time) and Figure 8.16 (versus maturity). Both tests show a swift increase in AD (contraction) up to two days. However, while *ANL FA +28FA (20/44)* continues to develop AD (contraction) gradually over time, the AD curve representing *ANL FA +28FA (10/26)* experiences a small expansion before it flattens out and stays constant during the rest of the measurement, i.e. for 11 weeks.

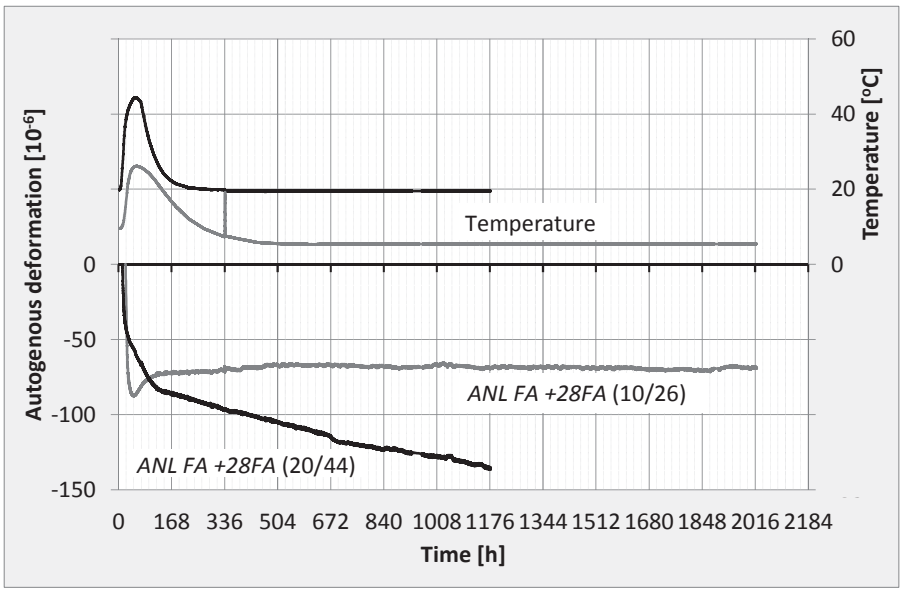

Figure 8.15; Measured autogenous deformation, ANL FA +28FA, realistic temperature conditions representing summer and winter, respectively

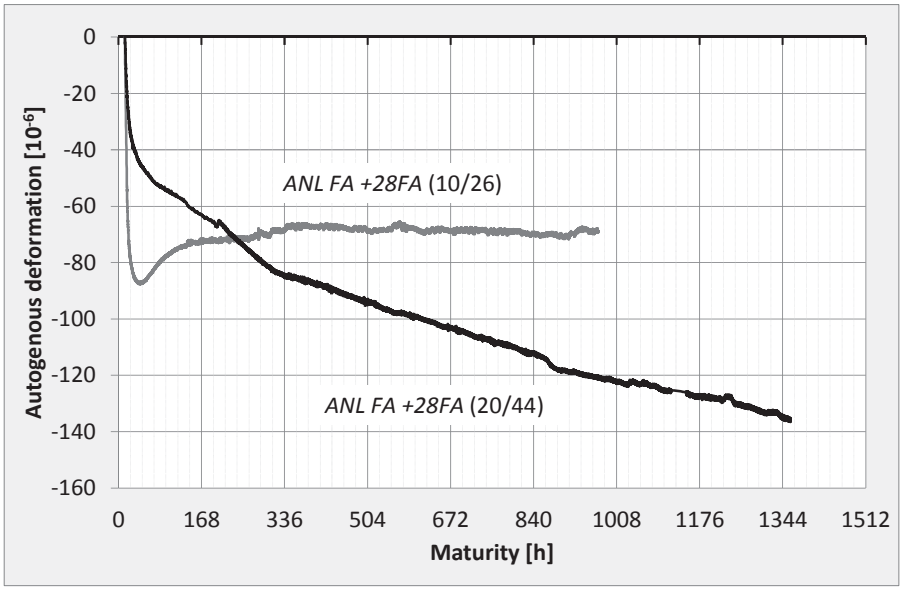

Figure 8.16; Measured autogenous deformation versus maturity, ANL FA +28FA, realistic temperature conditions representing summer and winter, respectively

8.2.7 Discussion of autogenous deformation results

AD curves for *ANL Ref.*, *ANL FA* and *ANL FA +16FA* under 20 °C isothermal conditions are presented in Figure 8.17. All concretes show a rapid initial AD development (contraction) between t_0 and 24 hours. However, while AD for *ANL Ref.* continuous to contract at a constant (but somewhat slower) rate also after 24 hours, the AD for the two fly ash concretes transits into an expansion. After 8 days of expansive AD development, the AD gradually changes back into a small but continuous contraction. *ANL FA* and *ANL FA +16FA* show very similar behaviour in AD under 20 °C isothermal conditions, but they differ considerably from the much more pronounced AD development found for *ANL Ref.* Hence, the two cements ANL and ANL FA seem to induce quite different AD under 20 °C isothermal conditions. Further, due to the very similar AD development found for the two fly ash concretes, the increasing replacement of cement by fly ash does not seem to affect the AD behaviour under 20 °C isothermal conditions. However, it should be noticed that this observation is based on AD curves from two fly ash concretes only, and could not be said to constitute a general validity.

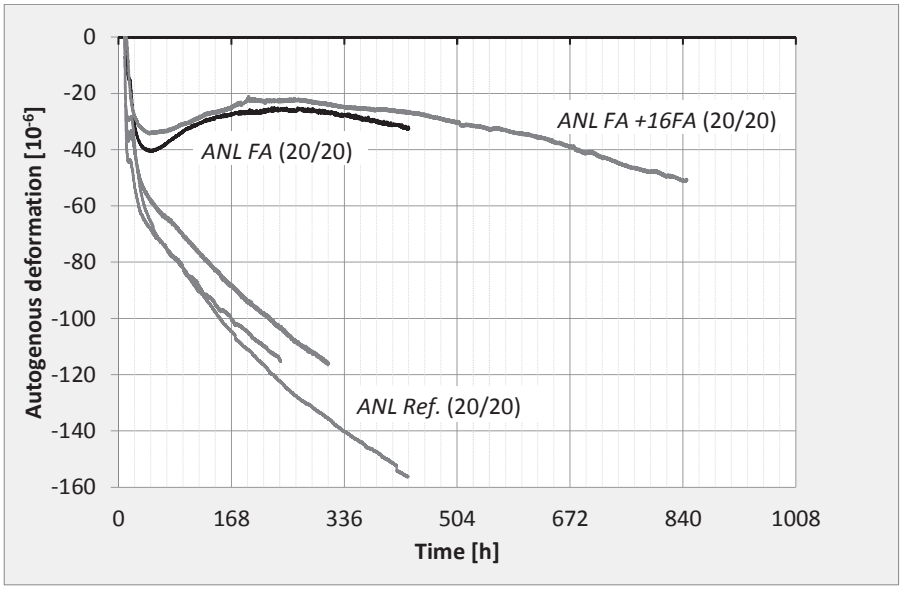

Figure 8.17; Autogenous deformation, 20 °C isothermal conditions, all tests

During the realistic temperature tests, each concrete was subjected to its own temperature history representing an 800 mm thick wall as described in Section 7.3. Three series of realistic temperature histories (differed by surrounding temperature conditions and cement batch) were used: *Summer I*, *Summer II* and *Winter*, see Table 8.2. The two summer conditions *Summer I* and *Summer II* simulate the wall cast with two different batches of cement. As described in Chapter 7.4, the change in cement batch did not seem to affect the mechanical properties of the concretes, with exception from a small increase in tensile strength for *ANL Ref.* with the new cement batch. Hence, the main differences between the

two wall simulations, *Summer I* and *Summer II*, are the applied temperature histories (see Section 7.3) and the corresponding measured AD.

Table 8.2; Series of realistic temperature histories used for tests in the TSTM System

	Summer I	**Summer II**	**Winter**
Temp. from Cement batch*	TF3-11	TF5-14	TF5-14
Tests	*ANL Ref. (20/62)* *ANL FA (20/52)* *ANL FA +8FA (20/49)* *ANL FA +16FA (20/45)*	*ANL Ref. (20/62)* *ANL FA (20/59)* *ANL FA +16FA (20/50)* *ANL FA +28FA (20/44)*	*ANL FA (10/43)* *ANL FA +28FA (10/26)*

**) The applied temperature history in the test is based on heat evolution from the listed ANL FA cement batch, all fly ash concretes were actually tested with cement batch TF5-14*

Deduced AD curves for *Summer I* are given in Figure 8.18 (versus time) and Figure 8.19 (versus maturity), while AD curves for *Summer II* are presented in Figure 8.20 (versus time) and Figure 8.21 (versus maturity). AD curves deduced from the tests performed under winter conditions, *Winter*, are presented in Figure 8.22 (versus time) and Figure 8.23 (versus maturity). The AD obtained under isothermal conditions (Figure 8.17) appears to be fundamentally different from the corresponding AD deduced from realistic temperature tests. From this follows that for the current concretes, AD under realistic temperature conditions cannot be modelled and predicted based on isothermal test results and the maturity principle. Similar conclusions were made by e.g. [Bjøntegaard, 1999] and [Jensen et al., 1999]. [Orosz et al., 2014] evaluated two models previously used to describe AD at the Luleå University of Technology. One of the models was solely based on the maturity principle, while the other model was based on both the maturity principle and a separate temperature adjustment factor. The evaluation showed that neither of the models was found to give a satisfying description of the AD. Providing AD measurements in the laboratory for all occurring temperature histories in a complex concrete structure is however impossible. In such cases, the maturity concept could still be useful when combined with AD deduced from realistic temperature tests. This would still give a better description of the actual AD than when based on isothermal AD test results. For most cases, TD is still the most important driving force with respect to early age volume changes in concrete structures.

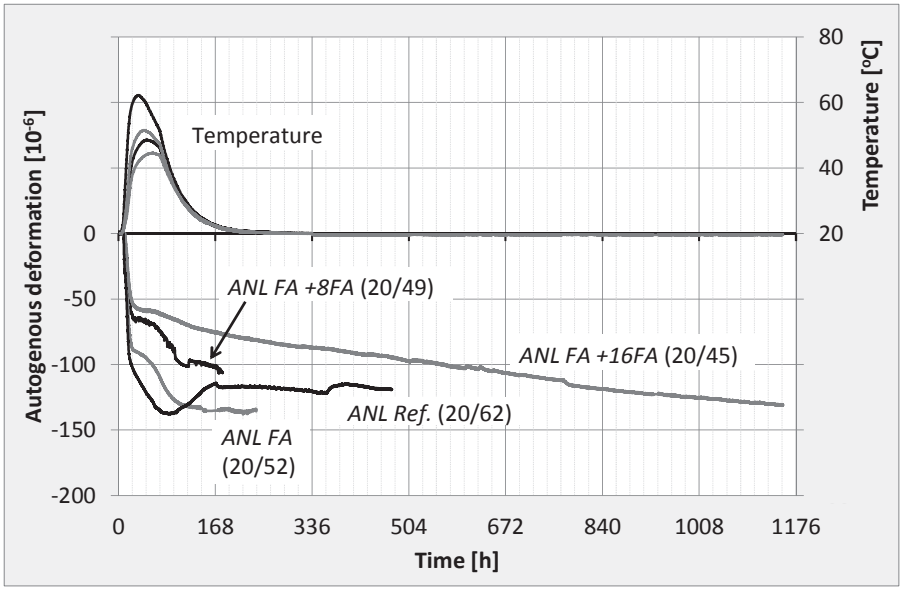

Figure 8.18; Autogenous deformation, realistic temperature conditions, Summer I (TF3-11 cement), ANL Ref., ANL FA, ANL FA +16FA and ANL FA +28FA

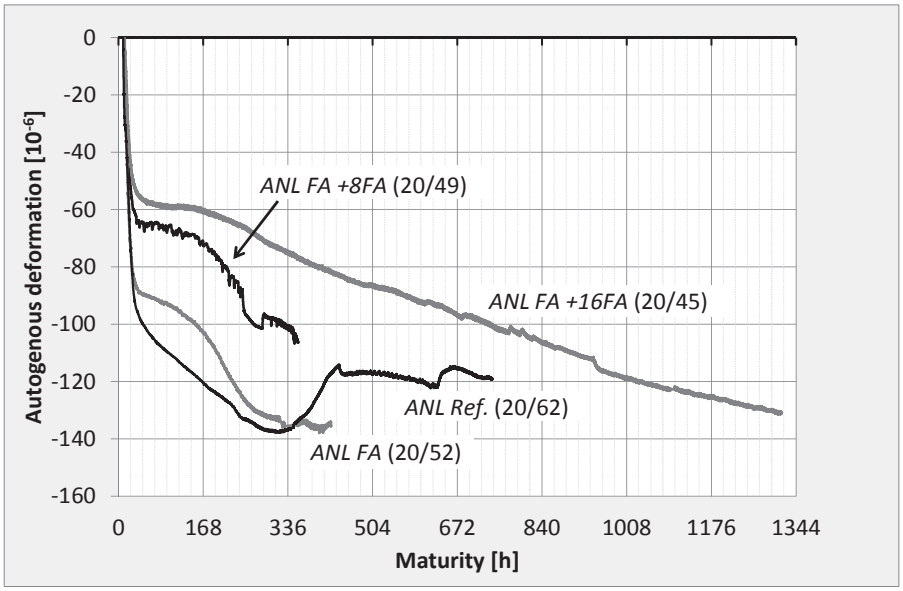

Figure 8.19; Autogenous deformation versus maturity, realistic temperature conditions, Summer I (TF3-11 cement), ANL Ref., ANL FA, ANL FA +16FA and ANL FA +28FA

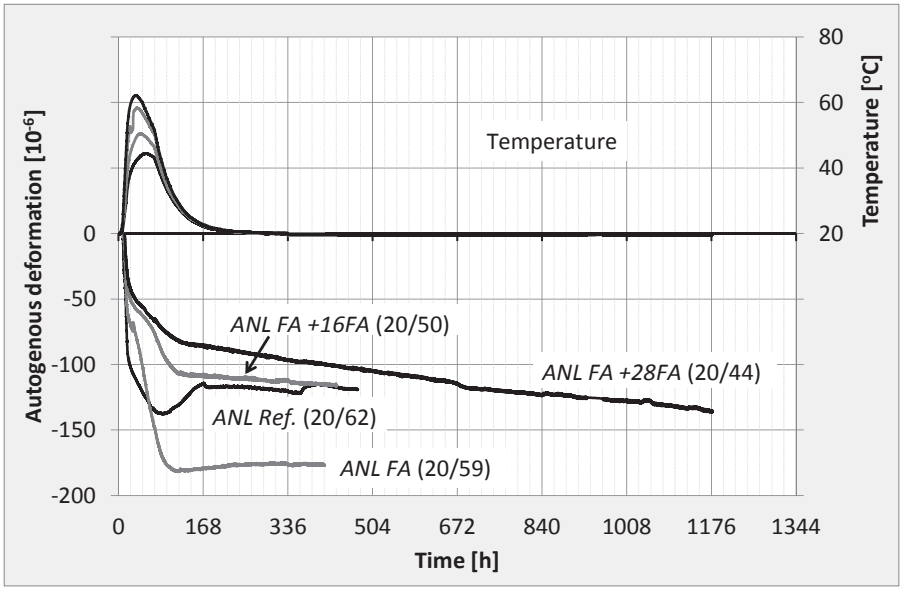

Figure 8.20; Autogenous deformation, realistic temperature conditions, Summer II (TF4-15 cement), ANL Ref., ANL FA, ANL FA +16FA and ANL FA +28FA

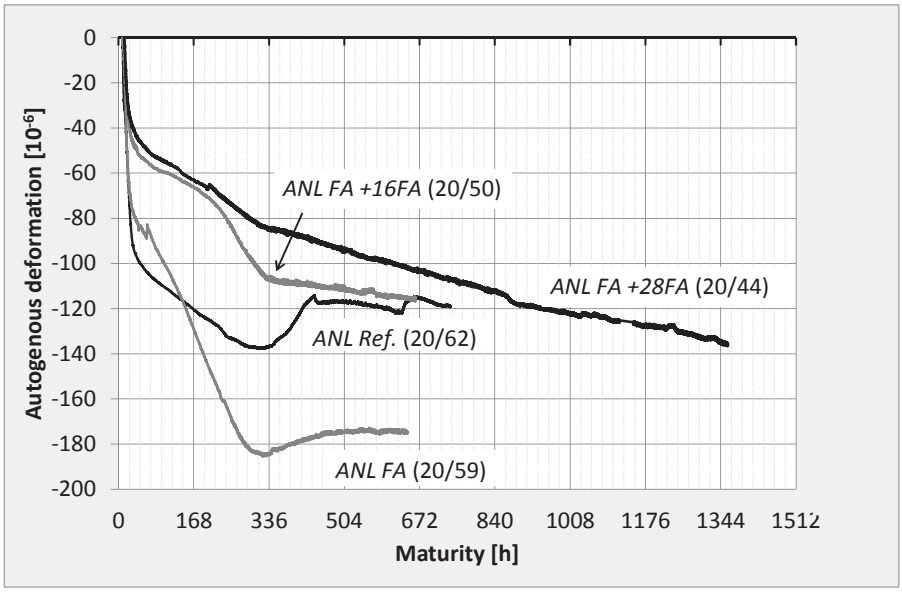

Figure 8.21; Autogenous deformation versus maturity, realistic temperature conditions, Summer II (TF4-15 cement), ANL Ref., ANL FA, ANL FA +16FA and ANL FA +28FA

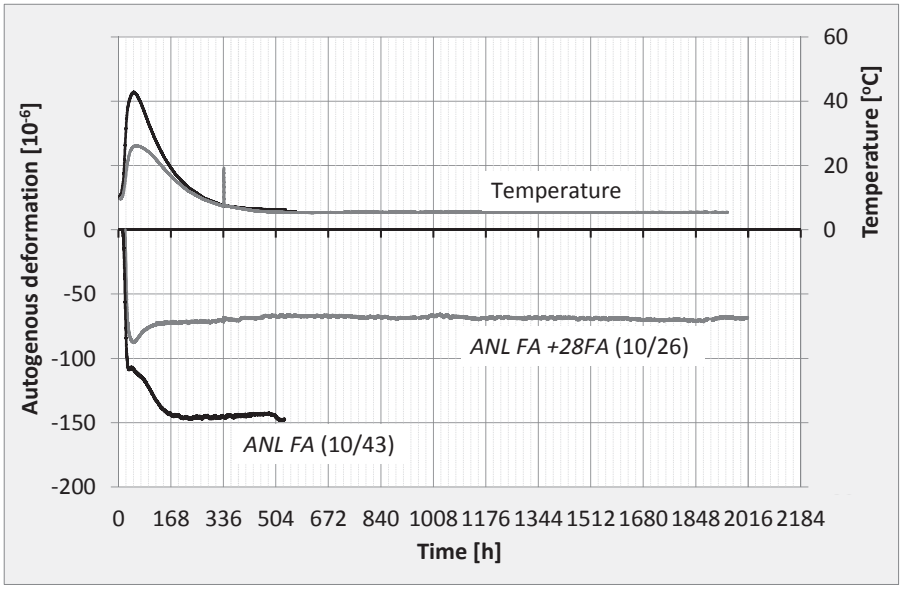

Figure 8.22; Autogenous deformation under realistic temperature conditions, Winter, ANL FA +16FA and ANL FA +28FA

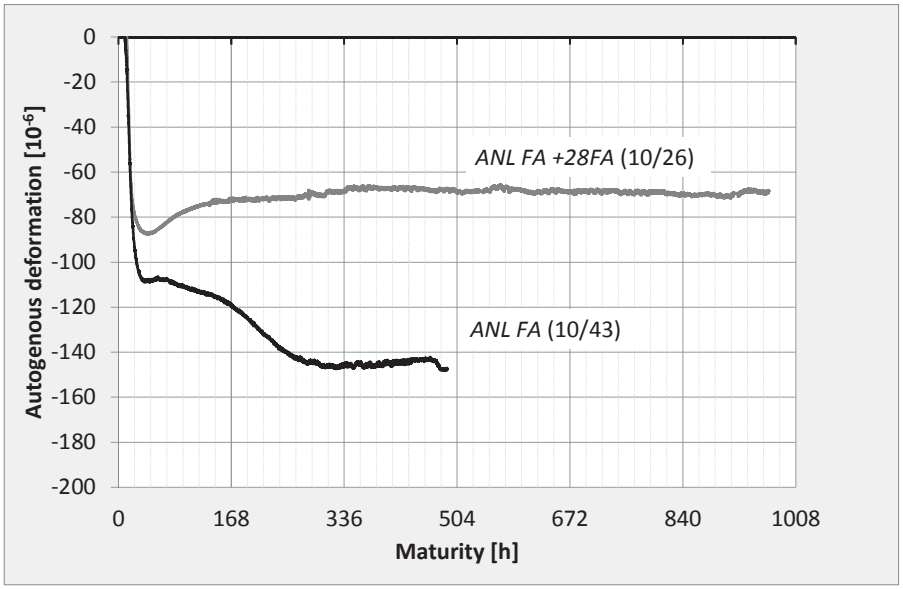

Figure 8.23; Autogenous deformation versus maturity under realistic temperature conditions, Winter, ANL FA +16FA and ANL FA +28FA

Analogous to the isothermal tests, *ANL Ref.* showed a different behaviour in AD when compared with the fly ash concretes also for realistic temperature conditions. The fly ash concretes showed a systematically decreasing AD (contraction) with increasing FA content (i.e. 17 %, 25 %, 33 % and 45 % fly ash as % by weight of cement and fly ash content). It could however be discussed whether the AD curves varied with the fly ash content, or rather with the maximum temperature increase ΔT_{max} which is strongly influenced by the given fly ash content. To study the effect of temperature increase on AD, all AD curves were compared, see Figure 8.24 (versus time) and Figure 8.25 (versus maturity). The figures show that for the fly ash concretes, the total AD (contraction) over the first 336 hours is systematically increasing with increasing ΔT_{max} independently of the fly ash content. This systematic relation between AD and ΔT_{max} is clearly illustrated in Figure 8.26, which shows deduced AD at 336 maturity hours versus ΔT_{max}. However, beyond 336 hours, the given AD curves show various behaviour and the relation between AD and ΔT_{max} is no longer as systematic. For the fly ash concretes, it seems as if the AD development could be divided into three phases:

1) *Between t_0 and T_{max}:* the temperature increase phase. During this phase, all tests showed an initial rapid increase in AD (contraction). Although no clear systematic relation was found, there was a tendency of an increasing initial AD (contraction) with increasing ΔT_{max}. This initial rapid AD contraction has also been seen in other studies, e.g. [Bjøntegaard, 1999], [Lee et al., 2003], [Lura et al., 2003] and [Termkhajornkit et al., 2005]. However, as described in Chapter 3.2, the currently applied simplification of a constant CTE will cause an early parallel displacement of the AD curve (increased contraction), and the deduced AD curves in this initial phase should therefore not be overinterpreted.
2) *Between T_{max} and approx. 336 hours*: the cooling phase. During this phase, the AD behaviour of the fly ash concretes seems to vary with ΔT_{max}. While AD for fly ash concretes subjected to a ΔT_{max} lower than 20 ^{o}C occurs as an expansion, the AD for tests with a ΔT_{max} higher than 20 ^{o}C occurs as a contraction which is increasing with increasing ΔT_{max}. Contradictorily, the concrete without fly ash, *ANL Ref. (20/62)* experienced an expansive AD despite its high ΔT_{max}, an observation which was also made by [Bjøntegaard, 1999] on a similar concrete.
3) *Beyond 336 hours:* isothermal conditions. During this phase, the concretes previously subjected to a ΔT_{max} lower than 30 ^{o}C kept developing AD (contraction) at a rate which tended to decrease with increasing ΔT_{max}. For the concretes previously subjected to a ΔT_{max} higher than 30 ^{o}C, a very limited AD development was observed beyond 336 hours. For the test subjected to the highest ΔT_{max}, *ANL FA (20/59)*, a small expansion in AD was seen beyond 336 hours. The only exception from these general observations was *ANL FA +28FA (10/26),* where no AD development beyond 336 hours was seen although the test was subjected to a ΔT_{max} lower than 30 ^{o}C.

Summarized, for the fly ash concretes, the AD development could be divided into three phases, where the AD behaviour during each phase varied systematically with T_{max} and/or ΔT_{max}. However, limited by the scope of the current work, to establish a numerical model describing the AD development for fly ash concretes has not been prioritized.

Only a limited amount of AD measurements on fly ash concretes subjected to realistic temperature conditions have been found in the literature. A brief summary is given in the following. AD measurements reported by [Bjøntegaard et al., 2003] and [Bjøntegaard, 2004] showed a small decrease in AD at 336 hours with increasing fly ash content, however, the currently found rapid initial AD contraction was not seen. AD measurements reported by [Ji, 2008] on the other hand, showed no relation between AD and fly ash content. [Bjøntegaard et al., 2012] reported a tendency of a small increase in AD (contraction) with increasing FA content in the cooling period, which is the opposite as found for the current test series.

[Sennour et al., 1989] measured AD on fly ash concretes under 20 ^{o}C isothermal conditions and found that partial replacement of cement by fly ash would increase the AD (contraction). Contradictorily, both [Lee et al., 2003] and [Bjøntegaard et al., 2012] found a clear tendency of decreasing AD (contraction) with increasing fly ash replacement under 20 ^{o}C isothermal conditions. [Termkhajornkit et al., 2005] reported AD measurements on concretes with three different types of fly ash, where the specimens were subjected to small temperature increases (less than 7 ^{o}C) during the concrete heat development phase. The AD behaviour was found to vary with the type of fly ash used, and no systematic relation between AD and fly ash content was found. Summarized, the contradicting AD results found in the literature underline the complex nature of the AD.

As previously described, it has been observed that AD (contraction) is increasing with increasing ΔT_{max}. Consequently, the new cement batch TF4-15 causes both an increased temperature as well as an increase in AD (contraction) when compared to the originally used cement batch TF3-11. The mechanical properties are however similar as discussed previously, which in combination with the increased volume changes (both TD and AD) makes the new cement batch TF4-15 unfavourable with respect to early age cracking. In addition, the observed change in AD development caused by the new cement batch illustrates how sensitive the AD development is to the properties and proportioning of the concrete components.

For the wall simulations which were applied the temperature set *Summer II*, it can be seen that *ANL FA* is subjected to early age volume changes (TD and AD) which are actually higher than for *ANL Ref.* (see Figure 8.27). In combination with the tensile strength (which is decreasing with increasing fly ash content) *ANL Ref.* must be considered a better choice than *ANL FA* with respect to low crack sensitivity for the current case.

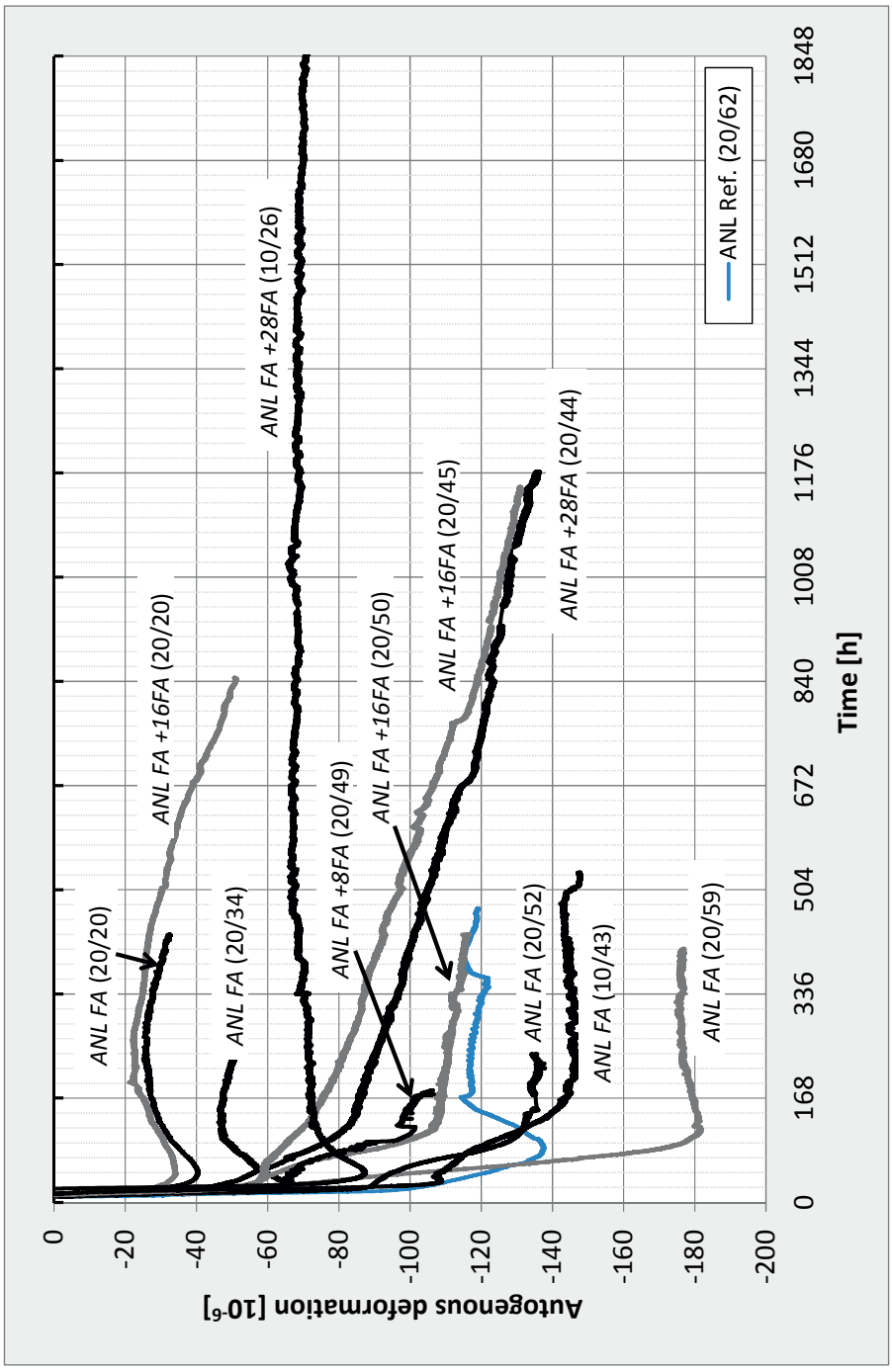

Figure 8.24; Measured autogenous deformation, effect of temperature increase

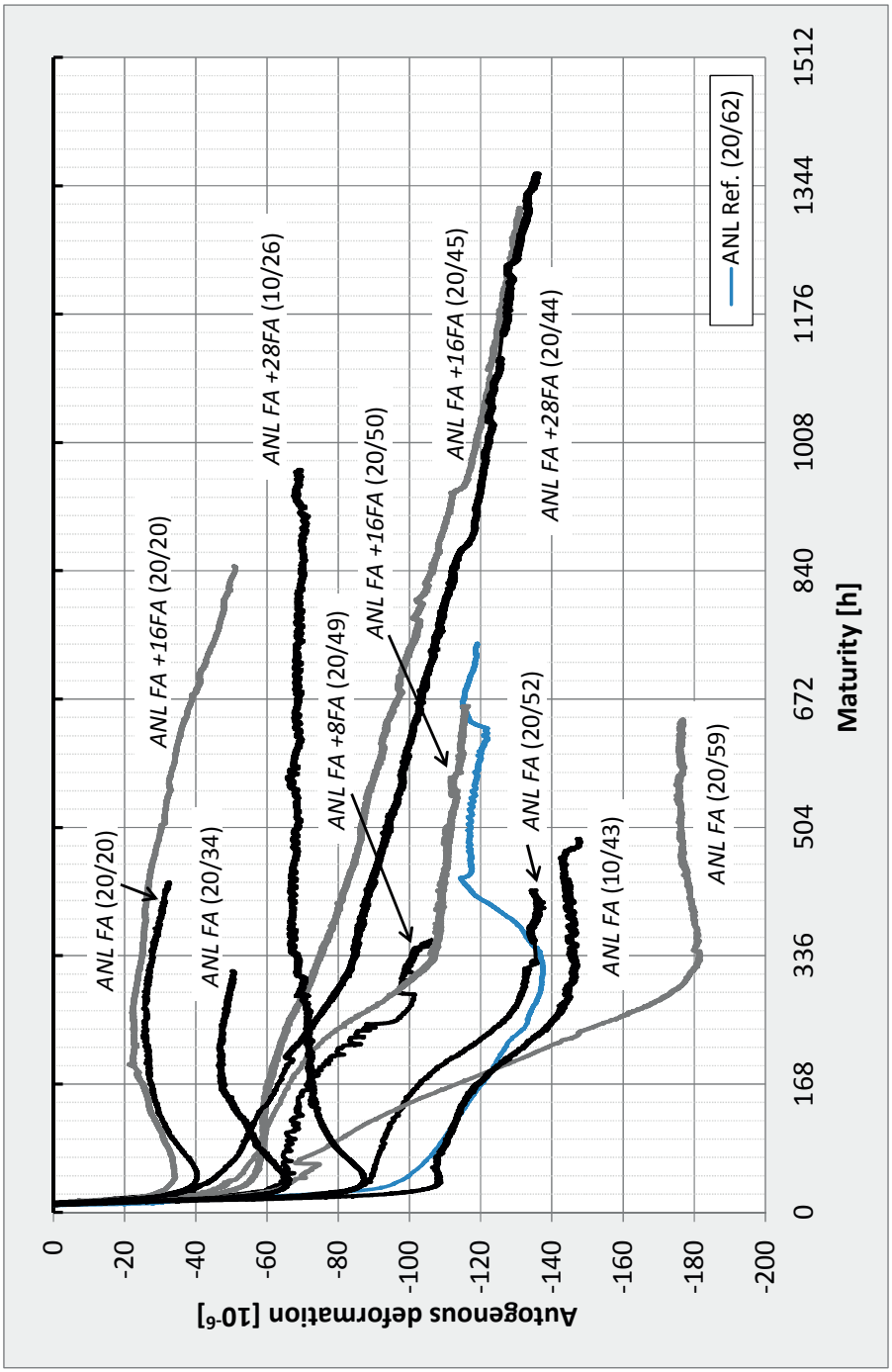

Figure 8.25; Autogenous deformation versus maturity, effect of temperature increase

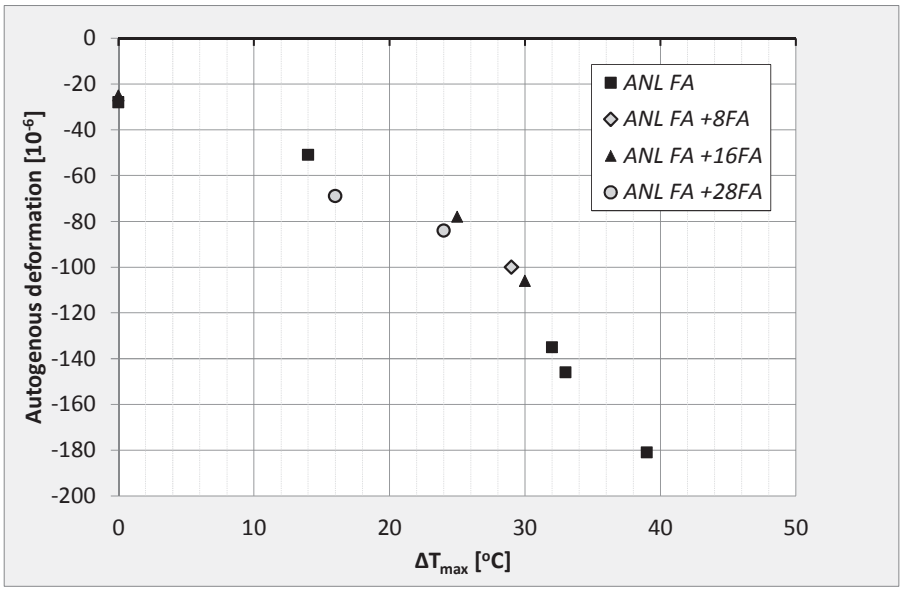

Figure 8.26; Autogenous deformation at 336 hours maturity versus maximum temperature increase for the fly ash concretes, i.e. effect of ΔT_{max} on AD

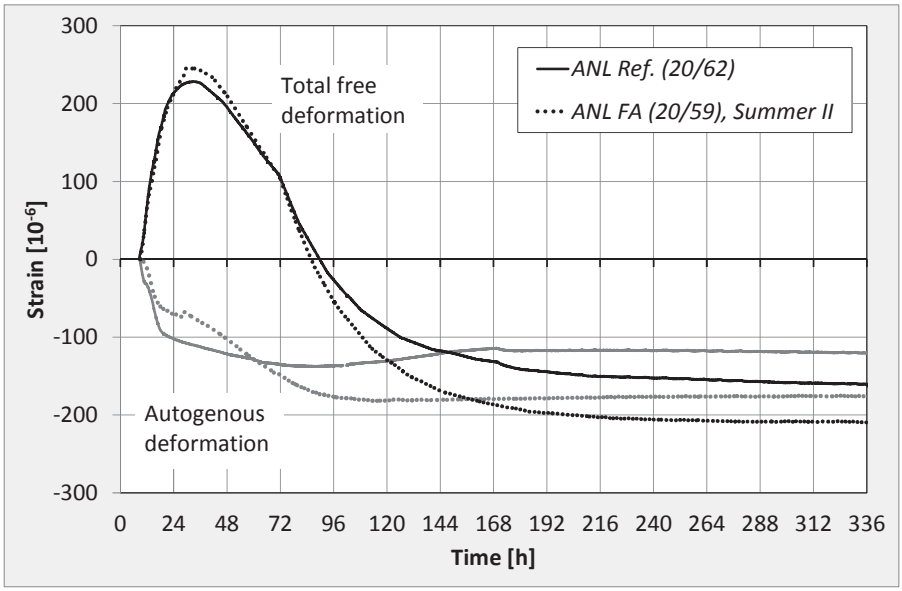

Figure 8.27; Measured free deformation and deduced autogenous deformation, ANL FA and ANL Ref., realistic temperature tests

AD is an important input for early age restrained stress calculations. The performed tests show that AD is a complex property which is dependent on both the concrete mix as well as on the actual temperature history. For the given tests, the temperature influence on AD could not be compensated for by the maturity principle. Hence, for restrained stress calculations, it is of major importance to know the AD development under temperature conditions which are as close to the actual case as possible. For instance, using a 20 °C isothermal AD curve when analysing a massive concrete structure subjected to a semi-adiabatic temperature history would, at least in a short term perspective, underestimate the calculated stress development considerably.

To further elaborate the temperature effects on AD, the temperature in the test *ANL FA+28FA (10/26)* was increased to 20 °C after 11 weeks with 5 °C isothermal conditions and a constant AD, (i.e. no AD development which was probably caused by reduced reactivity due to the low temperature). It was found that the temperature increase (+15 °C over 12 hours) initiated a revival of the AD development. During the 4 following weeks at 20 °C, i.e. until the test was ended, an AD development of -10 µstrain per week was measured (i.e. 40 µstrain and continuing), Figure 8.28. This rate was the same AD development rate as seen for *ANL FA +28FA (20/44)* under 20 °C isothermal conditions (i.e. beyond 2 weeks). This result underlines once again the complex nature of AD.

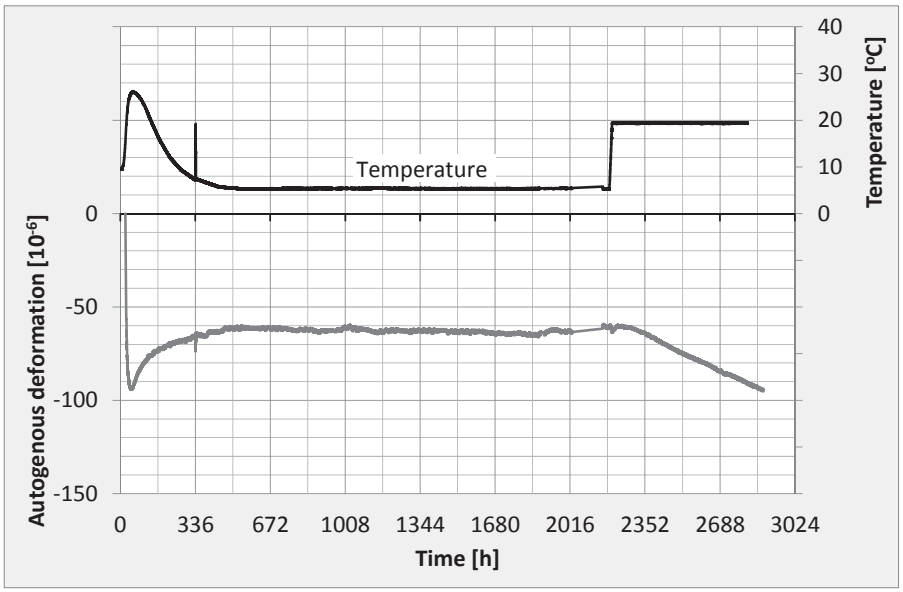

Figure 8.28; Autogenous deformation, ANL FA +28FA (10/26). Subjected to winter conditions and 5 °C isothermal temperatures for 13 weeks, followed by 20 °C isothermal temperature conditions for 4 weeks

8.3 Measured versus calculated stress in the TSTM

Calculated stress developments have been compared with restrained stress developments measured in the TSTM. Three programs were used for the uniaxial stress calculations: TSTM-sim (Excel), CrackTeSt COIN and DIANA, see Chapter 3.7. The applied input variables are listed in the following:

- Free deformation (sum of TD and AD) measured directly in the parallel Dilation Rig test, Chapter 8.2
- The degree of restraint R used during testing in the TSTM: R = 100 % for isothermal tests and R = 50 % for realistic temperature tests (i.e. as % of measured free deformation), see Chapter 6.3.6
- The actual temperature histories measured in the TSTM and in the Dilation Rig, Chapter 7.3
- Material parameters determined from parallel mechanical testing, Chapter 7.9

Figure 8.29 shows measured and calculated stress developments for *ANL Ref. (20/62)* subjected to a realistic temperature history. The stress developments have been calculated by the following four approaches: 1) TSTM-sim (Excel), 2) CrackTeSt COIN, 3) DIANA with double power law (DIANA DPL) and 4) DIANA with relaxation data (DIANA relaxation). The calculated stress curves show very good agreement, both with each other and also with the corresponding measured stress. The stress values obtained at 24 and 144 hours are presented in Table 8.3. All calculation approaches were based on the same material parameters for mechanical properties and creep. All calculations provided very accurate simulations of the compressive phase, however, the two DIANA calculations gave a slightly lower tensile stress development than the other approaches. Summarized, the calculation approaches combined with the previously determined material parameters must be said to provide a very accurate simulation of the stress development in the TSTM for *ANL Ref. (20/62)*.

A more advanced calculation approach was added for the stress calculations of the fly ash concretes. As described in Chapter 3.7.2, the specially designed program run in Excel was modified to open for a differentiation between creep in compression, creep recovery and creep in tension, and it was termed “TSTM-sim-mod”. The appurtenant sets of creep parameters (creep in compression, creep recovery and creep in tension) were determined based on dedicated creep tests in the TSTM System as presented in Chapter 7.7. Hence, creep in compression and tension were modelled by creep parameters as presented in Table 7.31, while the creep recovery when unloading the compressive load was set to zero.

Measured and calculated stress developments during the first two weeks for *ANL FA +16FA (20/45)* subjected to realistic temperature conditions are given in Figure 8.30. Measured and calculated stress curves for the whole test (7 weeks) are given in Figure 8.31. The calculated stress developments were found by the following five approaches: 1) TSTM-sim (Excel), 2) TSTM-sim-mod (Excel), 3) CrackTeSt COIN, 4) DIANA DPL and 5) DIANA relaxation.

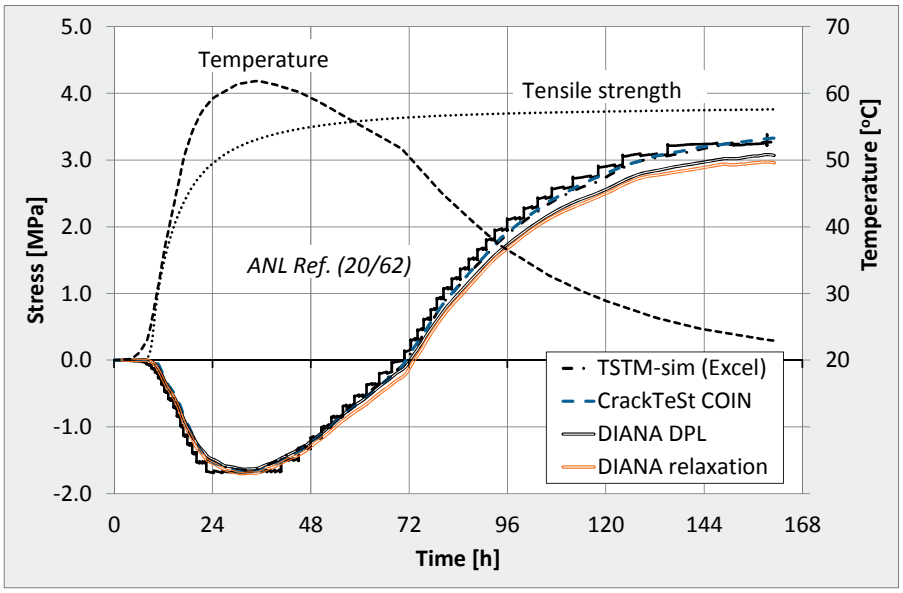

Figure 8.29; Measured and calculated stress development, ANL Ref. (20/62)

Table 8.3; Measured and calculated stress at 24 hours and 144 hours for ANL Ref. (20/62), calculated stress relative to the measured stress is given in parenthesis

Time	**Stress** [MPa]				
	Measured	Excel	CrackTeSt COIN	DIANA DPL	DIANA relaxation
24 hours	**-1.68**	-1.53 (0.91)	-1.53 (0.91)	-1.48 (0.88)	-1.54 (0.92)
144 hours	**3.24**	3.17 (0.98)	3.20 (0.99)	2.96 (0.91)	2.89 (0.89)

Measured and calculated stresses at 24, 168 and 1008 hours are presented in Table 8.4. All calculation approaches gave a very good description of the compressive phase. The most accurate description of the compressive unloading, i.e. between 55 and 85 hours, was provided by the modified Excel simulation which calculation routine includes the lack of creep recovery found in Section 7.7. For the tensile stress development, i.e. beyond 85 hours, the most accurate simulation was given by the two Excel approaches. CrackTeSt COIN and DIANA on the other hand, underestimate the tensile stress development over time. It is noticeable that the concrete continued to develop tensile stress at a constant rate beyond the cooling phase and up until the test was ended after 7 weeks. This trend was captured by the calculation approaches, except for CrackTeSt COIN which showed a small decrease in tensile stress beyond 6 weeks.

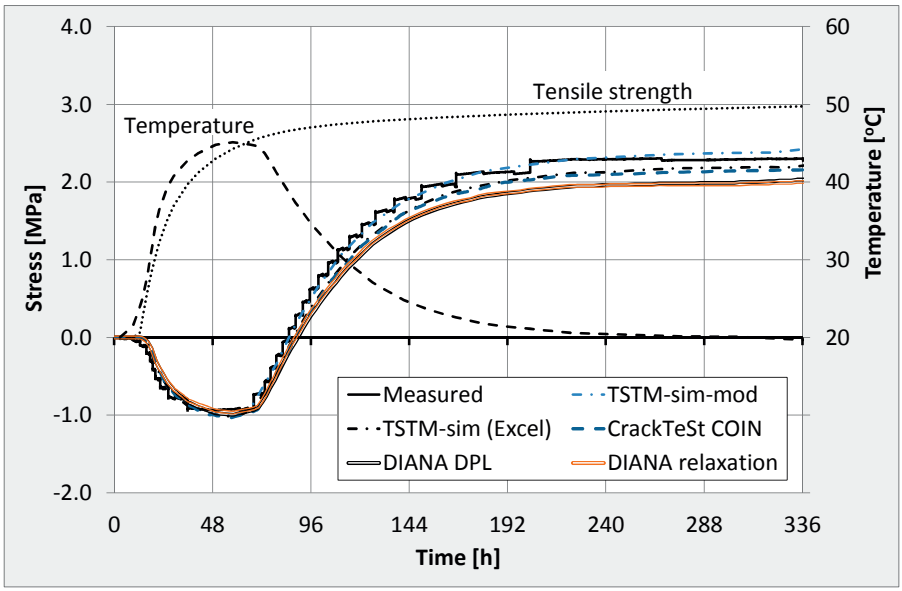

Figure 8.30; Measured and calculated stress development during the first two weeks, ANL FA +16FA (20/45)

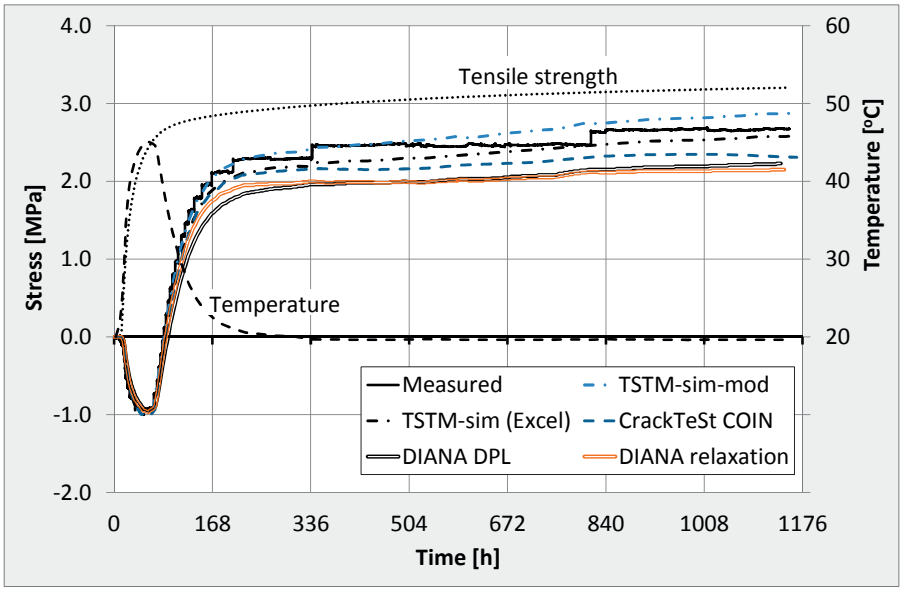

Figure 8.31; Measured and calculated stress development over 7 weeks, ANL FA +16FA

The DIANA DPL stress curve differs slightly between Figure 8.30 and Figure 8.31. This deviation was caused by the analysis' dependence on the defined time span, i.e. 2 weeks versus 7 weeks for the two analyses, respectively.

Table 8.4; Measured versus calculated stress at 24, 168 and 1008 hours for ANL FA +16FA (20/45), calculated stress relative to the measured stress is given in parenthesis

Time	**Stress** [MPa]					
	Measured	Excel	Excel modified	CrackTeSt COIN	DIANA DPL	DIANA relaxation
48 hours	**-0.93**	-0.99 (1.06)	-0.98 (1.05)	-0.99 (1.06)	-0.96 (1.03)	-0.93 (1.00)
168 hours	**2.10**	1.88 (0.89)	2.04 (0.97)	1.86 (0.89)	1.74 (0.83)	1.75 (0.83)
1008 hours	**2.68**	2.53 (0.94)	2.82 (1.05)	2.34 (0.87)	2.19 (0.82)	2.13 (0.79)

As a part of the verification of the different calculation approaches, the temperature development as well as the equivalent age (maturity) obtained from the various analyses were compared, Figure 8.32 and Figure 8.33. It was found that all calculation approaches provided exactly the same temperature development and equivalent age (maturity).

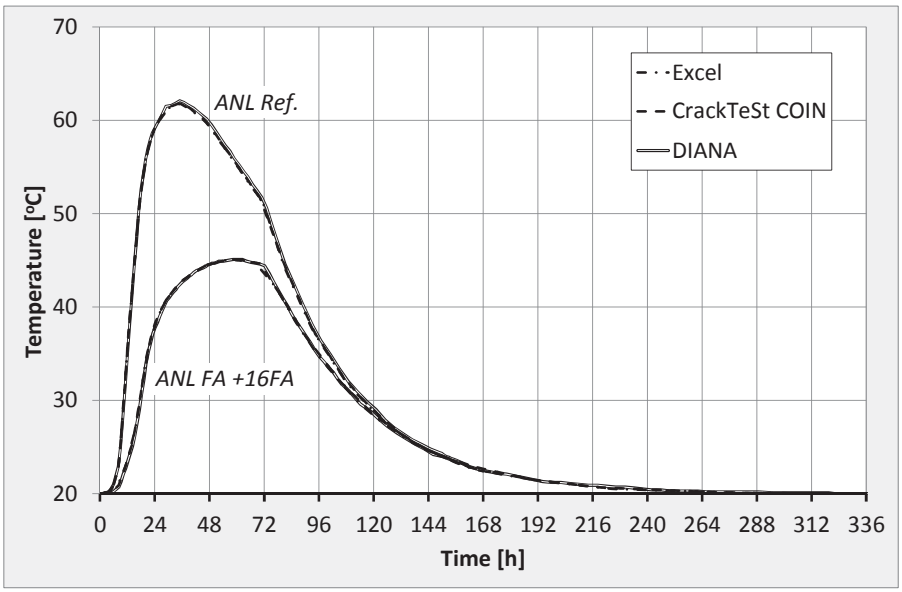

Figure 8.32; Obtained temperature history: Excel, CrackTeSt COIN and DIANA. ANL Ref. and ANL FA +16FA

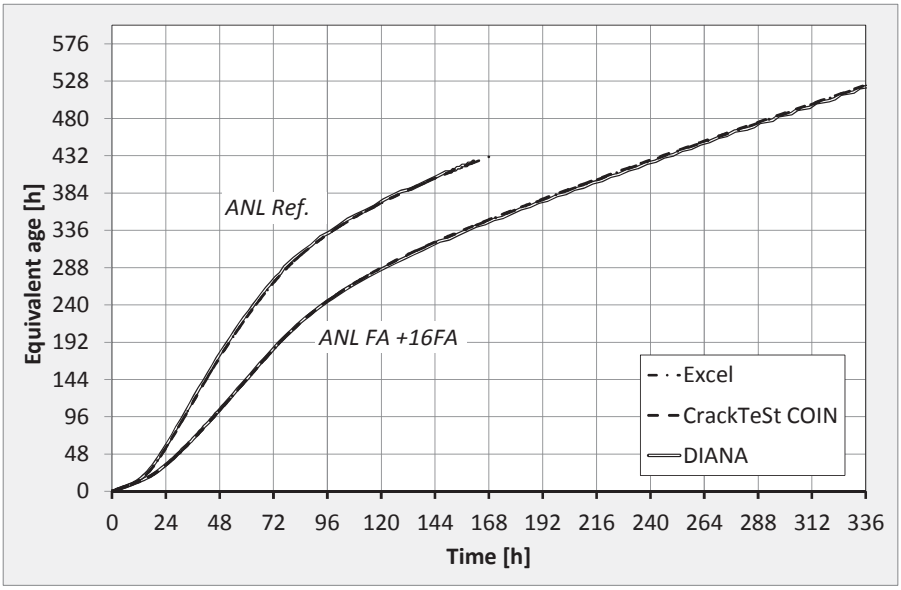

Figure 8.33; Obtained equivalent age (maturity hours): Excel, CrackTeSt COIN and DIANA. ANL Ref. and ANL FA +16FA

For the given examples, the various calculation approaches gave a good description of the measured TSTM stress development. All calculation approaches provided an accurate description of the compressive phase, while the two Excel approaches gave a slightly better description of the tensile stress development. The TSTM restrained stress curves presented in the following section are compared with stress curves calculated by the two calculation approaches run in Excel: 1) TSTM-sim and 2) TSTM-sim-mod (i.e. modified with a more comprehensive calculation routine with respect to creep).

8.4 Restrained stress test results, TSTM

8.4.1 General

An overview of the performed tests with various concretes and curing conditions is given in Table 8.5. As previously described, all realistic temperature TSTM tests were performed with individual temperature histories representing the given concrete cast in an 800 mm thick wall, see Chapter 7.3. It should however be noticed that while the calculated temperature histories were based on two different sets of cement batches as described in Table 8.5 and Chapter 7.3, most TSTM tests were actually performed with the cement batches EG1-10 (reference concrete) and TF5-14 (fly ash concretes), see Table 4.7.

Section 8.4.2 – Section 8.4.6 present the measured restrained stress developments for each concrete, respectively. In the following graphs, a cross at the end of the stress curve indicates that the given test developed failure in tension during testing. All other tests have been ended manually by first unloading the specimen and then reloading it until failure. All measured stress curves are compared with corresponding calculated stress curves as described in the previous section. Comparisons and discussions of the presented results are given in Section 8.4.7.

Table 8.5; Restrained stress tests in the TSTM, overview. All isothermal tests have been applied a degree of restraint of 100 %, and all realistic temperature tests a degree of restraint of 50 %

	Isothermal 20 °C	**Realistic temperature**		
		Summer*		**Winter***
		*Temp. from cement batch EG1-10/TF3-11**	*Temp. from cement batch EG1-14/TF5-14**	*Temp. from cement batch TF5-14**
ANL Ref	2	3	-	-
ANL FA	calculated**	1	2	1
ANL FA +8FA	-	1	calculated**	-
ANL FA +16FA	1	2	1	-
ANL FA +28FA	-	-	1	1

**) The applied temperature history in the test is based on heat evolution data for each individual cement batch. However, all fly ash concretes were actually mixed with cement batch TF5-14 during testing*

***) The stress development has only been calculated and not measured*

8.4.2 ANL Ref.

Measured stress developments for two nominally identical *ANL Ref. (20/20)* tests under 20 °C isothermal conditions are presented in Figure 8.34. Both tests were applied a degree of restraint of R = 100 %. The tests were evaluated numerically in Chapter 6.2.5 and show very good reproducibility with a standard deviation at 48 and 80 hours of only 0.04 and 0.15 MPa, respectively. The stress kept developing gradually over time, induced by the AD as presented in Section 8.2.

Figure 8.35 shows measured and calculated stress development (TSTM-sim (Excel), see Chapter 8.3) for three nominally identical realistic temperature tests performed with the reference concrete, *ANL Ref. (20/62)*. One of the tests was mixed with ANL cement batch EG1-10, while EG1-14 was used for the two other tests, however, the realistic temperature history was calculated based on heat evolvement data from cement batch EG1-10. All tests were applied a degree of restraint of R = 50 %. The measured stress showed very good reproducibility with a standard deviation at 48 and 96 hours of only 0.03 and 0.06 MPa, respectively, see Chapter 6.2.5. One of the tests developed failure in tension at 160 hours, one was unloaded at 100 hours, while one of the tests was ended after only 75 hours due to a software error.

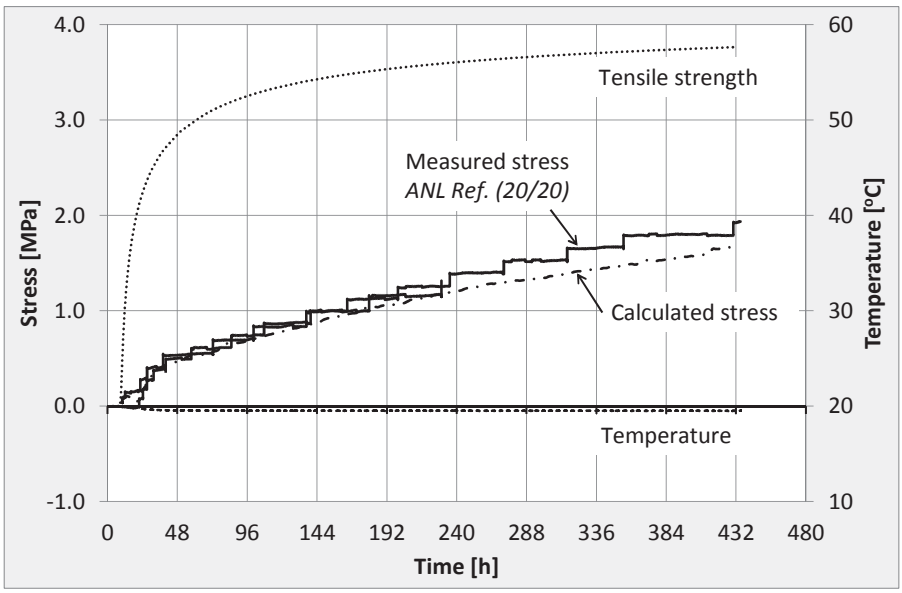

Figure 8.34; Measured and calculated (TSTM-sim (Excel)) restrained stress development, ANL Ref., two nominally identical tests, 20 °C isothermal conditions, R = 100 %

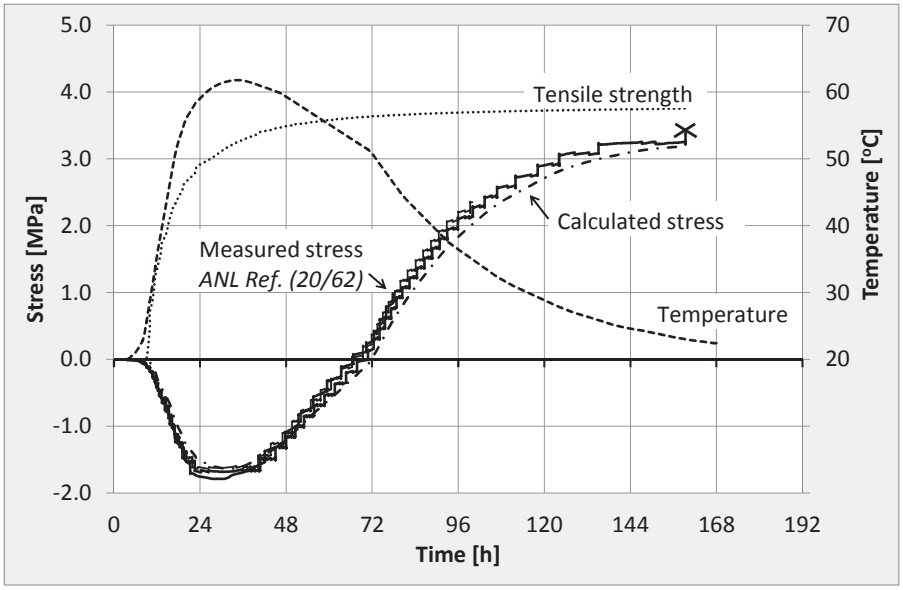

Figure 8.35; Measured and calculated (TSTM-sim (Excel)) restrained stress development, ANL Ref., three nominally identical tests, realistic temperature conditions, R = 50 %

8.4.3 ANL FA

For *ANL FA*, the following restrained stress tests, all with realistic temperature conditions, were performed:

- *ANL FA (20/52)* summer conditions (temp. from TF3-11 cement), Figure 8.36
- *ANL FA (20/59)* two nominally identical tests, summer conditions (temperature based on TF5-14 cement), Figure 8.37
- *ANL FA (10/43)* winter conditions (temperature from TF5-14 cem.), Figure 8.38

All *ANL FA* realistic temperature tests, Figure 8.36 - Figure 8.38, were applied a degree of restraint of R = 50 %. For all realistic temperature histories, the measured stress development show good agreement with the calculated stress development, especially for the calculation method that differentiate between creep in compression, creep recovery and creep in tension, i.e. TSTM-sim-mod. All tests were actually performed with cement batch TF5-14. *ANL FA (20/52)* developed failure in tension after 144 hours, while the other tests were ended by a controlled unloading. Two nominally identical tests were performed for *ANL FA (20/59)*, confirming the good reproducibility of the TSTM System.

There was not performed any restrained stress tests for *ANL FA* under isothermal conditions, however, the isothermal stress development was calculated based on AD determined from creep tests, Figure 8.39. As expected, the calculations show a very limited stress development, directly reflecting the slow AD development found in Section 8.2.3.

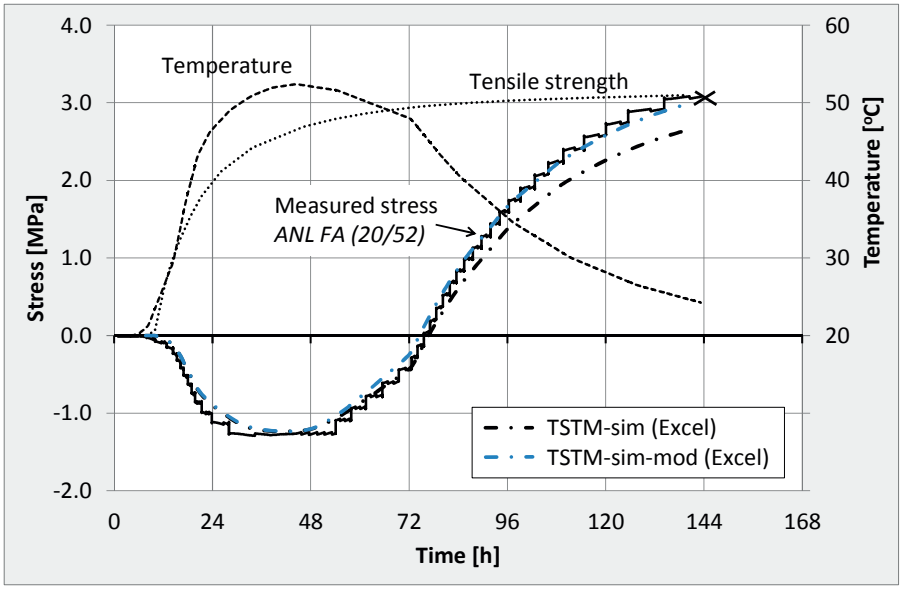

Figure 8.36; Measured and calculated stress development, ANL FA (20/52), summer conditions (based on cement batch TF3-11), R = 50 %, the test developed failure after 144 hours

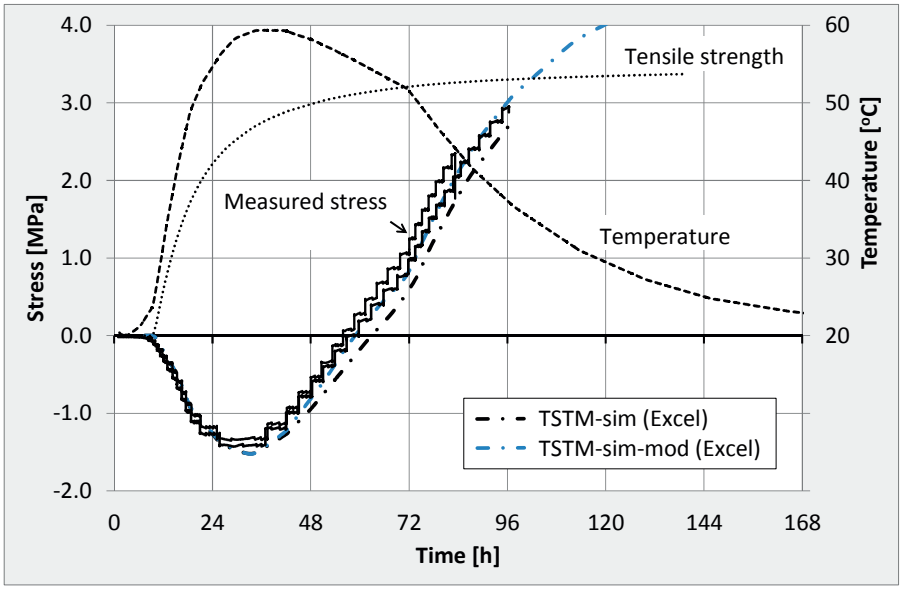

Figure 8.37; Measured and calculated stress development ANL FA (20/59), two nominally identical tests, summer conditions (based on cement batch TF5-14), R = 50 %

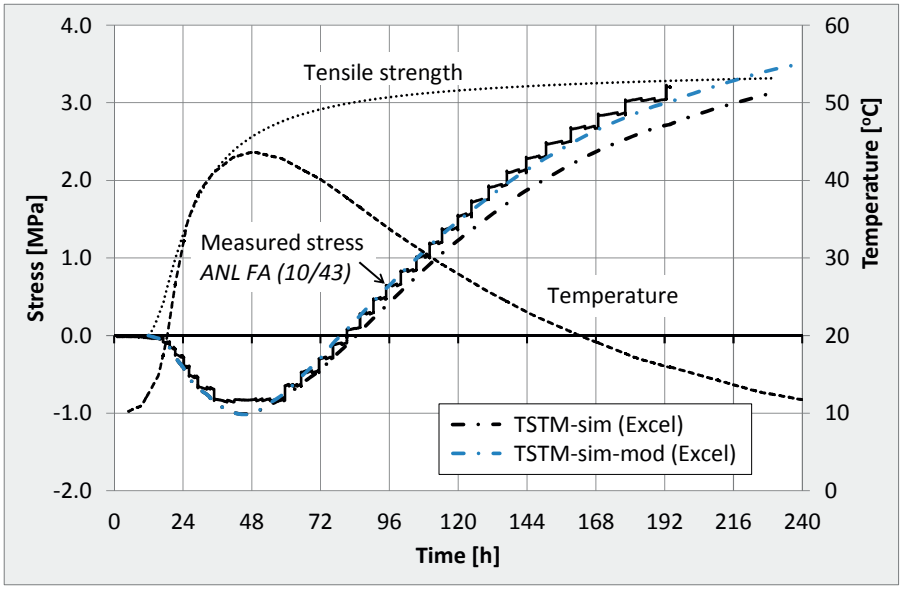

Figure 8.38; Measured and calculated stress development ANL FA (10/43), winter conditions (calculated from cement batch TF5-14), R = 50 %

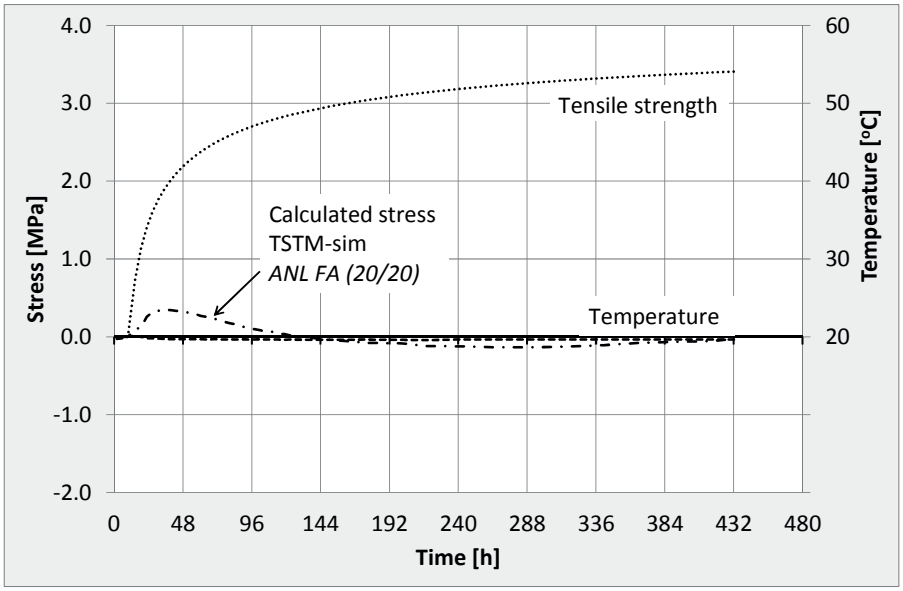

Figure 8.39; Calculated stress development ANL FA (20/20), 20 °C isothermal conditions, R = 100 %

8.4.4 ANL FA +8FA

Restrained stress development for *ANL FA +8FA (20/49)* when exposed to realistic temperature conditions is presented in Figure 8.40. The applied temperature history represents the wall described in Chapter 7.3 when cast with cement batch TF3-11 (i.e. *Summer I*), the test was however actually performed with cement batch TF5-14. The test specimen was applied a degree of restraint of R = 50 %. The measured and calculated stress development show good agreement in the compressive phase, however, a small deviation appears beyond 80 hours during the tensile stress development. One reason could be that the creep parameters for *ANL FA +8FA* were assumed from creep tests on *ANL FA* and *ANL FA +16FA*. The test developed failure in tension after 192 hours.

ANL FA +8FA (20/54) (i.e. when subjected to the curing condition *Summer II*) was not tested in the TSTM, however, the expected stress development was calculated by using the AD obtained from the curing condition *Summer I*. The calculated stress development for *ANL FA +8FA (20/54)* is presented in Figure 8.41. The calculated stress is probably slightly underestimated, as the AD for *Summer II* is expected to be somewhat higher than for *Summer I* due to the found increase in AD with increasing temperature, Section 8.2.7. In addition, the stress calculations for *ANL FA +8FA (20/49)* indicated that the used creep parameters slightly underestimates the stress development in the tensile phase.

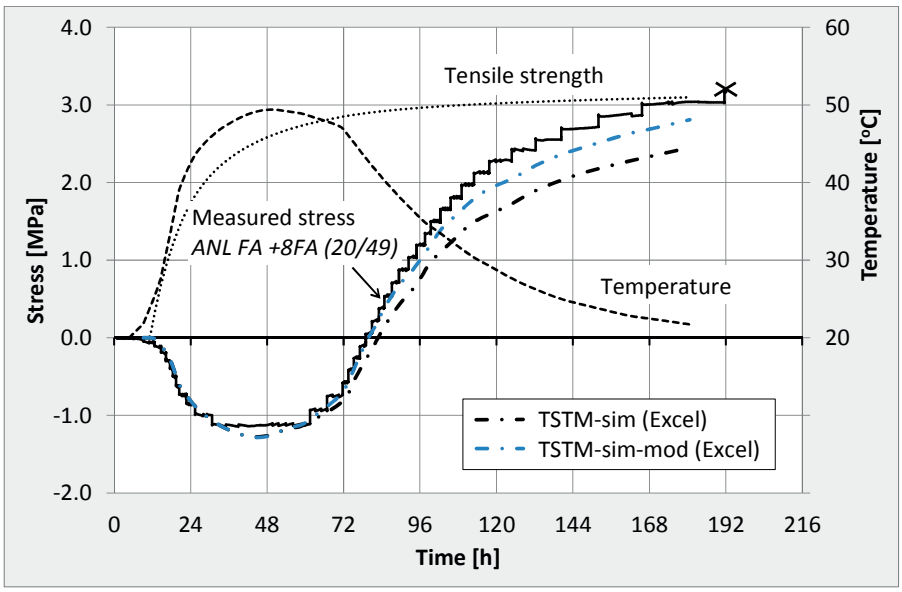

Figure 8.40; Measured and calculated stress development, ANL FA +8FA (20/49), summer conditions Summer I (i.e. temperature history based on heat evolution data for cement batch TF3-11), R = 50 %

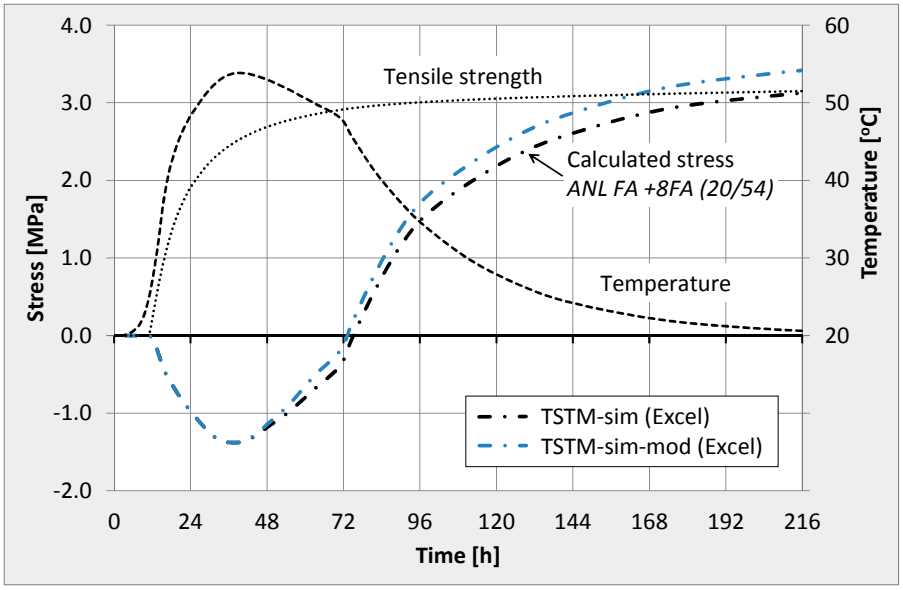

Figure 8.41; Calculated restrained stress development, ANL FA +8FA (20/54), summer conditions Summer II (i.e. temperature history based on heat evolution data for cement batch TF5-14), R = 50 %

8.4.5 ANL FA +16FA

The following restrained stress tests have been carried out for *ANL FA +16FA*:

- *ANL FA +16FA (20/20)* 20 °C isothermal conditions, Figure 8.42
- *ANL FA +16FA (20/45)* two nominally identical tests, realistic temperature conditions, *Summer I* (temperature history based on TF3-11 cement), Figure 8.43 and Figure 8.44
- *ANL FA +16FA (20/50)* realistic temperature conditions, *Summer II* (temp. based on TF5-14 cement), Figure 8.45

Measured stress development for *ANL FA +16FA* under 20 °C isothermal conditions and a degree of restraint of R = 100 % is presented in Figure 8.42. The results show a very slow stress development, which is as expected since there is almost no AD development, Section 8.2.5.

All the realistic temperature tests were applied a degree of restraint of *R* = 50 %. The two nominally identical *ANL FA +16FA (20/45)* tests show very similar behaviour during the compression phase, however, they seem to divert during the tensile stress development. At 168 hours, the difference in tensile stress between the two tests is 20 %. This deviation could be partly explained by a variation in the E-modulus, which from the TSTM was found to be approximately 1.5 GPa (i.e. 4.4 %) higher for the test with the highest tensile

stress development. In addition, the same test also showed an AD development which was approximately 7 μstrain higher (9 % at 168 hours) than for the other test.

One of the *ANL FA +16FA (20/45)* tests was run for as much as 7 weeks, Figure 8.44. The concrete kept developing stress at a slow but steady rate beyond the 2 first weeks and until the test was ended. This was as expected due to the long-term continuous AD development found from the parallel Dilation Rig test, see Section 8.2.5.

All realistic temperature tests were performed with the same cement batch TF5-14, the tests were however subjected to two different temperature histories: 1) *ANL FA +16FA (20/45)* based on heat development data from TF3-11, Figure 8.43 and Figure 8.44 and 2) *ANL FA +16FA (20/50)* based on heat development data from TF5-14, Figure 8.45. The results show the considerable influence of cement batch on the generated temperature history and the corresponding stress development. The stress development for *ANL FA +16FA (20/50)* reaches the tensile strength after approximately 144 hours, while the tensile stress obtained from *ANL FA +16FA (20/45)* is about 30 % lower at the corresponding time. The measured stress development show good agreement with the calculated stress development for all the realistic temperature tests.

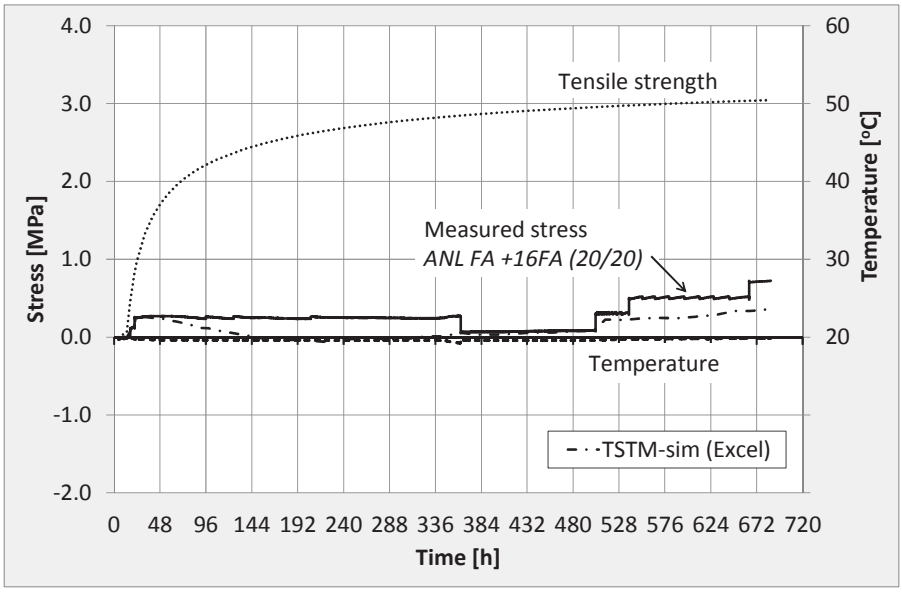

Figure 8.42; Measured and calculated restrained stress development, ANL FA +16FA (20/20), 20 °C isothermal conditions, R = 100 %

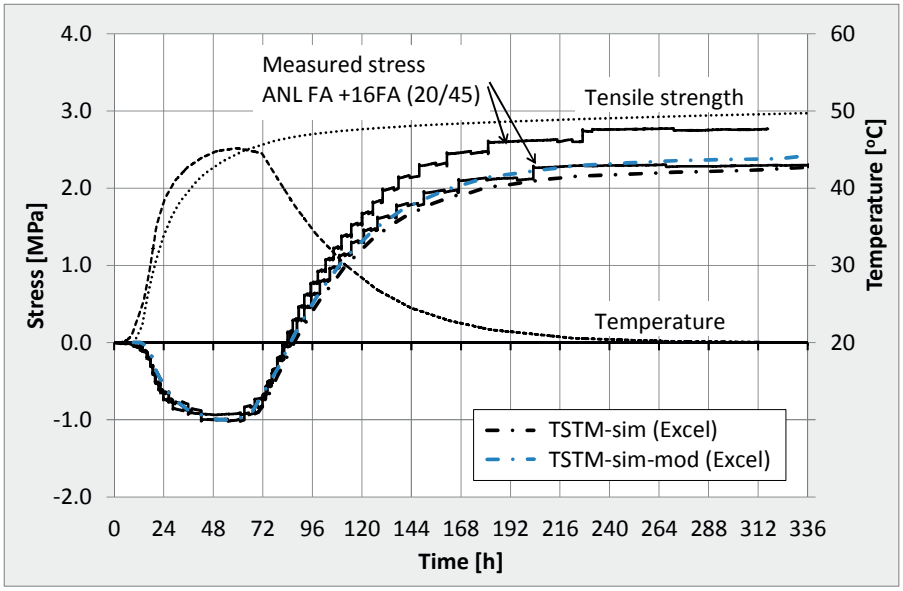

Figure 8.43; Measured and calculated restrained stress development, ANL FA +16FA (20/45), two nominally identical tests, summer conditions Summer I (temperature history based on cement batch TF3-11), R = 50 %

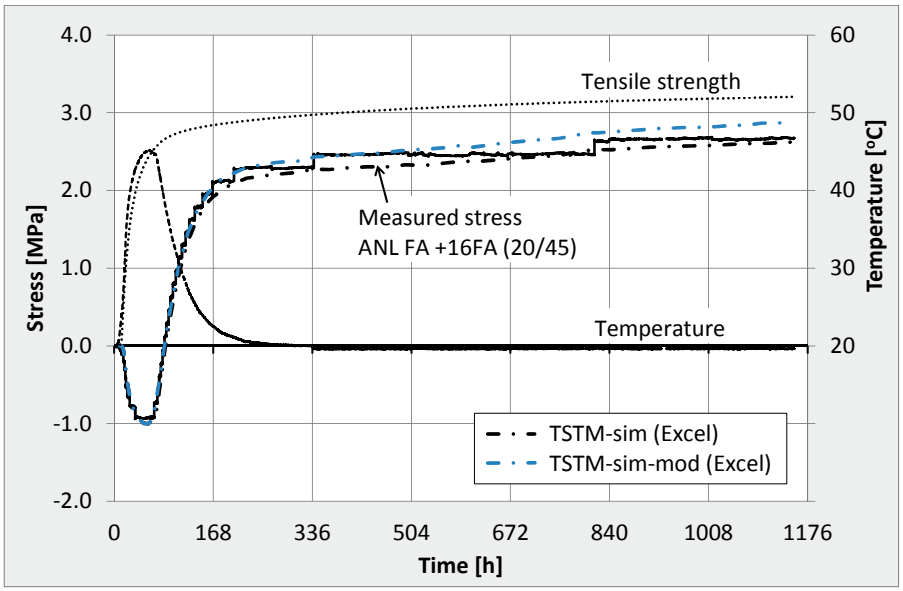

Figure 8.44; Measured and calculated restrained stress development, ANL FA +16FA (20/45), summer conditions Summer I (temperature history from cement batch TF3-11), R = 50 %, long-term measurements

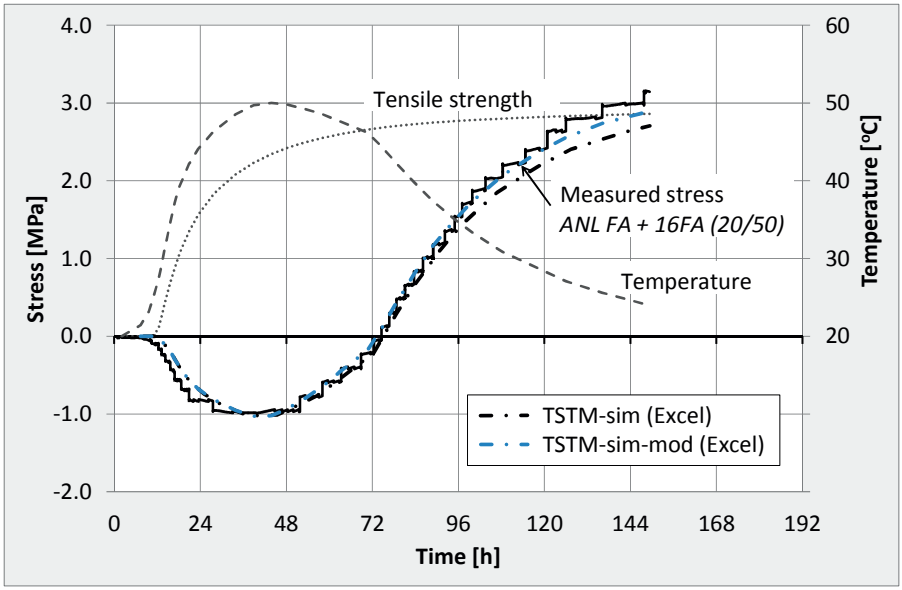

Figure 8.45; Measured and calculated restrained stress development, ANL FA +16FA (20/50), summer conditions Summer II (temperature from cement batch TF5-14), R = 50 %

8.4.6 ANL FA +28FA

Two realistic temperature stress tests were performed with *ANL FA +28FA*:

- *ANL FA +28FA (20/44)* summer conditions, *Summer II* (based on TF5-14)
- *ANL FA +28FA (10/26)* winter conditions, *Winter* (based on TF5-14)

Both tests were applied a degree of restraint of $R = 50$ %. The creep parameters used in the corresponding stress calculations were assumed based on creep parameters found by testing for *ANL FA* and *ANL FA +16FA*.

Figure 8.46 and Figure 8.47 show the stress developments during the first 2 weeks for *ANL FA +28FA (20/44)* and *ANL FA +28FA (10/26)*, respectively. Figure 8.48 shows the stress developments for the whole tests, i.e. 7 weeks for *ANL FA +28FA (20/44)* and 12 weeks for *ANL FA +28FA (10/26)*.

ANL FA +28FA (20/44) gradually developed increasing tensile stress beyond 2 weeks at a slow but steady rate until the test was ended. The tensile stress increase was however so small, that during the final 5 weeks it could only be seen by the length measurements of the TSTM specimen (i.e. the threshold value was not reached). The original Excel calculation TSTM-sim (without the enhanced creep routine) gave best agreement with the measured stress development. However, this might as well be related to a certain inaccuracy introduced by the assumed creep parameters.

The test subjected to winter conditions, *ANL FA +28FA (10/26),* reached a maximum tensile stress level after approximately 3 weeks, followed by an insignificant decrease in tensile stress over the next 6 weeks (the decrease was so small that the displacement threshold value was not reached, hence it was only seen by the displacement measurements of the TSTM). Beyond 9 weeks the tensile stress stayed at a constant level up until the test was ended after approximately 12 weeks. Due to the low T_{max}, *ANL FA +28FA (10/26)* achieved a very limited compressive phase. Therefore, only TSTM-sim (Excel) which is without the enhanced creep routine was used in the corresponding stress calculations. As seen from Figure 8.48, the calculation approach overestimated the above described tensile stress decrease (i.e. relaxation). While the stress calculations indicated a 26 % decrease in tensile stress between 3 and 12 weeks, an evaluation of the TSTM length displacement indicate a corresponding measured tensile stress decrease of only 3 %.

The latter described test *ANL FA +28FA (10/26)* was subjected to an increase and decrease in temperature at 336 hours, Figure 8.47. This change in temperature does not seem to have had any permanent effect on neither the AD nor the stress development.

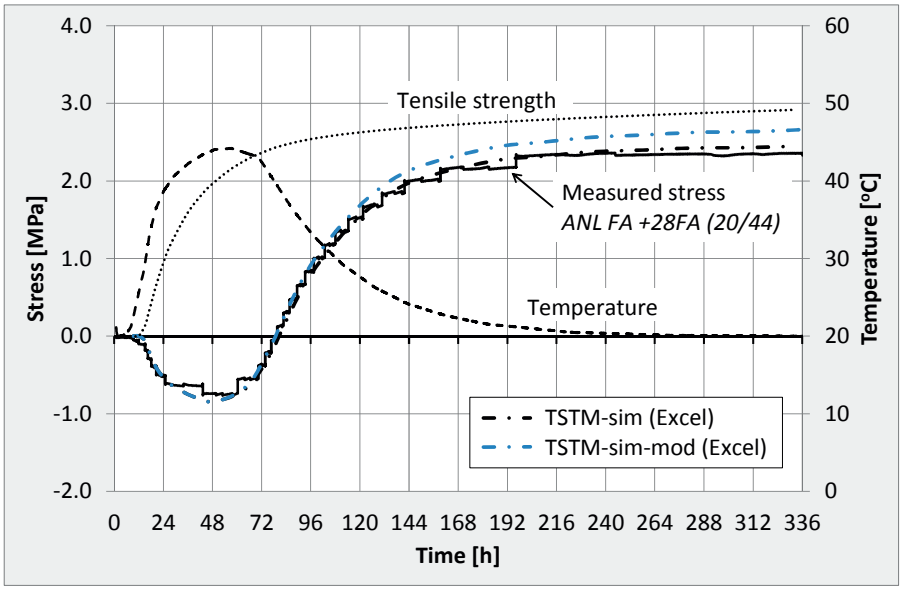

Figure 8.46; Measured and calculated stress development, ANL FA +28FA (20/44), summer conditions Summer II (temperature history based on cement batch TF5-14), R = 50 %

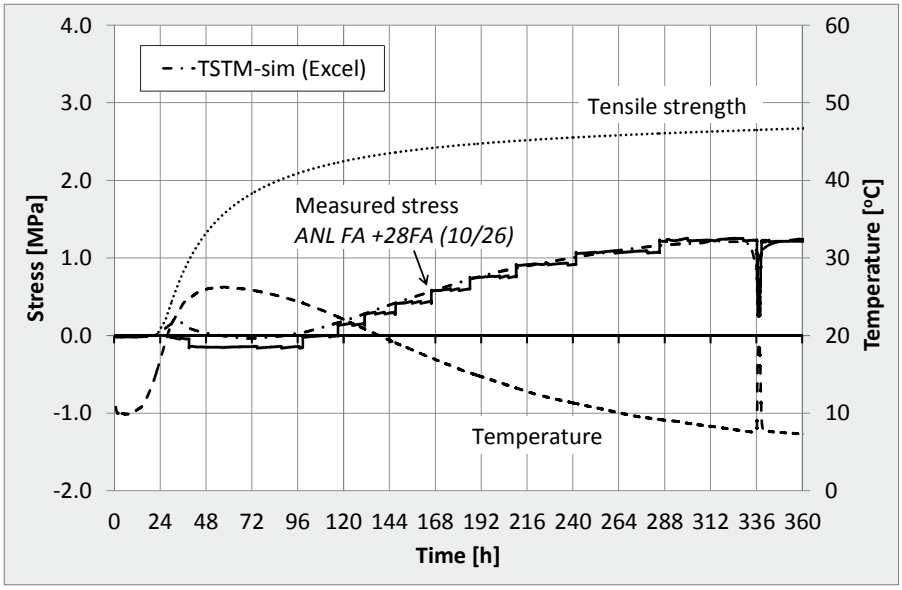

Figure 8.47; Measured and calculated stress development, ANL FA +28FA (10/26), winter conditions Winter (temperature history based on cement batch TF5-14), R = 50 %

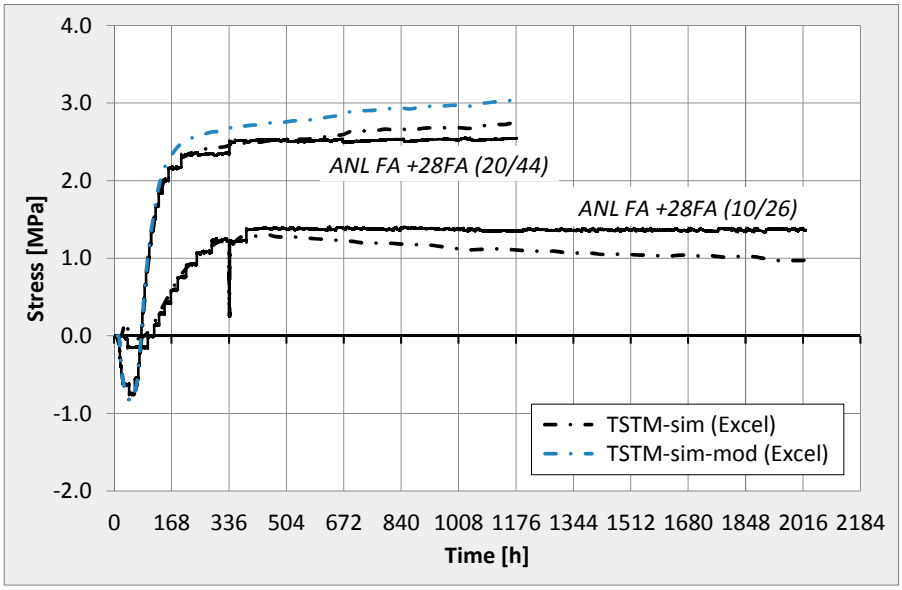

Figure 8.48; Measured and calculated stress development, ANL FA +28FA, summer and winter conditions, R = 50 %

8.4.7 Restrained stress measurements - comparisons and discussions

Stress curves from three isothermal TSTM tests: *ANL Ref.*, *ANL FA* and *ANL FA +16FA*, are compared in Figure 8.49. The corresponding crack indexes, Figure 8.50, were calculated from tensile strength development as determined in Chapter 7.4. The stress developments for *ANL Ref.* and *ANL FA +16FA* were measured in the TSTM, while the stress development for *ANL FA* was calculated based on AD found from creep tests.

The stress developments presented in Figure 8.49 are a direct reflection of the corresponding measured AD presented in Section 8.2 as AD constitutes the stress-inducing movement in the concrete under isothermal temperature conditions.

The fly ash concretes have a higher initial crack index due to the slower development of tensile strength, however, because of the much faster AD development found for *ANL Ref.*, the crack index for *ANL Ref.* keeps increasing and surpass the fly ash concretes at 40 hours. After two weeks, *ANL Ref.* has a crack index of 0.45, while the crack indexes for the fly ash concretes are close to zero. *ANL Ref.*'s crack index of 0.45 after 18 days, only induced by AD, must be regarded as very significant.

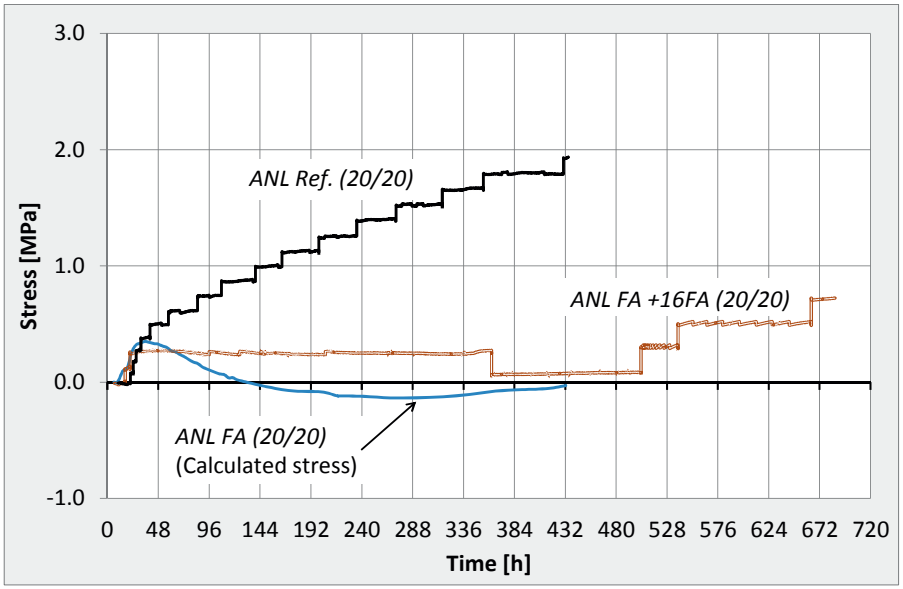

Figure 8.49; Stress development under 20 °C isothermal conditions, ANL Ref., ANL FA and ANL FA +16FA

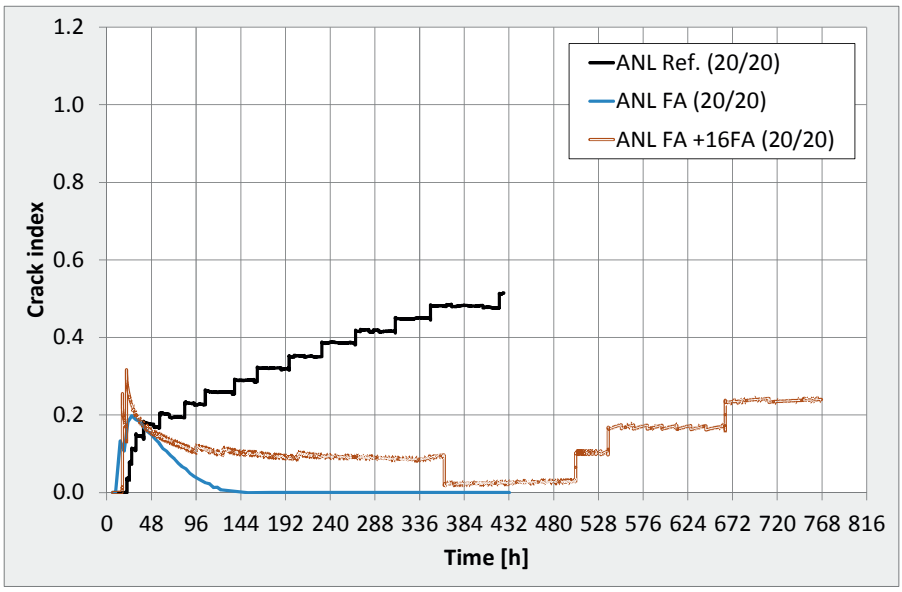

Figure 8.50; Crack index under 20 °C isothermal conditions, ANL Ref., ANL FA and ANL FA +16FA

Figure 8.51 compares stress development curves representing the wall described in Chapter 7.3 cast under temperature conditions *Summer I* (i.e. the temperature was based on the originally used ANL FA cement batch TF3-11, the tests were however cast with TF5-14). The corresponding crack indexes are given in Figure 8.52. As found in Chapter 7.3, T_{max} is decreasing with increasing fly ash content. A reduction in T_{max} reduces the concrete expansion and hence the initial compressive stress development during the first 1-2 days. Further, a decreasing T_{max} also decreases the thermal contraction to which the wall is subjected during the cooling phase. For the given wall and temperature conditions, both the compressive and tensile stresses were decreasing with increasing fly ash content. However, the reduced tensile stress development must be considered in combination with the also reduced tensile strength, see the crack indexes given in Figure 8.52. Due to the lower tensile strength, the crack risk for *ANL FA (20/52)* and *ANL FA +8FA (20/49)* surpass *ANL Ref. (20/62)* after 120 and 144 hours, respectively. In addition, *ANL FA (20/52)* actually developed failure in tension at an earlier point in time than *ANL Ref. (20/62)*.

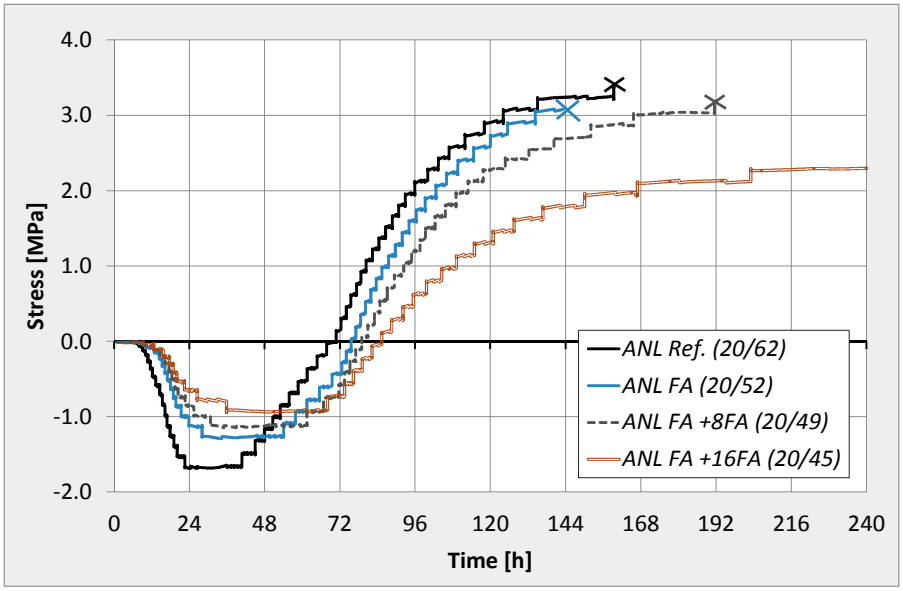

Figure 8.51; Stress development under realistic temperature conditions, Summer I (cement batch TF3-11), ANL Ref. (20/62), ANL FA (20/52), ANL FA +8FA (20/49) and ANL FA +16FA (20/45)

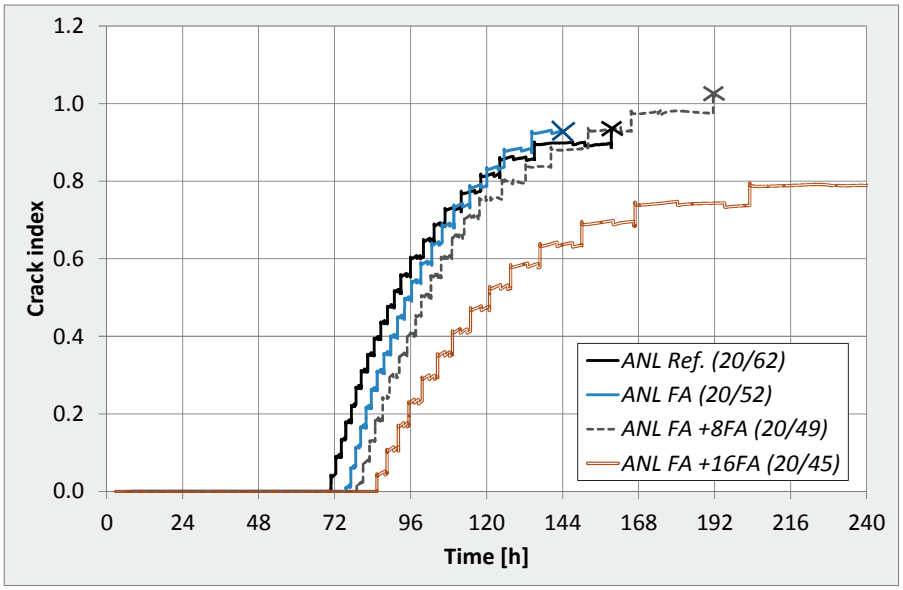

Figure 8.52; Crack index under realistic temperature conditions, Summer I (cement batch TF3-11), ANL Ref. (20/62), ANL FA (20/52), ANL FA +8FA (20/49) and ANL FA +16FA (20/45)

The stress development curves representing the wall cast under temperature conditions *Summer II* (i.e. with the cement batch TF5-14) are presented in Figure 8.53, while the corresponding crack indexes are given in Figure 8.54. When focusing on the fly ash concretes only (which all are based on the same cement ANL FA), both the stress developments and crack indexes are clearly reduced with increasing fly ash content.

When comparing the results obtained for temperature conditions *Summer I* and *Summer II*, it can be seen that the virtual change of cement batch had a high influence on the crack index. I.e. the cement batch actually used during testing, TF5-14, was not changed, however the applied temperature histories representing the two different cement batches were changed. Figure 8.55 and Figure 8.56 compare the stress developments and crack indexes for *ANL FA* and *ANL FA +16FA* cast with cement batch TF3-11 and TF5-14 (*Summer I* and *Summer II*, respectively). Thus, replacing the cement batch TF5-14 with TF3-11 would reduce the crack index at 96 hours for *ANL FA* with 37 %. The very same reduction in crack index could be achieved by changing the concrete *ANL FA* to *ANL FA +16FA* (i.e. increasing the total fly ash content from 16 to 33 %).

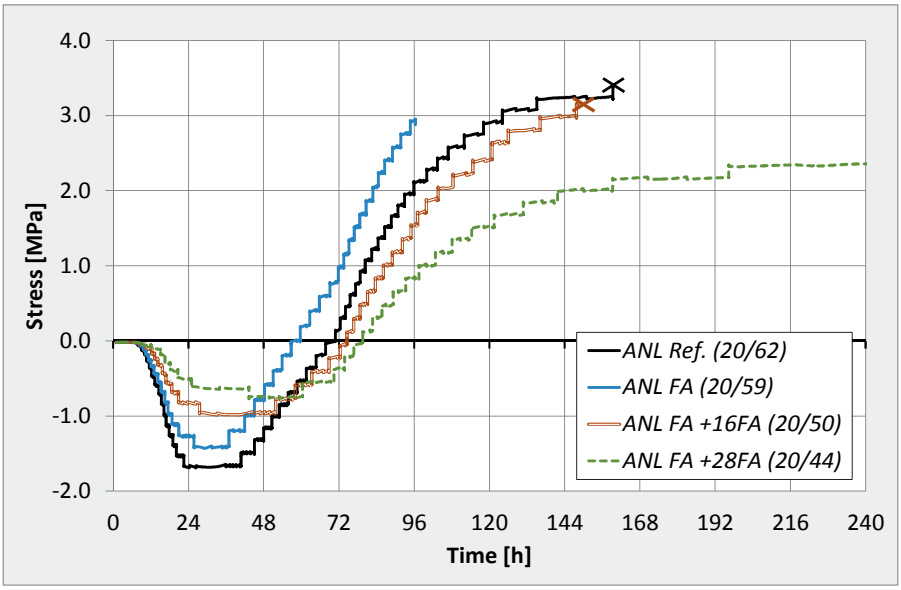

Figure 8.53; Stress development under realistic temperature conditions, Summer II (cement batch TF4-15), ANL Ref. (20/62), ANL FA (20/59), ANL FA +16FA (20/50) and ANL FA +28FA (20/44)

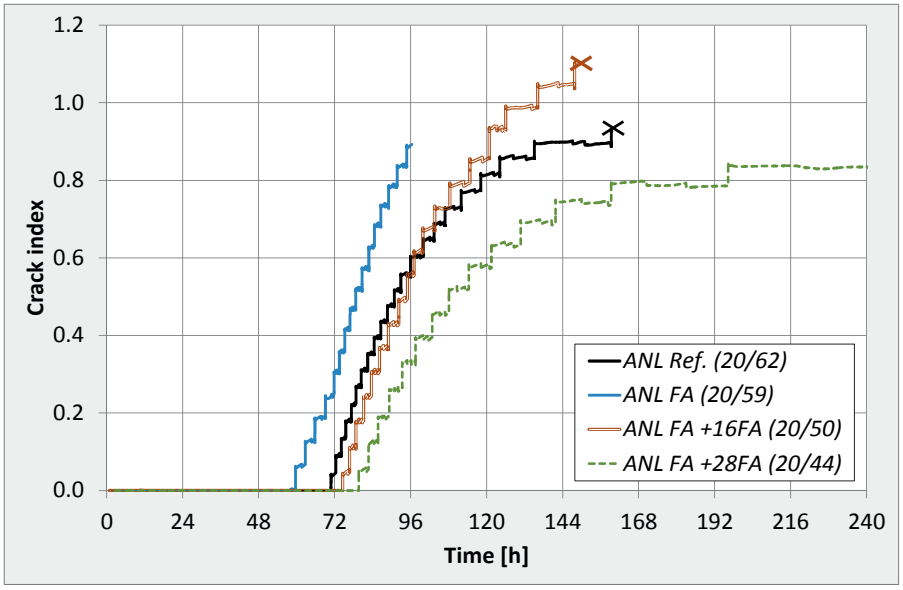

Figure 8.54; Crack index under realistic temperature conditions, Summer II (cement batch TF4-15), ANL Ref. (20/62), ANL FA (20/59), ANL FA +16FA (20/50) and ANL FA +28FA (20/44)

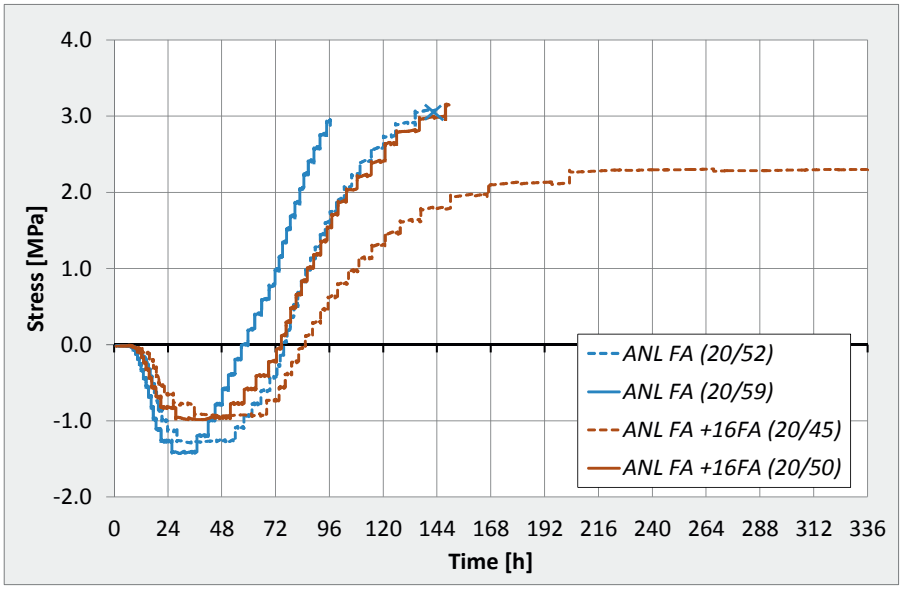

Figure 8.55; Stress development under realistic temperature conditions (summer), ANL FA and ANL FA +16FA, effect of cement batch: TF3-11 (dotted line) versus TF4-15 (continuous line)

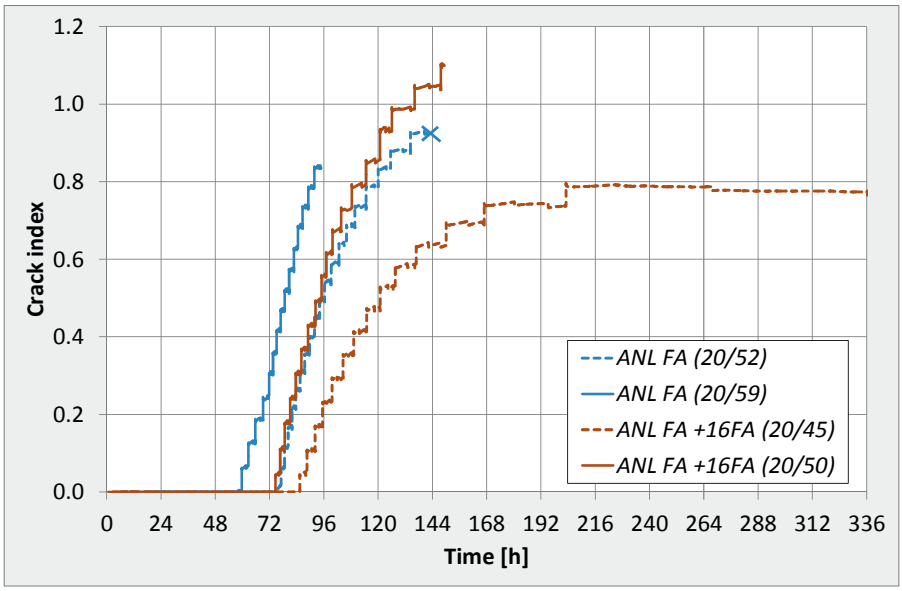

Figure 8.56; Crack index under realistic temperature conditions (summer), ANL FA and ANL FA +16FA, effect of cement batch: TF3-11 (dotted line) versus TF4-15 (continuous line)

The stress curves representing the wall cast under winter conditions are presented in Figure 8.57. Corresponding crack index curves are given in Figure 8.58. The temperature development for *ANL FA (10/43)* was quite high (ΔT_{max} = 33 °C) despite the winter conditions. The resulting calculated crack index was correspondingly high; it reached 1.0 within 8 days. *ANL FA +28FA (10/26)* on the other hand, had a T_{max} as low as 26 °C and the test hardly developed any initial compressive stress at all. Also the tensile stress development (which started as late as after 5 days) was slow, resulting in a fairly low crack index, below 0.5, despite winter conditions and the appurtenant slow property development.

All in all, the restrained stress development is reduced when increasing the fly ash content, but this has to be considered in combination with the correspondingly reduced tensile strength. For the given case (800 mm wall, summer and winter conditions), replacing cement by fly ash would reduce the cracking tendency. The concrete with the highest fly ash content, *ANL FA +28FA*, was found to provide the lowest crack index for both summer and winter conditions for the given case.

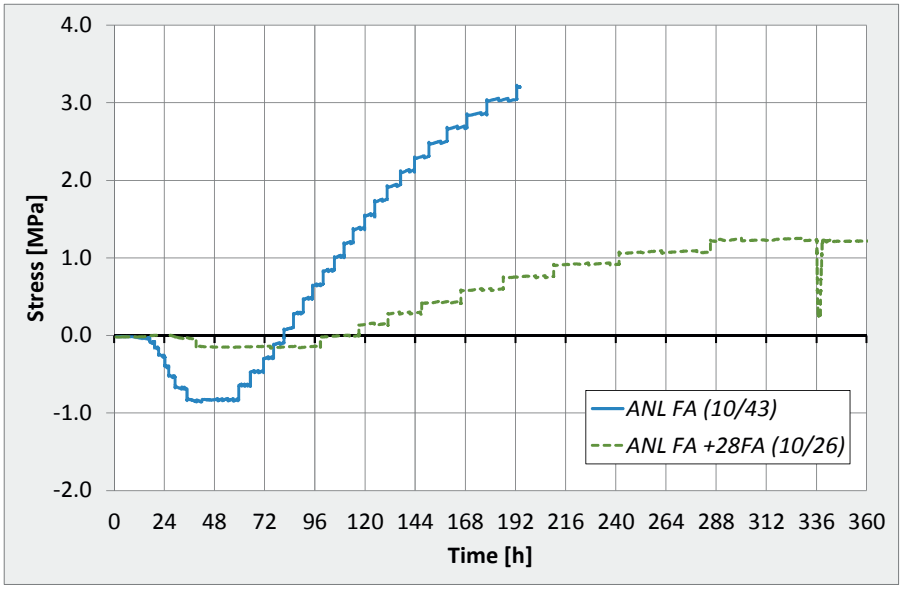

Figure 8.57; Stress development under realistic temperature conditions, Winter (cement batch TF4-15), ANL FA (10/43) and ANL FA +28FA (10/26)

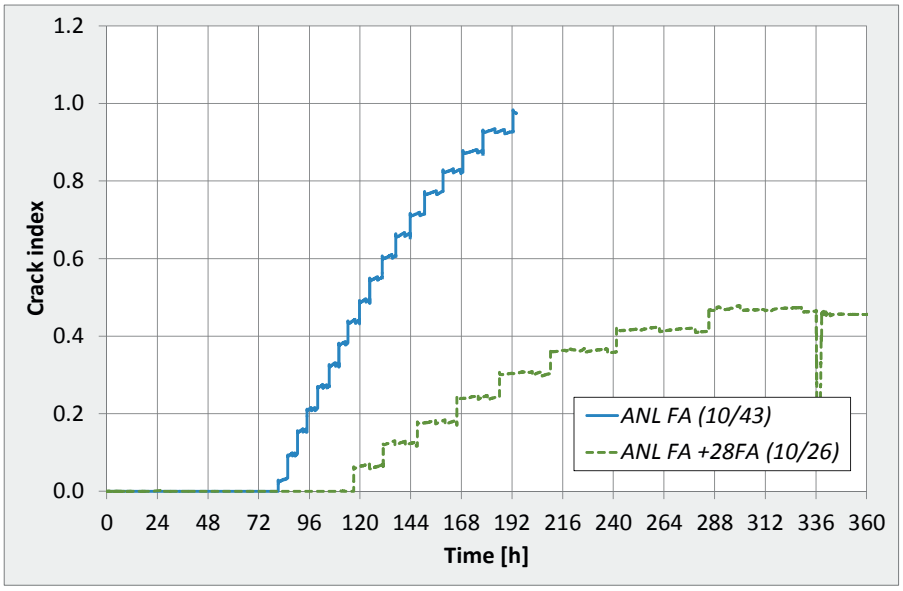

Figure 8.58; Crack index under realistic temperature conditions, Winter (cement batch TF4-15), ANL FA (10/43) and ANL FA +28FA (10/26)

Some of the TSTM tests were run for several weeks. *ANL FA +28FA (10/26)*, for instance, was run for as much as 12 weeks. Neither of these long-time tests experienced any

significant decrease in tensile stress over time. On the contrary, the tensile stress for *ANL FA +28FA (20/44)* was actually still increasing after 9 weeks. Long-time AD measurements on similar concretes [to be published by NTNU/SINTEF] show that the AD (contraction) is still increasing after as much as two years. From this follows that early age effects should be considered in combination with other structural and environmental loads when it comes to service limit state design after long time.

8.5 E-modulus and tensile strength determined from TSTM tests

8.5.1 General

The majority of the performed TSTM tests did not crack during testing. These tests were unloaded and thereafter subjected to a controlled loading until the specimens reached failure in tension, providing the tensile E-modulus and tensile stress capacities when loading until failure. In addition, the incremental E-modulus development during testing was determined for all TSTM tests as described in Chapter 6.3.7. The E-moduli and tensile strengths of the concrete series were also found by a mechanical test programme, Chapter 7.4.

The current section presents the various E-moduli and tensile strengths determined from the TSTM tests, and compare them with the material models and appurtenant material parameters described in Chapter 7.4.

8.5.2 E-modulus from the TSTM

The below listed E-moduli for *ANL Ref.*, *ANL FA*, *ANL FA +8FA*, *ANL FA +16FA* and *ANL FA +28FA* are presented in Figure 8.59, Figure 8.60, Figure 8.61, Figure 8.62 and Figure 8.63, respectively:

- E-modulus at the end of the TSTM test, 20 ^{o}C isothermal conditions
- E-modulus at the end of the TSTM test, realistic temperature conditions
- One incremental E-modulus from the TSTM, 20 ^{o}C isothermal conditions
- One incremental E-modulus from the TSTM, realistic temperature conditions
- Material model based on results from mechanical testing
- Material model with E_{28} assumed from TSTM tests

Generally, the E-modulus when loading until failure was found to be higher than the corresponding incremental E-modulus in the TSTM. This is related to the shape of the E-modulus - stress relation obtained when loading until failure in tension: the E-modulus decreases with increasing stress level. While the E-modulus when loading until failure was found from the strain-stress relation between 10 % and 40 % of the tensile strength, the incremental E-modulus was found from a corresponding relation over a much smaller stress range, see discussion in Chapter 6.3.7.

The E-moduli determined from the TSTM tests were generally higher than the corresponding values found from mechanical testing, a trend which was found to be increasing with increasing amount of fly ash. Hence, the material parameters determined from the mechanical test programme were decided adjusted to give a better fit with the TSTM E-moduli. This was achieved by using a 28-day E-modulus parameter (E_{28}) based on TSTM results, rather than using E_{28} determined from mechanical testing. The parameter E_{28} estimated from TSTM results was based on tests subjected to both 20 °C isothermal and realistic temperature conditions. For the fly ash concretes, the E-moduli was found to be higher for specimens subjected to realistic temperature conditions than for corresponding isothermal tests. This finding is supported by the mechanical test series performed for both isothermal and realistic temperature curing conditions presented in Chapter 7.6. Hence, by using an E-modulus found directly from the TSTM test, the described temperature effect on the 28-day E-modulus would be included in the material model.

It should be noticed that the test conditions varied between the currently determined E-moduli: the test specimen in the TSTM was subjected to loading from setting time up until the final testing, while the specimens used for mechanical testing were not subjected to loading prior to testing. In addition, the E-moduli found from mechanical testing are the average of the tensile and the compressive E-moduli, while the TSTM represents the tensile E-module only. In Chapter 7.4 it was found that the tensile E-modulus was slightly higher than the compressive E-modulus for all concretes and test ages.

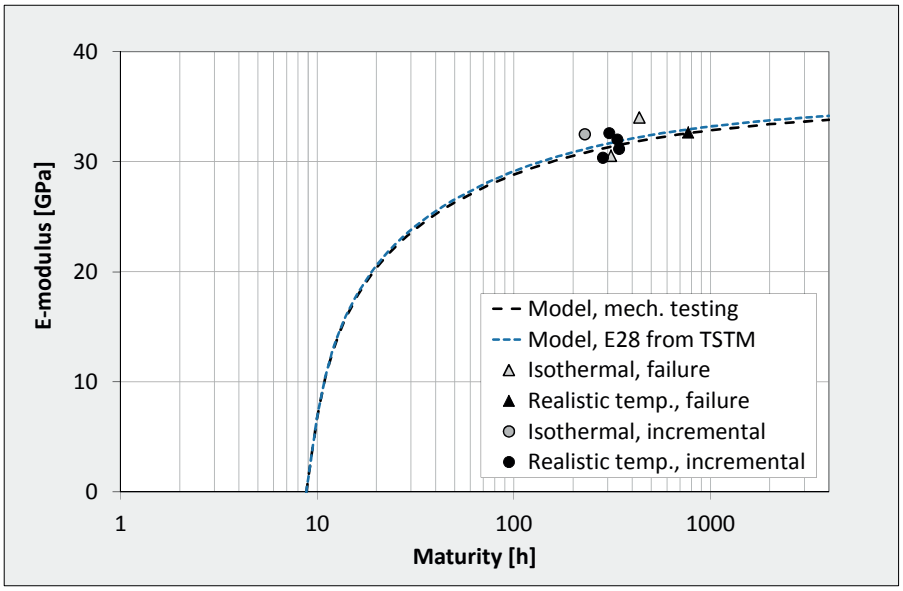

Figure 8.59; E-modulus versus maturity, ANL Ref., 20 °C isothermal and realistic temperature conditions

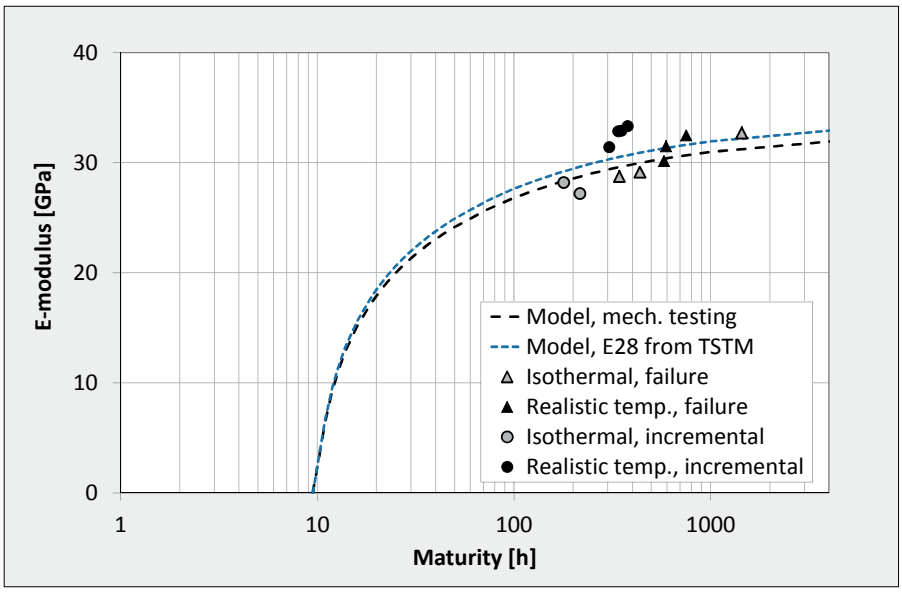

Figure 8.60; E-modulus versus maturity, ANL FA, 20 °C isothermal and realistic temperature conditions

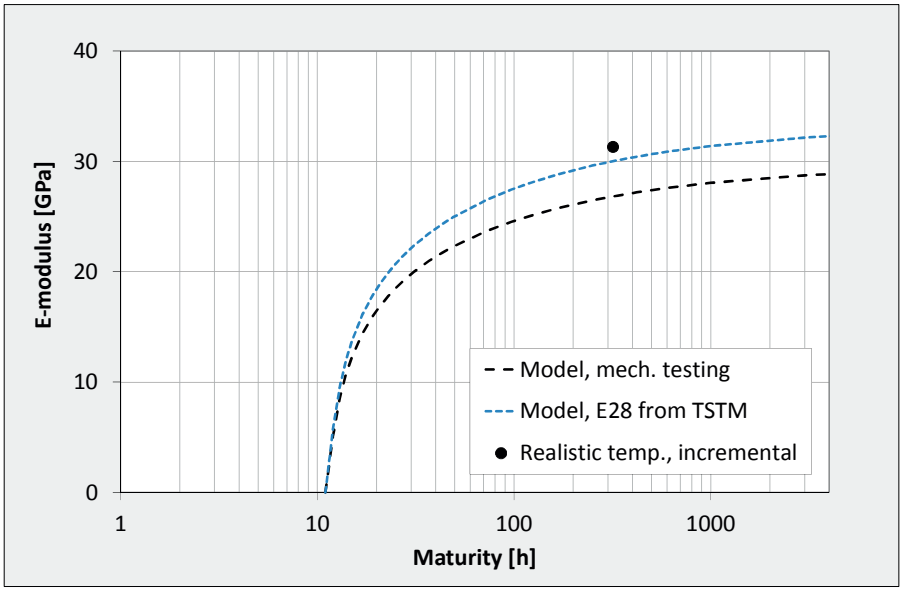

Figure 8.61; E-modulus versus maturity, ANL FA +8FA, 20 °C isothermal and realistic temperature conditions

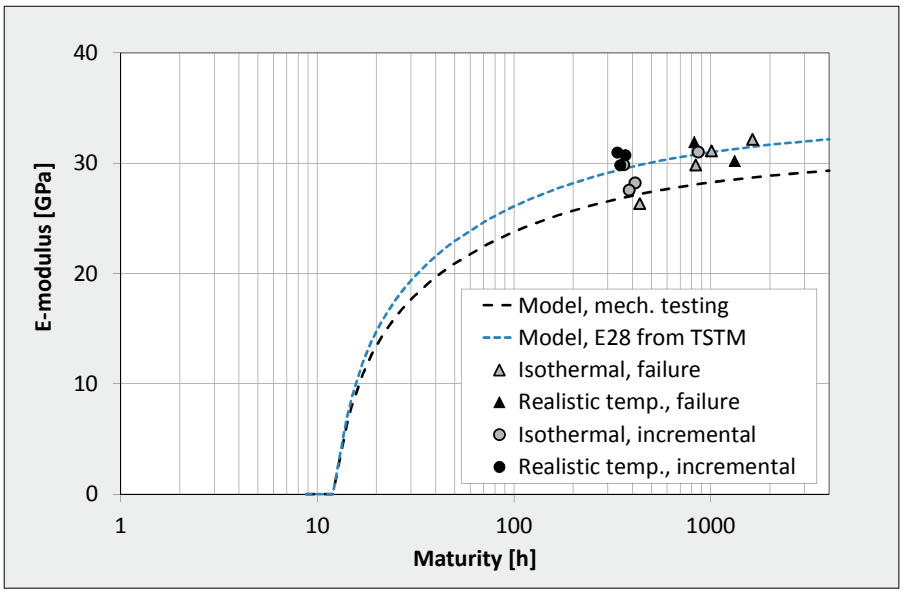

Figure 8.62; E-modulus versus maturity, ANL FA +16FA, 20 °C isothermal and realistic temperature conditions

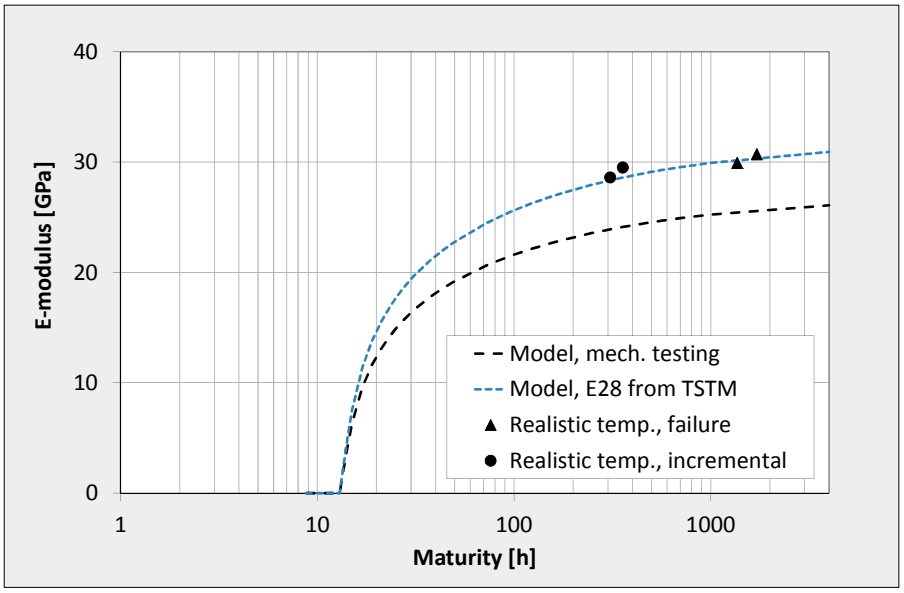

Figure 8.63; E-modulus versus maturity, ANL FA +28FA, 20 °C isothermal and realistic temperature conditions

As described in Chapter 6.3.7, the TSTM provides an incremental E-modulus development (i.e. obtained from incremental loading) over time for the concrete subjected to testing. Incremental E-modulus developments obtained for *ANL Ref.*, *ANL FA*, *ANL FA +8FA, ANL FA +16FA* and *ANL FA +28FA* are given in Figure 8.64, Figure 8.65, Figure 8.66, Figure 8.67 and Figure 8.68, respectively. The E-moduli are plotted versus maturity by a logarithmic scale, and all figures also show the modelled E-modulus development based on results from mechanical testing as found in Chapter 7.4.

The measured incremental E-modulus developments show a slightly faster development than the corresponding models. This is probably related to temperature effects caused by the realistic curing temperature as investigated and discussed in Chapter 7.6. The modified model, where a 28-day E-modulus parameter (E_{28}) based on TSTM results is used, gives better agreement with the measured development, especially for the fly ash concretes. However, there are still some deviations between measured and modelled E-modulus development for the *ANL Ref.* realistic temperature test (which is the test with the highest temperature increase during testing).

Elevated E-moduli values can be seen for all the tests at the time that the TSTM movement changes direction from expansion to contraction. These elevated values are most likely related to a small slowness/slippage in the TSTM System.

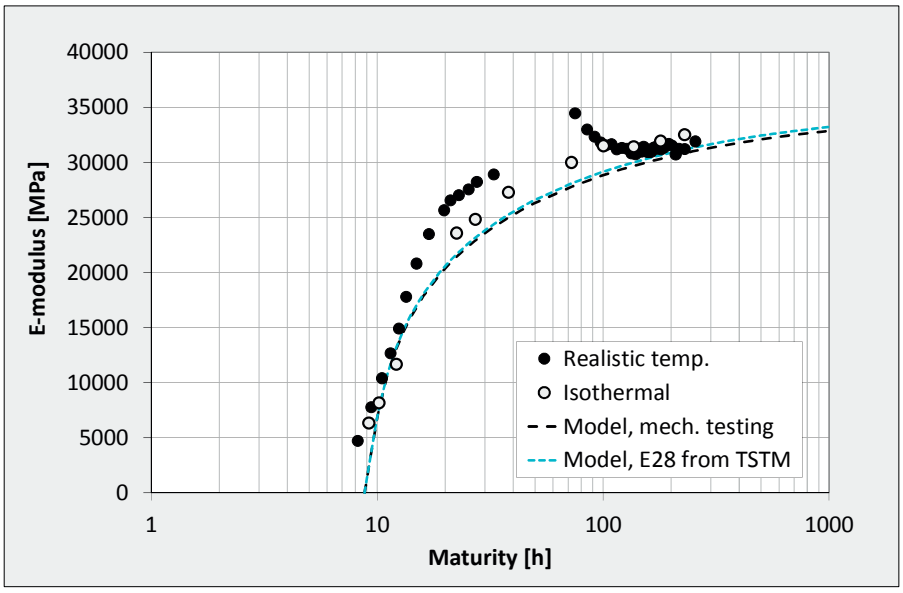

Figure 8.64; Incremental E-modulus development in the TSTM, ANL Ref., 20 °C isothermal and realistic temperature conditions

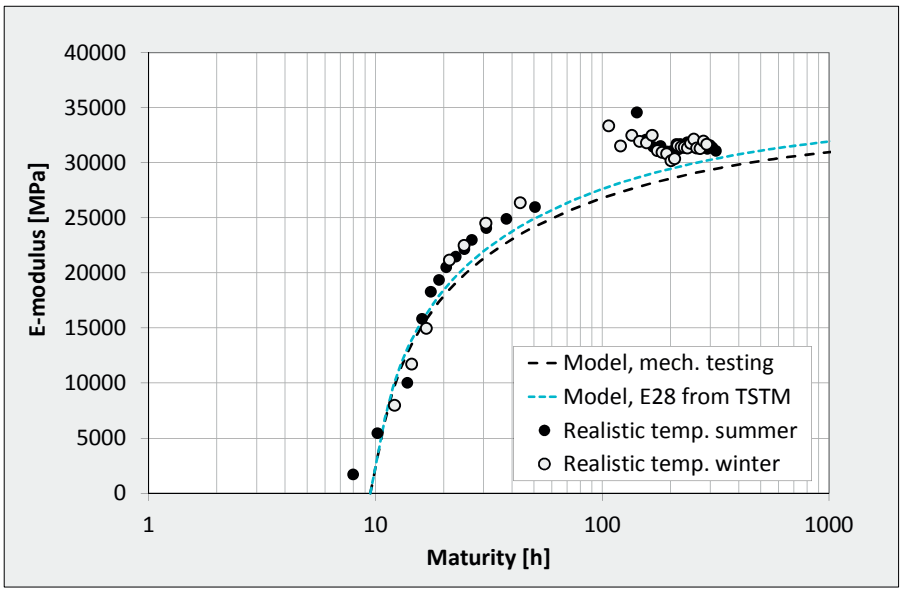

Figure 8.65; Incremental E-modulus development in the TSTM, ANL FA, realistic temperature conditions summer and winter

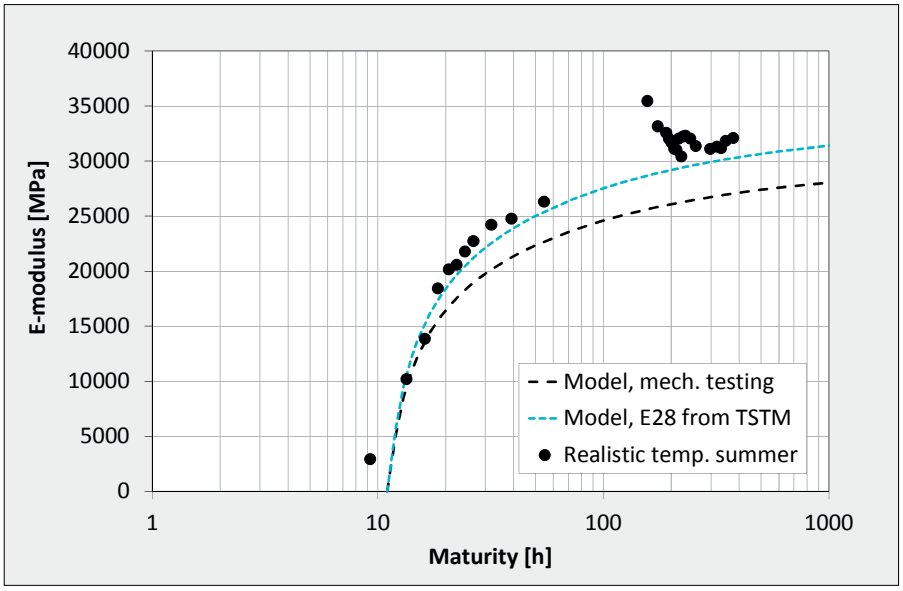

Figure 8.66; Incremental E-modulus development in the TSTM, ANL FA +8FA, realistic temperature conditions summer

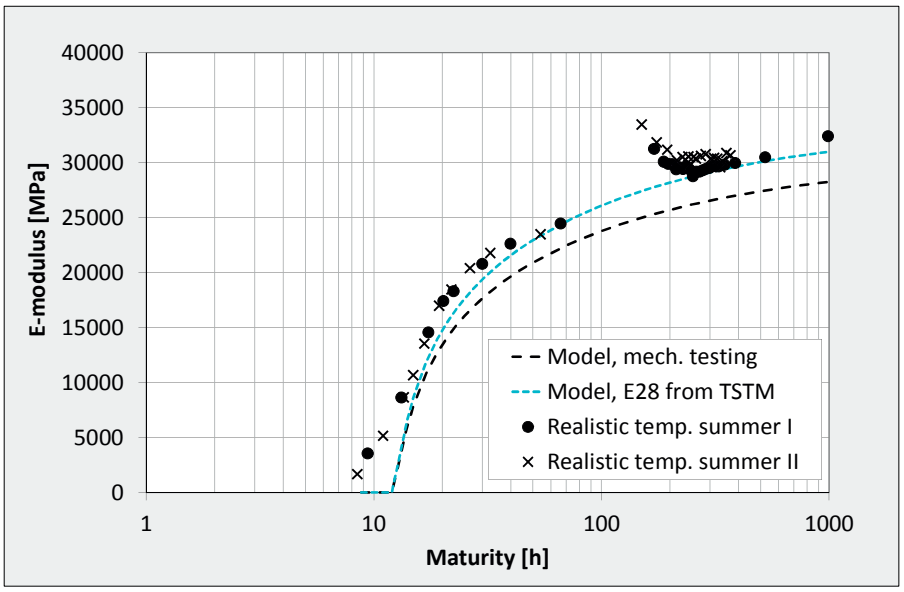

Figure 8.67; Incremental E-modulus development in the TSTM, ANL FA +16FA, realistic temperature conditions summer

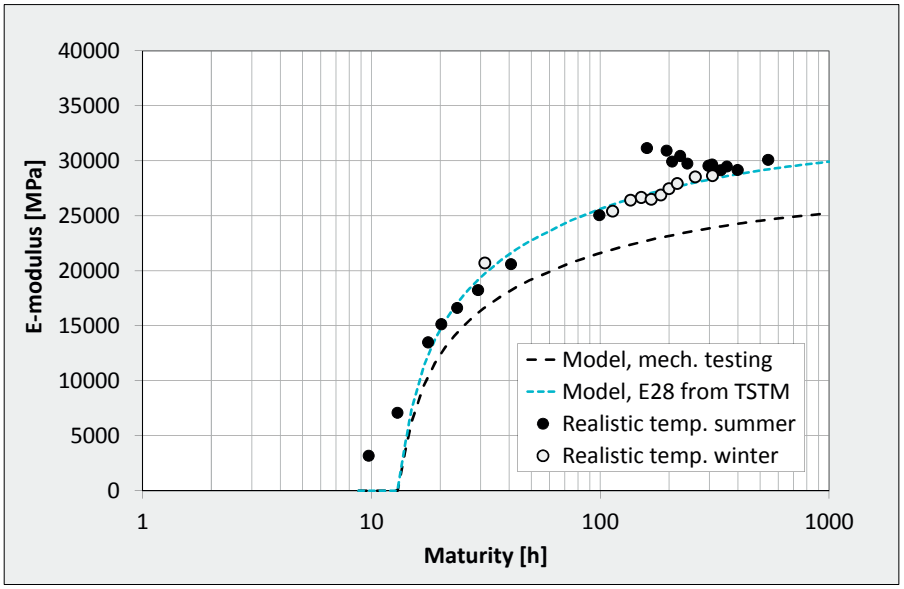

Figure 8.68; Incremental E-modulus development in the TSTM, ANL FA +28FA, realistic temperature conditions summer and winter

8.5.3 Tensile strength from the TSTM

Figure 8.69 - Figure 8.73 present tensile strengths obtained from the TSTM for the concretes *ANL Ref.*, *ANL FA*, *ANL FA +8FA*, *ANL FA +16FA* and *ANL FA +28FA*, respectively. The TSTM results are compared with the tensile strength model described in Chapter 3.4 in combination with model parameters as described in Chapter 7.4.

It should be noticed that there were some variations in test conditions between the mechanical tests and the TSTM tests: the specimens in the TSTM were subjected to loading from setting time up until the final testing, while the specimens used for mechanical testing were not subjected to any loading prior to testing. In addition, an analogous difference exists within the TSTM tests: while some of the tests developed failure in tension during testing (i.e. failure caused by sustained loading), the remaining tests were first unloaded and then reloaded until failure at a much higher loading rate than during testing. [Shkoukani et al., 1991] reported the following: "*The tensile strength obtained under sustained loading was smaller than under short-time loading"* and *"If short-term strength was determined within a failure time of 10 seconds, the corresponding sustained tensile strength was about 70 % of the short-term strength."* The same study also reported that the specimens that did not develop failure during sustained loading were unloaded and reloaded to failure in a short-term test: "*The strength obtained after this procedure was significantly higher than the corresponding strength obtained from short-term tests on virgin specimens."* This hardening mechanism was seen for both concentric and eccentric tensile tests, and corresponding behaviour is well known for compression [Neville, 1972]. According to these observations, the TSTM tests that developed failure during testing should provide a lower tensile strength than the tests that were unloaded and reloaded to failure. Considering all TSTM tensile strength values obtained, this tendency could actually be seen. However, no clear conclusion quantifying the effect could be made as the series of obtained tensile strengths is rather complex, see the discussion of additional varying test factors described below.

The TSTM results show that *ANL Ref.* exhibits the highest dispersion in tensile strength, Figure 8.69. However, the highest f_t value (4.4 MPa at 770 maturity hours) was obtained from the only test performed with the new cement batch EG1-14, and could thus be explained by the increased tensile strength found for EG1-14 when compared with the originally used batch EG1-11 [Kjellmark, 2015] (see Chapter 7.4). In addition, this particular test was the only realistic temperature test which did not develop failure under sustained loading (it was first unloaded and then reloaded to failure at a high loading rate, see discussion above). The low average tensile strength found for the realistic temperature tests could be explained both by: 1) sustained loading as discussed above and 2) reduction in tensile strength caused by curing at high temperatures as this effect is not covered by the maturity principle, see Chapter 7.6. The two tensile strengths obtained from isothermal TSTM tests give good agreement with the model.

TSTM tensile strengths obtained for *ANL FA* give a good fit with the model, Figure 8.70. This is as expected as the f_{t28} value used in the model was assumed based on TSTM test results, see Chapter 7.6.3. For *ANL FA +8FA*, Figure 8.71, only one tensile strength was obtained. This strength gives however very good agreement with the corresponding tensile strength model.

For *ANL FA +16FA*, the TSTM provided a higher tensile strength than the mechanical test series, Figure 8.72. This observation applies for both isothermal and realistic temperature conditions in the TSTM. For tensile strengths found from the TSTM beyond 672 maturity hours, the deviation could partly be explained by the observation from Section 7.6: The given material model is unable to describe the considerable increase in strength beyond 28 maturity days for the fly ash concretes. This argument could also explain the corresponding higher TSTM tensile strength seen for the concrete *ANL FA +28FA* when compared with the model, Figure 8.73. The uniaxial tensile strength tests reported in Chapter 7.6.3 show that *ANL FA +28FA* had a tensile strength of 3.99 MPa at 91 days (2184 hours), which corresponds well with the tensile strengths obtained from the TSTM tests. For *ANL FA +16FA,* the TSTM tests were performed with cement batch TF5-14, while the uniaxial tensile tests were performed with TF3-11. For *ANL FA +28FA* on the other hand, the same cement batch was used for both TSTM tests and mechanical testing.

Summarized, the presence of several different test factors complicated the comparison of the tensile strengths obtained from the various mechanical tests and TSTM tests: 1) Differences in testing conditions between mechanical tests and TSTM tests, 2) sustained loading versus short-time loading within the TSTM tests, 3) cement batch, 4) temperature conditions during curing and 5) the material model used to describe fly ash concretes. Allowing for the above listed sources that could cause deviating results, the TSTM tensile strength must still be said to give relatively good agreement with the corresponding results obtained from direct uniaxial tensile tests.

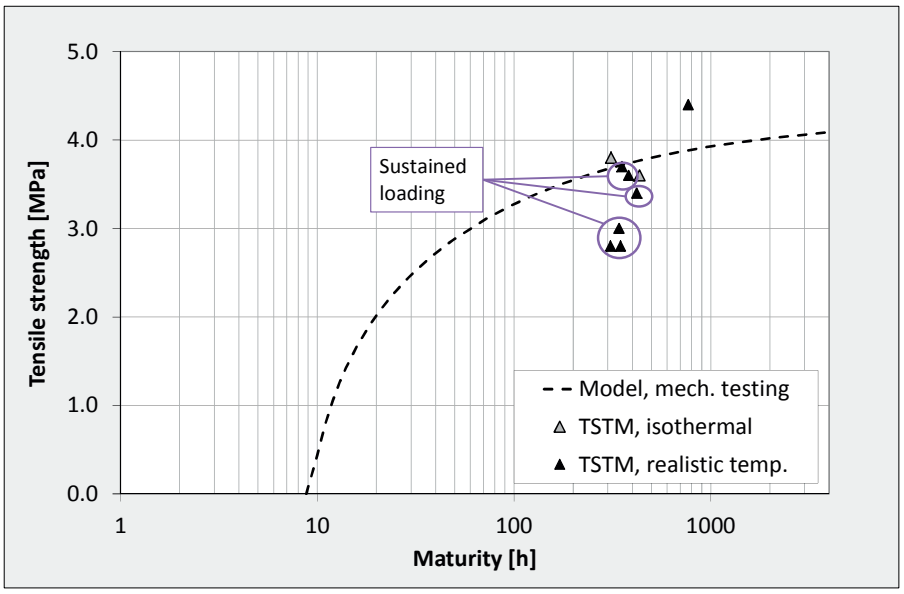

Figure 8.69; TSTM tensile strength versus maturity, ANL Ref., 20 °C isothermal and realistic temperature conditions

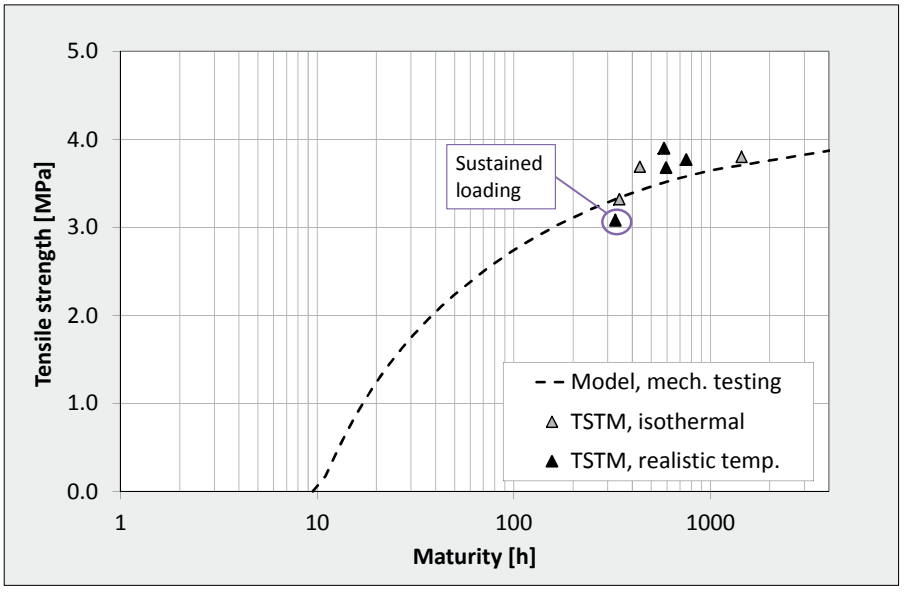

Figure 8.70; TSTM Tensile strength versus maturity, ANL FA, 20 °C isothermal and realistic temperature conditions

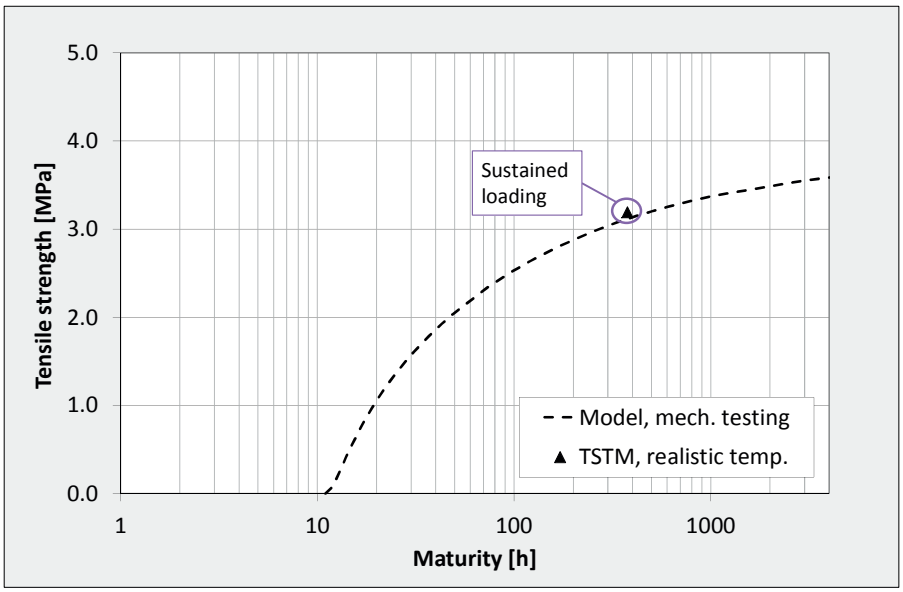

Figure 8.71; TSTM Tensile strength versus maturity, ANL FA +8FA, realistic temperature conditions

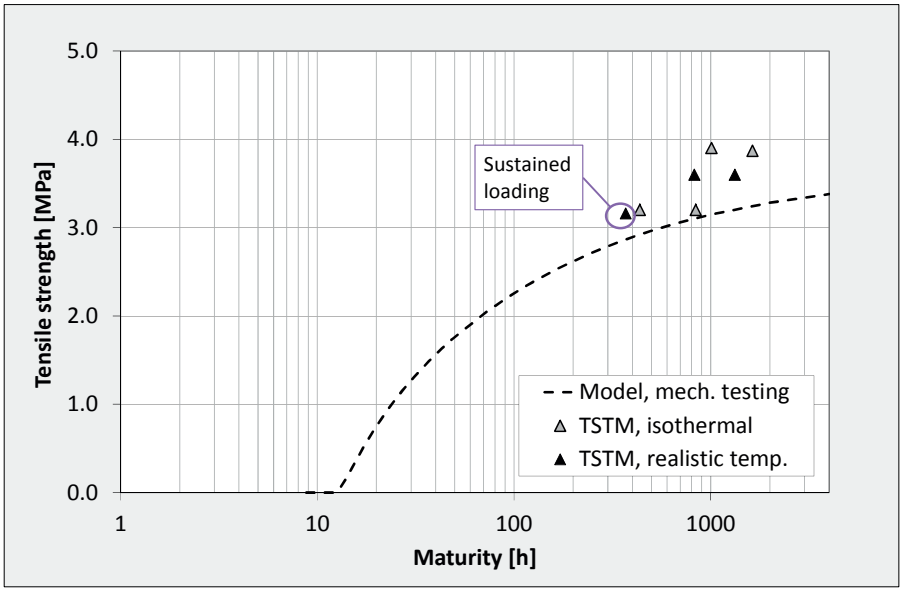

Figure 8.72; TSTM Tensile strength versus maturity, ANL FA +16FA, 20 °C isothermal and realistic temperature conditions

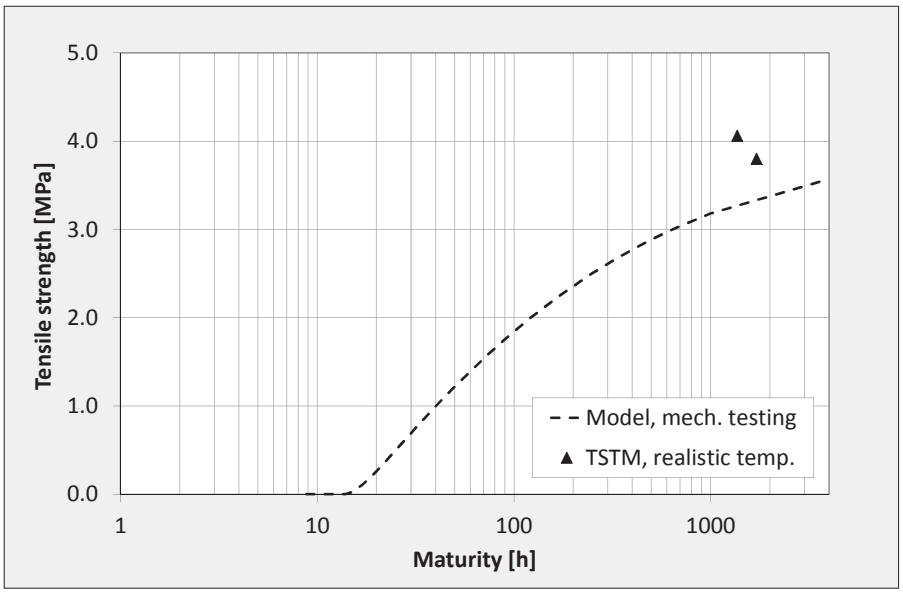

Figure 8.73; TSTM Tensile strength versus maturity, ANL FA +28FA, realistic temperature conditions

9 The influence of fly ash content on the various properties

A brief summary of the influence of fly ash content on the various investigated properties is given below. The summary is based on results previously presented and discussed in Chapter 7 and Chapter 8. Five concretes were included in the given investigation: *ANL Ref.*, *ANL FA*, *ANL FA +8FA*, *ANL FA +16FA* and *ANL FA +28FA*, with a fly ash content of 0 %, 17 %, 25 %, 33 % and 45 %, respectively. All concretes were made with $w/b = 0.40$ ($k_{FA} = 1.0$, $k_{silica} = 2.0$) and with the same cement paste volume (292 l/m^3). The increase in fly ash content was achieved by replacing cement with fly ash, and the fly ash content is given as percentage of the total amount of "cement + fly ash".

The heat development of each mix was measured in a semi-adiabatic calorimeter and used to calculate the temperature development in a defined wall structure. This is the "realistic" temperature development applied during testing (AD and TSTM), and it is off course different for each concrete mix.

Heat development: The research confirmed the well-known fact that the concrete heat development is systematically decreasing with increasing amount of fly ash.

Activation energy: The activation energy (with respect to mechanical properties) for temperatures above 20 °C, represented by the parameter *A,* was increasing with increasing amount of fly ash. The influence of fly ash on the parameter *B* was not found to be as systematic. However, there was a tendency of a decreasing *B* value with increasing fly ash content. In other words, the hydration rate was increasing with increasing amount of fly ash for temperatures above 20 °C, while it was quite similar for all concretes for temperatures below 20 °C.

Compressive strength: The 28-day compressive strength was systematically decreasing with increasing fly ash content. The average strength reduction was 0.8 MPa for each percentage increase in fly ash. Increasing the fly ash content from 0 % to 45 % caused a 35 MPa (44 %) decrease in the 28-day compressive strength. However, due to the fly ash concretes' property increase beyond 28 days, the corresponding decrease in the 91-day strength was reduced to 26 MPa (30 %).

Tensile strength: The tensile strength was systematically decreasing with increasing amount of fly ash. This trend was seen both for the direct uniaxial strength and for the tensile splitting strength. The average tensile strength was reduced with 0.8 MPa (22 %) when increasing the fly ash content from 0 % to 45 %. The corresponding decrease in the 91-day tensile strength was 0.6 MPa (13 %), confirming the enhanced property increase beyond 28 days seen for fly ash concretes.

E-modulus: Both the compressive and the tensile E-modulus were found to decrease with increasing fly ash content for all test ages. For the given concretes, the average reduction in the 28-day E-modulus was 0.2 GPa for each percentage increase in fly ash content. I.e. increasing the fly ash content from 0 % to 45 % caused a 7.6 GPa (23 %) decrease in the

28 day E-modulus. The corresponding decrease in the 91-day E-modulus was 4.4 GPa (13 %).

Coefficient of thermal expansion: The CTE was not systematically investigated during the current test series. However, a tendency of a slight increase in CTE with increasing amount of fly ash was seen.

Creep: For the investigated loading ages, the concrete creep was found to be slightly increasing over time with increasing amount of fly ash. This observation applies both for creep in compression and creep in tension.

Autogenous deformation: For 20 ^{o}C isothermal curing conditions, the reference concrete showed a much more pronounced AD development than the fly ash concretes. When looking at the fly ash concretes solely, the fly ash content did not seem to affect the AD behaviour. However, this latter observation was based on AD curves from two fly ash concretes only, and could therefore not be said to constitute a general validity. For realistic temperature conditions, AD (contraction) was systematically decreasing with increasing fly ash content. It could however be discussed whether the AD curves varied directly with the fly ash content, or rather with the applied maximum temperature increase, i.e. indirectly with the fly ash content.

Stress development: For the investigated wall and temperature conditions, both the compressive and tensile stresses were decreasing with increasing fly ash content. However, the reduced tensile stress development must be considered in combination with the corresponding reduced tensile strength, see *"Crack index"* below.

Crack index: For the investigated concretes and structural case (800 mm thick wall, summer and winter conditions), an increasing replacement of cement by fly ash was found to reduce the cracking tendency.

10 Summary, conclusions and further work

10.1 Summary and conclusions

The overall aim of the current PhD work was to contribute to an increased basic knowledge and understanding of early age concrete material properties (behavior) and also to investigate calculation methods to assess the concrete's structural behavior under realistic temperature curing conditions. This aim was approached both experimentally and analytically, resulting in an extensive experimental test program which has been performed during the current work.

In the following, the main conclusions are presented in relation to the originally defined objectives:

- *Finalize and verify the reconstruction of the TSTM System to provide a more advanced management of the experiments and more extensive outcome from each test*

During the current study, the TSTM System has been subjected to a reconstruction followed by a comprehensive and time-consuming verification and documentation period. The TSTM System is now considered operational, providing reliable results and very good reproducibility. As a result of the reconstruction, more advanced management of the experiments as well as more comprehensive outcome from each test have been achieved, e.g. optional degree of restraint and incremental E-modulus development. The TSTM is now able to directly simulate the stress development of a given section of a concrete structure by applying a representative temperature history and degree of restraint. The TSTM can thus be used as the answer for early age stress calculations, allowing for a calibration of the chosen calculation approach and appurtenant material parameters.

- *Provide knowledge about the effect of concrete composition and mineral additives, exemplified by fly ash content, on strain and stress development and cracking sensitivity in concrete structures*

An extensive experimental test program has been performed to investigate the effect of fly ash content on the various material properties. The results from the 20 ^{o}C isothermal tests showed that heat development as well as the compressive strength, tensile strength and E-modulus were systematically decreasing with increasing fly ash content. The property development rate beyond 28 days was found to increase systematically with increasing fly ash content. The concretes showed a small increase in creep with increasing fly ash content, and it was also found that the reference concrete had a much more pronounced AD development than the fly ash concretes under 20 ^{o}C isothermal curing conditions.

When subjected to realistic curing conditions, several of the material properties showed a different behaviour. "Realistic curing conditions" means that each concrete was subjected to its own semi-adiabatic temperature history representing the average temperature in a selected section of an 800 mm thick wall. While the reference concrete was affected by the

applied realistic temperature regime with a reduction in compressive strength, tensile strength and E-modulus, the investigated fly ash concrete was unaffected or even showed an increase in mechanical properties when compared to isothermal conditions. The fly ash concrete was for instance found to experience a temperature-induced increase in the 28-day E-modulus which was not captured by the maturity principle. As the heat development was found to be decreasing with increasing fly ash content, naturally also the concrete's temperature development and thus thermal dilation experienced a corresponding reduction. Also the AD (contraction) was decreasing with increasing fly ash content and reduced curing temperature, and a systematic relation between AD development and maximum temperature increase during curing was found.

Summarized, the tensile stresses under restrained conditions were found to be decreasing with increasing fly ash content. Also when seen in combination with the reduced tensile strength, the concrete's sensitivity to cracking was found to be systematically decreasing with increasing fly ash content for the given structural case. Consequently, by using laboratory experiments and analytical approaches, the concretes' sensitivity to cracking could be assessed and reduced with the use of mineral additives, which in the current study has been exemplified by fly ash content.

- *Check the validity and improve existing material models necessary to assess the structural behaviour of early age concrete*

Good agreement was found between early age stress developments calculated with TSTM-sim (Excel), CrackTeSt COIN and DIANA, respectively. The calculations also gave good agreement with the corresponding stress development measured in the TSTM, both for isothermal and realistic curing conditions (i.e. both summer- and winter conditions). This overall agreement supports the validity and robustness of both the calculation approaches and the applied model parameters. It should be noticed that the 28-day E-moduli used in the calculations were deduced from the TSTM tests, thus including the found temperature effect on the 28-day E-modulus for fly ash concretes. The applied creep parameters on the other hand, were deduced from isothermal tests.

A thorough material parameter database has been established for the investigated concretes. This database is about to be included in the program CrackTeSt COIN, making the currently established basis for early age stress calculations publicly available.

The TSTM allowed creep experiments to be carried out both in tension and compression under almost identical conditions. These tests gave very similar results, i.e. both compressive and tensile creep could be accurately described with the same creep parameters. More work will be performed to investigate this unique capability and corresponding results further. The obtained results also indicated no creep recovery when unloading the compressive load for the given case and load ages. Neglecting this found lack of creep recovery in early age stress calculations would cause a small underestimation of the tensile stress development over time. Originally, the creep parameters used for the early age stress calculations were assumed based on previous experience with similar

concretes. Compared with the creep parameters found from the current creep tests, the originally assumed values underestimated the tensile stress development of the fly ash concretes considerably (around 50 %). This illustrates the significance of a good overview of all relevant properties.

For all investigated concretes, AD obtained under isothermal conditions appears to be fundamentally different from the corresponding AD deduced from realistic temperature tests. From this follows that AD under realistic temperature conditions cannot be modelled and predicted based on isothermal test results and the maturity principle.

When exposed to 20 ^{o}C isothermal curing conditions, the fly ash concretes showed a much more pronounced mechanical property development beyond 28 days than the reference concrete without fly ash. It was found that the currently used material models failed to express this continuing development of properties beyond 28 days for the fly ash concretes. However, the above described long-term property development was significantly reduced when the specimens were exposed to realistic temperature curing conditions.

- *Final comments*

During the current work, two batches of cement run out and new ones were supplied. Heat development tests showed a considerable difference in the cement reactivity between the different batches, however, the corresponding change in material properties were surprisingly low. The realistic temperature histories calculated for the fly ash concretes were naturally found to be highly influenced by the given cement batch. This considerable change in curing temperature would further influence the TD and AD, and thus also the cracking sensitivity of the given concretes.

It was found that both mechanical properties and AD were affected by realistic temperature curing conditions in a way that could not be correctly adjusted for by using the maturity principle. Using isothermal values for AD under realistic conditions would underestimate the volume change and thus also the corresponding tensile stress generation. In addition, also the isothermal 28-day E-modulus value would underestimate the actual E-modulus occurring under realistic conditions and hence the tensile stress development. Both these properties should be determined under realistic temperature curing conditions, or at least be evaluated and if possible compensated for.

Several of the long-term TSTM tests continued to develop strain and stress for several months after casting, and the results reveal interesting aspects on the very limited or lacking ability of concrete to relax tensile stresses in the post-hardening phase. This illustrates the importance of long-term measurements when it comes to evaluating the concrete's sensitivity to cracking.

10.2 Further work

The existing material models for compressive strength, tensile strength and E-modulus development are not able to describe the enhanced property development beyond 28 days found for the fly ash concretes. More experiments are needed, and both long-term values (e.g. 91 days) and early age properties should be used to establish a new material model. With more AD tests, also an attempt to model AD in fly ash concretes could be carried out as a rather clear relation between temperature history and AD development was found during the current study.

During the AD measurements, some of the fly ash concretes were observed to experience a swelling in the cooling phase, i.e. between ΔT_{max} and 336 hours. The observation was made for the fly ash concretes which experienced a temperature increase of less than 20 ^{o}C during the hardening phase. The reason for this swelling could not be explained, and more research should be conducted to investigate this phenomenon further.

Realistic temperature curing conditions have been found to have a considerable influence on the material properties development, as found many times earlier by many researchers. Despite this, most laboratory experiments are performed under 20 ^{o}C isothermal conditions. Further testing on the effect of curing temperature on material properties development should be aspired. In addition, the found equality between tensile and compressive creep is planned investigated further, e.g. with more tests and with various times of loading.

For several long-term TSTM tests, the tensile stress development in the hardening phase was not seen to decrease over time. Consequently, it should be aspired to find measures to include early age stress development with other structural and environmental loads when it comes to service limit state design after long time. It would also be interesting to perform early age stress calculations for a full-scale realistic case to investigate the concretes and their sensitivity to cracking in a full-scale and possible more practical approach.

Finally, the most important future perspective would be to find feasible solutions and applications to implement the performed research into both the structural design and construction phase, and thus to be able to predict, reduce and if possible also avoid cracking of early age concrete.

References

Amin, Muhammad Nasir, Jeong-Su Kim, Yun Lee and Jin-Keun Kim (2009): *Simulation of the thermal stress in mass concrete using a thermal stress measuring device.* Cement and Concrete Research 39 (2009) 154

Atrushi, Dawood S. (2003): *Tensile and Compressive Creep of Early Age Concrete: Testing and Modelling*. PhD-Thesis, ISBN: 82-471-5565-6, Norwegian University of Science and Technology (NTNU), Trondheim, Norway

Bazant, Z.P. and E. Osman (1976): *Double power law for basic creep of concrete.* Materials and Structures 9 (49) (1976) 3-11

Bazant, Zdenek P. and Sandeep Baweja (1995): *Creep and shrinkage prediction model for analysis and design of concrete structures - model B3.* Materials and Structures 28 (1995) 357-365

Bazant, Zdenek P. (2001): *Prediction of concrete creep and shrinkage: past, present and future.* Nuclear Engineering and Design 203 (2001) 27-38

Bjøntegaard, Øyvind, Terje Kanstad, Erik J. Sellevold and Tor Arne Hammer (1999): *Stressinducing deformations and mechanical properties of high performance concrete at very early ages*. In the 5th International Symposium on Utilization of high Strength/High Performance Concrete. Sandefjord, Norway.

Bjøntegaard, Øyvind (1999): *Thermal Dilation and Autogenous Deformation as Driving Forces to Self-Induced Stresses in High Performance Concrete*. PhD-Thesis, ISBN: 82-7984-002-8, Norwegian University of Science and Technology (NTNU), Trondheim, Norway

Bjøntegaard, Øyvind, Terje Kanstad and Erik J. Sellevold (2000): *t0 - The startpoint of stress calculations*. For discussion at the IPACS meeting in Delft 20-21st of March. Norwegian University of Science and Technology, Trondheim.

Bjøntegaard, Øyvind and Erik J. Sellevold (2001): *Interaction between thermal dilation and autogenous deformation in high performance concrete.* Materials and Structures 34 (2001) 266-272

Bjøntegaard, Øyvind and Erik J. Sellevold (2003): *Bjørvika senketunnel, Fase I - Bestemmelse av betongegenskaper relevante for evaluering av risstendens i herdefasen.* Norwegian University of Science and Technology (NTNU), Trondheim, Norway

Bjøntegaard, Øyvind (2004): *Bjørvika senketunnel, Fase II - Bestemmelse av betongegenskaper relevante for evaluering av risstendens i herdefasen.* Norwegian University of Science and Technology (NTNU), Trondheim, Norway

Bjøntegaard, Øyvind and Erik J. Sellevold (2004a): *Effects of Silica Fume and Temperature on Autogenous Deformation of High Performance Concrete.* ACI, Special Publication 220

Bjøntegaard, Øyvind, Tor Arne Hammer and Erik J. Sellevold (2004b): *On the measurement of free deformation of early age cement paste and concrete.* Cement & Concrete Composites 26 (2004) 427-435

Bjøntegaard, Øyvind and E.J. Sellevold (2004c): *The Temperature-Stress Testing Machine (TSTM): Capabilities and Limitations*. Advances in Concrete Through Science and Engineering Northwestern University, Evanston, Illinois

Bjøntegaard, Øyvind (2011): *Basis for and practial approaches to stress calculations and crack risk estimation in hardening concrete structures - State of the art.* COIN Project report 31 - 2011, SINTEF Building and Infrastructure, Trondheim, Norway

Bjøntegaard, Øyvind and Knut O. Kjellsen (2012): *Property development and cracking tendency in hardening concrete: Effect of cement type and fly ash content.* COIN Project Report 40, SINTEF Building and Infrastructure, Trondheim, Norway

Bosnjak, Daniela (2000): *Self-induced Cracking Problems in Hardening Concrete Structures*. PhD-Thesis, Norwegian University of Science and Technology (NTNU), Trondheim, Norway

Breugel, K. van (2001): *Modelling of strength development in hardening concrete.* IPACS Report, Luleå University of Technology, ISBN: 91-89580-40-0, Sweden

Brooks, J. J. and A. M. Neville (1977): *A comparison of creep, elasticity and strength of concrete in tension and in compression.* Magazine of concrete research 29 (100) 131-141

Byfors, Jan (1980): *Plain Concrete at Early Ages.* CBI forskning/research 3:80, Swedish Cement and Concrete Research Institute, Stockholm, Sweden

Carette, Jérôme (2015): *Towards Early Age Characterisation of Eco-Concrete Containing Blast-Furnace Slag and Limestone Filler*. PhD-Thesis, Université Libre de Bruxelles (ULB), Bruxelles, Belgium

Case, R.J., K. Duan and T.G. Suntharavadivel (2013): *Effects of fly ash on compressive strength of structural concrete*. From Materials to Structures: Advancement through Innovation. Taylor & Francis Group, ISBN: 978-0-415-63318-5, London

CEB-FIP (1991): *CEB-FIP Model Code 1990: Design code*. CEB Bulletin No.203. Comité Euro-International du Béton, ISBN: 0727716964, 9780727716965, Lausanne, Switserland

Chengju, Guo (1989): *Maturity of Concrete: Method for Predicting Early-Stage Strength.* ACI Materials Journal no. 86 (1989) 341-353

COIN (2007-2014): *Concrete Innovation Centre - a centre for research based innovation.* www.coinweb.no, Established by the Research Counsil of Norway, Norway

Concreep 10 (2015): *Proceedings of the 10th International Conference on Mechanics and Physics of Creep, Shrinkage and Durability of Concrete and Concrete Structures*, C. Hellmich, B. Pichler and J. Kollegger, Vienna University of Technology, Austria

Czerny, F., K. van Breugel and E.A.B. Koenders (2005): *The reliability of crack predictions for hardening concrete structures*. 2005 International Congress - Global Construction: Ultimate Concrete Opportunities. Dundee, Scotland.

Darquennes, A., S. Staquet, M.P Delplancke-Ogletree and B. Espion (2011): *Effect of autogenous deformation on the crack risk of slag cement concretes.* Cement & Concrete Composites 33 (2011) 368-379

De Schutter, G. and L. Taerwe (1995): *General hydration model for Portland cement and blast furnace slag cement.* Cement and Concrete Research 25 (1995) 593-604

De Schutter, G. and L. Taerwe (1996): *Degree of hydration-based description of mechanical properties of early age concrete.* Materials and Structures 29 (1996) 335-344

De Schutter, G. (2004): *Applicability of degree of hydration concept and maturity method for thermo-visco-elastic behaviour of early age concrete.* Cement & Concrete Composites 26 (2004) 437-443

De Weerdt, K., M. Ben Haha, G. Le Saout, K. O. Kjellsen, H. Justnes and B. Lothenbach (2012): *The effect of temperature on the hydration of composite cements containing limestone powder an fly ash.* Materials and Structures 45 (2012) 1101-1114

Emborg, Mats (1989): *Thermal stresses in concrete structures at early ages*. PhD-Thesis, Luleå University of Technology, Sweden

Emborg, Mats (1998): *Development of Mechanical Behaviour at Early Ages*. Prevention of Thermal Cracking in Concrete at Early Ages. R. Springenschmid. ISBN: 0 419 22310 X, Technical University of Munich, Germany

Freiesleben Hansen, P. and E. J. Pedersen (1977): *Maturity computer for controlled curing and hardening of concrete (in Danish: Måleinstrument til kontrol af betons hærdning).* Nordisk Betong 1 (1977) 21-25

Freiesleben Hansen, P. (1978): *Curing technology - 1, Portlandcement (in Danish: Hærdeteknologi - 1, Portlandcement).* BFK-centralen, Lyngby, Denmark

Freiesleben Hansen, Per and Erik Jørgen Pedersen (1982): *Winter concreting (in Dansih: Vinterstøbning af beton. 1982.).* SBI Instruction 125. Danish Building Research Institute and Teknologisk Institutt, ISBN: 87-563-0445-5, Glostrup, Denmark

GmbH, JULABO (2013): *Operating Manual. Refrigerated/Heating Circulators. Julabo FP45.* JULABO GmbH, Seelbach, Germany

Grondin, F., M. Bouasker, P. Mounanga, A. Khelidj and A. Perronnet (2010): *Physico-chemical deformations of solidifying cementitious systems: multiscale modelling.* Materials and Structures 43 (2010) 151-165

Gutsch, Alexander-W. (2001): *Viscoelastic behaciour of Early Age Concrete.* IPACS Report, Luleå University of Technology, ISBN: 91-89580-38, Sweden

Hagihara, S, S Nakamura, Y Masuda, T Uenishi, T Okihashi and M Kono (2000): *Mechanical properties and creep behavior of high-strength concrete in early age*. In the Proceedings of the international workshop, Sendai Japan [Quoted by Ji (2008)]

Han, Sang-Hun, Jin-Keun Kim and Yon-Dong Park (2003): *Prediction of compressive strength of fly ash concrete by new apparent activation energy function.* Cement and Concrete Research 33 (2003) 965-971

Hedlund, Hans (1996): *Stresses in High Performance Concrete due to Temperature and Moisture Variations at Early Ages*. Licentiate Thesis, Luleå University of Technology, ISBN, Sweden

Hedlund, Hans (2000): *Hardening Concrete, Measurements and evaluation of non-elastic deformation and associated restraint stresses*. PhD-Thesis, ISBN: 91-89580-00-1, Luleå University of Technology, Sweden

Hedlund, Hans and Jan Olofsson (2001a): *Restraint Analyses and Simplifications, Typical Structure - Wall-on-Wall.* IPACS report, Luleå University of Technology, ISBN: 91 - 89580 - 67 - 2, Sweden

Hedlund, Hans and Jan-Erik Jonasson (2001b): *Temperature effect on autogenous deformation. Measurements and modelling of thermal and moisture related deformation and stress.* IPACS report, TU Luleå, ISBN: 91 - 89580 - 10 - 9, Sweden

Herholdt, Aage D., Chr. F. P. Justesen, Palle Nepper-Christensen and Anders Nielsen (1979): *Beton-Bogen*. Aalborg Portland, ISBN: 87-980816-0-8, Denmark

Houk, Ivan E., Orville E. Borge and Donald L. Houghton (1969): *Studies of Autogenous Volume Change in Concrete for Dworshak Dam.* Journal of Amer. Concr. Inst. (66) 560-568

Illston, J. M. (1965): *The creep of concrete under uniaxial tension.* Magazine of concrete research 17 (1965) 77-84

JCI, (Japan Concrete Institute) (1998): *Autogenous shrinkage of concrete: Proceedings of the international workshop organised by JCI (Japan Concrete Institute), Hiroshima, June 13-*

14, 1998, E.-i. Tazawa and N. K. K. Kyokai, E. & F.N. Spon ISBN: 0419238905, Hiroshima, Japan

JEJMS Concrete AB (2009-2012): *CrackTeSt COIN*. Luleå, Sweden.

Jensen, O. Mejlhede and P. Freiseleben Hansen (1995): *A dilatometer for measuring autogenous deformation in hardening Portland cement paste.* Materials and Structures 28 (1995) 406-409

Jensen, O. Mejlhede and P. Freiesleben Hansen (1996): *Autogenous Deformation and Change of the Relative Humidity in Silica Fume-Modified Cement Paste.* ACI Materials Journal no. 93 (6) (1996) 539-543

Jensen, Ole Mejlhede and Per Freiesleben Hansen (1999): *Influence of temperature on autogenous deformation and relative humidity change in hardening cement paste.* Cement and Concrete Research 29 (1999) 567-575

Ji, G. M., T. Kanstad, Ø. Bjøntegaard and E. J. Sellevold (2012): *Tensile and compressive creep deformations of hardening concrete containing mineral additives.* Materials and Structures 46 (2012) 1167-1182

Ji, Guomin (2008): *Cracking Risk of Concrete Structures in The Hardening Phase*. PhD-Thesis, Norwegian University of Science and Technology (NTNU), Trondheim, Norway

Jonasson, Jan-Erik (1994): *Modelling of Temperature, Moisture and Stresses in Young Concrete*. PhD-Thesis, Luleå University of Technology, Sweden

Jonasson, Jan-Erik and Gustaf Westman (2001): *RELAX - Conversion of creep data to relaxation data by the program RELAX.* IPACS report, TU Luleå, ISBN: 91 - 89580 - 45 - 1, Sweden

Jonasson, Jan-Erik, Peter Fjellström and Henrik Bäckström (2010): *Inverkan av variabel härdningstemperatur på betongens hållfasthetsutvikling* (The influence of variable curing temperature on the strength development of concrete - only available in Swedish), Bygg & Teknik (7)

Jonasson, Jan-Erik, Mats Emborg and Hans Hedlund (2014): *Measurement and Modelling of Strength and Heat of Hyddration for Young Concrete*. Proceedings of the XXII Nordic Concrete Research Symposium (p. 501-504), Reykjavik, Iceland

Justnes, H., A. Van Gernert, F. Verbovent and E. 1. Sellevold (1996): *Total and external chemical shrinkage of low w/c ratio cement pastes.* Advances in Cement Research 8, No. 31 (1996) 121-126

Kanstad, Terje (1990): *Nonlinear analysis considering timedependent deformations and capacity of reinforced and prestressed concrete*. PhD-Thesis, Norwegian University of Science and Technology, Norway

Kanstad, Terje, Daniela Bosnjak and Jan Arve Øverli (2001a): *3D Restraint Analyses of Typical Structures with Early Age Cracking Problems.* IPACS report, Luleå University of Technology, ISBN: 91 - 89580 - 32 - X, Sweden

Kanstad, Terje, Tor Arne Hammer, Øyvind Bjøntegaard and Erik J. Sellevold (2001b): *Mechanical properties of early age concrete: Evaluation of test methods for tensile strength and modulus of elasticity. Determination of model parameters.* IPACS Report, Luleå University of Technology, ISBN: 91-89580-49-4, Sweden

Kanstad, Terje, Tor Arne Hammer, Øyvind Bjøntegaard and Erik J. Sellevold (2003a): *Mechanical properties of young concrete: Part I: Experimental results related to test methods and temperature effects.* Materials and Structures 36 (2002) 218-225

Kanstad, Terje, Tor Arne Hammer, Øyvind Bjøntegaard and Erik J. Sellevold (2003b): *Mechanical properties of young concrete: Part II: Determination of model parameters and test program proposals.* Materials and Structures 36 (2002) 226-230

Khan, Arshad A., William D. Cook and Denis Mitchell (1996): *Tensile Strength of Low-, Medium-, and High-Strength Concretes at Early Ages.* ACI Materials Journal 93 (5) (1996) 487-493

Kim, Gyu-Yong, Eui-Bae Lee, Jeong-Soo Nam and Kyung-Mo Koo (2011): *Analysis of hydration heat and autogenous shrinkage of high-strength mass concrete.* Magazine of concrete research 63 (2011) 377-389

Kim, Jin-Keun, Sang Hun Han and Young Chul Song (2002): *Effect of temperature and aging on the mechanical properties of concrete Part I. Experimental results.* Cement and Concrete Research 32 (2002) 1087-1094

Kjellmark, Gunrid (2015): *Mechanical testing COIN P3.1-series, new cement batches.* COIN Project Report - draft, SINTEF Building and infrastructure, Trondheim, Norway

Kjellmark, Gunrid and Anja Estensen Klausen (2015): *Mechanical properties and calculation of model parameters for concrete with NORCEM cement and variable fly ash content.* COIN Project Report (55), SINTEF Building and infrastructure, Trondheim, Norway

Klausen, Anja Estensen (2013): *The Temperature-Stress Testing Machine - User Manual.* Norwegian University of Science and Technology (NTNU), Trondheim, Norway

Klausen, Anja Estensen, Terje Kanstad and Øyvind Bjøntegaard (2015): *Updated Temperature-Stress Testing Machine (TSTM): Introductory tests, calculations, verification and investigation of variable fly ash content*. Proceedings of CONCREEP 10, Vienna, Switzerland

Koenders, E.A.B. (1997): *Simulation of volume changes in hardening cement-based materials*. PhD-Thesis, ISBN: 90-407-1499-1, Delft University of Technology, Netherlands

Kuder, Katherine, Dawn Lehman, Jeffrey Berman, Gudmundur Hannesson and Rod Shogren (2012): *Mechanical properties of self consolidating concrete blended with high volumes of fly ash and slag*. Construction and Building Materials 34 (2012) 285-295

Larson, Mårten (2001): *Restraint from adjoining structures. Empirical, Analytical and Numerical Evaluation of Restraint Coefficients.* IPACS Reports, Luleå University of Technology, ISBN: 91 - 89580 - 57 - 5, Sweden

Lee, H. K., K. M. Lee and B. G. Kim (2003): *Autogenous shrinkage of high-performance concrete containing fly ash.* Magazine of concrete research 55 (2003) 507-515

Loser, Roman, Beat Münch and Pietro Lura (2010): *A volumetric technique for measuring the coefficient of thermal expansion of hardening cement paste and mortar.* Cement and Concrete Research 40 (2010) 1138-1147

Lura, Pietro (2003): *Autogenous Deformation and Internal Curing of Concrete*. PhD-Thesis, ISBN: 90-407-2404-0, Delft University of Technology, Netherlands

Lura, Pietro, Ole Mejlhede Jensen and Klaas von Breugel (2003): *Autogenous shrinkage in high-performance cement paste: An evaluation of basic mechanisms.* Cement and Concrete Research 33 (2003) 223-232

Lura, Pietro, Jon Couch, Ole Mejlhede Jensen and Jason Weiss (2009): *Early-age acoustic emission measurements in hydrating cement paste: Evidence for cavitation during solidification due to self-desiccation.* Cement and Concrete Research 39 (2009) 861-867

Lynam, C. G., O.B.E and M.C. (1934): *Growth and movement on Portland cement concrete*. Oxford University Press, ISBN, London, England

Löfquist, Bertil (1946): *Temperatureffekter i hårdnande betong (in English: Temperature effects in hardening concrete)*. PhD-Thesis, Chalmers tekniska høgskola, Kungl. Vattenfallsstyrelsen, Stockholm, Sweden

Maruyama, I. and A. Teramoto (2011): *Impact of time-dependant thermal expansion coefficient on the early-age volume changes in cement pastes.* Cement and Concrete Research 41 (2011) 380-391

Microsoft Office (2010): *Microsoft Excel*. Version: 14.0.6123.5001.

Morabito, P. (1998): *Methods to Determine the Heat of Hydration of Concrete*. Prevention of Thermal Cracking in Concrete at Early Ages. R. Springenschmid. ISBN: 0 419 22310 X, Technical University of Munich, Germany

Munch-Petersen, Gitte Normann and Christian Munch-Petersen (2014): *Early property development in concrete*. Proceedings of the XXII Nordic Concrete Research Symposium (p. 245-248), Reykjavik, Iceland

Möller, Göran, Nils Peterson and Paul Samuelsson (1982): *Betong-handbok*. AB Svensk Byggtjänst, ISBN: 91-7332-060-9, Stockholm, Sweden

Neville, A. M. (1970): *Creep of Concrete: Plain, Reinforced and Prestressed.* North-Holland publishing company, ISBN, University of Leeds, England

Neville, A. M. (1972): *Properties of Concrete*. Pitman Publishing Corporation, ISBN: 0 273 36150 3, New York, USA

Nilsson, Martin (2003): *Restraint Factors and Partial Coefficients for Crack Risk Analyses of Early Age Concrete Structures*. PhD-Thesis, ISBN: 91-89580-05-5, Luleå University of Technology, Sweden

NPRA, The Norwegian Public Roads Administration (2009): *Handbook R762E. General Specifications 2. Standard specification texts for bridges and quays*. Principal specification 8. Oslo.

NS-EN 197-1:2011: *Cement - Part 1: Composition, specifications and conformity criteria for common cements.* Standards Norway, Norway

NS-EN 206:2013+NA:2014: *Concrete - Specification, performance, production and conformity.* Standards Norway, Norway

NS 3657:1993: *Concrete testing - Determination of heat release.* Standards Norway, Norway

NS 3676:1987: *Concrete testing - Hardened concrete - Modules of elasticity in compression.* Standards Norway, Norway

Onken, P. and F. Rostasy (1995): *Effective concrete tensile strength in structures exposed to early restrained thermal loading.* Deutscher Auschuss für Stahlbeton, book 449, 1-93 (only avaiable in German), Germany

Orosz, Katalin, Peter Fjellström, Jan-Erik Jonasson, Mats Emborg and Hans Hedlund (2014): *Evaluation of thermal dilation and autogenous shrinkage at sealed conditions*. Proceedings of the XXII Nordic Concrete Research Symposium. Reykjavik, Iceland**:** 299-302.

Pane, Ivindra and Will Hansen (2008): *Investigation on key properties controlling early-age stress development of blended cement concrete.* Cement and Concrete Research 38 (2008) 1325

Pathak, Neelam and Rafat Siddique (2012): *Properties of self-compacting-concrete containing fly ash subjected to elevated temperatures.* Construction and Building Materials 30 (2012) 274-280

Pedersen, E. J. (1994): *Appendix 1. Curing of concrete structures*. Durable Concrete Structures: Design Guide (2nd Edition). C. E.-I. D. Béton. ISBN: 9780727739544**:** 86-104,

Radocea, Adrian (1992): *A study on the mechanism of plastic shrinkage of cement-based materials*. PhD-Thesis, Chalmers University of Technology, Göteborg, Sweden

Rastrup, Erik (1954): *Heat of hydration in concrete.* Magazine of concrete research 6 (17) 79-92

RILEM (1998): *State-of-the-Art Report: Prevention of Thermal Cracking in Concrete at Early Ages.* RILEM, Technical Committee 119, Technical University of Munich, ISBN: 0 419 22310 X, Germany

RILEM (2000): *International RILEM Workshop on Shrinkage of Concrete (Shrinkage 2000)*, V. Baroghel-Bouny and P.-C. Aïtcin, (586), ISBN: 2-912143-20-9, Paris, France

RILEM (2001): *EAC'01: International RILEM Conference on Early Age Cracking in Cementitious Systems*, K. Kovler and A. Bentur, ISBN: 2-912143-29-2, Haifa, Israel

RILEM (2002): *Early Age Cracking in Cementitious Systems*. RILEM Technical Comittee 181-EAS. A. Bentur. Bagneux, France.

RILEM (2003): *Early Age Cracking in Cementitious Systems.* RILEM, Technical Committee 181, ISBN: 2-912143-33-0,

RILEM (2006): *International RILEM Conference on Volume Changes of Hardening Concrete: Testing and Mitigation 20-23. August 2006*, P. L. a. K. K. O. M. Jensen, ISBN: 2-35158-004-4,Technical University of Denmark, Lyngby, Denmark

RILEM, Technical Committee 119 (1994): *Proceedings of the International RILEM Symposium: Thermal Cracking in Concrete at Early Ages.*, R. Springenschmid, ISBN: 0 419 18710 3, Technical University of Munich, Germany

Saul, A. G. A. (1951): *Principles underlying the steam curing of concrete at atmospheric pressure.* Magazine of concrete research Vol.2(6) (1951) 127-140

Sellevold, Erik, D.H. Bager, E. Klitgaard Jensen and T. Knudsen (1982): *Silica Fume Cement Paste - Hydration and Pore Structure*. Condensed Silica Fume in Concrete. O. E. Gjørv and K. E. Løland. ISBN, Division of Building Materials, Norwegian University of Science and Technology, Trondheim, Norway

Sellevold, Erik J. and et al. (1988): *Condensed Silica Fume in Concrete. FIP State of the Art Report.* Thomas Telford, ISBN: ISBN: 0 7277 1373 6, London, UK

Sellevold, Erik J. and Christine J. Hauck (1997): *Effect of curing temperature and silica fume on the pore structure of hardened cement paste.* Report TVBM-3078, Lund Insitute of Technology, Lund, Sweden

Sellevold, Erik J. and Øyvind Bjøntegaard (2006): *Coefficient of thermal expansion of cement paste and concrete: Mechanisms of moisture interaction.* Materials and Structures 39 (2006) 809-815

Sennour, Mohand L. and Ramon L. Carrasquillo (1989): *Creep and shrinkage properties in concrete containing fly ash.* The University of Texas at Austin, FHWA/TX-90+481-6, Austin, Texas

Shkoukani, Hisham and Joost Walraven (1991): *Sustained tensile strength of concrete.* IABSE reports = Rapports AIPC = IVBH Berichte 62 (1991) 725-729

Shoukry, Samir N., Gergis W. William, Brian Downie and Mourad Y. Riad (2011): *Effect of moisture and temperature on the mechanical properties of concrete.* Construction and Building Materials 25 (2011) 688-696

Smeplass, Sverre (1988): *Kalor - programdokumentasjon (In English: Kalor - program documentation).* SINTEF-report STF65 A88031, ISBN: 82-595-5096-2, Trondheim, Norway

Smeplass, Sverre (2001): *Herdekassen - bestemmelse av avkjølingstallet (in English: Curing box - determination of the cooling factor).* Nor-IPACS, Trondheim, Norway

Springenschmid, R., R. Breitenbücher and M. Mangold (1994): *Development of the cracking frame and the temperature-stress testing machine*. Thermal Cracking in Concrete at Early Ages, International Symposium held by RILEM. Munich. Proceedings 25.

Springenschmid, R. (1998): *Prevention of Thermal Cracking in Concrete at Early Ages - Preface.* RILEM Report 15, Great Britain, London

Staquet, S. and B. Espion (2005): *Deviations from the Principle of Superposition and their Consequenses on Structural Behaviour.* ACI Spring Convention: Shrinkage and Creep of Concrete 2005. N. J. Gardner and W. J. Weiss. New York, USA, American concrete institute**:** p. 67-83.

Takacs, Peter F. (2002): *Deformations in Concrete Cantilever Bridges: Observations and Theoretical Modelling*. PhD-Thesis, ISBN: 82-471-5415-3, Norwegian University of Science and Technology (NTNU), Norway

Termkhajornkit, Pipat, Toyoharu Nawa, Masashi Nakai and Toshiki Saito (2005): *Effect of fly ash on autogenous shrinkage.* Cement and Concrete Research 35 (2005) 473-482

TNO DIANA $_{BV}$ (2010): *DIANA*. Delft, The Netherlands. Manual -- Release 9.4.4.

Wang, Yuan-Feng, Yi-Shuo Ma and Lang Zhou (2011): *Creep of FRP-wrapped concrete columns with or without fly ash under axial load.* Construction and Building Materials 25 (2011) 697-704

Westman, Gustaf (1995): *Thermal Cracking in High Performance Concrete, Vicoelastic models and laboratory tests.* Licentiate Thesis, Luleå University of Technology, Sweden

Westman, Gustaf (1999): *Concrete Creep and Thermal Stresses, New Creep Models and their Effects on Stress Development*. PhD-Thesis, Luleå University of Technology, Sweden

Wyrzykowski, Mateusz and Pietro Lura (2013): *Moisture dependence of thermal expansion in cement-based materials at early ages.* Cement and Concrete Research 53 (2013) 25-35

Yoshitake, Isamu, Farshad Rajabipour, Yoichi Mimura and Andrew Scanlon (2012): *A prediction method of tensile Young's modulus of concrete at early ages.* Advances in Civil Engineering 2012 (Articel ID 391214) 10 pages

Yoshitake, Isamu, Wenbo Zhang, Yoichi Mimurac and Tadashi Saito (2013): *Uniaxial tensile strength and tensile Young's modulus of fly-ash concrete at early age.* Construction and Building Materials 40 (2013) 514-521

Yoshitake, Isamu, Howe Wong, Takeo Ishida and Ayman Y. Nassif (2014): *Thermal stress of high volume fly-ash (HVFA) concrete made with limestone aggregate.* Construction and Building Materials 71 (2014) 216-225

Appendix A: Cement composition

The cement compositions of the various cement batches used during the current work are given in the following:

EG1-10 (ANL) and TF3-11 (ANL FA)

EG1-10 (ANL) and TF3-11 (ANL FA) were the originally used cement batches. Their compositions are given in Table A.1. These cement batches were used during the semi-adiabatic calorimetry tests from which the heat developments were determined, and they were also used for the test series on mechanical properties under 20 ^{o}C isothermal curing conditions as presented in Chapter 7.4. In addition, most *ANL Ref.* TSTM tests were performed with EG1-10.

EG1-14 (ANL) and TF5-14 (ANL FA)

As EG1-10 and TF3-11 run out, they were replaced with EG1-14 and TF5-14, respectively. The cement composition of EG1-14 and TF5-14 are described in Table A.2. The latter cement batches were used for additional mechanical tests that investigated the effect of curing temperature (Chapter 7.6), the creep tests (Chapter 7.7) and all TSTM tests performed with the fly ash concretes (Chapter 8).

EG1-12 (ANL) and TZ1-12 (ANL FA)

EG1-12 and TZ1-12 were used at NORCEM when performing compressive strength tests for determination of activation energy (with exception from the fly ash concrete *ANL FA +28FA*, where TF5-14 was used). The cement compositions of EG1-12 and TZ1-12 are described in Table A.3.

Table A.1; Cement analyses for EG1-10 and TF3-11

Physical properties	**EG1-10 (ANL) CEM I 52,5 LA**	**TF3-11 (ANL FA) CEM II / A-V 42,5N**
1-day strength	18.6 MPa	12.1 MPa
2-day strength	29.7 MPa	21.5 MPa
7-day strength	46.6 MPa	33.7 MPa
28-day strength	56.0 MPa	-
Setting time	145 min	195 min
Fineness	382 m^2/kg	370 m^2/kg
+90my	0.5 %	0.07%
+64	1.7 %	1.34%
-24	74 %	75.4%
-30	82.6 %	83.3%
Specific weight	3160 kg/m^3	2980 kg/m^3
Fly ash	-	18.7 %
Loss on ignition (LOI)	2.02 %	1.30 %
Chemical composition		
SO3	3.45 %	2.75 %
SiO2	19.99 %	27.04 %
Al2O3	4.76 %	8.68 %
Fe2O3	3.72 %	4.60 %
CaO	62.90 %	52.73 %
MgO	1.99 %	1.94 %
P2O5	0.13 %	0.25 %
K2O	0.45 %	0.72 %
Na2O	0.30 %	0.42 %
Tot. Alkali (Na2O-ekv)	0.60 %	0.90 %
Cl-	0.024 %	0.024 %

Table A.2; Cement analyses for EG1-14 and TF5-14

Physical properties	**EG1-14 (ANL) CEM I 52,5 LA**	**TF5-14 (ANL FA) CEM II/A-V 42,5N**
1-day strength	20.9 MPa	15.9 MPa
2-day strength	32.4 MPa	25.5 MPa
7-day strength	52.5 MPa	40.7 MPa
28-day strength	64.1 MPa	58.6 MPa
Setting time	142 min	168 min
Fineness	421 m^2/kg	389 m^2/kg
+90my	0.0 %	0.5 %
+64	0.6 %	3.3 %
-24	75 %	67.4 %
-30	83.8 %	76.3 %
Specific weight	3160 kg/m^3	2980 kg/m^3
Fly ash	-	16.6 %
Loss on ignition (LOI)	2.31 %	1.03 %
Chemical composition		
SO3	3.40 %	2.71 %
SiO2	20.35 %	26.70 %
Al2O3	4.64 %	7.87 %
Fe2O3	3.51 %	4.53 %
CaO	62.97 %	53.37 %
MgO	1.63 %	1.71 %
P2O5	0.08 %	0.16 %
K2O	0.43 %	0.70 %
Na2O	0.32 %	0.43 %
Tot. Alkali (Na2O-ekv)	0.60 %	0.90 %
Cl-	-	0.024 %

Table A.3; Cement analyses for EG1-12 and TZ1-12

Physical properties	**EG1-12 (ANL)** **CEM I 52,5 LA**	**TZ1-12 (ANL FA)** **CEM II / A-V 42,5N**
1-day strength	19.8 MPa	16.4 MPa
2-day strength	32.3 MPa	25.6 MPa
7-day strength	48.3 MPa	40.2 MPa
28-day strength	63.2 MPa	56.4 MPa
Setting time	125 min	150 min
Fineness	396 m^2/kg	404 m^2/kg
+90my	0.0 %	2.3 %
+64	1.0 %	4.1 %
-24	74.1 %	71.2 %
-30	82.6 %	79.3 %
Specific weight	3160 kg/m^3	2980 kg/m^3
Fly ash	-	17.8 %
Loss on ignition (LOI)	2.15 %	1.13 %
Chemical composition		
SO3	3.25 %	2.57 %
SiO2	20.61 %	26.57 %
Al2O3	4.40 %	8.70 %
Fe2O3	3.53 %	4.42 %
CaO	63.24 %	53.55 %
MgO	1.73 %	1.71 %
P2O5	0.15 %	0.33 %
K2O	0.45 %	0.64 %
Na2O	0.32 %	0.33 %
Tot. Alkali (Na2O-ekv)	0.62 %	0.75 %
Cl-	0.030 %	0.024 %

Appendix B: Tabulated heat development

Semi-adiabatic calorimeter tests were performed to determine the hydration heat evolvement of the concretes for each of the two cement batches ANL and ANL FA. Since extra FA was added in three concretes in combination with ANL FA, this multiple testing involved all concretes (except the later added *ANL FA +28FA*).

A tabulated version of the isothermal heat development when using cement batch EG1-10 and TF3-11 is given in Table B.1. Corresponding results when using cement batch EG1-14 and TF5-14 is shown in Table B.2.

Table B.1; Resulting heat polygon when using cement batch EG1-10 and TF3-11

ANL Ref.		***ANL FA***		***ANL FA +8FA***		***ANL FA +16FA***	
[mh]	[kJ/kg cem]	[mh]	[kJ/kg cem]	[mh]	[kJ/kg cem]	[mh]	[kJ/kg cem]
0.0	0	0.0	0	0.0	0	0.0	0
4.2	5	5.6	5	8.8	10	8.4	5
5.9	10	7.6	10	10.5	20	11.5	20
7.6	20	9.3	20	11.7	30	13.0	30
9.4	40	10.5	30	12.9	40	14.4	40
10.8	60	11.6	40	14.1	50	15.8	50
12.2	80	13.5	60	15.2	60	17.2	60
13.6	100	15.5	80	17.3	80	19.8	80
14.9	120	17.3	100	18.5	90	21.4	90
16.4	140	19.6	120	19.7	100	23.9	100
18.5	160	23.2	140	23.5	120	27.3	110
21.5	180	29.2	160	30.2	140	31.7	120
25.7	200	38.8	180	40.5	160	44.4	140
32.6	220	52.2	200	55.4	180	62.1	160
42.7	240	60.3	210	73.6	200	85.3	180
56.2	260	69.5	220	96.4	220	113.1	200
74.3	280	91.8	240	134.3	240	149.3	220
102.8	300	135.0	260	163.3	250	176.2	230
156.9	320	270.5	278	207.8	260	211.5	240
287.0	340			298.5	270	262.8	250

Table B.2; Resulting heat polygon when using cement batch EG1-14 and TF5-14

ANL Ref.		***ANL FA***		***ANL FA +8FA***		***ANL FA +16FA***		***ANL FA +28FA***	
[mh]	[kJ/kg cem]	[mh]	[kJ/kg cem]	[mh]	[kJ/kg cem]	[mh]	[kJ/kg cem]	[mh]	[kJ/kg cem]
0.0	0	0.0	0	0.0	0	0.0	0	0.0	0
4.5	5	1.8	5	4.5	5	3.3	5	5.6	5
5.7	10	5.2	10	6.4	10	5.7	10	7.0	10
7.0	20	7.0	20	8.1	20	7.5	20	8.6	20
8.8	40	9.0	40	10.2	40	9.9	40	11.5	40
10.1	60	10.5	60	12.0	60	12.0	60	14.2	60
11.5	80	12.1	80	13.7	80	14.1	80	16.8	80
12.9	100	13.5	100	15.3	100	16.1	100	21.4	100
14.5	120	14.9	120	17.3	120	19.3	120	30.1	120
16.1	140	16.7	140	20.6	140	24.8	140	42.9	140
18.0	160	19.4	160	25.4	160	33.2	160	62.0	160
20.4	180	23.3	180	32.4	180	45.0	180	86.9	180
23.8	200	29.0	200	42.1	200	61.2	200	114.9	200
28.8	220	37.2	220	54.2	220	79.5	220	162.6	220
36.7	240	47.9	240	68.7	240	106.1	240	207.1	230
47.2	260	60.2	260	89.8	260	130.3	250	264.1	238
71.7	290	97.9	290	108.6	270	168.0	260	327.0	243
103.0	305	210.4	310	139.6	280	195.5	265		
145.3	312	306.5	315	192.6	290	261.2	272		
213.8	316			253.8	296	487.9	282		

Appendix C: Compressive strength results (NORCEM)

For all concretes, NORCEM performed compressive strength tests over time on cubes stored under isothermal conditions at 5 °C, 20 °C and 35 °C, respectively. The four concretes *ANL Ref.*, *ANL FA*, *ANL FA +8FA* and *ANL FA +16FA* were tested in 2013, while the later added concrete *ANL FA +28FA* was tested in 2015 with a different batch of ANL FA cement. The compressive test results for *ANL Ref.*, *ANL FA*, *ANL FA +8FA* and *ANL FA +16FA* are given in Table C.1, Table C.2, Table C.3 and Table C.4, respectively.

Table C.1; Cement analyses for EG1-14 and TF5-14

ANL Ref.					
5 °C		**20 °C**		**35 °C**	
Age [d]	[MPa]	Age [d]	[MPa]	Age [d]	[MPa]
1	3.7	0.5	6.3	0.25	6.3
1.5	10.4	0.67	11.1	0.33	13
2	18.9	1	25.2	0.5	26.4
3	32.1	2	41	0.67	32.2
4	41.2	3	52.2	1	40.2
5	48.6	7	65.1	2	50.3
7	56.8	28	84.8	4	61.7
28	70.7	90	89.4	28	72.3
		364	92.9		

Table C.2; Cement analyses for EG1-14 and TF5-14

ANL FA					
5 °C		**20 °C**		**35 °C**	
Age [d]	[MPa]	Age [d]	[MPa]	Age [d]	[MPa]
1	4.4	0.5	6.6	0.25	7.2
1.5	12	0.67	14.9	0.33	15.4
2	18.3	1	23.6	0.5	21.2
4	34.8	2	36.6	0.67	25.5
5	36.5	3	43.1	1	32.6
7	48.1	7	51	2	42.3
28	66.7	28	79.3	4	56.1
		90	94.2	28	81.4
		364	98.2		

Table C.3; Cement analyses for EG1-14 and TF5-14

ANL FA +8FA					
5 °C		**20 °C**		**35 °C**	
Age [d]	[MPa]	Age [d]	[MPa]	Age [d]	[MPa]
1	2.9	0.5	5.6	0.25	4.2
1.5	9	0.67	12.5	0.33	12.8
2	14.5	1	20.3	0.5	19.8
3	21.6	2	32.3	0.67	24.7
4	29.3	3	38.5	1	29.6
5	35.2	7	49.6	2	38.3
7	38.7	28	78.9	4	55.2
28	61.3	90	95.6	28	80.3
		364	100.3		

Table C.4; Cement analyses for EG1-14 and TF5-14

ANL FA +16FA					
5 °C		**20 °C**		**35 °C**	
Age [d]	[MPa]	Age [d]	[MPa]	Age [d]	[MPa]
1	2.1	0.5	3.8	0.25	3
1.5	7	0.67	7.6	0.33	8.8
2	10.8	1	15.5	0.5	15.7
3	18.3	2	25	0.67	18.7
4	21.7	3	30.7	1	23
5	26.7	7	40.4	2	32.6
7	31.9	28	66.9	4	46
28	47.7	90	83	28	77.4
		364	94.1		

DEPARTMENT OF STRUCTURAL ENGINEERING
NORWEGIAN UNIVERSITY OF SCIENCE AND TECHNOLOGY

N–7491 TRONDHEIM, NORWAY
Telephone: +47 73 59 47 00 Telefax: +47 73 59 47 01

"Reliability Analysis of Structural Systems using Nonlinear Finite Element Methods",
C. A. Holm, 1990:23, ISBN 82-7119-178-0.

"Uniform Stratified Flow Interaction with a Submerged Horizontal Cylinder",
Ø. Arntsen, 1990:32, ISBN 82-7119-188-8.

"Large Displacement Analysis of Flexible and Rigid Systems Considering Displacement-Dependent Loads and Nonlinear Constraints",
K. M. Mathisen, 1990:33, ISBN 82-7119-189-6.

"Solid Mechanics and Material Models including Large Deformations",
E. Levold, 1990:56, ISBN 82-7119-214-0, ISSN 0802-3271.

"Inelastic Deformation Capacity of Flexurally-Loaded Aluminium Alloy Structures",
T. Welo, 1990:62, ISBN 82-7119-220-5, ISSN 0802-3271.

"Visualization of Results from Mechanical Engineering Analysis",
K. Aamnes, 1990:63, ISBN 82-7119-221-3, ISSN 0802-3271.

"Object-Oriented Product Modeling for Structural Design",
S. I. Dale, 1991:6, ISBN 82-7119-258-2, ISSN 0802-3271.

"Parallel Techniques for Solving Finite Element Problems on Transputer Networks",
T. H. Hansen, 1991:19, ISBN 82-7119-273-6, ISSN 0802-3271.

"Statistical Description and Estimation of Ocean Drift Ice Environments",
R. Korsnes, 1991:24, ISBN 82-7119-278-7, ISSN 0802-3271.

“Properties of concrete related to fatigue damage: with emphasis on high strength concrete”,
G. Petkovic, 1991:35, ISBN 82-7119-290-6, ISSN 0802-3271.

"Turbidity Current Modelling",
B. Brørs, 1991:38, ISBN 82-7119-293-0, ISSN 0802-3271.

"Zero-Slump Concrete: Rheology, Degree of Compaction and Strength. Effects of Fillers as Part Cement-Replacement",
C. Sørensen, 1992:8, ISBN 82-7119-357-0, ISSN 0802-3271.

"Nonlinear Analysis of Reinforced Concrete Structures Exposed to Transient Loading",
K. V. Høiseth, 1992:15, ISBN 82-7119-364-3, ISSN 0802-3271.

"Finite Element Formulations and Solution Algorithms for Buckling and Collapse Analysis of Thin Shells",
R. O. Bjærum, 1992:30, ISBN 82-7119-380-5, ISSN 0802-3271.

"Response Statistics of Nonlinear Dynamic Systems",
J. M. Johnsen, 1992:42, ISBN 82-7119-393-7, ISSN 0802-3271.

"Digital Models in Engineering. A Study on why and how engineers build and operate digital models for decisison support",
J. Høyte, 1992:75, ISBN 82-7119-429-1, ISSN 0802-3271.

"Sparse Solution of Finite Element Equations",
A. C. Damhaug, 1992:76, ISBN 82-7119-430-5, ISSN 0802-3271.

"Some Aspects of Floating Ice Related to Sea Surface Operations in the Barents Sea",
S. Løset, 1992:95, ISBN 82-7119-452-6, ISSN 0802-3271.

"Modelling of Cyclic Plasticity with Application to Steel and Aluminium Structures",
O. S. Hopperstad, 1993:7, ISBN 82-7119-461-5, ISSN 0802-3271.

"The Free Formulation: Linear Theory and Extensions with Applications to Tetrahedral Elements
with Rotational Freedoms",
G. Skeie, 1993:17, ISBN 82-7119-472-0, ISSN 0802-3271.

"Høyfast betongs motstand mot piggdekkslitasje. Analyse av resultater fra prøving i Veisliter'n",
T. Tveter, 1993:62, ISBN 82-7119-522-0, ISSN 0802-3271.

"A Nonlinear Finite Element Based on Free Formulation Theory for Analysis of Sandwich Structures",
O. Aamlid, 1993:72, ISBN 82-7119-534-4, ISSN 0802-3271.

"The Effect of Curing Temperature and Silica Fume on Chloride Migration and Pore Structure of High Strength Concrete",
C. J. Hauck, 1993:90, ISBN 82-7119-553-0, ISSN 0802-3271.

"Failure of Concrete under Compressive Strain Gradients",
G. Markeset, 1993:110, ISBN 82-7119-575-1, ISSN 0802-3271.

"An experimental study of internal tidal amphidromes in Vestfjorden",
J. H. Nilsen, 1994:39, ISBN 82-7119-640-5, ISSN 0802-3271.

"Structural analysis of oil wells with emphasis on conductor design",
H. Larsen, 1994:46, ISBN 82-7119-648-0, ISSN 0802-3271.

"Adaptive methods for non-linear finite element analysis of shell structures",
K. M. Okstad, 1994:66, ISBN 82-7119-670-7, ISSN 0802-3271.

"On constitutive modelling in nonlinear analysis of concrete structures",
O. Fyrileiv, 1994:115, ISBN 82-7119-725-8, ISSN 0802-3271.

"Fluctuating wind load and response of a line-like engineering structure with emphasis on motion-induced wind forces",
J. Bogunovic Jakobsen, 1995:62, ISBN 82-7119-809-2, ISSN 0802-3271.

"An experimental study of beam-columns subjected to combined torsion, bending and axial actions",
A. Aalberg, 1995:66, ISBN 82-7119-813-0, ISSN 0802-3271.

"Scaling and cracking in unsealed freeze/thaw testing of Portland cement and silica fume concretes",
S. Jacobsen, 1995:101, ISBN 82-7119-851-3, ISSN 0802-3271.

"Damping of water waves by submerged vegetation. A case study of laminaria hyperborea",
A. M. Dubi, 1995:108, ISBN 82-7119-859-9, ISSN 0802-3271.

"The dynamics of a slope current in the Barents Sea",
Sheng Li, 1995:109, ISBN 82-7119-860-2, ISSN 0802-3271.

"Modellering av delmaterialenes betydning for betongens konsistens",
Ernst Mørtsell, 1996:12, ISBN 82-7119-894-7, ISSN 0802-3271.

"Bending of thin-walled aluminium extrusions",
Birgit Søvik Opheim, 1996:60, ISBN 82-7119-947-1, ISSN 0802-3271.

"Material modelling of aluminium for crashworthiness analysis",
Torodd Berstad, 1996:89, ISBN 82-7119-980-3, ISSN 0802-3271.

"Estimation of structural parameters from response measurements on submerged floating tunnels",
Rolf Magne Larssen, 1996:119, ISBN 82-471-0014-2, ISSN 0802-3271.

“Numerical modelling of plain and reinforced concrete by damage mechanics”,
Mario A. Polanco-Loria, 1997:20, ISBN 82-471-0049-5, ISSN 0802-3271.

“Nonlinear random vibrations - numerical analysis by path integration methods”,
Vibeke Moe, 1997:26, ISBN 82-471-0056-8, ISSN 0802-3271.

“Numerical prediction of vortex-induced vibration by the finite element method”,
Joar Martin Dalheim, 1997:63, ISBN 82-471-0096-7, ISSN 0802-3271.

“Time domain calculations of buffeting response for wind sensitive structures”,
Ketil Aas-Jakobsen, 1997:148, ISBN 82-471-0189-0, ISSN 0802-3271.

"A numerical study of flow about fixed and flexibly mounted circular cylinders",
Trond Stokka Meling, 1998:48, ISBN 82-471-0244-7, ISSN 0802-3271.

“Estimation of chloride penetration into concrete bridges in coastal areas”,
Per Egil Steen, 1998:89, ISBN 82-471-0290-0, ISSN 0802-3271.

“Stress-resultant material models for reinforced concrete plates and shells”,
Jan Arve Øverli, 1998:95, ISBN 82-471-0297-8, ISSN 0802-3271.

“Chloride binding in concrete. Effect of surrounding environment and concrete composition”,
Claus Kenneth Larsen, 1998:101, ISBN 82-471-0337-0, ISSN 0802-3271.

“Rotational capacity of aluminium alloy beams”,
Lars A. Moen, 1999:1, ISBN 82-471-0365-6, ISSN 0802-3271.

“Stretch Bending of Aluminium Extrusions”,
Arild H. Clausen, 1999:29, ISBN 82-471-0396-6, ISSN 0802-3271.

“Aluminium and Steel Beams under Concentrated Loading”,
Tore Tryland, 1999:30, ISBN 82-471-0397-4, ISSN 0802-3271.

"Engineering Models of Elastoplasticity and Fracture for Aluminium Alloys",
Odd-Geir Lademo, 1999:39, ISBN 82-471-0406-7, ISSN 0802-3271.

"Kapasitet og duktilitet av dybelforbindelser i trekonstruksjoner",
Jan Siem, 1999:46, ISBN 82-471-0414-8, ISSN 0802-3271.

“Etablering av distribuert ingeniørarbeid; Teknologiske og organisatoriske erfaringer fra en norsk ingeniørbedrift”,
Lars Line, 1999:52, ISBN 82-471-0420-2, ISSN 0802-3271.

“Estimation of Earthquake-Induced Response”,
Símon Ólafsson, 1999:73, ISBN 82-471-0443-1, ISSN 0802-3271.

“Coastal Concrete Bridges: Moisture State, Chloride Permeability and Aging Effects”
Ragnhild Holen Relling, 1999:74, ISBN 82-471-0445-8, ISSN 0802-3271.

”Capacity Assessment of Titanium Pipes Subjected to Bending and External Pressure”,
Arve Bjørset, 1999:100, ISBN 82-471-0473-3, ISSN 0802-3271.

“Validation of Numerical Collapse Behaviour of Thin-Walled Corrugated Panels”,
Håvar Ilstad, 1999:101, ISBN 82-471-0474-1, ISSN 0802-3271.

“Strength and Ductility of Welded Structures in Aluminium Alloys”,
Miroslaw Matusiak, 1999:113, ISBN 82-471-0487-3, ISSN 0802-3271.

“Thermal Dilation and Autogenous Deformation as Driving Forces to Self-Induced Stresses in High Performance Concrete”,
Øyvind Bjøntegaard, 1999:121, ISBN 82-7984-002-8, ISSN 0802-3271.

“Some Aspects of Ski Base Sliding Friction and Ski Base Structure”,
Dag Anders Moldestad, 1999:137, ISBN 82-7984-019-2, ISSN 0802-3271.

"Electrode reactions and corrosion resistance for steel in mortar and concrete",
Roy Antonsen, 2000:10, ISBN 82-7984-030-3, ISSN 0802-3271.

"Hydro-Physical Conditions in Kelp Forests and the Effect on Wave Damping and Dune Erosion. A case study on Laminaria Hyperborea",
Stig Magnar Løvås, 2000:28, ISBN 82-7984-050-8, ISSN 0802-3271.

"Random Vibration and the Path Integral Method",
Christian Skaug, 2000:39, ISBN 82-7984-061-3, ISSN 0802-3271.

"Buckling and geometrical nonlinear beam-type analyses of timber structures",
Trond Even Eggen, 2000:56, ISBN 82-7984-081-8, ISSN 0802-3271.

”Structural Crashworthiness of Aluminium Foam-Based Components”,
Arve Grønsund Hanssen, 2000:76, ISBN 82-7984-102-4, ISSN 0809-103X.

“Measurements and simulations of the consolidation in first-year sea ice ridges, and some aspects of mechanical behaviour”,
Knut V. Høyland, 2000:94, ISBN 82-7984-121-0, ISSN 0809-103X.

”Kinematics in Regular and Irregular Waves based on a Lagrangian Formulation”,
Svein Helge Gjøsund, 2000-86, ISBN 82-7984-112-1, ISSN 0809-103X.

”Self-Induced Cracking Problems in Hardening Concrete Structures”,
Daniela Bosnjak, 2000-121, ISBN 82-7984-151-2, ISSN 0809-103X.

"Ballistic Penetration and Perforation of Steel Plates",
Tore Børvik, 2000:124, ISBN 82-7984-154-7, ISSN 0809-103X.

"Freeze-Thaw resistance of Concrete. Effect of: Curing Conditions, Moisture Exchange and Materials",
Terje Finnerup Rønning, 2001:14, ISBN 82-7984-165-2, ISSN 0809-103X

"Structural behaviour of post tensioned concrete structures. Flat slab. Slabs on ground",
Steinar Trygstad, 2001:52, ISBN 82-471-5314-9, ISSN 0809-103X.

"Slipforming of Vertical Concrete Structures. Friction between concrete and slipform panel",
Kjell Tore Fosså, 2001:61, ISBN 82-471-5325-4, ISSN 0809-103X.

"Some numerical methods for the simulation of laminar and turbulent incompressible flows",
Jens Holmen, 2002:6, ISBN 82-471-5396-3, ISSN 0809-103X.

“Improved Fatigue Performance of Threaded Drillstring Connections by Cold Rolling”,
Steinar Kristoffersen, 2002:11, ISBN: 82-421-5402-1, ISSN 0809-103X.

"Deformations in Concrete Cantilever Bridges: Observations and Theoretical Modelling",
Peter F. Takâcs, 2002:23, ISBN 82-471-5415-3, ISSN 0809-103X.

"Stiffened aluminium plates subjected to impact loading",
Hilde Giæver Hildrum, 2002:69, ISBN 82-471-5467-6, ISSN 0809-103X.

"Full- and model scale study of wind effects on a medium-rise building in a built up area",
Jónas Thór Snæbjørnsson, 2002:95, ISBN82-471-5495-1, ISSN 0809-103X.

“Evaluation of Concepts for Loading of Hydrocarbons in Ice-infested water”,
Arnor Jensen, 2002:114, ISBN 82-417-5506-0, ISSN 0809-103X.

”Numerical and Physical Modelling of Oil Spreading in Broken Ice”,
Janne K. Økland Gjøsteen, 2002:130, ISBN 82-471-5523-0, ISSN 0809-103X.

”Diagnosis and protection of corroding steel in concrete”,
Franz Pruckner, 20002:140, ISBN 82-471-5555-4, ISSN 0809-103X.

“Tensile and Compressive Creep of Young Concrete: Testing and Modelling”,
Dawood Atrushi, 2003:17, ISBN 82-471-5565-6, ISSN 0809-103X.

“Rheology of Particle Suspensions. Fresh Concrete, Mortar and Cement Paste with Various Types of Lignosulfonates”,
Jon Elvar Wallevik, 2003:18, ISBN 82-471-5566-4, ISSN 0809-103X.

“Oblique Loading of Aluminium Crash Components”,
Aase Reyes, 2003:15, ISBN 82-471-5562-1, ISSN 0809-103X.

“Utilization of Ethiopian Natural Pozzolans”,
Surafel Ketema Desta, 2003:26, ISSN 82-471-5574-5, ISSN:0809-103X.

"Behaviour and strength prediction of reinforced concrete structures with discontinuity regions", Helge Brå, 2004:11, ISBN 82-471-6222-9, ISSN 1503-8181.

"High-strength steel plates subjected to projectile impact. An experimental and numerical study", Sumita Dey, 2004:38, ISBN 82-471-6282-2 (printed version), ISBN 82-471-6281-4 (electronic version), ISSN 1503-8181.

"Alkali-reactive and inert fillers in concrete. Rheology of fresh mixtures and expansive reactions."
Bård M. Pedersen, 2004:92, ISBN 82-471-6401-9 (printed version), ISBN 82-471-6400-0 (electronic version), ISSN 1503-8181.

"On the Shear Capacity of Steel Girders with Large Web Openings".
Nils Christian Hagen, 2005:9 ISBN 82-471-6878-2 (printed version), ISBN 82-471-6877-4 (electronic version), ISSN 1503-8181.

"Behaviour of aluminium extrusions subjected to axial loading".
Østen Jensen, 2005:7, ISBN 82-471-6873-1 (printed version), ISBN 82-471-6872-3 (electronic version), ISSN 1503-8181.

"Thermal Aspects of corrosion of Steel in Concrete".
Jan-Magnus Østvik, 2005:5, ISBN 82-471-6869-3 (printed version), ISBN 82-471-6868 (electronic version), ISSN 1503-8181.

"Mechanical and adaptive behaviour of bone in relation to hip replacement." A study of bone remodelling and bone grafting.
Sébastien Muller, 2005:34, ISBN 82-471-6933-9 (printed version), ISBN 82-471-6932-0 (electronic version), ISSN 1503-8181.

"Analysis of geometrical nonlinearities with applications to timber structures".
Lars Wollebæk, 2005:74, ISBN 82-471-7050-5 (printed version), ISBN 82-471-7019-1 (electronic version), ISSN 1503-8181.

"Pedestrian induced lateral vibrations of slender footbridges",
Anders Rönnquist, 2005:102, ISBN 82-471-7082-5 (printed version), ISBN 82-471-7081-7 (electronic version), ISSN 1503-8181.

"Initial Strength Development of Fly Ash and Limestone Blended Cements at Various Temperatures Predicted by Ultrasonic Pulse Velocity",
Tom Ivar Fredvik, 2005:112, ISBN 82-471-7105-8 (printed version), ISBN 82-471-7103-1 (electronic version), ISSN 1503-8181.

"Behaviour and modelling of thin-walled cast components",
Cato Dørum, 2005:128, ISBN 82-471-7140-6 (printed version), ISBN 82-471-7139-2 (electronic version), ISSN 1503-8181.

“Behaviour and modelling of selfpiercing riveted connections”,
Raffaele Porcaro, 2005:165, ISBN 82-471-7219-4 (printed version), ISBN 82-471-7218-6 (electronic version), ISSN 1503-8181.

”Behaviour and Modelling og Aluminium Plates subjected to Compressive Load”,
Lars Rønning, 2005:154, ISBN 82-471-7169-1 (printed version), ISBN 82-471-7195-3 (electronic version), ISSN 1503-8181.

”Bumper beam-longitudinal system subjected to offset impact loading”,
Satyanarayana Kokkula, 2005:193, ISBN 82-471-7280-1 (printed version), ISBN 82-471-7279-8 (electronic version), ISSN 1503-8181.

“Control of Chloride Penetration into Concrete Structures at Early Age”,
Guofei Liu, 2006:46, ISBN 82-471-7838-9 (printed version), ISBN 82-471-7837-0 (electronic version), ISSN 1503-8181.

“Modelling of Welded Thin-Walled Aluminium Structures”,
Ting Wang, 2006:78, ISBN 82-471-7907-5 (printed version), ISBN 82-471-7906-7 (electronic version), ISSN 1503-8181.

”Time-variant reliability of dynamic systems by importance sampling and probabilistic analysis of ice loads”,
Anna Ivanova Olsen, 2006:139, ISBN 82-471-8041-3 (printed version), ISBN 82-471-8040-5 (electronic version), ISSN 1503-8181.

“Fatigue life prediction of an aluminium alloy automotive component using finite element analysis of surface topography”.
Sigmund Kyrre Ås, 2006:25, ISBN 82-471-7791-9 (printed version), ISBN 82-471-7791-9 (electronic version), ISSN 1503-8181.

”Constitutive models of elastoplasticity and fracture for aluminium alloys under strain path change”,
Dasharatha Achani, 2006:76, ISBN 82-471-7903-2 (printed version), ISBN 82-471-7902-4 (electronic version), ISSN 1503-8181.

“Simulations of 2D dynamic brittle fracture by the Element-free Galerkin method and linear fracture mechanics”,
Tommy Karlsson, 2006:125, ISBN 82-471-8011-1 (printed version), ISBN 82-471-8010-3 (electronic version), ISSN 1503-8181.

“Penetration and Perforation of Granite Targets by Hard Projectiles”,
Chong Chiang Seah, 2006:188, ISBN 82-471-8150-9 (printed version), ISBN 82-471-8149-5 (electronic version), ISSN 1503-8181.

"Deformations, strain capacity and cracking of concrete in plastic and early hardening phases",
Tor Arne Hammer, 2007:234, ISBN 978-82-471-5191-4 (printed version), ISBN 978-82-471-5207-2 (electronic version), ISSN 1503-8181.

"Crashworthiness of dual-phase high-strength steel: Material and Component behaviour", Venkatapathi Tarigopula, 2007:230, ISBN 82-471-5076-4 (printed version), ISBN 82-471-5093-1 (electronic version), ISSN 1503-8181.

"Fibre reinforcement in load carrying concrete structures",
Åse Lyslo Døssland, 2008:50, ISBN 978-82-471-6910-0 (printed version), ISBN 978-82-471-6924-7 (electronic version), ISSN 1503-8181.

"Low-velocity penetration of aluminium plates",
Frode Grytten, 2008:46, ISBN 978-82-471-6826-4 (printed version), ISBN 978-82-471-6843-1 (electronic version), ISSN 1503-8181.

"Robustness studies of structures subjected to large deformations",
Ørjan Fyllingen, 2008:24, ISBN 978-82-471-6339-9 (printed version), ISBN 978-82-471-6342-9 (electronic version), ISSN 1503-8181.

"Constitutive modelling of morsellised bone",
Knut Birger Lunde, 2008:92, ISBN 978-82-471-7829-4 (printed version), ISBN 978-82-471-7832-4 (electronic version), ISSN 1503-8181.

"Experimental Investigations of Wind Loading on a Suspension Bridge Girder",
Bjørn Isaksen, 2008:131, ISBN 978-82-471-8656-5 (printed version), ISBN 978-82-471-8673-2 (electronic version), ISSN 1503-8181.

"Cracking Risk of Concrete Structures in The Hardening Phase",
Guomin Ji, 2008:198, ISBN 978-82-471-1079-9 (printed version), ISBN 978-82-471-1080-5 (electronic version), ISSN 1503-8181.

"Modelling and numerical analysis of the porcine and human mitral apparatus",
Victorien Emile Prot, 2008:249, ISBN 978-82-471-1192-5 (printed version), ISBN 978-82-471-1193-2 (electronic version), ISSN 1503-8181.

"Strength analysis of net structures",
Heidi Moe, 2009:48, ISBN 978-82-471-1468-1 (printed version), ISBN 978-82-471-1469-8 (electronic version), ISSN1503-8181.

"Numerical analysis of ductile fracture in surface cracked shells",
Espen Berg, 2009:80, ISBN 978-82-471-1537-4 (printed version), ISBN 978-82-471-1538-1 (electronic version), ISSN 1503-8181.

"Subject specific finite element analysis of bone – for evaluation of the healing of a leg lengthening and evaluation of femoral stem design",
Sune Hansborg Pettersen, 2009:99, ISBN 978-82-471-1579-4 (printed version), ISBN 978-82-471-1580-0 (electronic version), ISSN 1503-8181.

"Evaluation of fracture parameters for notched multi-layered structures",
Lingyun Shang, 2009:137, ISBN 978-82-471-1662-3 (printed version), ISBN 978-82-471-1663-0 (electronic version), ISSN 1503-8181.

"Modelling of Dynamic Material Behaviour and Fracture of Aluminium Alloys for Structural Applications"
Yan Chen, 2009:69, ISBN 978-82-471-1515-2 (printed version), ISBN 978-82 471-1516-9 (electronic version), ISSN 1503-8181.

"Nanomechanics of polymer and composite particles"
Jianying He 2009:213, ISBN 978-82-471-1828-3 (printed version), ISBN 978-82-471-1829-0 (electronic version), ISSN 1503-8181.

"Mechanical properties of clear wood from Norway spruce"
Kristian Berbom Dahl 2009:250, ISBN 978-82-471-1911-2 (printed version) ISBN 978-82-471-1912-9 (electronic version), ISSN 1503-8181.

"Modeling of the degradation of TiB_2 mechanical properties by residual stresses and liquid Al penetration along grain boundaries"
Micol Pezzotta 2009:254, ISBN 978-82-471-1923-5 (printed version) ISBN 978-82-471-1924-2 (electronic version) ISSN 1503-8181.

"Effect of welding residual stress on fracture"
Xiabo Ren 2010:77, ISBN 978-82-471-2115-3 (printed version) ISBN 978-82-471-2116-0 (electronic version), ISSN 1503-8181.

"Pan-based carbon fiber as anode material in cathodic protection system for concrete structures"
Mahdi Chini 2010:122, ISBN 978-82-471-2210-5 (printed version) ISBN 978-82-471-2213-6 (electronic version), ISSN 1503-8181.

"Structural Behaviour of deteriorated and retrofitted concrete structures"
Irina Vasililjeva Sæther 2010:171, ISBN 978-82-471-2315-7 (printed version) ISBN 978-82-471-2316-4 (electronic version) ISSN 1503-8181.

"Prediction of local snow loads on roofs"
Vivian Meløysund 2010:247, ISBN 978-82-471-2490-1 (printed version) ISBN 978-82-471-2491-8 (electronic version) ISSN 1503-8181.

"Behaviour and modelling of polymers for crash applications"
Virgile Delhaye 2010:251, ISBN 978-82-471-2501-4 (printed version) ISBN 978-82-471-2502-1 (electronic version) ISSN 1503-8181.

"Blended cement with reducted CO_2 emission – Utilizing the Fly Ash-Limestone Synergy",
Klaartje De Weerdt 2011:32, ISBN 978-82-471-2584-7 (printed version) ISBN 978-82-471-2584-4 (electronic version) ISSN 1503-8181.

"Chloride induced reinforcement corrosion in concrete" Concept of critical chloride content – methods and mechanisms.
Ueli Angst 2011:113, ISBN 978-82-471-2769-9 (printed version) ISBN 978-82-471-2763-6 (electronic version) ISSN 1503-8181.

"A thermo-electric-Mechanical study of the carbon anode and contact interface for Energy savings in the production of aluminium".
Dag Herman Andersen 2011:157, ISBN 978-82-471-2859-6 (printed version) ISBN 978-82-471-2860-2 (electronic version) ISSN 1503-8181.

"Structural Capacity of Anchorage Ties in Masonry Veneer Walls Subjected to Earthquake". The implications of Eurocode 8 and Eurocode 6 on a typical Norwegain veneer wall.
Ahmed Mohamed Yousry Hamed 2011:181, ISBN 978-82-471-2911-1 (printed version) ISBN 978-82-471-2912-8 (electronic ver.) ISSN 1503-8181.

"Work-hardening behaviour in age-hardenable Al-Zn-Mg(-Cu) alloys".
Ida Westermann , 2011:247, ISBN 978-82-471-3056-8 (printed ver.) ISBN 978-82-471-3057-5 (electronic ver.) ISSN 1503-8181.

"Behaviour and modelling of selfpiercing riveted connections using aluminium rivets".
Nguyen-Hieu Hoang, 2011:266, ISBN 978-82-471-3097-1 (printed ver.) ISBN 978-82-471-3099-5 (electronic ver.) ISSN 1503-8181.

"Fibre reinforced concrete".
Sindre Sandbakk, 2011:297, ISBN 978-82-471-3167-1 (printed ver.) ISBN 978-82-471-3168-8 (electronic ver) ISSN 1503:8181.

"Dynamic behaviour of cablesupported bridges subjected to strong natural wind".
Ole Andre Øiseth, 2011:315, ISBN 978-82-471-3209-8 (printed ver.) ISBN 978-82-471-3210-4 (electronic ver.) ISSN 1503-8181.

"Constitutive modeling of solargrade silicon materials"
Julien Cochard, 2011:307, ISBN 978-82-471-3189-3 (printed ver). ISBN 978-82-471-3190-9 (electronic ver.) ISSN 1503-8181.

"Constitutive behavior and fracture of shape memory alloys"
Jim Stian Olsen, 2012:57, ISBN 978-82-471-3382-8 (printed ver.) ISBN 978-82-471-3383-5 (electronic ver.) ISSN 1503-8181.

“Field measurements in mechanical testing using close-range photogrammetry and digital image analysis”
Egil Fagerholt, 2012:95, ISBN 978-82-471-3466-5 (printed ver.) ISBN 978-82-471-3467-2 (electronic ver.) ISSN 1503-8181.

“Towards a better under standing of the ultimate behaviour of lightweight aggregate concrete in compression and bending”,
Håvard Nedrelid, 2012:123, ISBN 978-82-471-3527-3 (printed ver.) ISBN 978-82-471-3528-0 (electronic ver.) ISSN 1503-8181.

“Numerical simulations of blood flow in the left side of the heart”
Sigrid Kaarstad Dahl, 2012:135, ISBN 978-82-471-3553-2 (printed ver.) ISBN 978-82-471-3555-6 (electronic ver.) ISSN 1503-8181.

“Moisture induced stresses in glulam”
Vanessa Angst-Nicollier, 2012:139, ISBN 978-82-471-3562-4 (printed ver.) ISBN 978-82-471-3563-1 (electronic ver.) ISSN 1503-8181.

“Biomechanical aspects of distraction osteogensis”
Valentina La Russa, 2012:250, ISBN 978-82-471-3807-6 (printed ver.) ISBN 978-82-471-3808-3 (electronic ver.) ISSN 1503-8181.

“Ductile fracture in dual-phase steel. Theoretical, experimental and numerical study”
Gaute Gruben, 2012:257, ISBN 978-82-471-3822-9 (printed ver.) ISBN 978-82-471-3823-6 (electronic ver.) ISSN 1503-8181.

“Damping in Timber Structures”
Nathalie Labonnote, 2012:263, ISBN 978-82-471-3836-6 (printed ver.) ISBN 978-82-471-3837-3 (electronic ver.) ISSN 1503-8181.

“Biomechanical modeling of fetal veins: The umbilical vein and ductus venosus bifurcation”
Paul Roger Leinan, 2012:299, ISBN 978-82-471-3915-8 (printed ver.) ISBN 978-82-471-3916-5 (electronic ver.) ISSN 1503-8181.

“Large-Deformation behaviour of thermoplastics at various stress states”
Anne Serine Ognedal, 2012:298, ISBN 978-82-471-3913-4 (printed ver.) ISBN 978-82-471-3914-1 (electronic ver.) ISSN 1503-8181.

“Hardening accelerator for fly ash blended cement”
Kien Dinh Hoang, 2012:366, ISBN 978-82-471-4063-5 (printed ver.) ISBN 978-82-471-4064-2 (electronic ver.) ISSN 1503-8181.

“From molecular structure to mechanical properties”
Jianyang Wu, 2013:186, ISBN 978-82-471-4485-5 (printed ver.) ISBN 978-82-471-4486-2 (electronic ver.) ISSN 1503-8181.

"Experimental and numerical study of hybrid concrete structures"
Linn Grepstad Nes, 2013:259, ISBN 978-82-471-4644-6 (printed ver.) ISBN 978-82-471-4645-3 (electronic ver.) ISSN 1503-8181.

"Mechanics of ultra-thin multi crystalline silicon wafers"
Saber Saffar, 2013:199, ISBN 978-82-471-4511-1 (printed ver.) ISBN 978-82-471-4513-5 (electronic ver). ISSN 1503-8181.

"Through process modelling of welded aluminium structures"
Anizahyati Alisibramulisi, 2013:325, ISBN 978-82-471-4788-7 (printed ver.) ISBN 978-82-471-4789-4 (electronic ver.) ISSN 1503-8181.

"Combined blast and fragment loading on steel plates"
Knut Gaarder Rakvåg, 2013:361, ISBN978-82-471-4872-3 (printed ver.) ISBN 978-82-4873-0 (electronic ver.). ISSN 1503-8181.

"Characterization and modelling of the anisotropic behaviour of high-strength aluminium alloy"
Marion Fourmeau, 2014:37, ISBN 978-82-326-0008-3 (printed ver.) ISBN 978-82-326-0009-0 (electronic ver.) ISSN 1503-8181.

"Behaviour of threated steel fasteners at elevated deformation rates"
Henning Fransplass, 2014:65, ISBN 978-82-326-0054-0 (printed ver.) ISBN 978-82-326-0055-7 (electronic ver.) ISSN 1503-8181.

"Sedimentation and Bleeding"
Ya Peng, 2014:89, ISBN 978-82-326-0102-8 (printed ver.) ISBN 978-82-326-0103-5 (electric ver.) ISSN 1503-8181.

"Impact against X65 offshore pipelines"
Martin Kristoffersen, 2014:362, ISBN 978-82-326-0636-8 (printed ver.) ISBN 978-82-326-0637-5 (electronic ver.) ISSN 1503-8181.

"Formability of aluminium alloy subjected to prestrain by rolling"
Dmitry Vysochinskiy, 2014:363,, ISBN 978-82-326-0638-2 (printed ver.) ISBN 978-82-326-0639-9 (electronic ver.) ISSN 1503-8181.

"Experimental and numerical study of Yielding, Work-Hardening and anisotropy in textured AA6xxx alloys using crystal plasticity models"
Mikhail Khadyko, 2015:28, ISBN 978-82-326-0724-2 (printed ver.) ISBN 978-82-326-0725-9 (electronic ver.) ISSN 1503-8181.

"Behaviour and Modelling of AA6xxx Aluminium Alloys Under a Wide Range of Temperatures and Strain Rates"
Vincent Vilamosa, 2015:63, ISBN 978-82-326-0786-0 (printed ver.) ISBN 978-82-326-0787-7 (electronic ver.) ISSN 1503-8181.

"A Probabilistic Approach in Failure Modelling of Aluminium High Pressure Die-Castings"
Octavian Knoll, 2015:137, ISBN 978-82-326-0930-7 (printed ver.) ISBN 978-82-326-0931-4 (electronic ver.) ISSN 1503-8181.

"Ice Abrasion on Marine Concrete Structures"
Egil Møen, 2015:189, ISBN 978-82-326-1034-1 (printed ver.) ISBN 978-82-326-1035-8 (electronic ver.) ISSN 1503-8181.

"Fibre Orientation in Steel-Fibre-Reinforced Concrete"
Giedrius Zirgulis, 2015:229, ISBN 978-82-326-1114-0 (printed ver.) ISBN 978-82-326-1115-7 (electronic ver.) ISSN 1503-8181.

"Effect of spatial variation and possible interference of localised corrosion on the residual capacity of a reinforced concrete beam"
Mohammad Mahdi Kioumarsi, 2015:282, ISBN 978-82-326-1220-8 (printed ver.) ISBN 978-82-1221-5 (electronic ver.) ISSN 1503-8181.

"The role of concrete resistivity in chloride-induced macro-cell corrosion"
Karla Horbostel, 2015:324, ISBN 978-82-326-1304-5 (printed ver.) ISBN 978-82-326-1305-2 (electonic ver.) ISSN 1503-8181.

"Flowable fibre-reinforced concrete for structural applications"
Elena Vidal Sarmiento, 2015-335, ISBN 978-82-326-1324-3 (printed ver.) ISBN 978-82-326-1325-0 (electronic ver.) ISSN 1503-8181.

"Development of chushed sand for concrete production with microproportioning"
Rolands Cepuritis, 2016:19, ISBN 978-82-326-1382-3 (printed ver.) ISBN 978-82-326-1383-0 (electronic ver.) ISSN 1503-8181.

"Withdrawal properties of threaded rods embedded in glued-laminated timer elements"
Haris Stamatopoulos, 2016:48, ISBN 978-82-326-1436-3 (printed ver.) ISBN 978-82-326-1437-0 (electronic ver.) ISSN 1503-8181.

"An Experimental and numerical study of thermoplastics at large deformation"
Marius Andersen, 2016:191, ISBN 978-82-326-1720-3 (printed ver) ISBN 978-82-326-1721-0 (electronic ver.) ISSN 1503-8181.